Targeting inter-organ cross-talk in cardiometabolic diseases
Liu, C.

Citation

Liu, C. (2023, May 16). *Targeting inter-organ cross-talk in cardiometabolic diseases*. Retrieved from https://hdl.handle.net/1887/3618361

Version:	Publisher's Version
License:	Licence agreement concerning inclusion of doctoral thesis in the Institutional Repository of the University of Leiden
Downloaded from:	https://hdl.handle.net/1887/3618361

Note: To cite this publication please use the final published version (if applicable).

Targeting Inter-Organ Cross-Talk in Cardiometabolic Diseases

Cong Liu

Targeting Inter-Organ Cross-Talk in Cardiometabolic Diseases

Cong Liu

Targeting Inter-Organ Cross-Talk in Cardiometabolic Diseases
© 2023, Cong Liu

Targeting Inter-Organ Cross-Talk in Cardiometabolic Diseases

Proefschrift

ter verkrijging van
de graad van doctor aan de Universiteit Leiden,
op gezag van rector magnificus prof. dr. ir. H. Bijl,
volgens besluit van het college voor promoties
te verdedigen op dinsdag 16 mei 2023
klokke 10:00 uur

door

Cong Liu

geboren te Shandong, China,
in 1993

Promotores
Prof. dr. P.C.N. Rensen
Prof. dr. Y. Wang (Xi'an Jiaotong University, Xi'an, Shaanxi Province, China)

Co-promotor
Dr. M. Schönke

Leden promotiecommissie
Prof. dr. P.H.A. Quax
Prof. dr. A.K. Groen (Amsterdam University Medical Center)
Prof. dr. S.W.C. Van Mil (University Medical Center Utrecht)
Prof. dr. E. Blaak (Maastricht University)

TABLE OF CONTENTS

1

General introduction and outline

Cardiometabolic health is tightly controlled by highly coordinated cross-talk among various tissues and organs. In this thesis, by using dietary and pharmacological interventions, I explored the therapeutic potential of targeting inter-organ communication in cardiometabolic diseases. By the end I hope you will realize that when talking about therapeutic strategies for cardiometabolic diseases - it's all about inter-organ cross-talk.

GENERAL INTRODUCTION

Cardiometabolic health is achieved through a complex network of organ communication. Dysfunction of these lines of communication contributes to the development of cardiometabolic diseases, which are quickly becoming pressing public-health concerns globally.

1. Cardiometabolic diseases

Definition of cardiometabolic diseases. Cardiometabolic diseases are a collective term referring to metabolic disorders, non-alcoholic fatty liver disease (NAFLD) and cardiovascular diseases (CVDs). Metabolic disorders that are driven by abnormal fat expansion are a group of conditions including dyslipidemia, hyperglycemia, insulin resistance, obesity, type 2 diabetes (T2D) and hypertension, and these metabolic abnormalities are all well-documented risk factors for the development of NAFLD and CVDs [1-4]. Given the close association between NAFLD and CVD risk factors encapsulated by the metabolic disorders, it is not surprising that NAFLD was recently proposed to be associated with increased risk of CVDs. Substantial epidemiological evidence and population-based cohort studies indeed link NAFLD to subclinical atherosclerosis and a high prevalence of clinically manifest CVDs. In case control studies, NAFLD has been shown to be associated with increased artery intima-media thickness and arterial wall stiffness [5, 6]. Likewise, cohort studies in people with biopsy-proven NAFLD demonstrate that CVDs are the most common cause of death in this population [7-9]. According to these available findings, there seems little doubt that NAFLD is also a risk factor of CVDs.

NAFLD is an umbrella term for a group of liver diseases ranging from hepatic steatosis, featured by hepatocyte lipid overload, to nonalcoholic steatohepatitis (NASH) with hepatic steatosis, lobular inflammation, hepatocyte ballooning and varying degrees of fibrosis [2]. People diagnosed with NASH are predisposed to developing cirrhosis and hepatocellular carcinoma, among whom people with severe hepatic fibrosis are at highest risk of overall and liver-related mortality [10]. Currently, there are no established pharmacological agents for NASH. Rather, lifestyle interventions remain

1

the first-line treatment for it, despite that lifestyle changes are rarely attainable in the long term, and the liver transplantation is still the sole intervention to treat the end-stage of NASH [2, 11].

CVDs, as indicated by the name, are a broad term of diseases affecting the heart and/ or blood vessels. The main cause of CVDs is atherosclerosis, which is defined by the build-up of atherogenic lipoprotein-derived cholesterol and immune cells in the vessel wall, to form so-called atherosclerotic plaques [12]. The most clinically dangerous plaques, by rupturing or eroding, can trigger occlusive luminal thrombosis, thereby causing a heart attack or stroke, depending on the specific artery that is occluded by the thrombus [12]. Of note, almost 18 million people die from CVDs each year, making it the number one cause of death globally [13]. Although alleviation of dyslipidemia largely decreases cardiovascular morbidity and mortality as consistently observed in large clinical trials, many at-risk patients either fail to reach their target lipid levels using current therapeutics like statins or are intolerant to statins owing to their adverse effects [14]. This leaves many patients with obvious residual risks.

Collectively, there is an unmet need for additional therapeutic targets and strategies that control the development of cardiometabolic diseases, in particular of NAFLD and atherosclerotic CVD, or even reverse the underlying pathophysiology.

Pathogenesis of insulin resistance and obesity. The etiology of cardiometabolic diseases is associated with a positive energy balance. In the human body, energy is stored as glycogen and, to much larger extent, as lipids, which represents long-term energy storage. In health, lipids are mainly stored as triglycerides (TGs) located within lipid droplets in white adipose tissue (WAT), and, to much lesser extent, stored ectopically in non-adipose tissues. In obesity, a dysfunction of long-term fat storage in WAT resulting from chronic overnutrition, impaired adipogenesis, restricted hyperplasia and other factors, leads to increased circulating free fatty acids (FAs) and consequently increased ectopic fat deposition in e.g. the liver and skeletal muscle. Excessive lipid accumulation in these non-adipose tissues can disturb their metabolic function, thereby promoting disease progression. FAs in the circulation are partially derived from the lipolysis of chylomicron- and very-low density lipoprotein (VLDL)-derived TGs by the action of lipoprotein lipase (LPL) [15]. Most circulating FAs are derived from TG stores in WAT, released via the action of the cyclic adenosine monophosphate (cAMP)-dependent enzymes, including adipose triglyceride lipase (ATGL), hormone sensitive lipase (HSL), and monoglyceride lipase (MGL) [16]. Insulin secreted by pancreatic β cells is crucial for inhibition of FA release from WAT; inhibition of adipose tissue lipolysis is even the most sensitive pathway of insulin action. When

insulin resistance develops, intracellular lipolysis in adipocytes increases to produce more FAs, which further inhibit the anti-lipolytic effect of insulin and thus promote additional lipolysis [1].

Pathogenesis of NAFLD. A 'two-hit' theory was posited for several years to explain NAFLD pathogenesis [17]. This theory indicates that in the setting of the first 'hit', namely steatosis alone, which is caused by a chronic lipid accumulation in hepatocytes, a second 'hit', such as endoplasmic reticulum (ER) stress, oxidant stress and inflammasome activation, is required for the development of NAFLD by activating inflammatory cascades and fibrogenesis. However, this view appeared too simplistic and is now considered outdated [18]. There are various molecular pathways that contribute to NAFLD development, and it is even uncertain whether NAFLD is always preceded by fatty liver. Therefore, a 'multi-hit' concept has recently been proposed and is currently used for understanding NAFLD pathogenesis. The 'multi-

1
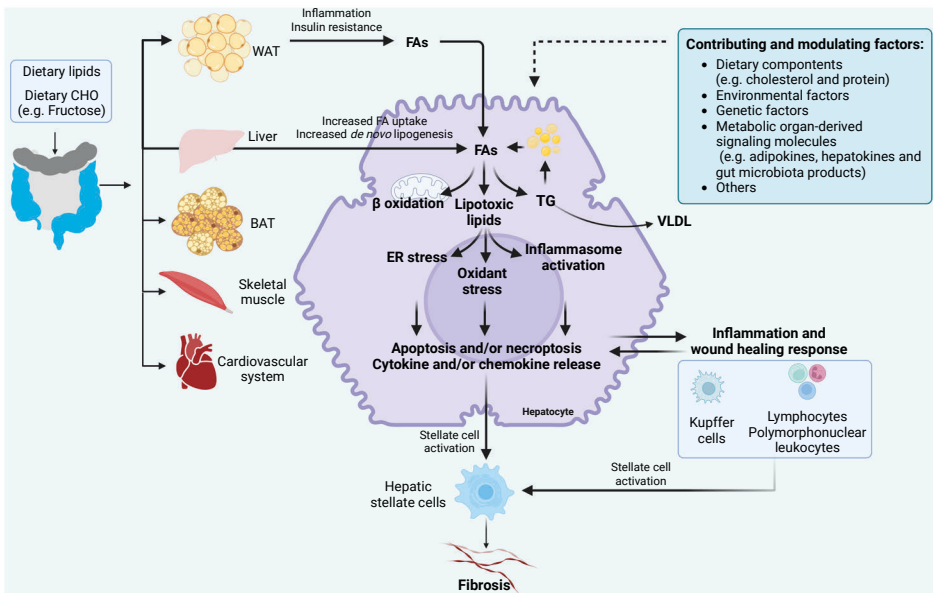
Figure 1-1. Pathogenesis of NAFLD. Fatty acids (FAs) derived from dietary lipids or white adipose tissue (WAT) circulate in the blood as bound to albumin, and can then be delivered to the liver. The liver itself can also produce FAs via *de novo* lipogenesis, the process through which hepatocytes convert excess dietary carbohydrates (CHO) like glucose to FAs. The two main fates of FAs in hepatocytes are breakdown through mitochondrial β-oxidation and re-esterification to form triglycerides (TGs) that can be stored in lipid droplets. Lipid droplet-derived TGs undergo precisely-controlled lipolysis to release FAs back into the hepatocyte FA pool. When the disposal of FAs through β-oxidation or TGs synthesis is overwhelmed, FAs can form toxic lipid species that can cause endoplasmic reticulum (ER) stress, oxidant stress and inflammasome activation. These processes can lead to hepatocellular injury, inflammation, stellate cell activation and fibrogenesis. BAT, brown adipose tissue; WAT, white adipose tissue.

hit' theory is based on the concept that various factors (e.g. dietary, environmental and genetic) can induce insulin resistance, obesity and abnormal changes of the gut microbiota, all of which are all risk factors contributing to NAFLD initiation and progression [11]. The conceptual frame work behind this theory is that the capacity of the liver to handle the primary metabolic energy substrates, e.g. FAs and carbohydrates (CHO), is overwhelmed, leading to aberrant accumulation of toxic lipid species in hepatocytes, which can induce hepatocellular stress, injury and death (**Figure 1-1**).

Pathogenesis of atherosclerosis. Atherosclerosis, the main cause of CVDs, is considered to be a lipid-driven inflammatory disease [19]. In the early stage, apolipoprotein B (ApoB)-containing lipoproteins, such as TG-rich lipoprotein (TRL) remnants and low-density lipoprotein (LDL) particles, are deposited and accumulate in the vessel wall, where these particles can undergo oxidative and other modifications that can render them pro-inflammatory and immunogenic. This is followed by the recruitment of classic monocytes into the intima of the vessel wall. Bloodstream monocytes can bind to adhesion molecules expressed by the endothelial cells. Chemokines can promote the migration of these bound monocytes into the vessel wall. Once in the intima, monocytes can differentiate into macrophages, and attain a phenotype related to the reparative macrophage population [19]. These macrophages express scavenger receptors that allow them to bind to and take up modified lipoprotein particles, which turns them into lipid-rich foam cells. At this stage, mild lesions or 'fatty streaks' are formed that are still reversible. With disease progression, these foam cells and endothelial cells can release pro-inflammatory cytokines, and T lymphocytes, despite numerically less abundant than macrophages, also enter into the intima, where they can affect the function of innate immune cells, endothelial and smooth muscle cells (SMCs) [19]. SMCs within the media are able to migrate into the intima in response to factors released by the accumulating leukocytes. These SMCs can produce extracellular matrix molecules (such as collagen), that contribute to the intimal thickening. T cell-derived factors, such as interferon γ, can dampen collagen synthesis by SMCs and impair the ability of SMCs to repair and maintain the fibrous cap that overlines the fatty streak. Foam cells and SMCs may eventually die, resulting in the formation of a necrotic core within the plaque. Furthermore, pro-inflammatory macrophages and other immune cells can increase their production of matrix metalloproteinases to degrade collagen and consequently impair fibrous cap strength. Thinning and structural weakening of the fibrous cap can upregulate the susceptibility of the plaque to rupture (**Figure 1-2**).
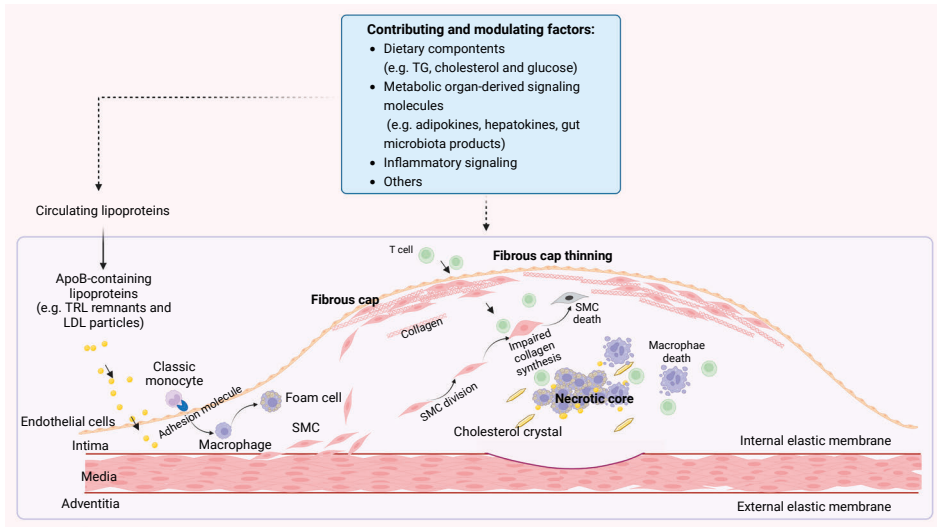
Figure 1-2. Pathogenesis of atherosclerosis. Increased circulating levels of atherogenic lipoproteins, caused by multiple factors e.g. dietary lipids and metabolic organ-associated signaling molecules, can promote atherosclerosis development. Early events of atherosclerosis include infiltration of atherogenic lipoproteins into the intima and adhesion of blood leukocytes, primarily monocytes, to the activated endothelial monolayer. This is followed by migration of monocytes into the intima and their maturation into macrophages. These macrophages can then take up large amounts of lipids to transform into lipid-laden foam cells. Lesion progression involves smooth muscle cell (SMC) migration from the media into the intima, resident intimal and media-derived SMC proliferation and extracellular matrix synthesis (e.g. collagen synthesis). Macrophages and SMCs within plaques can die in advancing lesions. Extracellular lipids derived from dead and dying cells can accumulate in the central region of a plaque, often denoted the lipid or necrotic core. TRL, triglyceride-rich lipoprotein; LDL, low-density lipoprotein.

2. Inter-organ cross-talk: a gatekeeper for cardiometabolic health

In multicellular organisms, maintenance of whole-body homeostasis and response to nutritional and environmental challenges require the coordination of different tissues and organs. To respond to metabolic demands, higher organisms have evolved multidirectional interactions among various metabolic organs and tissues in periphery and in the central nervous system (CNS). In this regard, inter-organ cross-talk represents a system of biological communication which relays important information about metabolic fluxes between physiological distant cells. Although how these metabolic organ systems interact with one another is still not completely understood, one key strategy for modulating whole-body metabolism is communication among tissues through signaling molecules including peptide/protein hormones, bioactive lipids, functional small molecules and other factors (e.g. micro-vesicles and exosomes). These molecules allow multiple organ systems to work together to absorb, store, sense and use energy, and to regulate the efficiency of energy metabolism of the body. Thus, tightly controlled inter-organ cross-talk is crucial for maintaining cardiometabolic health.

Gastrointestinal tract-derived signaling molecules. The gastrointestinal (GI) tract, the key interface between ingested dietary nutrients and the body, plays a pivotal
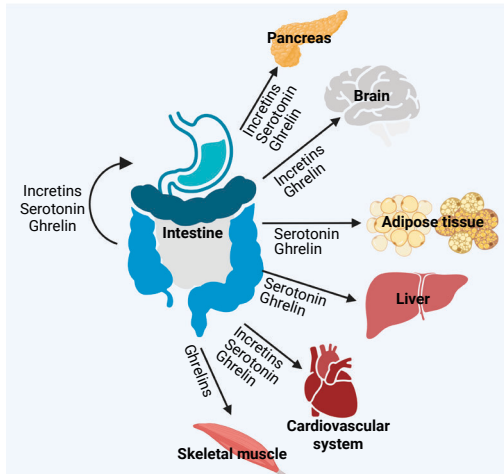

role in regulating energy utilization. The GI tract harbors enteroendocrine cells (EECs) along its entirety. EECs are the main sensors of the ingested nutrients, and can release peptide hormones into the paracellular space where they either act locally or enter into the bloodstream and circulate to other organs [20]. Recently, it has also been identified that many EECs contain basolateral cytoplasmic elongations known as neuropods that not only contain peptide/protein hormones but also connect to nerves of the GI tract, which allows the transduction of nutrient signals from the GI tract directly to the brain [21]. Accordingly, in response to various challenges (e.g. dietary changes) within a proper range, the GI tract has the ability to maintain a homeostatic status through inter-organ cross-talk (**Figure 2-1**).

Figure 2-1. Gastrointestinal tract-derived signaling factors. Hormones secreted by the gastrointestinal (GI) tract, such as the incretin hormones GIP and GLP-1, serotonin and ghrelin, play an important role in the regulation of nutrient uptake and storage. These hormones act on the brain to modify energy metabolism, and also have diverse metabolic effects on target organs, such as pancreas, adipose tissue, the liver, skeletal muscle and cardiovascular system (selected GI tract-derived factors and selected target organs are shown).

Among GI-derived signaling molecules, glucagon-like peptide-1 (GLP-1) and glucose-dependent insulinotropic peptide (GIP) are the best-characterized. GLP-1 and GIP are released from enteroendocrine L and K cells, respectively, within the gut upon consumption of dietary nutrients, primarily simple carbohydrates (CHO). Upon secretion, the majority of GLP-1 is rapidly degraded by dipeptidyl peptidase-4 (DPP4); only approximately 25% reaches the hepatoportal circulation and 10% reaches the systemic circulation [22, 23]. GLP-1 exerts its function through binding to and activating its specific G-protein-coupled receptor (GPCR), e.g. the GLP-1 receptor (GLP-1R) [24]. Likewise, most of GIP is rapidly degraded by DPP4 after releasing from the gut following nutrient intake, and the remaining GIP in the circulation can act on its receptor, the GIPR, to confer its function. Since the GLP-1R and GIPR are highly expressed in pancreas, these two GI-derived peptide hormones can act on pancreatic β cells to exert insulinotropic effects in a glucose-dependent manner [25]. Functional GLP-1R and GIPR are also expressed on extra-pancreatic organs, such as the brain,

where GLP-1 and GIP can achieve the control of energy intake (e.g. food consumption) and expenditure (e.g. BAT thermogenesis) [26]. GI tract also produces serotonin. After releasing to the bloodstream, the GI-derived serotonin interacts with multiple metabolic organs (e.g. the liver and adipose tissue) to regulate whole-body metabolism [27]. Other GI-derived signaling molecules, such as ghrelin, also relay metabolic information to multiple metabolic organs to influence whole-body metabolism in response to different metabolic conditions [20, 27].

Gut microbiota-associated signaling molecules. Besides producing signaling molecules itself, the GI tract also harbors a complex and dynamic population of microorganisms, the microbiota, the density of which increases from proximal to the distal end of the intestine. The gut microbiota is dominated by bacteria, while fungi, viruses, archaea and protozoa are also present. It forms a bioreactor which is fueled by exogenous dietary components and endogenous compounds generated from microorganisms and the host to produce bioactive compounds. These gut microbiota-derived metabolites signal to various metabolic organs in the body, which adds to cross-talk between the gut and the host. The structural components of the microbes also contribute to organ cross-talk under pathological conditions. Owning to the gut microbiota-host communication, the gut microbiota plays critical roles in regulating physiological functions of the host (**Figure 2-2**).

Short-chain fatty acids (SCFAs) are important signaling molecules produced by the gut microbiota. They are the end products of the gut microbial fermentation of non-digestible CHO. The most abundant SCFAs in the gut are acetate, butyrate and propionate, which constitute >95% of the total SCFAs, while caproate, formate and valerate are present in substantially lower amounts and make up the remaining 5% [28]. SCFAs exert their functions partially by acting on specific GPCRs, including GPR41 and GPR43, which are widely expressed [29]. The binding of SCFAs to their receptors on EECs can trigger GLP-1 secretion, which improves pancreatic function and reduces appetite [30]. Moreover, butyrate and

Figure 2-2. Gut microbiota-associated signaling molecules. Gut microbiota convert environmental signals and dietary molecules into signaling metabolites to communicate with the host. These gut microbiota-associated bioactive compounds, such as short chain fatty acids (SCFAs), bile acids (BAs), branch-chain amino acids (BCAAs), trimethylamine (TMA) and microbe-associated molecular patterns (MAMPs) including lipopolysaccharide (LPS), can signal to different organs and tissues (e.g. intestine, the gut microbiota, brain, liver, adipose tissue, skeletal muscle and cardiovascular system), in the host to modulate the function of these organs and tissues (selected gut microbiota-associated factors and selected target organs are shown).

acetate have been shown to act on the vagus nerve to increase energy metabolism, and acetate can also cross the blood-brain barrier and act centrally to increase satiety [31]. Propionate acts as a precursor for intestinal glucogenesis, which contributes to the inhibition hepatic glucose production and the improvement of hyperglycemia [32]. Moreover, SCFAs can act on WAT to decrease lipolysis and suppress inflammation, act on brown adipose tissue (BAT) to increase thermogenesis, and act on skeletal muscle and the liver to increase fat oxidation and decrease inflammation, thereby contributing to the whole-body metabolic homeostasis [22]. According to the available literature, SCFAs may be potential therapeutic targets for treating cardiometabolic disorders.

In addition to SCFAs, bile acids (BAs) have also been regarded as important gut microbiota-associated metabolites. BAs are metabolites of amphipathic cholesterol, and they solubilize dietary lipids by forming mixed micelles in the small intestine and facilitate the absorption of those lipids [33]. They are also hormones that regulate BA biosynthesis, lipid and glucose metabolism as well as immune signaling. The BA pool contains primary BAs, synthesized by hepatocytes, and secondary BAs, the products of primary BA metabolism by the gut microbiota. Primary BAs are conjugated in the liver with glycine/taurine in humans or primarily taurine in mice, to form bile salts that are stored in the gall bladder [33]. After being released into the small intestine upon the intake of dietary nutrients, primary BAs can be deconjugated by the gut microbes, which enables these BAs to escape reabsorption [34]. BAs have been shown to activate farnesoid X (FXR) and Takeda G-protein receptor 5 (TGR5), and the intestinal microbiota can affect the metabolism of BAs to modulate signaling mediated by these two receptors [35]. For instance, liver-derived primary BAs mainly activate FXR in enterocytes to induce the expression of fibroblast growth factor (FGF)15 that suppresses hepatic BA synthesis, and thus leads to reduced BA pool through the gut-liver feedback loop [36]. In addition to generating signaling molecules to modulate CHO and lipid metabolism, the gut microbiota can also regulate amino acid metabolism to control metabolic health. Recent clinical trials have reported that elevated circulating levels of branched-chain amino acids (BCAAs), including isoleucine, leucine and valine, are implicated in the development of cardiometabolic diseases [37]. Intriguingly, several gut microbes (e.g. *Parabacteroides merdae*) have been shown to enhance BCAA degradation, thereby reducing blood BCAA and improving cardiometabolic disorders [38].

Not all gut microbiota-derived signals exert beneficial effects to maintain metabolic health, and recent studies reported that several gut microbiota-associated signaling molecules can trigger the development of cardiometabolic diseases via communication with multiple metabolic organs [39]. A well-studied example is trimethylamine oxide (TMAO) that is derived from dietary choline [40-42]. Gut microbiota convert choline

into trimethylamine (TMA) that is delivered via the portal vein to the liver where hepatocytes rapidly oxidize TMA into TMAO by flavin monooxygenases (FMOs) [42]. Studies conducted in *Apoe*^{-/-} and *Ldlr*^{-/-} mice showed that TMAO aggravates atherosclerosis via various mechanisms, including promoting formation of foam cells and activating the inflammatory response [42, 43]. Besides, by feeding choline-enriched diet to C57BL/6 mice, TMAO has been reported to induce insulin resistance and adiposity, which is partially attributed to the stimulation of hepatic glucose production [39]. These available data likely indicate that TMAO-lowering interventions may have therapeutic potential to reduce cardiometabolic disease. However, *Apoe*^{-/-}, *Ldlr*^{-/-} and C57BL/6 mice are suboptimal models for human metabolism, and studies in more humanized animal models and humans are still needed to validate TMAO as therapeutic target.

Likewise, microbe-associated molecular patterns (MAMPs), such as lipopolysaccharide (LPS), are also important bioactive molecules contributing to the development of cardiometabolic diseases. They are recognized by pattern-recognition receptors, such as Toll-like receptors (TLRs), on epithelial and immune cells [29]. Under physiological conditions, these MAMPs hardly translocate across the epithelial barrier. Occasionally, low amounts of microbial components (e.g. LPS) might reach the lymph and circulation via paracellular diffusion, transcellular transport or co-transport with chylomicrons. In pathological conditions, such as obesity, the gut-blood barrier can become leaky, thereby increasing LPS levels in the circulation, which induces local and systemic inflammation to initiate and exacerbate cardiometabolic diseases [44, 45].

Liver-derived signaling molecules. As a key regulator of energy metabolism, the liver is able to adapt quickly to various metabolic conditions. For instance, during the postprandial state, the hepatic uptake of glucose is increased in response to elevated blood glucose, and hepatocytes then convert glucose into glycogen and into TGs through *de novo* lipogenesis (DNL). Simultaneously, the influx of glucose into the liver decreases the hepatic glucose production. In the fasting state, hepatic glucose production is increased via glycogenolysis and gluconeogenesis to supply glucose as a fuel source to extra-hepatic tissues. In addition, the liver can also generate ketones from lipid oxidation, and produce very-low density lipoproteins (VLDL) to supply lipids to peripheral tissues. To maintain the balance of aforementioned metabolic processes and other pathways involved in whole-body metabolism, the liver needs to communicate with other organs in periphery and/or in the CNS via functional molecules. The term 'hepatokines' has recently been coined to indicate liver-secreted hormones, which are essential for transmitting information regarding the metabolic status of the liver to other tissues (**Figure 2-3**).
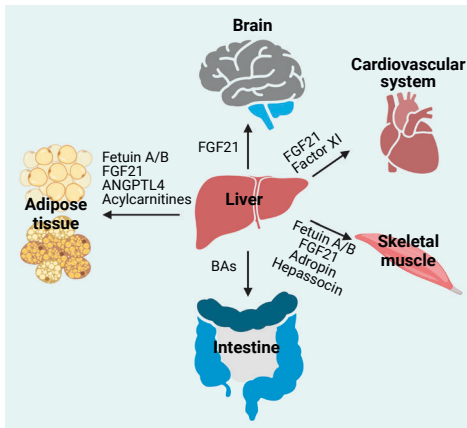
Figure 2-3. Liver-derived factors. The liver plays a central role in energy metabolism and communicates with other organ systems via many secreted signaling molecules. These factors, including hepatokines, lipids and other small molecules, have diverse effects on target organs including adipose tissues, the brain, cardiovascular system, skeletal muscle and the intestine, which help maintain energy homeostasis in response to rapidly changing nutritional states (selected liver-derived factors are shown). ANGPTL4, angiopoietin-like 4; BA, bile acids.

Fetuin-A is one of well-studied liver-derived factors proposed to regulate metabolic balance through integrated organ cross-talk. Fetuin-A is expressed predominately in the liver, but also in the placenta and the tongue to a lesser extent. It was identified as an endogenous inhibitor of the insulin receptor tyrosine kinase in the adipose tissue and skeletal muscle [46]. Another hepatokine is FGF21, an atypical member of the endocrine FGF family that lacks mitogenic activity. Although mRNA levels of FGF21 can be detected in numerous tissues, including the liver, adipose tissue, pancreas and muscle, under physiological conditions circulating FGF21 levels are known to be mainly derived from the liver. FGF21 elicits its biological effects by binding and activating a receptor complex comprised of FGF receptors (FGFRs) and its co-receptor-klotho (KLB) [47]. Whereas FGFRs exhibit a ubiquitous expression pattern, the expression of KLB is primarily restricted to specific metabolic organs (e.g. the liver and adipose tissue). Being a stress-induced hormone, hepatic FGF21 expression is markedly increased by myriad of nutritional and cellular stress signals, and FGF21 released from the liver into the circulation exerts paracrine and endocrine control of many aspects of energy metabolism in multiple tissues. For instance, FGF21 acts on the liver in an autocrine manner to protect hepatocytes from metabolic stress-induced lipid overload, and acts in an endocrine manner on WAT to increase lipid lipolysis under fasting conditions, and on BAT to increase thermogenesis upon cold exposure [48]. FGF21 also reduces sweet food intake via signaling through the paraventricular nucleus in hypothalamus [48]. In fact, most of the hepatokines are secreted in response to an adverse metabolic state like obesity, dyslipidemia and insulin resistance. In particular, liver lipid overload is the most important signal that promotes the production and release of these signaling molecules. In line with this, circulating levels of many hepatokines including FGF21 have been shown to rise in metabolically compromised states, such as obesity, NAFLD and CVDs [47-49]. The induction of FGF21 is thought to mediate a compensatory response to limit metabolic dysfunction, although the response is inadequate to

counteract the metabolically compromised state. This likely indicates that increasing FGF21 levels or activity is a potent target for combating cardiometabolic diseases. Other hepatokines (e.g. angiopoietin-like proteins and acylcarnitine) and liver-derived bioactive compounds (e.g. BAs) also participate in this inter-organ communication to maintain cardiometabolic balance [46, 50]. Therefore, a better understanding of how liver-secreted factors affect other organ systems during the development of cardiometabolic diseases may lead to new therapeutic targets and tools.

Adipose tissue-derived signaling molecules. Three main types of adipocytes (e.g. white, brown and beige) can be found in the human body. Among these adipose tissue depots, WAT is the most abundant form of adipose tissue. In general, white adipocytes contain a single, large lipid droplet occupying most of the cell, and relatively few mitochondria, and they are specialized for lipid storage and release in response to changing nutritional status. BAT is a highly vascularized organ rich in brown adipocytes, and beige adipocytes mainly reside in subcutaneous WAT. In contrast to white adipocytes, brown and beige adipocytes are characterized by multilocular lipid droplets and high mitochondria density. Brown and beige fat depots are unique to mammals and function to generate heat by metabolizing FAs and glucose, called "adaptive" (non-shivering) thermogenesis, which is associated with high expression of uncoupling protein 1 (UCP1). Upon activation, UCP-1 separates nutrient catabolism from ATP synthesis by dissipating the proton gradient in the inner mitochondria membrane, releasing potential energy in the form of heat [51, 52]. The thermogenic fat, although representing a small part of total adipose tissue, can exert a profound metabolic impact because of their capacity to engage in thermogenesis. When fully active, the thermogenic adipose tissue can upregulate whole-body energy expenditure by over 100% in mice [53, 54]. Although the abundance of these thermogenic fat depots in humans (~0.1% of body mass) is relatively smaller than that in mice (> 0.5% of body mass), it has been shown that human brown fat burns ~20% of the basal caloric need [55]. Many studies have shown the beneficial effects BAT

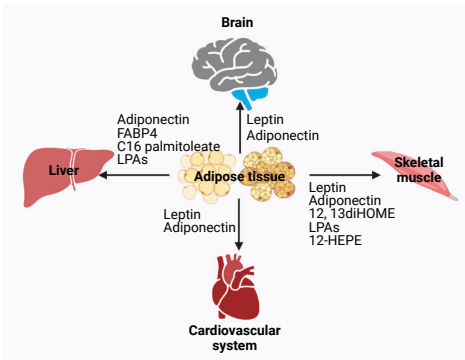**Figure 2-4. Adipose tissue-derived factors**. Some adipocyte-secreted molecules signal to the brain to regulate energy metabolism. Others, including adipokines and lipokines, have diverse effects on their target organs, such as the liver, skeletal muscle and cardiovascular system (selected adipose tissue-associated factors and selected target organs are shown). FABP4, fatty-acid-binding proteins; LPA, lysophosphatidic acid.

activation and WAT browning on not only suppressing body weight gain, but also improving systemic metabolism [16, 56]. In addition to their role in lipid and glucose handling, both white adipocytes and thermogenic brown and beige adipocytes secrete bioactive molecules, which can be peptides (adipokines), lipids (lipokines) and exosomal microRNAs, which have profound impact on adjacent or remote tissues (**Figure 2-4**).

Of those factors, leptin is one of well-established endocrine hormones that acts on its receptor (also known as obesity receptor, Ob-Rs), which is a member of class I cytokine receptor family [56]. The leptin receptor is expressed in various cell types both in the brain and the periphery. In the brain, leptin signaling is important for mediating its metabolic effects (e.g. reduction of food intake), as evidenced by increased body fat and increased plasma levels of glucose and insulin in neuron-specific leptin receptor-deficient mice [57]. Leptin signaling also occurs in skeletal muscle and the heart to increase glucose and fatty acid metabolism [58, 59]. Adiponectin is another adipocyte-secreted hormone with systemic insulin-sensitizing and anti-inflammatory properties. Adiponectin signaling is initiated by binding of adiponectin to either of two associated cell surface receptors, AdipoR1 which is widely expressed or AdipoR2 which is mainly located in the livers [60]. The adiponectin signaling pathway, which can be mediated by the activation of e.g. peroxisome proliferator-activated receptor-α (PPARα), plays a pivotal role in modulating whole-body metabolism. For example, adiponectin has been shown to decrease gluconeogenesis and increase FA oxidation in the liver and skeletal muscle, and to increase glucose uptake in WAT and skeletal muscle [61]. Also, adiponectin acts on the brain to promote weight loss [62], and exerts protective effects on cardiovascular diseases [63]. Other adipokines (e.g. adipsin; FA binding protein 4, FABP; and neuregulin 4), lipokines (e.g. 12-HEPE, palmitoleate and 12,13-dihydroxy-(9Z)-octadecenoic acid) and microRNAs [56] also play important roles in regulating whole-body energy metabolism and influence cardiometabolic health by modulating organ-specific functions [64]. Overall, considering the critical role of adipose tissue and its secreted factors in metabolic health, targeting adipose tissue function and adipose tissue-derived factors may provide novel options in treating cardiometabolic diseases.

Other metabolic organ-derived signaling molecules. Muscle-secreted factors, known as myokines, have also been shown to play a role in cardiometabolic health [65]. Irisin, one of the important myokines, can increase muscle oxidative metabolism and uptake of substrates (e.g. glucose and fatty acids), and reduce hepatic glucose output. Irisin was also shown to induce WAT remodeling by increasing p38 signaling, UCP1 expression, and therefore browning [66]. The heart can also secrete signaling compounds, such as atrial natriuretic peptide (ANP) and B-type natriuretic peptide (BNP). However, a wide range of cardiac hormones remain largely uncharacterized [67]. Inflammatory

mediators released by the immune system are also involved in whole-body metabolism. Tissue resident immune cells can release numerous cytokines, chemokines, and other bioactive molecules, which can trigger pro- or anti-inflammatory signaling to regulate the metabolic function of their targeted organs [68].

3. Inter-organ cross-talk: therapeutic target for cardiometabolic diseases

As aforementioned, inter-organ cross-talk is a gatekeeper for cardiometabolic health. Currently, interventions that regulate cross-talk among metabolic organ systems are being explored as promising strategies to prevent and treat a wide variety of cardiometabolic diseases.

Drugging the gut microbiota. Accumulating evidence demonstrates that the gut microbiota has profound impact on the susceptibility for cardiometabolic diseases of the host. The gut microbiota-host axis contains various layers, including dietary components, gut microbial profiles and meta-organismal pathways, and they are all potential therapeutic targets for cardiometabolic diseases. Therefore, researchers have started to develop gut microbiota-oriented strategies to combat these diseases.

The use of anti-microbial drugs, such as poorly absorbed antibiotics, has been proposed as a strategy for treating cardiometabolic diseases. Several studies indeed reported an association between the development of atherosclerosis and the presence of pathogens *Helicobacter pylori* and *Cytomegalovirus*, but many prospective randomized trials with antibiotics treatment have failed to show clinical benefits [69-71]. A recent research screened more than 1000 commonly prescribed non-antibiotic drugs for their influence on the gut microbiota. Almost 25% of these medications had antibiotic-like effects, as shown by decreasing at least one human commensal gut microbial species [72]. The anti-diabetic drug metformin, for example, improves metabolic dysfunction, including hyperglycemia, in part by decreasing the abundance of *Bacteroides fragilis* in the gut of individuals with T2D [73]. These findings thus indicate that commonly prescribed medications may exert their beneficial effects at least in part through modulating the gut microbiota. Given that drug-microbiota cross-talk varies between metabolic conditions and individuals, investigating the effects of commonly used non-antibiotic therapeutics on the gut microbiota composition and function might reveal therapeutic handles possible use in drug development and personalized medicine.

Beyond classical therapeutics, probiotics have also been proposed to alleviate cardiometabolic diseases. For example, a mouse study showed that *Akkermansia muciniphila* (*A. muciniphila*), a SCFA producer, exerts protective effects on NAFLD and atherosclerosis [74, 75]. Besides, administration of a butyrate producer *Roseburia*

intestinalis (R. intestinalis) can protect against various cardiometabolic diseases, including atherosclerosis [76]. Although probiotic treatment has shown the ability to favorably modulate metabolic phenotypes in several clinical trials, results are highly variable [77]. Moreover, the current probiotic selection is likely driven by abundance-based analyses of the microbial composition. However, the key commensal providing a crucial gain of function may be a low abundant component and is often not easily detected by the current techniques.

Dietary interventions remain the most effective strategy for modulating the gut microbiota-host interactions. This is perhaps best exemplified by production of the compound TMAO from choline-enriched diet (e.g. red meat and eggs) [40-42]. Studies in *Apoe*$^{-/-}$ and *Ldlr*$^{-/-}$ mice have shown that high circulating TMAO levels caused by high dietary choline intake can promote the development of cardiometabolic diseases [39], indicating the potential of TMAO-reducing therapies for the treatment of cardiometabolic diseases. In contrast to dietary choline, dietary fiber has been shown to alleviate cardiometabolic diseases through increasing the production of SCFAs by the gut bacteria [78]. Several studies have determined the impact of a SCFA-enriched diet on cardiometabolic health, and established a direct causal relationship between fermentation of dietary fiber and improvement of cardiometabolic health. For example, mice fed a high-fat diet (HFD) enriched in butyrate showed decreased food consumption and increased energy expenditure [79-81]. Likewise, in obese and diabetic mice, oral administration of acetate reduced weight gain and improved glucose tolerance [82]. In humans, propionate administration reduced obesity, lowered blood glucose levels and increased insulin release during an oral glucose tolerance test [83]. Thus, dietary interventions that directly or indirectly increase intestinal levels of SCFAs may be an efficient strategy to combat cardiometabolic diseases. In addition, given that the SCFAs and TMAO have opposite effects on cardiometabolic diseases, treatment with SCFAs may have the potential to protect against TMAO-induced cardiometabolic disturbance.

Activating brown fat. It has been speculated that decreased cold-induced thermogenesis, for instance due to advances in home insulation and heating, contributes to increased prevalence of obesity-related cardiometabolic diseases [84]. Indeed, in people with dyslipidemia, long-term BAT activation by cold exposure has been shown to lower plasma lipids, such as TGs and atherogenic cholesterol [85]. In fact, our research group has shown that BAT activation in *APOE*3-Leiden.CETP* mice, a well-established model with human-like lipoprotein metabolism, lowers plasma lipid levels and reduces obesity, hepatic steatosis and atherosclerosis [86]. These findings indicate BAT as a potential therapeutic target for cardiometabolic diseases.

Previous studies have reported that cold exposure to 17℃ for 2 hours per day over 6 weeks induces the detectability of BAT by [¹⁸F]fluorodeoxyglucose (FDG) PET-CT scan in human adults in whom BAT was undetectable at baseline. The increased BAT volume after cold exposure was associated with reduced fat mass [87]. However, the long-term cold exposure was shown to be associated with an increased FA release from WAT in overweight/obese men [88], which could induce excess ectopic fat deposition and thus could be detrimental to cardiometabolic health. As such, although using cold exposure to recruit and activate BAT has been provided valuable insight into cardiometabolic benefits, concerns related to long-term tolerability and potential adverse effects possibly limit its use as a therapy for obesity and its related diseases.

In addition to cold exposure, researchers have been working on searching for potential targets for BAT activation in humans. For example, β3-adrenergic receptor (β3-AR) agonists (e.g. mirabegron), which are potent activators of BAT thermogenesis in mice, have been tested in humans for BAT thermogenesis. However, whether β3-AR activation stimulate human BAT thermogenesis remains controversy [89]. A study reported that β3-ARs in human brown adipocytes are required to regulate the lipolytic and thermogenic cellular processes, and that β3-AR agonists might have cardiometabolic benefits in people with obesity [90]. Another study, however, proposed that β2-adrenergic receptor (β3-AR) rather than β3-AR is the primary target for pharmacological activation of human brown adipocytes [91]. In addition to β-adrenergic receptors (β-ARs), researchers have also uncovered an alternative pathway of GPCR-mediated adipose thermogenesis via the constitutively active receptor GPR3 in mice [92]. However, the potential of targeting β-ARs and GPR3 signaling in treating cardiometabolic diseases in humans remains further investigation.

Aside from catecholamines such as norepinephrine, other hormones can act on various adipose tissue depots, including BAT, independent of adrenergic receptors. For instance, liver-derived FGF21 can act on its receptors expressed in adipose tissue to increase expression of thermogenic genes, thereby enhancing the heat-producing capacity of BAT and promoting browning of WAT [93]. In line with this, FGF21 has been shown to promote weight loss and lower systemic lipid and glucose levels in obese mice and non-human primates [93, 94]. Given that hepatokine FGF21 plays pivotal roles in mediating the cross-talk between the liver and adipose tissue and in maintaining cardiometabolic health, extensive efforts have been made with the use of recombinant FGF21 or FGF21 variants as potential therapy for obesity and associated cardiometabolic diseases [95]. While analogues FGF21 are in clinical development for obesity and T2D [48], the therapeutic potential of FGF21 in the treatment of NASH and atherosclerotic CVD remains unclear.

1

OUTLINE OF THIS THESIS

Chapter 1 provided an introduction on inter-organ cross-talk as a gatekeeper for cardiometabolic health. It was explained that metabolic organs can interact to regulate whole-body metabolism through signaling molecules, such as peptide/protein hormones, bioactive lipids and functional small molecules. These molecules allow various metabolic tissues and organs to work together to absorb, store, sense and use energy, and to maintain energy balance of the body. However, aberrant production of these signaling molecules is associated with energy imbalance and contributes to the development of cardiometabolic diseases, indicating inter-organ crosstalk as a therapeutic target for cardiometabolic diseases. In this thesis, by using dietary and pharmacological interventions, I explored the therapeutic potential of targeting inter-organ communication in cardiometabolic diseases, aimed to reveal novel and effective inter-organ cross-talk-directed therapeutic strategies for these diseases.

Studies in *Apoe*^{-/-} and *Ldlr*^{-/-} mice have linked dietary choline to the pathogenesis of cardiometabolic diseases, related to production of TMAO, which could theoretically be counteracted by the anti-inflammatory and antiatherogenic properties of butyrate. Therefore, in **Chapter 2**, we aimed to investigate whether butyrate can alleviate choline-induced atherosclerosis. To this end, we used *APOE*3-Leiden.CETP* mice, a well-established atherosclerosis-prone model with human-like lipoprotein metabolism, and fed these mice with an atherogenic diet alone or supplemented with choline, butyrate or their combination. In addtion to its atherogenic effects, dietary choline or its metabolite TMAO has also been reported to promote adiposity in diet-induced (DIO) obese and *ob/ob* mice. However, several clinical trials have reported anti-obesity effects of high dietary choline intake. Therefore, in **Chapter 3**, we aimed to assess the effects of dietary choline on adiposity in humanized *APOE*3-Leiden.CETP* mice exposed to a Western-type diet, and to elucidate underlying mechanisms.

Narcolepsy is a clinical condition of severely disturbed sleep that is characterized by an increase in body weight after disease onset, frequently leading to obesity. Clinical studies have reported that the narcolepsy drug γ-hydroxybutyric acid (GHB), a SCFA that is structurally similar to butyrate, promotes weight loss. Due to its central effects and its misuse-associated adverse effects, GHB is unlikely to be prescribed as anti-obesity drug. Nonetheless, elucidating the mechanisms by which GHB reduces body weight may reveal therapeutic handles for the development of effective body weight control medications. Therefore, in **Chapter 4**, we aimed to to unveil the metabolic mechanisms underlying GHB-induced weight reduction in obesity. Furthermore, we aimed to examine whether GHB administration also confers weight loss during

the development of obesity. To this end, C57BL/6J mice that were lean and fed HFD to induce obesity, or that were obese due to previous HFD feeding, were orally administered with GHB.

Besides the SCFAs butyrate and GHB, FGF21 is another promising therapeutic tool for treatment of cardiometabolic diseases. Currently, analogues of FGF21 are in clinical development for treatment of obesity and type 2 diabetes. Although their glucose-lowering and insulin-sensitizing effects have been largely unraveled, the mechanisms by which they alleviate liver injury have only been scarcely addressed. In **Chapter 5**, we thus aimed to unveil the mechanisms underlying FGF21-mediated improvement of NASH, in particular with respect to steatohepatitis and fibrogenesis. To this end, liver-specific FGF21 overexpression was achieved in *APOE*3-Leiden.CETP* mice, followed by administration of a high-fat high-cholesterol diet (HFCD). Finally, in **Chapter 6**, we investigated the importance of FGF21 in other aspects of cardiometabolic health, particularly in lipoprotein metabolism in relation to atherogenesis, by administration of long-acting recombinant FGF21 to *APOE*3-Leiden.CETP* mice fed an atherogenic diet.

In the last part of this thesis, **Chapter 7**, the findings of these experimental studies and their implications for future research will be discussed.

1

REFERENCES

1. Eckel, R.H., S.M. Grundy, and P.Z. Zimmet, *The metabolic syndrome.* The Lancet, 2005. **365**(9468): p. 1415-1428.

2. Stefan, N., H.U. Haring, and K. Cusi, *Non-alcoholic fatty liver disease: causes, diagnosis, cardiometabolic consequences, and treatment strategies.* Lancet Diabetes Endocrinol, 2019. **7**(4): p. 313-324.

3. Leong, D.P., et al., *Reducing the Global Burden of Cardiovascular Disease, Part 2 Prevention and Treatment of Cardiovascular Disease.* Circulation Research, 2017. **121**(6): p. 695-710.

4. Lonardo, A., et al., *Hypertension, diabetes, atherosclerosis and NASH: Cause or consequence?* J Hepatol, 2018. **68**(2): p. 335-352.

5. Salvi, P., et al., *Increased arterial stiffness in nonalcoholic fatty liver disease: the Cardio-GOOSE study.* J Hypertens, 2010. **28**(8): p. 1699-707.

6. Kozakova, M., et al., *Fatty liver index, gamma-glutamyltransferase, and early carotid plaques.* Hepatology, 2012. **55**(5): p. 1406-15.

7. Stepanova, M. and Z.M. Younossi, *Independent Association Between Nonalcoholic Fatty Liver Disease and Cardiovascular Disease in the US Population.* Clinical Gastroenterology and Hepatology, 2012. **10**(6): p. 646-650.

8. Ekstedt, M., et al., *Fibrosis Stage Is the Strongest Predictor for Disease-Specific Mortality in NAFLD After Up to 33 Years of Follow-Up.* Hepatology, 2015. **61**(5): p. 1547-1554.

9. Angulo, P., et al., *Liver Fibrosis, but No Other Histologic Features, Is Associated With Long-term Outcomes of Patients With Nonalcoholic Fatty Liver Disease.* Gastroenterology, 2015. **149**(2): p. 389-+.

10. Taylor, R.S., et al., *Association Between Fibrosis Stage and Outcomes of Patients With Nonalcoholic Fatty Liver Disease: A Systematic Review and Meta -Analysis.* Gastroenterology, 2020. **158**(6): p. 1611-+.

11. Friedman, S.L., et al., *Mechanisms of NAFLD development and therapeutic strategies.* Nat Med, 2018. **24**(7): p. 908-922.

12. Boren, J., et al., *Low-density lipoproteins cause atherosclerotic cardiovascular disease: pathophysiological, genetic, and therapeutic insights: a consensus statement from the European Atherosclerosis Society Consensus Panel.* Eur Heart J, 2020. **41**(24): p. 2313-2330.

13. Benjamin, E.J., et al., *Heart Disease and Stroke Statistics-2018 Update: A Report From the American Heart Association.* Circulation, 2018. **137**(12): p. e67-e492.

14. Reiner, Z., *Resistance and intolerance to statins.* Nutr Metab Cardiovasc Dis, 2014. **24**(10): p. 1057-66.

15. Eckel, R.H., *Lipoprotein lipase. A multifunctional enzyme relevant to common metabolic diseases.* N Engl J Med, 1989. **320**(16): p. 1060-8.

16. Sakers, A., et al., *Adipose-tissue plasticity in health and disease.* Cell, 2022. **185**(3): p. 419-446.

17. Peverill, W., L.W. Powell, and R. Skoien, *Evolving concepts in the pathogenesis of NASH: beyond steatosis and inflammation.* Int J Mol Sci, 2014. **15**(5): p. 8591-638.

18. Alonso, C., et al., *Metabolomic Identification of Subtypes of Nonalcoholic Steatohepatitis.* Gastroenterology, 2017. **152**(6): p. 1449-1461 e7.

19. Libby, P., et al., *Atherosclerosis.* Nat Rev Dis Primers, 2019. **5**(1): p. 56.

20. Monteiro, M.P. and R.L. Batterham, *The Importance of the Gastrointestinal Tract in Controlling Food Intake and Regulating Energy Balance.* Gastroenterology, 2017. **152**(7): p. 1707-1717 e2.

21.   Liddle, R.A., *Neuropods.* Cell Mol Gastroenterol Hepatol, 2019. **7**(4): p. 739-747.

22.   Canfora, E.E., J.W. Jocken, and E.E. Blaak, *Short-chain fatty acids in control of body weight and insulin sensitivity.* Nat Rev Endocrinol, 2015. **11**(10): p. 577-91.

23.   Calanna, S., et al., *Secretion of glucose-dependent insulinotropic polypeptide in patients with type 2 diabetes: systematic review and meta-analysis of clinical studies.* Diabetes Care, 2013. **36**(10): p. 3346-52.

24.   Campbell, J.E. and D.J. Drucker, *Pharmacology, physiology, and mechanisms of incretin hormone action.* Cell Metab, 2013. **17**(6): p. 819-837.

25.   Drucker, D.J., *The biology of incretin hormones.* Cell Metab, 2006. **3**(3): p. 153-65.

26.   Boer, G.A., D.L. Hay, and A. Tups, *Obesity pharmacotherapy: incretin action in the central nervous system.* Trends Pharmacol Sci, 2022.

27.   Yabut, J.M., et al., *Emerging Roles for Serotonin in Regulating Metabolism: New Implications for an Ancient Molecule.* Endocr Rev, 2019. **40**(4): p. 1092-1107.

28.   Cummings, J.H., et al., *Short chain fatty acids in human large intestine, portal, hepatic and venous blood.* Gut, 1987. **28**(10): p. 1221-7.

29.   Schroeder, B.O. and F. Backhed, *Signals from the gut microbiota to distant organs in physiology and disease.* Nat Med, 2016. **22**(10): p. 1079-1089.

30.   Tolhurst, G., et al., *Short-chain fatty acids stimulate glucagon-like peptide-1 secretion via the G-protein-coupled receptor FFAR2.* Diabetes, 2012. **61**(2): p. 364-71.

31.   Frost, G., et al., *The short-chain fatty acid acetate reduces appetite via a central homeostatic mechanism.* Nat Commun, 2014. **5**: p. 3611.

32.   De Vadder, F., et al., *Microbiota-generated metabolites promote metabolic benefits via gut-brain neural circuits.* Cell, 2014. **156**(1-2): p. 84-96.

33.   Collins, S.L., et al., *Bile acids and the gut microbiota: metabolic interactions and impacts on disease.* Nat Rev Microbiol, 2022.

34.   Midtvedt, T., *Microbial bile acid transformation.* Am J Clin Nutr, 1974. **27**(11): p. 1341-7.

35.   Swann, J.R., et al., *Systemic gut microbial modulation of bile acid metabolism in host tissue compartments.* Proc Natl Acad Sci U S A, 2011. **108 Suppl 1**: p. 4523-30.

36.   Sayin, S.I., et al., *Gut microbiota regulates bile acid metabolism by reducing the levels of tauro-beta-muricholic acid, a naturally occurring FXR antagonist.* Cell Metab, 2013. **17**(2): p. 225-35.

37.   Li, T., et al., *Defective Branched-Chain Amino Acid Catabolism Disrupts Glucose Metabolism and Sensitizes the Heart to Ischemia-Reperfusion Injury.* Cell Metab, 2017. **25**(2): p. 374-385.

38.   Qiao, S., et al., *Gut Parabacteroides merdae protects against cardiovascular damage by enhancing branched-chain amino acid catabolism.* Nat Metab, 2022. **4**(10): p. 1271-1286.

39.   Agus, A., K. Clement, and H. Sokol, *Gut microbiota-derived metabolites as central regulators in metabolic disorders.* Gut, 2021. **70**(6): p. 1174-1182.

40.   Koeth, R.A., et al., *Intestinal microbiota metabolism of L-carnitine, a nutrient in red meat, promotes atherosclerosis.* Nat Med, 2013. **19**(5): p. 576-85.

41.   Zhu, W., et al., *Gut Microbial Metabolite TMAO Enhances Platelet Hyperreactivity and Thrombosis Risk.* Cell, 2016. **165**(1): p. 111-124.

42.   Wang, Z., et al., *Gut flora metabolism of phosphatidylcholine promotes cardiovascular disease.* Nature, 2011. **472**(7341): p. 57-63.

1

43. Tang, W.H.W. and S.L. Hazen, *The contributory role of gut microbiota in cardiovascular disease.* Journal of Clinical Investigation, 2014. **124**(10): p. 4204-4211.

44. Cani, P.D., et al., *Metabolic endotoxemia initiates obesity and insulin resistance.* Diabetes, 2007. **56**(7): p. 1761-72.

45. Ferro, D., et al., *New Insights into the Pathogenesis of Non-Alcoholic Fatty Liver Disease: Gut-Derived Lipopolysaccharides and Oxidative Stress.* Nutrients, 2020. **12**(9).

46. Stefan, N. and H.U. Haring, *The role of hepatokines in metabolism.* Nat Rev Endocrinol, 2013. **9**(3): p. 144-52.

47. Fisher, F.M. and E. Maratos-Flier, *Understanding the Physiology of FGF21.* Annu Rev Physiol, 2016. **78**: p. 223-41.

48. Geng, L., K.S.L. Lam, and A. Xu, *The therapeutic potential of FGF21 in metabolic diseases: from bench to clinic.* Nat Rev Endocrinol, 2020. **16**(11): p. 654-667.

49. Zarei, M., et al., *Targeting FGF21 for the Treatment of Nonalcoholic Steatohepatitis.* Trends Pharmacol Sci, 2020. **41**(3): p. 199-208.

50. Cao, Y., et al., *Liver-heart cross-talk mediated by coagulation factor XI protects against heart failure.* Science, 2022. **377**(6613): p. 1399-1406.

51. Garlid, K.D., M. Jaburek, and P. Jezek, *The mechanism of proton transport mediated by mitochondrial uncoupling proteins.* FEBS Lett, 1998. **438**(1-2): p. 10-4.

52. Nedergaard, J., et al., *UCP1: the only protein able to mediate adaptive non-shivering thermogenesis and metabolic inefficiency.* Biochim Biophys Acta, 2001. **1504**(1): p. 82-106.

53. Angueira, A.R., et al., *Early B Cell Factor Activity Controls Developmental and Adaptive Thermogenic Gene Programming in Adipocytes.* Cell Rep, 2020. **30**(9): p. 2869-2878 e4.

54. Ouellet, V., et al., *Brown adipose tissue oxidative metabolism contributes to energy expenditure during acute cold exposure in humans.* J Clin Invest, 2012. **122**(2): p. 545-52.

55. Elattar, S. and A. Satyanarayana, *Can Brown Fat Win the Battle Against White Fat?* J Cell Physiol, 2015. **230**(10): p. 2311-7.

56. Scheja, L. and J. Heeren, *The endocrine function of adipose tissues in health and cardiometabolic disease.* Nat Rev Endocrinol, 2019. **15**(9): p. 507-524.

57. Cohen, P., et al., *Selective deletion of leptin receptor in neurons leads to obesity.* J Clin Invest, 2001. **108**(8): p. 1113-21.

58. Ceddia, R.B., W.N. William, and R. Curi, *The response of skeletal muscle to leptin.* Frontiers in Bioscience-Landmark, 2001. **6**: p. D90-D97.

59. Poetsch, M.S., A. Strano, and K. Guan, *Role of Leptin in Cardiovascular Diseases.* Front Endocrinol (Lausanne), 2020. **11**: p. 354.

60. Yamauchi, T. and T. Kadowaki, *Adiponectin Receptor as a Key Player in Healthy Longevity and Obesity-Related Diseases.* Cell Metabolism, 2013. **17**(2): p. 185-196.

61. Fang, H. and R.L. Judd, *Adiponectin Regulation and Function.* Compr Physiol, 2018. **8**(3): p. 1031-1063.

62. Qi, Y., et al., *Adiponectin acts in the brain to decrease body weight.* Nat Med, 2004. **10**(5): p. 524-9.

63. den Ruijter, H.M., G. Pasterkamp, and S.C. de Jager, *Adiponectin regulation in cardiovascular disease: is diseased fat showing its true color?* Arterioscler Thromb Vasc Biol, 2014. **34**(10): p. 2180-1.

64. Fasshauer, M. and M. Blüher, *Adipokines in health and disease.* Trends in Pharmacological Sciences, 2015. **36**(7): p. 461-470.

65. Severinsen, M.C.K. and B.K. Pedersen, *Muscle-Organ Crosstalk: The Emerging Roles of Myokines.* Endocr Rev, 2020. **41**(4).

66. Arhire, L.I., L. Mihalache, and M. Covasa, *Irisin: A Hope in Understanding and Managing Obesity and Metabolic Syndrome.* Front Endocrinol (Lausanne), 2019. **10**: p. 524.

67. Severinsen, M.C.K. and B.K. Pedersen, *Muscle-Organ Crosstalk: The Emerging Roles of Myokines.* Endocr Rev, 2020. **41**(4): p. 594-609.

68. Clerico, A., et al., *Thirty years of the heart as an endocrine organ: physiological role and clinical utility of cardiac natriuretic hormones.* American Journal of Physiology-Heart and Circulatory Physiology, 2011. **301**(1): p. H12-H20.

69. Zmora, N., et al., *The Role of the Immune System in Metabolic Health and Disease.* Cell Metab, 2017. **25**(3): p. 506-521.

70. Epstein, S.E., et al., *The role of infection in restenosis and atherosclerosis: focus on cytomegalovirus.* Lancet, 1996. **348 Suppl 1**: p. s13-7.

71. Patel, P., et al., *Association of Helicobacter pylori and Chlamydia pneumoniae infections with coronary heart disease and cardiovascular risk factors.* BMJ, 1995. **311**(7007): p. 711-4.

72. Saikku, P., et al., *Serological evidence of an association of a novel Chlamydia, TWAR, with chronic coronary heart disease and acute myocardial infarction.* Lancet, 1988. **2**(8618): p. 983-6.

73. Maier, L., et al., *Extensive impact of non-antibiotic drugs on human gut bacteria.* Nature, 2018. **555**(7698): p. 623-628.

74. Wu, H., et al., *Metformin alters the gut microbiome of individuals with treatment-naive type 2 diabetes, contributing to the therapeutic effects of the drug.* Nat Med, 2017. **23**(7): p. 850-858.

75. Kim, S., et al., *Akkermansia muciniphila Prevents Fatty Liver Disease, Decreases Serum Triglycerides, and Maintains Gut Homeostasis.* Appl Environ Microbiol, 2020. **86**(7).

76. He, X., et al., *Akkermansia muciniphila Alters Gut Microbiota and Immune System to Improve Cardiovascular Diseases in Murine Model.* Front Microbiol, 2022. **13**: p. 906920.

77. Kasahara, K., et al., *Interactions between Roseburia intestinalis and diet modulate atherogenesis in a murine model.* Nature Microbiology, 2018. **3**(12): p. 1461-1471.

78. Witkowski, M., T.L. Weeks, and S.L. Hazen, *Gut Microbiota and Cardiovascular Disease.* Circ Res, 2020. **127**(4): p. 553-570.

79. Nogal, A., A.M. Valdes, and C. Menni, *The role of short-chain fatty acids in the interplay between gut microbiota and diet in cardio-metabolic health.* Gut Microbes, 2021. **13**(1).

80. Li, Z., et al., *Butyrate reduces appetite and activates brown adipose tissue via the gut-brain neural circuit.* Gut, 2018. **67**(7): p. 1269-1279.

81. Wang, D., et al., *LSD1 mediates microbial metabolite butyrate-induced thermogenesis in brown and white adipose tissue.* Metabolism, 2020. **102**: p. 154011.

82. Gao, Z., et al., *Butyrate improves insulin sensitivity and increases energy expenditure in mice.* Diabetes, 2009. **58**(7): p. 1509-17.

83. Hernandez, M.A.G., et al., *The Short-Chain Fatty Acid Acetate in Body Weight Control and Insulin Sensitivity.* Nutrients, 2019. **11**(8).

84. Chambers, E.S., et al., *Effects of targeted delivery of propionate to the human colon on appetite regulation, body weight maintenance and adiposity in overweight adults.* Gut, 2015. **64**(11): p. 1744-54.

85. Keith, S.W., et al., *Putative contributors to the secular increase in obesity: exploring the roads less traveled.* Int J Obes (Lond), 2006. **30**(11): p. 1585-94.

86. Hoeke, G., et al., *Role of Brown Fat in Lipoprotein Metabolism and Atherosclerosis.* Circ Res, 2016. **118**(1): p. 173-82.

87. Berbee, J.F., et al., *Brown fat activation reduces hypercholesterolaemia and protects from atherosclerosis development.* Nat Commun, 2015. **6**: p. 6356.

88. Cheng, L., et al., *Brown and beige adipose tissue: a novel therapeutic strategy for obesity and type 2 diabetes mellitus.* Adipocyte, 2021. **10**(1): p. 48-65.

89. Chondronikola, M., et al., *Brown Adipose Tissue Activation Is Linked to Distinct Systemic Effects on Lipid Metabolism in Humans.* Cell Metabolism, 2016. **23**(6): p. 1200-1206.

90. Larsen, T.M., et al., *Effect of a 28-d treatment with L-796568, a novel beta(3)-adrenergic receptor agonist, on energy expenditure and body composition in obese men.* Am J Clin Nutr, 2002. **76**(4): p. 780-8.

91. Cero, C., et al., *beta3-Adrenergic receptors regulate human brown/beige adipocyte lipolysis and thermogenesis.* JCI Insight, 2021. **6**(11).

92. Blondin, D.P., et al., *Human Brown Adipocyte Thermogenesis Is Driven by beta2-AR Stimulation.* Cell Metab, 2020. **32**(2): p. 287-300 e7.

93. Sveidahl Johansen, O., et al., *Lipolysis drives expression of the constitutively active receptor GPR3 to induce adipose thermogenesis.* Cell, 2021. **184**(13): p. 3502-3518 e33.

94. Lewis, J.E., et al., *Going Back to the Biology of FGF21: New Insights.* Trends Endocrinol Metab, 2019. **30**(8): p. 491-504.

95. Andersen, B., et al., *FGF21 decreases body weight without reducing food intake or bone mineral density in high-fat fed obese rhesus macaque monkeys.* Int J Obes (Lond), 2018. **42**(6): p. 1151-1160.

96. Jin, L., et al., *Fibroblast Growth Factor-Based Pharmacotherapies for the Treatment of Obesity-Related Metabolic Complications.* Annu Rev Pharmacol Toxicol, 2022.

2

Choline and butyrate beneficially modulate the gut microbiome without affecting atherosclerosis in *APOE*3-Leiden.CETP* mice

Cong Liu[1,2], Zhuang Li[1,2], Zikuan Song[1,2], Xiayue Fan[3], Hua Shao[3], Milena Schönke[1,2], Mariëtte R. Boon[1,2], Patrick C.N. Rensen[1,2,3], Yanan Wang[1,2,3]

[1] Department of Medicine, Division of Endocrinology, Leiden University Medical Center, Leiden, The Netherlands.
[2] Einthoven Laboratory for Experimental Vascular Medicine, Leiden University Medical Center, Leiden, The Netherlands.
[3] Med-X institute, Center for Immunological and Metabolic Diseases, and Department of Endocrinology, First Affiliated Hospital of Xi'an Jiaotong University, Xi'an Jiaotong University, Xi'an, China.

ABSTRACT
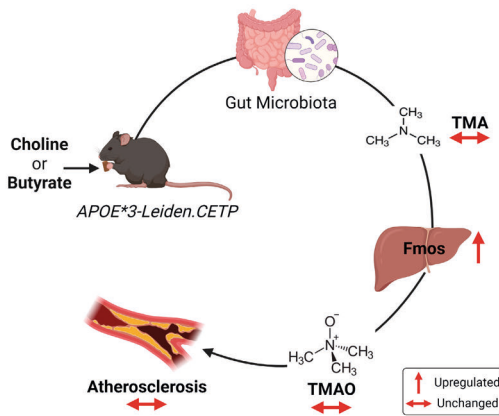
Choline has been shown to exert atherogenic effects in *Apoe⁻/⁻* and *Ldlr⁻/⁻* mice, related to its conversion by gut bacteria into trimethylamine (TMA) that is converted by the liver into the proinflammatory metabolite trimethylamine-N-oxide (TMAO). Since butyrate beneficially modulates the gut microbiota and has anti-inflammatory and antiatherogenic properties, the aim of the present study was to investigate whether butyrate can alleviate choline-induced atherosclerosis. To this end, we used *APOE*3-Leiden.CETP* mice, a well-established atherosclerosis-prone model with human-like lipoprotein metabolism. Female *APOE*3-Leiden.CETP* mice were fed an atherogenic diet alone or supplemented with choline, butyrate or their combination for 16 weeks. Interestingly, choline protected against fat mass gain, increased the abundance of anti-inflammatory gut microbes, and increased the expression of gut microbial genes involved in TMA and TMAO degradation. Butyrate similarly attenuated fat mass gain and beneficially modulated the gut microbiome, as shown by increased abundance of anti-inflammatory and short chain fatty acid-producing microbes, and inhibited expression of gut microbial genes involved in lipopolysaccharide synthesis. Both choline and butyrate upregulated hepatic expression of flavin-containing monooxygenases, and their combination resulted in highest circulating TMAO levels. Nonetheless, choline, butyrate and their combination did not influence atherosclerosis development, and TMAO levels were not associated with atherosclerotic lesion size. While choline and butyrate have been reported to oppositely modulate atherosclerosis development in *Apoe⁻/⁻* and *Ldlr⁻/⁻* mice as related to changes in the gut microbiota, both dietary constituents did not affect atherosclerosis development while beneficially modulating the gut microbiome in *APOE*3-Leiden.CETP* mice.

INTRODUCTION

Atherosclerosis, the main underlying cause of cardiovascular diseases (CVD), is a chronic disease arising from an imbalanced cholesterol metabolism and a maladaptive immune response [1]. Hypercholesterolemia induces the retention of apolipoprotein (Apo) B-containing cholesterol-rich lipoproteins in the arterial intima, which triggers infiltration of circulating monocytes into the intima, induces cholesterol-laden foam cell formation and accumulation, and subsequently initiates and aggravates atherosclerosis [1]. Therefore, cholesterol-lowering therapy potently reduces morbidity and mortality of atherosclerotic CVD (asCVD) [2]. Yet, a significant burden of asCVD remains, at least partly due to the residual inflammatory risk [3]. Therefore, there is an urgent need to search for additional therapeutic targets which govern atherogenesis, particularly those regulating both cholesterol metabolism and inflammation.

Several lines of evidence have linked the gut microbiota to atherogenesis [4, 5]. The gut microbiota is mainly shaped by dietary factors. Bacteria in the gut can metabolize complex dietary components to generate various functional small-molecule metabolites [4, 5]. Trimethylamine N-oxide (TMAO) is a gut-derived metabolite that has been described to aggravate atherosclerosis in $Apoe^{-/-}$ and $Ldlr^{-/-}$ mice [6, 7]. Gut microbiota generate TMAO from dietary choline via a two-step meta-organismal pathway to first produce trimethylamine (TMA) that is delivered via the portal vein to the liver where it can be rapidly oxidized into TMAO by flavin monooxygenases (FMOs). TMAO aggravates atherosclerosis via various mechanisms, such as promoting foam cell formation and activation of the inflammatory response [6, 8]. Hence, TMAO-lowering interventions may have therapeutic potential to reduce asCVD risk. Interestingly, butyrate, a short chain fatty acid (SCFA), has been shown to protect against atherosclerosis in $Apoe^{-/-}$ and $Ldlr^{-/-}$ mice [9-12]. This is in part mediated through its action on the gut microbiota, since butyrate suppresses the overgrowth of pathogenic gut microbes, inhibits the synthesis of endotoxins, and prevents bacterial translocation. As a result, butyrate alleviates systemic inflammation, thereby halting atherosclerosis progression [9].

Based on the hypothesis that butyrate may be able to protect against dietary choline-induced atherosclerosis development, the aim of the present study was to examine the effects of choline, butyrate and their combination on atherosclerosis in *APOE*3-Leiden.CETP* mice, a well-established translational model for human-like lipoprotein metabolism. In contrast to our expectations, we demonstrate that both choline and butyrate beneficially modulate the gut microbiome without affecting atherosclerosis development, and TMAO levels were not associated with atherosclerotic lesion size.

MATERIALS AND METHODS

For details of animals and antibodies used, please see the Major Resources Table in the **Supplementary Materials**.

Mice

Female *APOE*3-Leiden.CETP* mice were generated as previously described [13]. Mice at the age of 8-12 weeks were housed under standard conditions (22℃; 12/12-hour light/dark cycle) with *ad libitum* access to water and a cholesterol-containing Western-type diet (WTD; 0.15% cholesterol and 16% fat; ssniff, Soest, Germany). All mice were acclimatized to housing and WTD for 3 weeks prior to the dietary intervention. Then, based on 4-hour fasted plasma lipid levels, body weight as well as body composition, these mice were randomized to 4 treatment groups using RandoMice [14] (n=17 per group) receiving either WTD (ctrl group), WTD+choline (1.2% w/w, according to previous studies [6, 15]; choline group), WTD+butyrate (5% w/w, according to previous studies [16, 17]; butyrate group) or WTD+butyrate+choline (1.2% w/w choline and 5% w/w butyrate; butyrate+choline group) for 16 weeks according to a well-established protocol in our group [18-20]. The sample size was calculated based on the average atherosclerotic lesion area of $1×10^5$ µm^2 in the ctrl group with a standard deviation lesion size of $0.3×10^5$ µm^2. We considered a difference in plaque size of 30% to be biologically relevant. To achieve the differences with α=5% and a power of 80%, 17 animals per group were therefore needed. Mice were group housed (4-5 per cage) during the experimental period to avoid stress caused by single housing. All animal experiments were performed in accordance with the Institute for Laboratory Animal Research Guide for the Care and Use of Laboratory Animals, and were approved by the National Committee for Animal Experiments and by the Ethics Committee on Animal Care (Protocol No. AVD1160020172927) and Experimentation of the Leiden University Medical Center (Protocol No. PE.18.063.006). All animal procedures were conform the guidelines from Directive 2010/63/EU of the European Parliament on the protection of animal used for scientific purposes.

Body weight and body composition

Body weight was measured weekly with a scale, and body composition of conscious mice was measured biweekly using an EchoMRI-100 analyzer (EchoMRI, Houston, TX, USA).

Plasma lipid profiles and choline metabolites

Every 4 weeks, after 4 hours of fasting (9:00-13:00), tail vein blood was collected into paraoxon-coated glass capillaries. These capillaries were placed on ice and centrifuged, and plasma was collected and stored at -20℃. Plasma total cholesterol (TC) and

triglyceride (TG) levels were determined (n=17 per group) using commercial enzymatic kits from Roche Diagnostics (Mannheim, Germany). Plasma high density lipoprotein cholesterol (HDL-C) and non-HDL-C levels (n=17 per group) were determined as previously described [19]. At week 16, plasma choline, betaine, TMA and TMAO levels were quantified (n=10 per group) using liquid chromatography-tandem mass spectrometry as described under Expanded Methods in the **Supplementary Materials**.

Gene expression

Total RNA was extracted from snap-frozen tissues using the Tripure RNA isolation reagent (Roche, Mijdrecht, The Netherlands), according to the manufacturer's instructions. Complementary DNA for quantitative reverse transcriptase-PCR was generated as previously described [18]. The expression of mRNA was normalized to *Actb* and *Rplp0* mRNA levels and expressed as fold change compared with the ctrl group. The primer sequences are listed in the **Supplementary Materials**.

Genomic DNA extraction and metagenomic sequencing

At week 16, cecal contents were collected, and genomic bacterial DNA was isolated with the fast DNA stool mini kit (QIAamp, Germany) following the manufacturer's instructions. Then, these DNA samples were used for determination of gut microbial gene expression via qPCR as well as metagenomics sequencing. Sequencing data was processed as described under Expanded Methods in the **Supplementary Materials**.

Atherosclerotic plaque characterization and quantification

Hearts were collected and fixated in phosphate-buffered 4% formaldehyde, embedded in paraffin after dehydration in 70-100% ethanol and cross-sectioned (5 μm) perpendicular to the axis of the aorta throughout the aortic root area, starting from the appearance of open aortic valve leaflets. Per mouse, 4 sections with 50 μm intervals were used for atherosclerosis measurements. Sections were stained with haematoxylin-phloxine-saffron for histological analysis. Lesions were categorized by severity according to the guidelines of the American Heart Association adapted for mice [21]. Sirius Red staining was used to quantify the collagen area. Monoclonal mouse antibody M0851 (1:800; Dako, Heverlee, The Netherlands) against smooth muscle cell actin was used to quantify the smooth muscle cell area. Rat monoclonal anti-mouse MAC-3 antibody (1:1000; BD Pharmingen, San Diego, CA, USA) was used to quantify the macrophage area. Immunostainings were amplified using Vector Laboratories Elite ABC kit (Vector Laboratories Inc., Burlingame, CA, USA) and the immune-peroxidase complex was visualized with Nova Red (Vector Laboratories Inc., Burlingame, CA, USA). Lesion area and composition were analyzed using Image J software. The stability index was calculated by dividing the relative collagen and smooth muscle cell area by the relative area of macrophages within the same lesion.

Statistical analyses

Statistical analyses among these 4 groups were assessed using One-way ANOVA followed by a Fisher's LSD post hoc test, unless indicated otherwise. The square root of the lesion area was taken to linearize the relationship with the plasma TC, non-HDL-C, HDL-C and TG exposures and plasma TMAO levels (at 16 week). To assess significant correlations between atherosclerotic lesion size and plasma lipids and TMAO, univariate regression analyses were performed. Then, to predict the contribution of these plasma parameters to the atherosclerotic lesion size, multiple regression analysis was performed. Data are presented as mean±SEM, and a *P* value less than 0.05 is considered statistically significant. All statistical analyses were performed with GraphPad Prism 9 (GraphPad Software Inc., California, CA, USA) except for univariate and multiple regression analyses which were performed with SPSS 20.0 (SPSS, Chicago, IL USA) for Windows and metagenomic data analysis using R packages.

RESULTS

Choline and butyrate attenuate WTD-induced fat mass gain in *APOE*3-Leiden.CETP* mice

To address how choline and butyrate affect atherosclerosis in a mouse model for human-like lipoprotein metabolism, we fed female *APOE*3-Leiden.CETP* mice a cholesterol-containing WTD alone or supplemented with choline, butyrate or a combination of
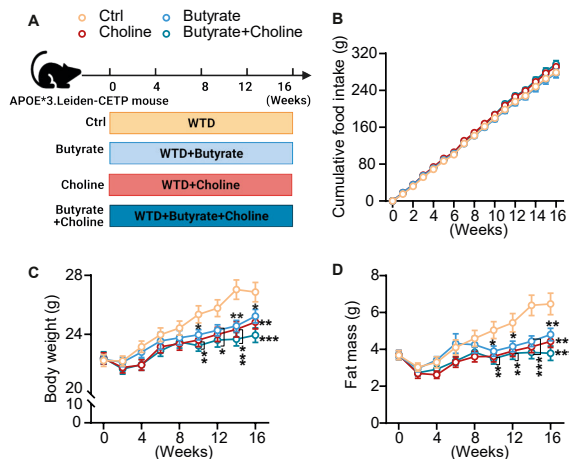
Fig. 1. Choline and butyrate attenuate WTD-induced fat mass gain in *APOE*3-Leiden.CETP* mice. (**A**) Experimental set up. (**B**) Cumulative food intake (n=4-5 per group), (**C**) body weight (n=16-17 per group), and (**D**) body fat mass (n=16-17 per group) were monitored throughout the experimental period. Data are shown as mean±SEM. Differences were assessed using one-way ANOVA followed by a Fisher's LSD post-test. *P<0.05; **P<0.01, ***P<0.001, compared with the control (ctrl) group. WTD, Western-type diet.

both supplements for 16 weeks (**Fig. 1A**). Neither choline nor butyrate affected food intake (**Fig. 1B**). Despite this, choline and butyrate attenuated WTD-induced body weight gain (**Fig. 1C**), which was explained by reduced fat mass gain (**Fig. 1D**) without affecting body lean mass (**Fig. S1**).

Choline and butyrate beneficially modulate the gut microbiome in *APOE*3-Leiden.CETP* mice

Previous studies have shown that the gut microbiota participates in choline- and butyrate-induced modulation of body weight and atherogenesis [16, 22, 23]. We thus performed whole metagenome shotgun sequencing to assess the impact of choline, butyrate and their combination on the gut microbiota composition and function. While principal component analysis revealed great similarities of the gut microbiome structure among the groups (**Fig. 2A**), choline reduced the gut microbial α diversity, regardless of butyrate supplementation (**Fig. 2B**). At the phylum level, most gut commensal microbes belonged to *Bacteroidetes*, *Firmicutes*, *Proteobacteria*, which, along with *Actinobacteria* and *Verrucomicrobia*, represented approximately 95% of the total microbial community (**Fig. S2A**). At the species level, *Faecalibaculum rodentium* (*F. rodentium*), *Parabacteroides distasonis* (*P. distasonis*) and *Bacteroides uniforms* (*B. uniforms*) were abundant among the groups (**Fig. 2C**). As compared to control treatment, butyrate enriched species with proposed anti-inflammatory properties, such as *Duncaniella spB8* (*D. spB8*) [24, 25] and *Blautia producta* (*B. producta*) [26], *Faecalibaculum* (*F. prausnitzii*) [27, 28] and *Ruthenibacterium lactatiformans* (*R. lactatiformans*) [29] (**Fig. 2D**).

Simultaneously, butyrate downregulated gut microbial genes involved in lipopolysaccharide (LPS) biosynthesis when compared to control treatment (**Fig. 2E**, **S2B**). In addition, choline increased several bacterial species compared to control treatment, including a probiotic microbe *Lactobacillus reuteria* (*L. reuteria*) [30] and three anti-inflammatory species of the *Olsenella* genus [31] (**Fig. 2F**). Interestingly, choline treatment did not affect TMA-producing bacteria, had no impact on gut microbial genes associated with TMA synthesis (**Fig. 2G**), and did not affect the expression of choline trimethylamine-lyase (*CutC*), an essential bacterial choline TMA-lyase gene (**Fig. 2H**). Rather, choline treatment upregulated gene expression of enzymes involved in TMA and TMAO degradation, including TMA corrinoid protein and TMAO reductase (**Fig. 2I**), effects that were blunted upon concomitant butyrate administration (**Fig. S2C-E**). Moreover, choline treatment upregulated gut microbial genes involved in starch and sugar metabolism (**Fig. 2G**), which are associated with SCFA production [32]. Furthermore, the combination group shared greater similarities in the gut composition and function compared to the choline group than the butyrate

group (**Fig. S3A-E**). Taken together, both choline and butyrate beneficially affected the gut microbial composition and function in WTD-fed *APOE*3-Leiden-CETP* mice, with a greater impact on the gut microbiome induced by choline versus butyrate.
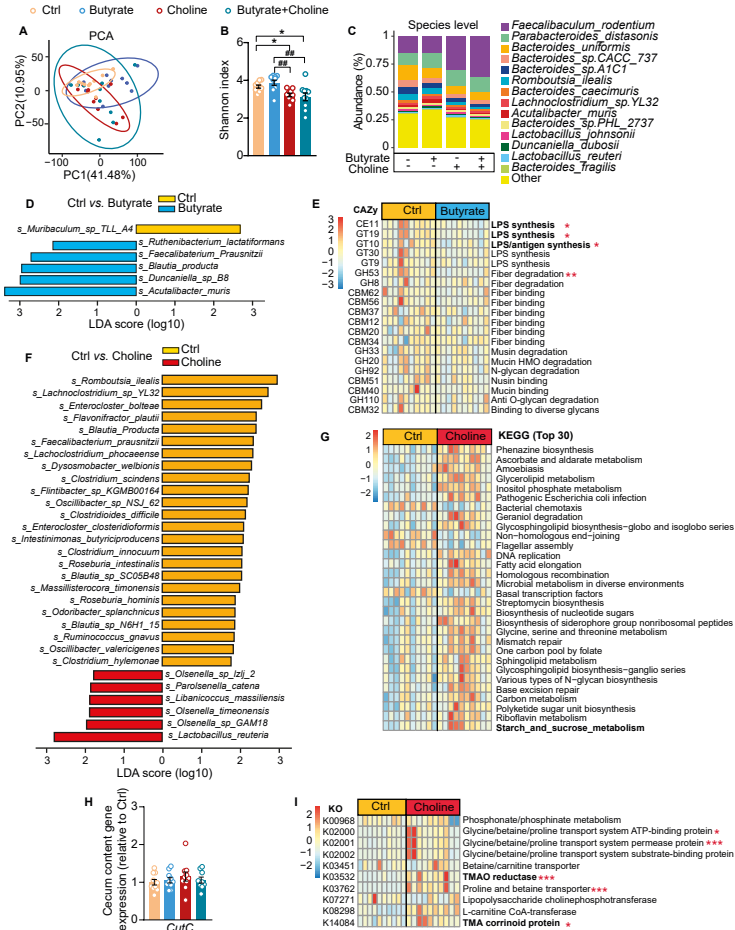
Fig. 2. Choline and butyrate beneficially modulate the gut microbiome in *APOE*3-Leiden.CETP* mice. At the end of the study, the cecal content was collected and sequenced using metagenomics sequencing (n=10 per group). (**A**) Principal component analysis (PCA) at the species level. (**B**) The Shannon index at the species level. (**C**) The abundance of the top 15 microbial species. (**D** and **F**) Linear discrimination analysis (LDA) effect size analysis was performed, and LDA scores calculated for differences in species-level abundance between groups. (**E** and **I**) Relative changes of the gut microbial genes involved in lipopolysaccharide (LPS) signaling and the metabolic pathway of TMA. (**G**) Top 30 significantly regulated KEGG pathways between the ctrl and choline groups. (**H**) Relative gut microbial *CutC* (choline TMA lyase) expression. (**B**, **H**) Data are represented as means±SEM. Differences were assessed using one-way ANOVA followed by a Fisher's LSD post-test. (**E**, **G**, **I**) Comparisons between groups were performed using Wilcoxon test. *$P<0.05$; **$P<0.01$, ***$P<0.001$, compared with the ctrl group. ##$P<0.01$, compared to the butyrate group.

Co-administration of choline and butyrate, instead of choline or butyrate alone, increases plasma TMAO levels in *APOE*3-Leiden.CETP* mice

Then, we investigated the role of dietary choline and butyrate in choline metabolism. To this end, we performed targeted metabolomics analyses to measure choline-related metabolites in plasma. Dietary choline increased plasma levels of choline and its oxidation product betaine (**Fig. 3A-B**) without affecting plasma TMA levels (**Fig. 3C**), while butyrate did not alter the levels of choline and its metabolites (**Fig. 3A-D**). Of note, only combination treatment increased TMAO levels (**Fig. 3D**). We observed that both choline and butyrate upregulated the hepatic expression of *Fmos* (i.e., *Fmo2* and *Fmo3*; **Fig. 3E**). Co-administration of choline and butyrate caused the highest expression of *Fmo3* in the liver (**Fig. 3E**), which may explain the highest plasma TMAO levels in the combination group.
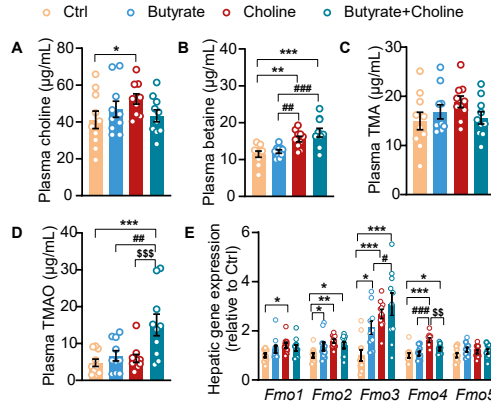
Fig. 3. Co-administration of choline and butyrate, instead of choline or butyrate alone, increases plasma TMAO levels in *APOE*3-Leiden.CETP* mice. At week16, plasma levels of **(A)** choline, (**B**) betaine, (**C**) TMA and (**D**) TMAO were determined. (**E**) At the end of the study, the relative mRNA expression of flavin-containing monooxygenases (*Fmos*) was determined in the liver. Data are shown as mean±SEM (n=10 per group). Differences were assessed using one-way ANOVA followed by a Fisher's LSD post hoc test. *$P<0.05$; **$P<0.01$, ***$P<0.001$, compared with the ctrl group; #$P<0.05$, ##$P<0.01$, ###$P<0.001$, compared to the butyrate group; $$$P<0.01$, $$$$P<0.001$, compared to the choline group. *Fmos*, flavin monooxygenases; TMA, trimethylamine; TMAO, trimethylamine N-oxide.

Choline and butyrate do not affect plasma lipid levels in *APOE*3-Leiden. CETP* mice

Choline and butyrate have been suggested to modulate reverse cholesterol transport (RCT) [11, 33]. However, choline upregulated to only some extent the expression of genes involved in HDL assembly (e.g. ATP-binding cassette subfamily A member 1, *Abca1*; **Fig. 4A**;), HDL uptake (e.g. scavenger receptor class B type 1, *Srb-1*; **Fig. 4B**),

bile acid secretion (e.g. bile salt export pump, *Bsep*; **Fig. 4C**), sterol secretion (e.g. ATP-binding cassette transporter G member 5, *Abcg5*; **Fig. 4D**), *Ldlr* and *CETP* (**Fig. 4E**). And, butyrate had minor impact on the expression of these genes (**Fig. 4A-E**). Similarly, neither choline nor butyrate had any evident effects on levels of plasma TG, TC, HDL-C and non-HDL-C (**Fig. S4A-B**, **4F-G**).
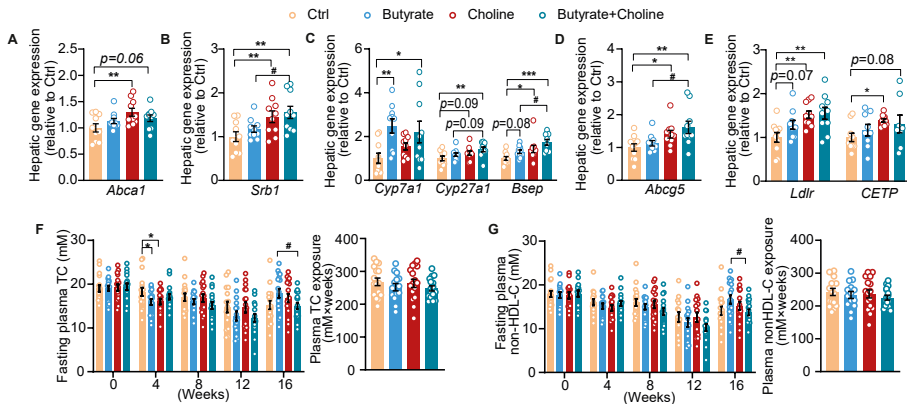
Fig. 4. Choline and butyrate do not affect plasma lipid levels in *APOE*3-Leiden.CETP* mice. The relative expression of genes involved in high-density lipoprotein (HDL) assembly and clearance (**A** and **B**), bile acid synthesis and secretion (**C**), and sterol secretion (**D**) was determined. (**E**) The mRNA levels of low-density lipoprotein receptor and cholesteryl ester transfer protein (*CETP*) were measured. Fasting plasma levels of total cholesterol (TC; **F**) and non-high-density lipoprotein cholesterol (non-HDL-C; **G**) were determined throughout the experimental period. Data are represented as mean±SEM (**A-E**, n=9-10 per group; **F-G**, n=16-17 per group). Differences were assessed using one-way ANOVA followed by a Fisher's LSD post hoc test. *$P<0.05$; **$P<0.01$, ***$P<0.001$, compared with the ctrl group; #$P<0.05$, compared to the butyrate group. *Abca1*, ATP-binding cassette subfamily A member 1; *Abcg5*, ATP-binding cassette transporter G member 5; *Bsep*, bile salt export pump; *Cyp27a1*, sterol 27-hydroxylase; *Cyp7a1*, cholesterol 7α-hydroxylase; *Ldlr*, low density lipoprotein receptor; *Srb-1*, scavenger receptor class B type 1.

Choline and butyrate have no impact on atherosclerosis development in *APOE*3-Leiden-CETP* mice

We next assessed the size, severity and composition of atherosclerotic lesions throughout the aortic root in the heart isolated after 16 weeks of treatment. Neither choline, butyrate nor their combination affected atherosclerotic plaque area, severity and composition (**Fig. 5A-D, S5A-C**). In accordance, choline and butyrate had no impact on atherosclerotic plaque stability (**Fig. 5E**), as calculated from dividing the relative collagen and smooth muscle cell area by the relative area of macrophages within the same lesion. While univariate regression analysis revealed that the atherosclerotic lesion area was to some extent predicted by plasma cholesterol levels (**Fig. 5F, S5D-F**), plasma TMAO levels were not associated with atherosclerotic lesion size in *APOE*3.Leiden-CETP* mice (**Fig. 5G**).
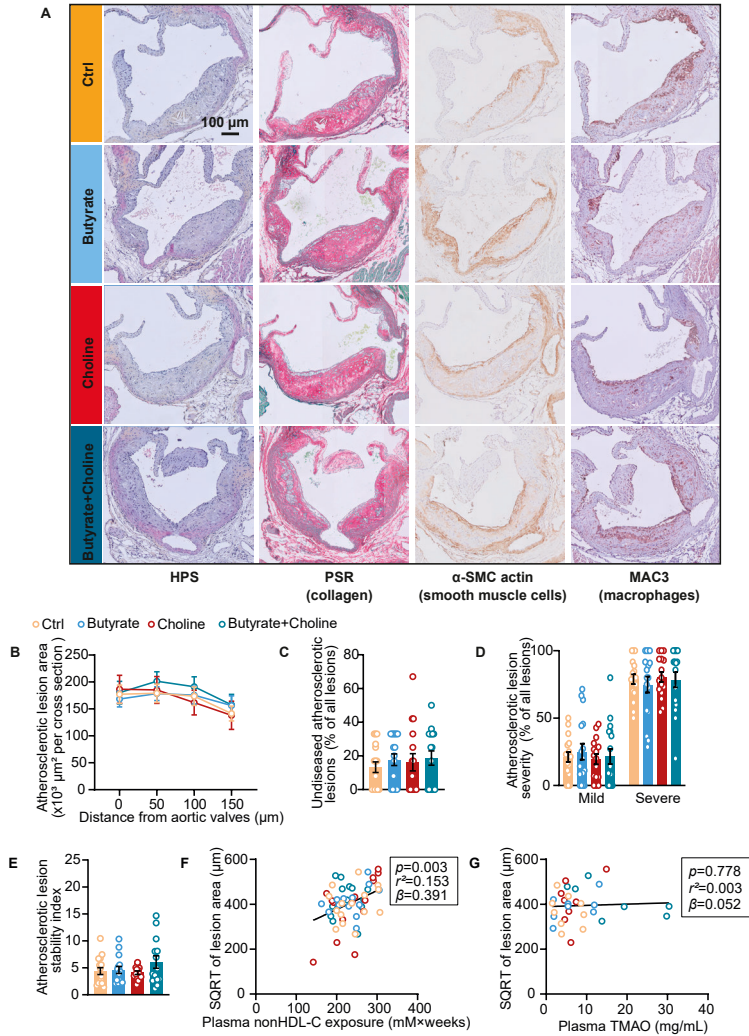
Fig. 5. Choline and butyrate have no impact on atherosclerosis development in *APOE*3-Leiden. CETP* mice. At 16 weeks, hearts were collected, and the valve area in the aortic root was stained with haematoxylin–phloxine–saffron (HPS). To quantify the contents of collagen, smooth muscle cells and macrophages within the lesion, the valve area in the aortic root was stained with Picrosirius red (PSR), anti-α-smooth muscle cell actin (α-SMC actin) antibody and anti-MAC3 antibody, respectively. (**A**) Representative pictures of every staining. (**B**) The relationship between atherosclerotic lesion area and the distance from aortic valve was determined by calculating the lesion area of 4 consecutive sections (with 50 µm intervals) beginning with the appearance of open aortic valve leaflets (n=13-16 per group). Lesions were categorized into undiseased (**C**), mild, and severe (**D**) lesions (n=13-16 per group). (**E**) The stability index was calculated by dividing the smooth muscle cell and collagen area by macrophage area within the same lesion. The square root (SQRT) of the atherosclerotic lesion area plotted against plasma (**F**) non-HDL-C exposure and TMAO (**G**) levels, and linear regression analyses were performed. Data are represented as means±SEM (**B-F**, n=13-16 per group; **G**, n=10 per group). Comparisons among four groups were performed using one-way ANOVA followed by a Fisher's LSD post hoc test.

DISCUSSION

Choline has been reported to aggravate atherosclerosis development, as caused by generation of TMAO through the gut-liver axis [6, 33], while butyrate beneficially modulates the gut microbiota and shows antiatherogenic effects, in *Apoe*$^{-/-}$ and *Ldlr*$^{-/-}$ mice [9-11]. Based on our hypothesis that butyrate is able to alleviate choline-induced atherosclerosis, we set out to evaluate the effects of choline, butyrate and their combination in *APOE*3.Leiden-CETP* mice, a well-established model for human-like lipid metabolism and atherosclerosis development. In contrast to expectations, we here report that both choline and butyrate beneficially modulate the gut microbiome, without affecting atherosclerosis development. Likewise, the combination of choline and butyrate did not influence atherosclerosis development, and TMAO levels were not associated with atherosclerotic lesion size.

First, we demonstrated that choline exerts beneficial effects on the gut microbial composition and function without influencing atherosclerosis. Choline increased cecal abundance of *L. reuteria* and three species in the *Olsenella* genus. *L. reuteria* has been reported to improve gut barrier function via reducing inflammation [30, 34], and bacteria of the *Olsenella* genus enhance the efficacy of immune checkpoint inhibitors in cancer by enhancing anti-inflammatory capacities of T cells [31]. In this study, choline did not affect the cecum content expression of bacterial *CutC*, a key gene responsible for converting choline into TMA by the gut microbiota. In line with this finding, choline did not affect plasma TMA levels. Choline did upregulate hepatic expression of *Fmos* (especially *Fmo3*), encoding the rate-limiting enzymes responsible for the oxidation of TMA to TMAO [15, 33]. However, choline did not influence plasma TMAO levels, which may be explained by upregulated gut microbial gene expression of TMAO reductase that reduces TMAO to TMA, and TMA corrinoid that catabolizes TMA to methane [35, 36]. It has been shown that excess choline can also be metabolized to other metabolites, such as phosphocholine and acetylcholine [37-39], and the mouse model used here may have different choline metabolism compared to other mouse models such as *Apoe*$^{-/-}$ and *Ldlr*$^{-/-}$ mice. Thus, future studies are needed to explore the differences in choline metabolism between in the various mouse models. In addition, we observed that choline slightly upregulated hepatic expression of RCT-related genes. This is in contrast to previous studies in *Apoe*$^{-/-}$ mice, which proposed that choline suppresses expression of RCT-related genes to aggravate atherosclerosis [33], although it is in fact in line with the absence of effects of choline on atherosclerosis in *APOE*3-Leiden. CETP* mice. We did observe that choline profoundly upregulates hepatic expression of *CETP* and *Ldlr*. Therefore, the seeming discrepancies between the different mouse models might be explained by a choline-mediated increase of CETP-mediated transfer

of neutral lipids between lipoproteins and a APOE-LDLR mediated clearance pathway of triglyceride-rich lipoprotein remnants, which are both operational in *APOE*3-Leiden. CETP* mice but not in *ApoE^-/-* mice. In fact, and in line with our findings, a very recent study showed that choline does not affect atherosclerosis in CETP-expressing *Apoe^-/-* mice [40].

Similarly to choline, butyrate also beneficially modulated the gut microbiome although in different aspects. Butyrate increased cecal abundance of the anti-inflammatory species *D. spB8* [24, 25] as well as three strains known for producing SCFAs, including acetate-producing *B. producta* [26], butyrate-producing *F. Prausnitzii* [27, 28] and lactate-producing *R. lactatiformans* [29]. Furthermore, butyrate downregulated cecal microbial genes involved in LPS synthesis, which may imply that butyrate alleviates LPS-induced damage of gut barrier integrity [41]. Previous studies showed that butyrate reduces atherosclerotic lesion size in *Apoe^-/-* and *Ldlr^-/-* mice partially via improving gut barrier function [9-12, 42]. This was attributed to maintained gut microbiota homeostasis and inhibited LPS synthesis, which reduces gut barrier permeability and thus reduces systemic inflammation [42-44]. Probably as a combined result, butyrate inhibited macrophage infiltration into atherosclerotic plaques and halts plaque progression [9, 45]. In contrast, we found no influence of butyrate on atherosclerotic size, severity and composition including macrophage content within atherosclerotic lesions in *APOE*3-Leiden.CETP* mice. In addition to beneficially modulating gut microbiome, butyrate has been demonstrated to promote RCT and thus to improve cholesterol metabolism, by primarily stimulating ABCA1-mediated cholesterol efflux in macrophages and increasing hepatic bile acid synthesis and secretion, thereby alleviating atherosclerosis in *Apoe^-/-* mice [11]. In our mouse model, butyrate only slightly affected hepatic expression of RCT-related genes including *Abca1* and did not affect cholesterol levels. Moreover, plasma non-HDL-C levels were positively correlated to atherosclerotic size. Therefore, it is likely that atherosclerosis is more inflammation-driven in *Apoe^-/-* and *Ldlr^-/-* mice, and more cholesterol-driven in *APOE*3-Leiden.CETP* mice, explaining why butyrate is not atheroprotective in our model.

TMAO has been identified as the main mediator of the previously described atherogenic effects of choline in *Apoe^-/-* and *Ldlr^-/-* mice [6, 33]. In the present study, we observed that treatment with the combination of choline and butyrate increased plasma TMAO levels as compared to single treatments. This is likely due to the observation that butyrate impaired the choline-induced TMA and TMAO degradation signaling. Indeed, the gut microbial gene expression of TMA corrinoid protein and TMAO reductase in the combination group was comparable to that of the control and butyrate groups. However, in spite of increased plasma TMAO levels, combined choline and butyrate

administration did not affect atherosclerosis. Of note, plasma TMAO levels were not associated with atherosclerotic lesion size. The fact that TMAO induces atherosclerosis in *Apoe*^{-/-} and *Ldlr*^{-/-} mice but not in *APOE*3-Leiden.CETP* mice, may suggest that TMAO lacks atherogenic properties in humans. Indeed, many human dietary trials did not find any association between plasma TMAO and CVD risk [46-48]. Multiple meta-analyses and systematic reviews have shown that the intake of eggs, rich in TMAO precursors, is not correlated to heart disease risk and mortality [49]. Similarly, another systematic review and a cohort study have concluded that TMAO does not associate with CVD risk [50].

In conclusion, we demonstrate that in *APOE*3-Leiden.CETP* mice, a well-established model for human-like lipoprotein metabolism, both choline and butyrate beneficially modulate the gut microbiome and increase TMAO, however without affecting atherosclerosis.

Author contributions

CL designed the study, carried out the research, analyzed and interpreted the results, and wrote and revised the manuscript. ZL carried out the research, interpreted the results, reviewed and revised the manuscript, and obtained funding. ZS carried out the research, interpreted the results, reviewed and revised the manuscript. XF and HS analyzed metagenomics data and reviewed the manuscript. MS interpreted the results, reviewed and revised the manuscript. MRB advised the study and reviewed the manuscript. PCNR designed and advised the study, interpreted the results, edited, reviewed and revised the manuscript and obtained funding. YW designed and advised the study, interpreted the results, reviewed and revised the manuscript and obtained the funding.

REFERENCES

1. Back M, Yurdagul A, Jr., Tabas I, Oorni K, Kovanen PT. Inflammation and its resolution in atherosclerosis: mediators and therapeutic opportunities. *Nat Rev Cardiol.* 2019;16:389-406. doi: 10.1038/s41569-019-0169-2

2. Hegele RA, Gidding SS, Ginsberg HN, McPherson R, Raal FJ, Rader DJ, Robinson JG, Welty FK. Nonstatin Low-Density Lipoprotein-Lowering Therapy and Cardiovascular Risk Reduction-Statement From ATVB Council. *Arterioscler Thromb Vasc Biol.* 2015;35:2269-2280. doi: 10.1161/ATVBAHA.115.306442

3. Aday AW, Ridker PM. Targeting Residual Inflammatory Risk: A Shifting Paradigm for Atherosclerotic Disease. *Front Cardiovasc Med.* 2019;6:16. doi: 10.3389/fcvm.2019.00016

4. Jonsson AL, Backhed F. Role of gut microbiota in atherosclerosis. *Nat Rev Cardiol.* 2017;14:79-87. doi: 10.1038/nrcardio.2016.183

5. Tang WHW, Li DY, Hazen SL. Dietary metabolism, the gut microbiome, and heart failure. *Nat Rev Cardiol.* 2019;16:137-154. doi: 10.1038/s41569-018-0108-7

6. Wang Z, Klipfell E, Bennett BJ, Koeth R, Levison BS, Dugar B, Feldstein AE, Britt EB, Fu X, Chung YM, et al. Gut flora metabolism of phosphatidylcholine promotes cardiovascular disease. *Nature.* 2011;472:57-63. doi: 10.1038/nature09922

7. Seldin MM, Meng Y, Qi H, Zhu W, Wang Z, Hazen SL, Lusis AJ, Shih DM. Trimethylamine N-Oxide Promotes Vascular Inflammation Through Signaling of Mitogen-Activated Protein Kinase and Nuclear Factor-kappaB. *J Am Heart Assoc.* 2016;5. doi: 10.1161/JAHA.115.002767

8. Collins HL, Drazul-Schrader D, Sulpizio AC, Koster PD, Williamson Y, Adelman SJ, Owen K, Sanli T, Bellamine A. L-Carnitine intake and high trimethylamine N-oxide plasma levels correlate with low aortic lesions in ApoE(-/-) transgenic mice expressing CETP. *Atherosclerosis.* 2016;244:29-37. doi: 10.1016/j.atherosclerosis.2015.10.108

9. Kasahara K, Krautkramer KA, Org E, Romano KA, Kerby RL, Vivas EI, Mehrabian M, Denu JM, Backheds F, Lusis A, et al. Interactions between Roseburia intestinalis and diet modulate atherogenesis in a murine model. *Nat Microbiol.* 2018;3:1461-1471. doi: 10.1038/s41564-018-0272-x

10. Chen Y, Xu C, Huang R, Song J, Li D, Xia M. Butyrate from pectin fermentation inhibits intestinal cholesterol absorption and attenuates atherosclerosis in apolipoprotein E-deficient mice. *J Nutr Biochem.* 2018;56:175-182. doi: 10.1016/j.jnutbio.2018.02.011

11. Du Y, Li X, Su C, Xi M, Zhang X, Jiang Z, Wang L, Hong B. Butyrate protects against high-fat diet-induced atherosclerosis via up-regulating ABCA1 expression in apolipoprotein E-deficiency mice. *Br J Pharmacol.* 2020;177:1754-1772. doi: 10.1111/bph.14933

12. Brandsma E, Kloosterhuis NJ, Koster M, Dekker DC, Gijbels MJJ, van der Velden S, Rios-Morales M, van Faassen MJR, Loreti MG, de Bruin A, et al. A Proinflammatory Gut Microbiota Increases Systemic Inflammation and Accelerates Atherosclerosis. *Circ Res.* 2019;124:94-100. doi: 10.1161/CIRCRESAHA.118.313234

13. Westerterp M, van der Hoogt CC, de Haan W, Offerman EH, Dallinga-Thie GM, Jukema JW, Havekes LM, Rensen PC. Cholesteryl ester transfer protein decreases high-density lipoprotein and severely aggravates atherosclerosis in APOE*3-Leiden mice. *Arterioscler Thromb Vasc Biol.* 2006;26:2552-2559. doi: 10.1161/01.ATV.0000243925.65265.3c

14. van Eenige R, Verhave PS, Koemans PJ, Tiebosch I, Rensen PCN, Kooijman S. RandoMice, a novel, user-friendly randomization tool in animal research. *PLoS One.* 2020;15:e0237096. doi: 10.1371/journal.pone.0237096

15. Tang WH, Wang Z, Levison BS, Koeth RA, Britt EB, Fu X, Wu Y, Hazen SL. Intestinal microbial metabolism of phosphatidylcholine and cardiovascular risk. *N Engl J Med.* 2013;368:1575-1584. doi: 10.1056/NEJMoa1109400

16. Li Z, Yi CX, Katiraei S, Kooijman S, Zhou E, Chung CK, Gao Y, van den Heuvel JK, Meijer OC, Berbee JFP, et al. Butyrate reduces appetite and activates brown adipose tissue via the gut-brain neural circuit. *Gut.* 2018;67:1269-1279. doi: 10.1136/gutjnl-2017-314050

17. Gao Z, Yin J, Zhang J, Ward RE, Martin RJ, Lefevre M, Cefalu WT, Ye J. Butyrate improves insulin sensitivity and increases energy expenditure in mice. *Diabetes.* 2009;58:1509-1517. doi: 10.2337/db08-1637

18. Liu C, Schonke M, Zhou E, Li Z, Kooijman S, Boon MR, Larsson M, Wallenius K, Dekker N, Barlind L, et al. Pharmacological treatment with FGF21 strongly improves plasma cholesterol metabolism to reduce atherosclerosis. *Cardiovasc Res.* 2022;118:489-502. doi: 10.1093/cvr/cvab076

19. Berbee JF, Boon MR, Khedoe PP, Bartelt A, Schlein C, Worthmann A, Kooijman S, Hoeke G, Mol IM, John C, et al. Brown fat activation reduces hypercholesterolaemia and protects from atherosclerosis development. *Nat Commun.* 2015;6:6356. doi: 10.1038/ncomms7356

20. In Het Panhuis W, Kooijman S, Brouwers B, Verhoeven A, Pronk ACM, Streefland TCM, Giera M, Schrauwen P, Rensen PCN, Schonke M. Mild Exercise Does Not Prevent Atherosclerosis in APOE*3-Leiden.CETP Mice or Improve Lipoprotein Profile of Men with Obesity. *Obesity (Silver Spring).* 2020;28 Suppl 1:S93-S103. doi: 10.1002/oby.22799

21. Wong MC, van Diepen JA, Hu L, Guigas B, de Boer HC, van Puijvelde GH, Kuiper J, van Zonneveld AJ, Shoelson SE, Voshol PJ, et al. Hepatocyte-specific IKKbeta expression aggravates atherosclerosis development in APOE*3-Leiden mice. *Atherosclerosis.* 2012;220:362-368. doi: 10.1016/j.atherosclerosis.2011.06.055

22. Agus A, Clement K, Sokol H. Gut microbiota-derived metabolites as central regulators in metabolic disorders. *Gut.* 2021;70:1174-1182. doi: 10.1136/gutjnl-2020-323071

23. Schugar RC, Gliniak CM, Osborn LJ, Massey W, Sangwan N, Horak A, Banerjee R, Orabi D, Helsley RN, Brown AL, et al. Gut microbe-targeted choline trimethylamine lyase inhibition improves obesity via rewiring of host circadian rhythms. *Elife.* 2022;11. doi: 10.7554/eLife.63998

24. Forster SC, Clare S, Beresford-Jones BS, Harcourt K, Notley G, Stares MD, Kumar N, Soderholm AT, Adoum A, Wong H, et al. Identification of gut microbial species linked with disease variability in a widely used mouse model of colitis. *Nat Microbiol.* 2022;7:590-599. doi: 10.1038/s41564-022-01094-z

25. Feng P, Li Q, Liu L, Wang S, Wu Z, Tao Y, Huang P, Wang P. Crocetin Prolongs Recovery Period of DSS-Induced Colitis via Altering Intestinal Microbiome and Increasing Intestinal Permeability. *Int J Mol Sci.* 2022;23. doi: 10.3390/ijms23073832

26. Aoki R, Onuki M, Hattori K, Ito M, Yamada T, Kamikado K, Kim YG, Nakamoto N, Kimura I, Clarke JM, et al. Commensal microbe-derived acetate suppresses NAFLD/NASH development via hepatic FFAR2 signalling in mice. *Microbiome.* 2021;9:188. doi: 10.1186/s40168-021-01125-7

27. Machiels K, Joossens M, Sabino J, De Preter V, Arijs I, Eeckhaut V, Ballet V, Claes K, Van Immerseel F, Verbeke K, et al. A decrease of the butyrate-producing species Roseburia hominis and Faecalibacterium prausnitzii defines dysbiosis in patients with ulcerative colitis. *Gut.* 2014;63:1275-1283. doi: 10.1136/gutjnl-2013-304833

28. Olsson LM, Boulund F, Nilsson S, Khan MT, Gummesson A, Fagerberg L, Engstrand L, Perkins R, Uhlen M, Bergstrom G, et al. Dynamics of the normal gut microbiota: A longitudinal one-year population study in Sweden. *Cell Host Microbe.* 2022;30:726-739 e723. doi: 10.1016/j.chom.2022.03.002

29. Shkoporov AN, Chaplin AV, Shcherbakova VA, Suzina NE, Kafarskaia LI, Bozhenko VK, Efimov BA. Ruthenibacterium lactatiformans gen. nov., sp. nov., an anaerobic, lactate-producing member of the family Ruminococcaceae isolated from human faeces. *Int J Syst Evol Microbiol.* 2016;66:3041-3049. doi: 10.1099/ijsem.0.001143

30. Zhou Q, Wu F, Chen S, Cen P, Yang Q, Guan J, Cen L, Zhang T, Zhu H, Chen Z. Lactobacillus reuteri improves function of the intestinal barrier in rats with acute liver failure through Nrf-2/HO-1 pathway. *Nutrition.* 2022;99-100:111673. doi: 10.1016/j.nut.2022.111673

31. Mager LF, Burkhard R, Pett N, Cooke NCA, Brown K, Ramay H, Paik S, Stagg J, Groves RA, Gallo M, et al. Microbiome-derived inosine modulates response to checkpoint inhibitor immunotherapy. *Science.* 2020;369:1481-1489. doi: 10.1126/science.abc3421

32. Arpaia N, Campbell C, Fan X, Dikiy S, van der Veeken J, deRoos P, Liu H, Cross JR, Pfeffer K, Coffer PJ, et al. Metabolites produced by commensal bacteria promote peripheral regulatory T-cell generation. *Nature.* 2013;504:451-455. doi: 10.1038/nature12726

33. Koeth RA, Wang Z, Levison BS, Buffa JA, Org E, Sheehy BT, Britt EB, Fu X, Wu Y, Li L, et al. Intestinal microbiota metabolism of L-carnitine, a nutrient in red meat, promotes atherosclerosis. *Nat Med.* 2013;19:576-585. doi: 10.1038/nm.3145

34. Wu H, Xie S, Miao J, Li Y, Wang Z, Wang M, Yu Q. Lactobacillus reuteri maintains intestinal epithelial regeneration and repairs damaged intestinal mucosa. *Gut Microbes.* 2020;11:997-1014. doi: 10.1080/19490976.2020.1734423

35. Ferguson DJ, Jr., Krzycki JA. Reconstitution of trimethylamine-dependent coenzyme M methylation with the trimethylamine corrinoid protein and the isozymes of methyltransferase II from Methanosarcina barkeri. *J Bacteriol.* 1997;179:846-852. doi: 10.1128/jb.179.3.846-852.1997

36. Ellenbogen JB, Jiang R, Kountz DJ, Zhang L, Krzycki JA. The MttB superfamily member MtyB from the human gut symbiont Eubacterium limosum is a cobalamin-dependent gamma-butyrobetaine methyltransferase. *J Biol Chem.* 2021;297:101327. doi: 10.1016/j.jbc.2021.101327

37. Corbin KD, Zeisel SH. Choline metabolism provides novel insights into nonalcoholic fatty liver disease and its progression. *Curr Opin Gastroen.* 2012;28:159-165. doi: 10.1097/MOG.0b013e32834e7b4b

38. Zeisel SH. Metabolic crosstalk between choline/1-carbon metabolism and energy homeostasis. *Clin Chem Lab Med.* 2013;51:467-475. doi: 10.1515/cclm-2012-0518

39. Garcia-Molina P, Sola-Leyva A, Luque-Navarro PM, Laso A, Rios-Marco P, Rios A, Lanari D, Torretta A, Parisini E, Lopez-Cara LC, et al. Anticancer Activity of the Choline Kinase Inhibitor PL48 Is Due to Selective Disruption of Choline Metabolism and Transport Systems in Cancer Cell Lines. *Pharmaceutics.* 2022;14. doi: ARTN 426. doi: 10.3390/pharmaceutics14020426

40. Collins HL, Adelman SJ, Butteiger DN, Bortz JD. Choline Supplementation Does Not Promote Atherosclerosis in CETP-Expressing Male Apolipoprotein E Knockout Mice. *Nutrients.* 2022;14. doi: 10.3390/nu14081651

41. Guo SH, Nighot M, Al-Sadi R, Alhmoud T, Nighot P, Ma TY. Lipopolysaccharide Regulation of Intestinal Tight Junction Permeability Is Mediated by TLR4 Signal Transduction Pathway Activation of FAK and MyD88. *J Immunol.* 2015;195:4999-5010. doi: 10.4049/jimmunol.1402598

42. Fang W, Xue H, Chen X, Chen K, Ling W. Supplementation with Sodium Butyrate Modulates the Composition of the Gut Microbiota and Ameliorates High-Fat Diet-Induced Obesity in Mice. *J Nutr.* 2019;149:747-754. doi: 10.1093/jn/nxy324

43. Tang G, Du Y, Guan H, Jia J, Zhu N, Shi Y, Rong S, Yuan W. Butyrate ameliorates skeletal muscle atrophy in diabetic nephropathy by enhancing gut barrier function and FFA2-mediated PI3K/Akt/mTOR signals. *Br J Pharmacol*. 2022;179:159-178. doi: 10.1111/bph.15693

44. Bach Knudsen KE, Laerke HN, Hedemann MS, Nielsen TS, Ingerslev AK, Gundelund Nielsen DS, Theil PK, Purup S, Hald S, Schioldan AG, et al. Impact of Diet-Modulated Butyrate Production on Intestinal Barrier Function and Inflammation. *Nutrients*. 2018;10. doi: 10.3390/nu10101499

45. Aguilar EC, Leonel AJ, Teixeira LG, Silva AR, Silva JF, Pelaez JM, Capettini LS, Lemos VS, Santos RA, Alvarez-Leite JI. Butyrate impairs atherogenesis by reducing plaque inflammation and vulnerability and decreasing NFkappaB activation. *Nutr Metab Cardiovasc Dis*. 2014;24:606-613. doi: 10.1016/j.numecd.2014.01.002

46. Bordoni L, Samulak JJ, Sawicka AK, Pelikant-Malecka I, Radulska A, Lewicki L, Kalinowski L, Gabbianelli R, Olek RA. Trimethylamine N-oxide and the reverse cholesterol transport in cardiovascular disease: a cross-sectional study. *Sci Rep*. 2020;10:18675. doi: 10.1038/s41598-020-75633-1

47. Richard C, Cristall L, Fleming E, Lewis ED, Ricupero M, Jacobs RL, Field CJ. Impact of Egg Consumption on Cardiovascular Risk Factors in Individuals with Type 2 Diabetes and at Risk for Developing Diabetes: A Systematic Review of Randomized Nutritional Intervention Studies. *Can J Diabetes*. 2017;41:453-463. doi: 10.1016/j.jcjd.2016.12.002

48. Shin JY, Xun P, Nakamura Y, He K. Egg consumption in relation to risk of cardiovascular disease and diabetes: a systematic review and meta-analysis. *Am J Clin Nutr*. 2013;98:146-159. doi: 10.3945/ajcn.112.051318

49. Meyer KA, Shea JW. Dietary Choline and Betaine and Risk of CVD: A Systematic Review and Meta-Analysis of Prospective Studies. *Nutrients*. 2017;9. doi: 10.3390/nu9070711

50. Nagata C, Wada K, Tamura T, Konishi K, Kawachi T, Tsuji M, Nakamura K. Choline and Betaine Intakes Are Not Associated with Cardiovascular Disease Mortality Risk in Japanese Men and Women. *J Nutr*. 2015;145:1787-1792. doi: 10.3945/jn.114.209296

SUPPLEMENT

Expanded methods

Plasma targeted metabolome

Plasma samples (20 μL per sample; n=10 per group) were prepared for quantitation of choline, betaine, TMA and TMAO level. The measurement was performed by BGI genomics (Shenzhen, Guang Zhou, China). In brief, plasma protein was precipitated by adding methanol/acetonitrile (15/85; 180 μL per sample). These plasma samples were then centrifuged (20,000 × g, 15 min, 4℃). The supernatants (10 μL per sample) were taken and mixed with pure acetonitrile (190 μL per sample). After the centrifugation (20,000 × g, 15 min, 4℃), the supernatants (5 μL per sample) were mixed with pure acetonitrile (55 μL per sample), and tested using liquid chromatography with tandem mass spectrometry (LC-MS/MS). Standard curve was prepared as follows. 1000 ppm (mg/mL) of each standard solution was prepared using methanol/acetonitrile (15:85), and then pure acetonitrile was used to gradually dilute standard solution to prepare a 0-200 ppb mixed standard into 9 standard concentration points. LC-MS/MS analysis was carried out using an ACQUITY UPLC I-Class (Waters, Framingham, MA, USA) coupled to QTRAP6500+ mass spectrometry (SCIEX, Framingham, MA, USA). Reversed-phase separation was performed on a BEH HILIC column (100 mm × 2.1 mm, 1.7 μm; Waters, Framingham, MA, USA) according to the manufacturer's instruction. The mobile phase consisted of ultrapure water, 0.15% formic acid, 10 mM ammonium formate and acetonitrile. Mass spectrometry was performed using ESI ion source in a positive ion mode. Using MultiQuant software (SCIEX, Framingham, MA, USA), the default parameters are used for automatic identification and integration of each multiple reaction monitoring (MRM) transition (ion pair), and manual inspection is assisted. The concentration of choline-related metabolites was obtained by substituting the integrated peak area of the targeted index in the sample into the standard curve, followed by multiplying by the dilution factor.

Metagenomics sequencing and analysis

Whole-genome shotgun sequencing of all samples (n=10 per group) was carried out on a DNBSEQ platform at BGI Genomics (Shenzhan, Guang Zhou, China). SOAPnuke was used to remove low quality sequences. Human sequences were removed using Bowtie2 [1]. The filtered high-quality reads were assembled into contigs using MEGAHIT [2], and only contigs of ≥ 300 bp were used. Genes were predicated by MetaGeneMark [3]. A non-redundant gene catalogue was constructed using CD-HIT [4]. Gene taxonomy was annotated to Kraken2 [5] database. High-quality reads were mapped back to the constructed non-redundant gene catalogue using Salmon [6] to calculate gene

2

abundance within each sample. Gene functional identification was annotated to Kyoto Encyclopedia of Genes and Genomes (KEGG) [7] and KEGG orthology (KO), and Carbohydrate-Active EnZymes (CAZy) [8]. Principal component analysis (PCA) [59] at the species level, linear discriminant analysis (LDAL) and relative abundance of pathways and enzymes were analysed using R packages.

Supplementary Table 1 List of primer sequences for the targeted mouse genes used in mRNA expression analysis

Gene	Forward primer (5'-3')	Reverse Primer (5'-3')
Abca1	CCCAGAGCAAAAAGCGACTC	GGTCATCATCACTTTGGTCCTTG
Abcg5	TGTCCTACAGCGTCAGCAACC	GGCCACTCTCGATGTACAAGG
Actb	AACCGTGAAAAGATGACCCAGAT	CACAGCCTGGATGGCTACGTA
Bsep	CTGCCAAGGATGCTAATGCA	CGATGGCTACCCTTTGCTTCT
CETP	CAGATCAGCCACTTGTCCAT	CAGCTGTGTGTTGATCTGGA
CutC	AGRGTTHGATYMTGGCTCAG	TGCTGCCTCCCGTAGGAGT
Cyp27a1	TCTGGCTACCTGCACTTCCT	CTGGATCTCTGGGCTCTTTG
Cyp7a1	CAGGGAGATGCTCTGTGTTCA	AGGCATACATCCCTTCCGTGA
Fmo1	AAACAAGCATAGCGGGTTTG	ATCCGGTTTTGCGTTGATAG
Fmo2	AGCTGTGGTCTTCGAGGATG	GGCAAGCTACACAAGCCTTT
Fmo3	GGAACTTGCACTTTGCCTTC	TAGGAGATTGGGCTTTGCAC
Fmo4	CGGAGCAGCTCATTAAAAGG	CTGAGTGAGCTCGTCCATGT
Fmo5	TGCCCTCACAAAGTGAAATG	GCTGGCTGTCCACATACCTT
Ldlr	GCATCAGCTTGGACAAGGTGT	GGGAACAGCCACCATTGTTG
Rplp0	GGACCCGAGAAGACCTCCTT	GCACATCACTCAGAATTTCAATGG
Srb-1	GTGCTGCTGGGGCTTGGAGG	CACTGGTGGGCTGTCCGCTG

Abca1, ATP-binding cassette subfamily A member 1; *Abcg5*, ATP-binding cassette transporter G member 5; *Actb*, β-actin; *ApoB*, apolipoprotein B; *Bsep*, bile salt export pump; *CETP*, CETP cholesteryl ester transfer protein; *CutC*, choline trimethylamine-lyase *Cyp27a1*, sterol 27-hydroxylase; *Cyp7a1*, cholesterol 7α-hydroxylase; *Fmo*, flavin monooxygenase; *Ldlr*, low density lipoprotein receptor; *Mttp*, microsomal triglyceride transfer protein; *Rplp0*, ribosomal protein lateral stalk subunit P0; *Srb-1*, scavenger receptor class B type 1.

REFERENCES

1. Langmead, B. and S.L. Salzberg, *Fast gapped-read alignment with Bowtie 2.* Nat Methods, 2012. **9**(4): p. 357-9.

2. Li, D., et al., *MEGAHIT: an ultra-fast single-node solution for large and complex metagenomics assembly via succinct de Bruijn graph.* Bioinformatics, 2015. **31**(10): p. 1674-6.

3. Zhu, W., A. Lomsadze, and M. Borodovsky, *Ab initio gene identification in metagenomic sequences.* Nucleic Acids Res, 2010. **38**(12): p. e132.

4. Fu, L., et al., *CD-HIT: accelerated for clustering the next-generation sequencing data.* Bioinformatics, 2012. **28**(23): p. 3150-2.

5. Wood, D.E., J. Lu, and B. Langmead, *Improved metagenomic analysis with Kraken 2.* Genome Biol, 2019. **20**(1): p. 257.

6. Patro, R., et al., *Salmon provides fast and bias-aware quantification of transcript expression.* Nat Methods, 2017. **14**(4): p. 417-419.

7. Kanehisa, M. and S. Goto, *KEGG: kyoto encyclopedia of genes and genomes.* Nucleic Acids Res, 2000. **28**(1): p. 27-30.

8. Lombard, V., et al., *The carbohydrate-active enzymes database (CAZy) in 2013.* Nucleic Acids Res, 2014. **42**(Database issue): p. D490-5.

9. Jolliffe, I.T. and J. Cadima, *Principal component analysis: a review and recent developments.* Philos Trans A Math Phys Eng Sci, 2016. **374**(2065): p. 20150202.

2
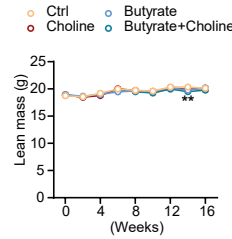
Fig. S1. Choline and butyrate have no effects on body lean mass in *APOE*3-Leiden.CETP* mice. Body lean mass was measured throughout the experimental period. Data are represented as mean±SEM (n=16-17 per group). Differences were assessed using one-way ANOVA followed by a Fisher's LSD post-test. **$P<0.01$, compared with the ctrl group.

Fig. S2. Butyrate downregulates gut microbial genes involved in lipopolysaccharide biosynthesis in *APOE*3-Leiden.CETP* mice. At the end of the study, the cecal content was collected and sequenced using metagenomics (n=10 per group). (**A**) The abundance of top 15 microbial phyla. (**B**) Top 30 significantly regulated KEGG pathway between the ctrl and butyrate groups. (**C-E**) Relative changes of the gut microbial genes involved TMA metabolic pathway between groups. (**B-E**) Comparisons between groups were performed using Wilcoxon test. *$P<0.05$; **$P<0.01$, compared with the ctrl group. KEGG, Kyoto Encyclopedia of Genes and Genomes; KO, KEGG Ortholog; TMA, trimethylamine; TMAO, trimethylamine N-oxide.
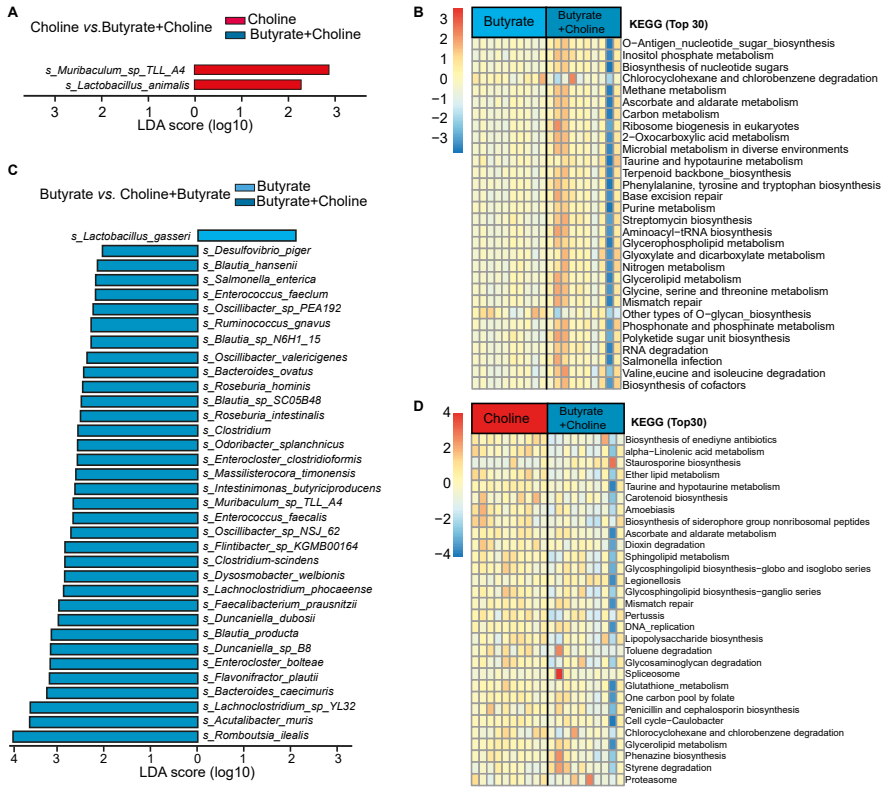
Fig. S3. Choline exerts greater effects on the gut microbial composition and function compared to butyrate in *APOE*3-Leiden.CETP* mice. (A and **C)** Linear discrimination analysis (LDA) effect size analysis was performed, and LDA scores calculated for differences in species-level abundance between groups. (**B** and **D**) Top 30 significantly regulated KEGG pathway between groups. (**B** and **D**) Comparisons between groups were performed using Wilcoxon test.
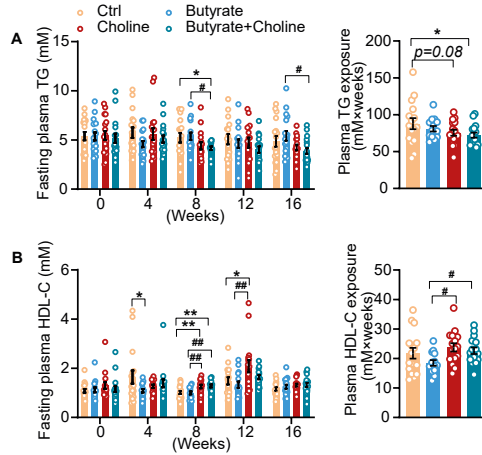
Fig. S4. Choline and butyrate do not evidently alter plasma lipid levels in *APOE*3-Leiden.CETP* mice. (A-B) Fasting plasma triglyceride (TG) and high-density lipoprotein cholesterol (HDL-C) levels were measured throughout the experimental period, and plasma TG and HDL exposure (mM x weeks) throughout the experimental period was calculated. Data are represented as mean±SEM (n=16-17 per group). Differences were assessed using one-way ANOVA followed by a Fisher's LSD post hoc test. *$P<0.05$; **$P<0.01$, compared with the ctrl group; #$P<0.05$, ##$P<0.01$, compared to the butyrate group.
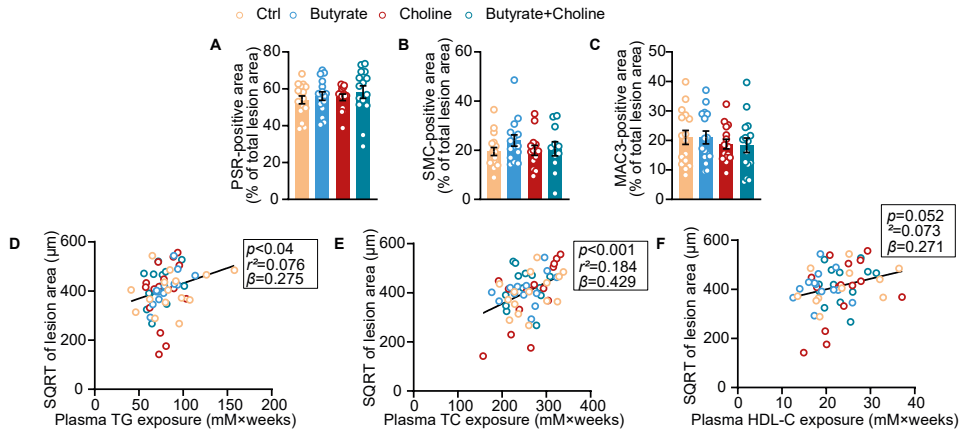
Fig. S5. Choline and butyrate have no impact on atherosclerotic lesion composition in *APOE*3-Leiden.CETP* mice. At the end of the study, atherosclerotic lesion composition was evaluated. To quantify the contents of collagen (**A**), smooth muscle cells (**B**) and macrophages (**C**) within the lesion, the valve area in the aortic root was stained with Picrosirius red (PSR), anti-α-smooth muscle cell actin (α-SMC actin) antibody and anti-MAC3 antibody, respectively. (**D-F**) The square root (SQRT) of the atherosclerotic lesion area was plotted against plasma TG exposure, total cholesterol (TC) exposure and HDL-C exposure during the 16-week treatment period, and linear regression analyses were performed. Data are represented as mean±SEM (n=13-16 per group). Differences were assessed using one-way ANOVA followed by a Fisher's LSD post hoc test.

3

Dietary choline increases brown adipose tissue activation markers and improves cholesterol metabolism in female *APOE*3-Leiden.CETP* mice

Cong Liu[1,2], Zikuan Song[1,2], Zhuang Li[1,2], Mariëtte R. Boon[1,2], Milena Schönke[1,2], Patrick C.N. Rensen[1,2,3], Yanan Wang[1,2,3]

[1] Department of Medicine, Division of Endocrinology, Leiden University Medical Center, Leiden, The Netherlands.
[2] Einthoven Laboratory for Experimental Vascular Medicine, Leiden University Medical Center, Leiden, The Netherlands.
[3] Med-X institute, Center for Immunological and Metabolic Diseases, and Department of Endocrinology, First Affiliated Hospital of Xi'an Jiaotong University, Xi'an Jiaotong University, Xi'an, China.

ABSTRACT
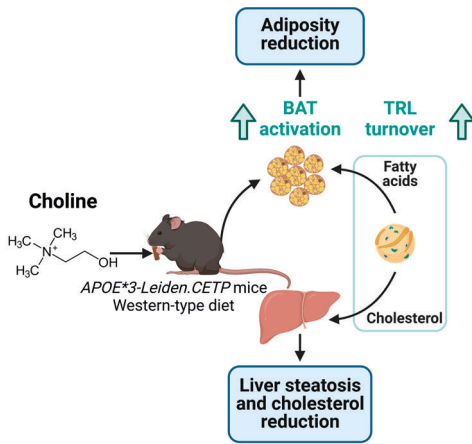
Studies in mice have recently linked increased dietary choline consumption to increased incidence of obesity-related metabolic diseases, while several clinical trials have reported an anti-obesity effect of high dietary choline intake. Since the underlying mechanisms by which choline affects obesity are incompletely understood, the aim of the present study was to investigate the role of dietary choline supplementation in adiposity. Female *APOE*3-Leiden.CETP* mice, a well-established model for human-like lipoprotein metabolism and cardiometabolic diseases, were fed a Western-type diet supplemented with or without choline (1.2%, w/w) for up to 16 weeks. Dietary choline reduced body fat mass gain, prevented adipocyte enlargement, and attenuated adipose tissue inflammation. Besides, choline ameliorated liver steatosis and damage, associated with an upregulation of hepatic genes involved in fatty acid oxidation. Moreover, choline reduced plasma cholesterol, as explained by a reduction of plasma non-HDL-cholesterol. Mechanistically, choline reduced hepatic VLDL-cholesterol secretion and enhanced the selective uptake of fatty acids from triglyceride-rich lipoprotein (TRL)-like particles by brown adipose tissue (BAT), consequently accelerating the clearance of the cholesterol-enriched TRL remnants by the liver. In *APOE*3-Leiden.CETP* mice, dietary choline reduces body fat by enhancing TRL-derived fatty acids by BAT, resulting in accelerated TRL turnover to improve hypercholesterolemia. These data provide a mechanistic basis for the observation in human intervention trials that high choline intake is linked with reduced body weight.

INTRODUCTION

Choline is an essential nutrient that has important biological functions, such as being a precursor for phospholipids (PLs) and a regulator of hepatic lipoprotein secretion [1]. However, since 2011 studies in *Apoe*$^{-/-}$ and *Ldlr*$^{-/-}$ mice have linked dietary choline to the pathogenesis of cardiometabolic diseases, related to its conversion by the gut-liver axis into trimethylamine N-oxide (TMAO) [2-4]. TMAO was shown to aggravate atherosclerosis via various mechanisms, such as promoting foam cell formation and disturbing cholesterol metabolism [3-6]. However, very recently, we and others reported that a diet rich in choline or its precursor phosphatidylcholine does not aggravate atherosclerosis development in various mouse models of atherosclerosis [7-9]. Furthermore, by using *APOE*3-Leiden.CETP mice*, a well-established mouse model for human-like cardiometabolic diseases, we also showed that plasma TMAO levels do not associate with atherosclerosis development [9].

Moreover, TMAO was previously shown to exacerbate insulin resistance and promote adiposity in diet-induced obese (DIO) and *ob/ob* mice [10-13]. Interestingly, such a correlation between plasma TMAO levels and obesity-associated metabolic disorders is not supported by clinical studies [14-19]. Studies even showed that high choline intake failed to increase plasma TMAO levels in healthy populations [20, 21] and people with obesity [22, 23]. In fact, several clinical trials reported that high choline intake is linked to reduced body weight [24, 25], lowered insulin resistance [26], and decreased cholesterol synthesis [27].These clinical findings likely indicate a beneficial effect of high dietary choline on obesity in humans.

Obesity, originating from a chronic positive energy balance, is one of the most prevalent public health concerns worldwide. Over the past decades, researchers have searched for interventions that can increase energy expenditure and/or decrease energy intake, thereby effectively combating obesity. Of note, the detection of brown adipose tissue (BAT) in human adults has sparked interest in enhancing energy expenditure through increasing thermogenic activity in brown adipocytes. BAT thermogenesis is primarily mediated by uncoupling protein 1 (UCP-1). UCP-1 transports protons, generated from the electron transport chain resulting from oxidation of glucose and fatty acids, across the mitochondrial inner membrane in a process uncoupled from adenosine triphosphate (ATP) synthesis, generating heat for non-shivering thermogenesis [28, 29]. As such, BAT activation can induce fat loss, but it remains unclear whether dietary choline promotes weight loss through activation of BAT. Thus, the aim of the present was to investigate the effect of high dietary consumption on adiposity and BAT function using a well-established humanized mouse model, i.e. *APOE*3-Leiden.CETP* mice.

3

MATERIALS AND METHODS

Animals

Female *APOE*3-Leiden.CETP* mice were generated as previously described [30]. Mice aged at 8-12 weeks were housed under standard conditions (22℃; 12/12-hour light/dark cycle) with *ad libitum* access to water and a Western-type diet (WTD; 0.15% cholesterol and 16% fat; ssniff, Soest, Germany). All mice were acclimatized to housing and the WTD for 3 weeks prior to the dietary intervention with choline. Then, based on 4-hour fasted plasma lipids, body weight and body composition, mice were randomized into two groups using RandoMice [31] to receive either WTD ('Ctrl') or WTD with free choline (1.2% w/w; 'Choline') for up to 16 weeks.

In study 1, mice (n=16 per group) were treated for 9 weeks, during which an oral lipid tolerance test (OLTT) was performed at week 6 (n=8 per group). Thereafter, *in vivo* assays tracing very low-density lipoprotein (VLDL) clearance (n=8 per group) and hepatic VLDL production (n=8 per group) were conducted at week 9.

To gain more insight in the function of adipose tissue and the liver, various adipose tissue depots and liver samples were collected (for histological analysis, n=17 per group; for mRNA expression analysis, n=10 per group) from study 2 in which mice were treated with choline for 16 weeks. Unless indicated otherwise, mice were group housed (3–5 per cage) during the experimental period to avoid stress caused by single housing.

All animal experiments were carried out according to the Institute for Laboratory Animal Research Guide for the Care and Use of Laboratory Animals, and were approved by the National Committee for Animal Experiments (Protocol No. AVD1160020172927) and by the Ethics Committee on Animal Care and Experimentation of the Leiden University Medical Center (Protocol No. PE.18.063.006 and No. PE.18.063.007). All animal procedures were conform with the guidelines from Directive 2010/63/EU of the European Parliament on the protection of animals used for scientific purposes.

Measurement of body weight and body composition

Body weight was measured weekly with a scale, and body composition of conscious mice was measured every 4 weeks using an EchoMRI-100 analyzer (EchoMRI, Houston, TX, USA).

Plasma lipid profiles and alanine transaminase measurement

Every 4 weeks, after 4-hour fasting (9:00–13:00), tail vein blood (n=16 per group) was collected into paraoxon-coated glass capillaries. Plasma was collected and measured for triglyceride (TG) and total cholesterol (TC) levels. In brief, TG and TC levels were

measured using Cobas Triglycerides (106571) and Cobas Total Cholesterol (106570) enzymatic kits (both from Roche Diagnostics, Mannheim, Germany), by adding 200 μL reagent (undiluted for TG and 3x diluted in water for TC) to 7.5 μL 5x diluted samples and incubating at room temperature for 30 min prior to measuring absorption at 492 nm versus 650 nm (for TG) or at 505 nm versus 650 nm (for TC). Plasma high-density lipoprotein cholesterol (HDL-C) and non-HDL-C levels were measured using a previously published approach [32]. Plasma alanine transaminase (ALT) levels were determined at the end of the study using Mouse ALT ELISA Kit (Abcam, Cambridge, MA, USA)

Oral lipid tolerance test

At week 6, mice (n=8 per group) were fasted for 4 hours. Then, these mice received olive oil (10 mL/kg body weight; Carbonell Traditional, Cordoba, Spain) via oral gavage. Blood was collected into paraoxon-coated glass capillaries at 0, 2, 4, 6 and 8 hours following the gavage, spun down, and plasma was used for TG measurement as described above.

In vivo plasma decay and organ uptake of fatty acids derived from very low-density lipoprotein (VLDL)-like particles

VLDL-like particles (average size 80 nm) labelled with glycerol tri[^{3}H]oleate ([^{3}H]TO) and [^{14}C]cholesteryl oleate ([^{14}C]CO) were prepared as described[33]. At week 9, mice (n=8 per group) were fasted for 4 hours (9:00–13:00) and intravenously injected (t=0 min) with the VLDL-like particles (1.0 mg TG in 200 μL PBS). Blood samples were collected from the tail vein at 0 min (before injection) and 2, 5, 10, and 15 min after injection to measure the plasma decay of [^{3}H]TO and [^{14}C]CO. After 15 min, all mice were sacrificed by CO_2 inhalation and perfused via the heart with ice cold PBS. Subsequently, tissues were isolated, transferred into High Performance glass vials (PerkinElmer, Groningen, The Netherlands) and dissolved overnight at 56℃ in 0.5 mL Solvable (PerkinElmer, Groningen, The Netherlands). Dissolved organs were mixed with 5 mL Ultima Gold scintillation fluid (PerkinElmer, Groningen, The Netherlands), and vials were placed in a Tri-Carb 2910TR Low Activity Liquid Scintillation Analyzer (PerkinElmer, Groningen, The Netherlands) to assess ^{3}H and ^{14}C activity. Disintegrations per minute of ^{3}H and ^{14}C were expressed as percentage of the injected dose per gram tissue and whole organ weight.

Hepatic VLDL production

After 9 weeks of dietary intervention, mice (n=8 per group) were fasted for 4 hours (9:00–13:00) and anaesthetized via an intraperitoneal injection (once) of 6.25 mg/kg Acepromazine (Alfasan, Woerden, The Netherlands), 6.25 mg/kg Midazolam (Roche, Mijdrecht, The Netherlands), and 0.31 mg/kg Fentanyl (Janssen-Cilag, Tilburg, The Netherlands). Anesthesia was maintained by intraperitoneal injection (3 times; every 45 min) of 0.03 mg/kg Acepromazine, 0.03 mg/kg Midazolam, and 0.001 mg/kg Fentanyl.

To ensure a deep anesthesia throughout the experimental procedure, the reflexes of mice were checked by pinching the toes of the paws, and body temperature was maintained using a heating pad. Hepatic VLDL production was assessed as previously described [34]. Using commercial kits, TG, TC, and PL (Instruchemie, Delfzijl, The Netherlands) concentrations were determined.

Adipose tissue histology

At week 16, various adipose tissue depots, including interscapular brown adipose tissue (iBAT), subscapular brown adipose tissue (sBAT), subcutaneous white adipose tissue (sWAT) and gonadal white adipose tissue (gWAT), were collected and weighed (n=17 per group). Then, formalin-fixed paraffin-embedded iBAT, sWAT and gWAT sections (5 µm thickness) were prepared for hematoxylin-eosin (H&E) staining. Moreover, iBAT and sWAT sections were processed for UCP-1 staining. Using Image J software (version 1.52a; National Institutes of Health, Bethesda, Maryland), the areas occupied by intracellular lipid vacuoles and UCP-1, as well as the size of adipocyte of gWAT and sWAT were assessed using Image J software.

Liver histology and lipid measurements

Formalin-fixed paraffin-embedded liver samples (collected at week 16; n=17 per group) were stained with H&E. The areas occupied by intracellular lipid vacuoles were quantified using Image J software. Hepatic lipids were extracted from frozen liver samples (n=10 per group) using a modified protocol from Bligh and Dyer [35]. Commercial kits were used for the measurement of hepatic TG, TC, PL and protein (Pierce, Thermo Fisher Scientific, Waltham, MA, USA). Hepatic lipids were expressed as nmol lipid per mg protein.

Gene expression analysis

Using Tripure RNA isolation reagent (Roche, Mijdrecht, The Netherlands), total RNA was extracted from snap-frozen tissues (collected at week 16; n=10 per group). Using Moloney Murine Leukemia Virus Reverse Transcriptase (Promega, Leiden, The Netherlands), complementary DNA for quantitative reverse transcriptase-PCR was generated by reverse transcription of total RNA. Then, mRNA expression was normalized to *b-actin* and *Rplp0* mRNA levels and expressed as fold change compared with the Ctrl group. Primer sequences are listed in the Supplementary material online.

Statistical analyses

Comparisons between Ctrl and Choline groups were performed using unpaired two-tailed Student's *t*-tests or two-way analysis of variance (ANOVA). Data are presented as mean ± SEM, and a *P* value less than 0.05 is considered statistically significant. All statistical analyses were performed with GraphPad Prism 9 (GraphPad Software Inc., CA, USA).

RESULTS

Dietary choline supplementation attenuates fat mass gain

To assess the effects of choline on adiposity, we fed *APOE*3-Leiden.CETP* mice a WTD with or without choline. Dietary choline supplementation did not affect food intake (**Fig. 1A**). However, choline attenuated WTD-induced body weight gain (-7% at week 9; **Fig. 1B**), as explained by reduced gain of fat mass (-18% at week 8; **Fig. 1D**) rather than lean mass (**Fig. 1C**). Furthermore, choline reduced weights of gWAT (-38%) and sWAT (-29%) (**Fig. 1E**), attenuated adipocyte enlargement of these WAT depots (gWAT, -31%; sWAT, -33%; **Fig. 1F, G**), and tended to increase UCP-1 content in sWAT (+169%; **Fig. 1G**). In gWAT, choline did not affect gene expression of adiponectin i.e. *Adipoq* (**Fig. S1A**) and common macrophage (Mφ) surface makers, but downregulated the expression of pro-inflammatory M1φ markers, including tumor necrosis factor α (*Tnfa*; -60%), C-C motif chemokine ligand 2 (*Ccl2*; -63%) and inducible nitric oxide synthase (*iNos*; -32%), and upregulated the expression of anti-inflammatory M2φ markers, including V-set immunoglobulin-domain-containing 4 (*Vsig4*; +48%) and mannose receptor C-type 1 (*Mrc1*; +28%) (**Fig. 1H**).

Choline reduces hepatic steatosis and inflammation

To evaluate the consequence of attenuated adiposity as induced by choline for hepatic steatosis, histological and biochemistry analyses were performed in livers obtained after 16 weeks of intervention. Choline reduced liver weight (-18%; **Fig. 2A**), and alleviated WTD-induced hepatic steatosis, as shown by reduced intracellular lipid vacuoles (-40%; **Fig. 2B**) and reduced hepatic TG (-30%), TC (-24%) and PL (-19%) levels (**Fig. 2C**). Choline did not affect hepatic expression of genes involved in cholesterol synthesis including 3-hydroxy-3-methylglutaryl-CoA reductase (*Hmgcr*), mevalonate kinase (*Mvk*) and sterol regulatory element-binding protein 2 (*Srebp2*), apart from slightly increasing sterol regulatory element-binding protein 1c (*Srebp1c*; +37%) (**Fig. S1B**). In contrast, choline increased hepatic expression of genes involved in fatty acid (FA) oxidation, including carnitine palmitoyl transferase 1a (*Cpt1a*, +49%) and peroxisome proliferator-activated receptor α (*Ppara*; +38%) (**Fig. 2D**). Choline also attenuated hepatic inflammation, as evidenced by downregulated hepatic mRNA expression of *Tnfa* (-56%), interleukin 1β (*Il1b*; -47%) and *Ccl2* (-75%) (**Fig. 2E**). In line with these findings, choline induced a profound reduction of plasma ALT levels (-81%; **Fig. 2F**).

Choline ameliorates hypercholesterolemia

Next, we evaluated the effects of choline on WTD-induced dyslipidemia. While choline had no effects on plasma TG levels (**Fig. S1A**), it tended to improve lipid intolerance after 6 weeks of dietary choline supplementation (**Fig. S1B**). Of note, choline reduced plasma TC levels (-29% at week 8), which was explained by lowered non-HDL-C (-29%
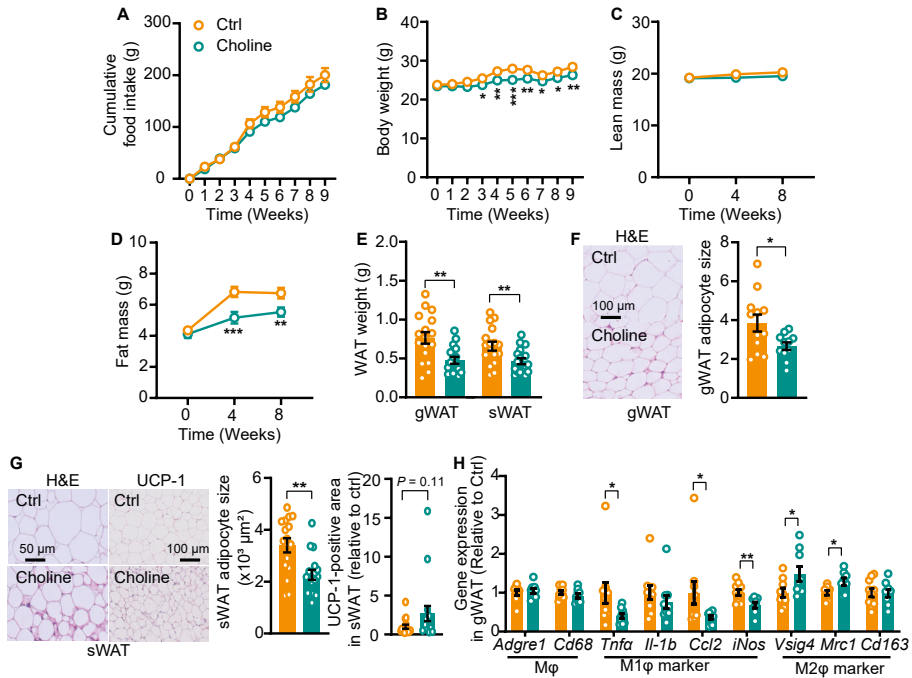
Fig 1. Choline attenuates fat mass gain and improves WAT function. (**A**) cumulative food intake, (**B**) body weight, (**C**) body lean mass and (**D**) body fat mass were monitored throughout the experimental period. (**E**) At the end of the study, various white adipose tissue depots were collected and weighed. (**F** and **G**) white adipocyte enlargement was assessed by hematoxylin-eosin (H&E) staining, and (**G**) subcutaneous white adipose tissue (sWAT) browning was evaluated by uncoupling protein-1 (UCP-1) immunostaining. (**H**) Gonadal white adipose tissue (gWAT) inflammation was assessed by quantifying expression of proinflammatory and anti-inflammatory genes. (**A-D**), data were obtained from study 1; (**E-H**) data were obtained from study 2. Data are represented as mean ± SEM (**A**, n=4-5 per group; **B-G**, n=16-17 per group; **H**, n=9-10 per group). Differences were assessed using (**A-D**) two-way ANOVA followed by Fisher's LSD test or (**E-H**) unpaired two-tailed Student's *t*-test. *$P<0.05$, **$P<0.01$, ***$P<0.001$. *Adgre1*, adhesion G protein-coupled receptor E1; *Ccl2*, chemokine C–C motif ligand 2; *Cd68*, cluster of differentiation 68; *Cd163*, cluster of differentiation 163; *Il1b*, interleukin-1β; *iNos*, inducible nitric oxide synthase; *Mrc1*, mannose receptor C-type 1; *Vsig4*, V-set and immunoglobulin domain containing 4; *Tnfa*, tumor necrosis factor α.-

at week 8) rather than HDL-C (**Fig. 3A-C**). To examine the mechanism underlying the choline-induced changes of plasma lipid levels, we examined whether choline affects hepatic VLDL production. Despite choline upregulating the hepatic mRNA expression of microsomal triglyceride transfer protein (*Mttp*; +45%) and apolipoprotein B (*Apob*; +58%), choline did not affect the production rate of VLDL-TG and VLDL-apolipoprotein B (ApoB) (**Fig. 3D-F**). In contrast, choline decreased the amount of PL (-30%) and TC (-38%) per ApoB, respectively (**Fig. 3G**). Since each VLDL particle contains a single apoB molecule, these data indicate that choline does not affect VLDL particle production, but largely reduces the hepatic secretion of cholesterol within VLDL.
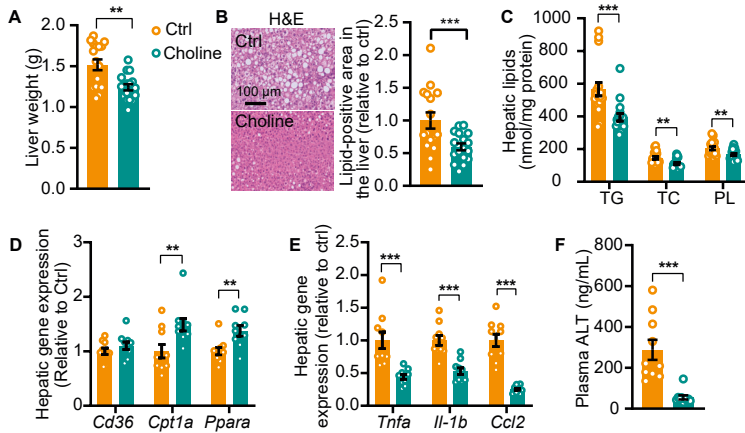
Fig 2. Choline reduces hepatic steatosis and inflammation. At the end of the study, (**A**) liver weight was measured, (**B**) hepatic lipid content was assessed by H&E staining, and hepatic levels of (**C**) triglyceride (TG), total cholesterol (TC) and phospholipid (PL) were determined. The relative mRNA expression of genes involved in lipid handling (**D**) and inflammation (**E**) was determined in the liver. (**F**) Plasma alanine transaminase (ALT) was also measured. Data were obtained from study 2 and are represented as mean ± SEM (**A-C**, n=16-17 per group; **D-F**, n=9-10 per group). Differences were assessed using unpaired two-tailed Student's *t*-test. **P<0.01, ***P<0.001. *Cd36*, cluster of differentiation 36; *Cpt1*, carnitine palmitoyl transferase 1; transcription factor 1; *Ppara*, peroxisome proliferator activated receptor α; *Tnfa*, tumor necrosis factor α; *Il1b*, interleukin-1β; *Ccl2*, chemokine C–C motif ligand 2.

Choline activates BAT to accelerate TG-derived FA uptake, accompanied by increased hepatic uptake of cholesterol-enriched remnants

Besides profoundly reducing VLDL-cholesterol secretion, we hypothesized that choline may also improve hypercholesterolemia by accelerating VLDL-cholesterol clearance. Therefore, after 9 weeks of treatment, we intravenously injected mice with VLDL-like particles labelled with [³H]TO and [¹⁴C]CO. Interestingly, choline accelerated the clearance of [³H]TO from plasma (**Fig. 4A**), which was primarily caused by increased uptake of [³H]TO-derived [³H]oleate by BAT (iBAT, +66%; sBAT, 75%; **Fig. 4B, S2A**). Concomitantly, choline increased the plasma clearance of [¹⁴C]CO (**Fig. 4C**), which was attributed to the increased uptake of [¹⁴C]CO by the liver (+85%; **Fig. 4D, S2B**). We did not observe significant effects of choline on the expression of key genes involved in BAT thermogenesis (i.e. *Ucp1*; PRD1-BF1-RIZ1 homologous-domain containing 16; *Prdm16*; and iodothyronine deiodinase 2; *Dio2*; data not shown). However, as the increased FA uptake by BAT is an indicator of activated BAT, we next quantified intracellular lipid vacuoles and UCP-1 protein content in BAT obtained from this study. Consistently, choline reduced BAT weight (-17%; **Fig. 4E**), and decreased lipid droplet content (-45%; **Fig. 4F**) and increased UCP-1 level (+11%; **Fig. 4F**) in BAT, which further evidences BAT activation.
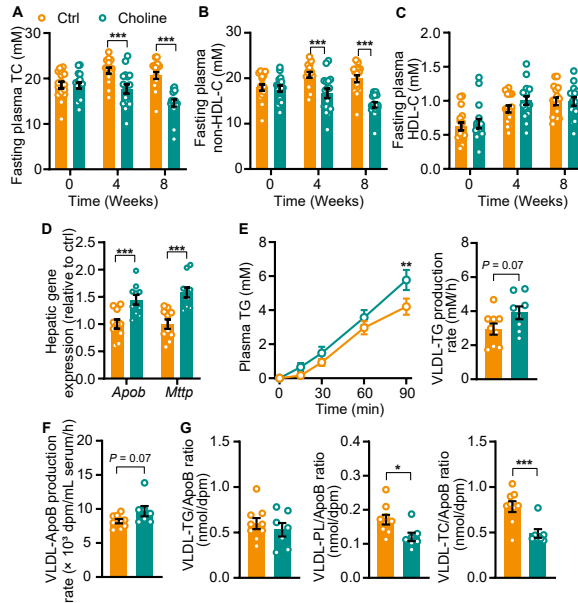
Fig 3. Choline ameliorates hypercholesterolemia. (**A-C**) Plasma cholesterol levels (n=14-16 per group) were measured throughout the study. (**D**) Hepatic expression of genes involved in very low-density lipoprotein (VLDL) production was quantified (n=9-10 per group). At week 9, the production rate of (**E**) VLDL-TG and (**F**) VLDL-apolipoprotein B (ApoB) was determined (n=6-8 per group), and (**G**) the amount of TG, protein, PL and TC within VLDL was measured (n=6-8 per group). Data were obtained from study 1 and are represented as mean±SEM. Differences were assessed using (**A-C** and **E** line graph) two-way ANOVA followed by Fisher's LSD test or unpaired two-tailed Student's t-test. *$P<0.05$, **$P<0.01$, ***$P<0.001$.

DISCUSSION

Previous studies in mice reported that choline promotes the development of obesity-related metabolic diseases, as caused by the generation of TMAO through the gut-liver axis [2-4]. However, several clinical trials reported that high choline intake is linked to reduced body weight [24, 25] and lowered insulin resistance [26]. Since the underlying mechanisms by which choline affects obesity remain unclear, the present study thus aimed to investigate the role of choline in adiposity by exposing *APOE*3-Leiden.CETP* mice to a WTD supplemented with or without choline. We demonstrated that dietary choline supplementation reduces body fat, ameliorate hepatic steatosis and lowers plasma cholesterol in this model.

First, by performing mechanistic studies we demonstrated the reduction in body fat induced by choline is accompanied by activation of BAT. Interestingly, previous mouse studies reported that choline and its metabolite TMAO promote obesity [11-13]. This seemingly discrepancy with our study is likely explained by different mouse models.
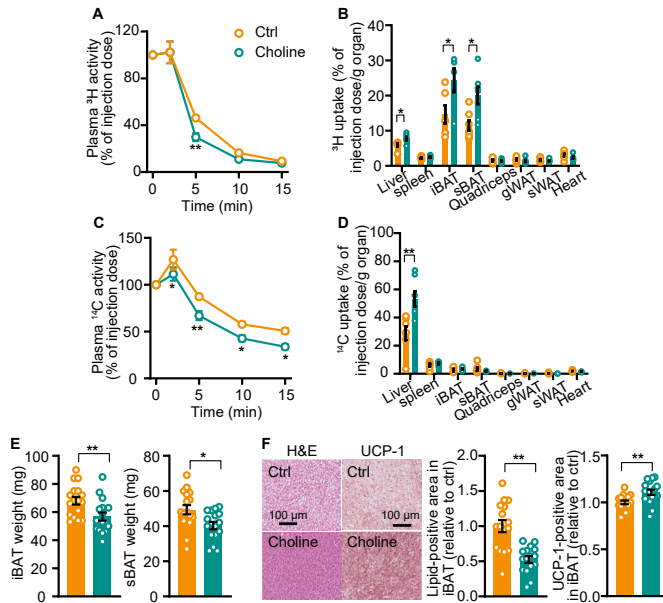
Fig 4. Choline activates BAT to accelerate TG-derived FA uptake, accompanied by increased hepatic uptake of cholesterol-enriched remnants. At week 9, the clearance of ^{3}H (**A**) and ^{14}C (**C**) from plasma and the uptake of ^{3}H (**B**) and ^{14}C (**D**) by various tissues were assessed. At week 16, various BAT deports were collected and weighed (**E**). In iBAT, lipid droplet content and UCP-1 content were assessed by H&E staining and UCP-1 immunostaining, respectively (**F**). (**A-D**) Data were obtained from study 1. (**E-F**) Data were obtained from study 2. Data are represented as mean±SEM (**A-D**, n=6-8; **E-F**, n=16-17). Differences were assessed using (**A and C**) two-way ANOVA followed by Fisher's LSD test or unpaired two-tailed Student's *t*-test. *$P<0.05$, **$P<0.01$. iBAT, interscapular brown adipose tissue; sBAT, subscapular brown adipose tissue.

While we used *APOE*3-Leiden.CETP* mice, a well-established model with human-like lipoprotein metabolism, other studies used either DIO or *ob/ob* mice [11-13]. It should be noted that we recently showed that dietary choline beneficially modulates the gut microbiome and has no impact on plasma TMAO levels in *APOE*3-Leiden.CETP* mice when fed the same diet as in the present study [36]. Similarly, another study showed that by feeding a choline-enriched diet, *Apoe$^{-/-}$* mice expressing CETP have lower TMAO levels than *ApoE$^{-/-}$* without CETP expression [37]. Likewise, long-term high-choline diet consumption did not increase TMAO levels in clinical trials, possibly as a consequence of human CETP expression [20-23]. In fact, high dietary choline intake has been associated with favorable body composition [24], which might be attributed to increased energy metabolism. In the present study, we observed that choline had no impact on food intake while promoting BAT activation as evidenced by increasing VLDL-derived FA uptake by BAT. BAT has a high metabolic demand, and metabolic substrates are crucial for BAT to initiate and maintain thermogenic function [38].

Activated BAT leads to increased utilization of various metabolic substrates, mainly TG-derived FAs, which results in heat production through uncoupling of mitochondrial respiration from ATP synthesis. Indeed, choline prevented lipid overloading in both BAT and WAT, accompanied by alleviation of WAT inflammation. Given that BAT is present and active in human adults [39], we thus speculate that our data provide a mechanistic explanation for the observation that choline improves body composition in humans. Future studies are needed to investigate the role of dietary choline intake in energy expenditure in relation to BAT activation in various animal models and humans. Besides, in the present study we used free choline, so it would be also interesting to investigate the effects of choline precursors (e.g. phosphatidylcholine) on adiposity.

We also demonstrated that choline ameliorates liver steatosis and inflammation. In obesity, adipose tissue dysfunction induces a high free FA flux from WAT towards the liver, leading to liver steatosis [40]. Therefore, the fact that choline attenuated adiposity and improved adipose tissue function may already in part explain reduced ectopic lipid deposition in organs such as the liver. In addition, we observed increased hepatic expression of genes involved in hepatic FA oxidation. In line with our findings, choline has been shown to upregulate β-oxidation in an *in vitro* hepatocellular steatosis model [41]. Although choline had minor effects on hepatic mRNA expression of the transcription factors involved in cholesterol synthesis, we cannot exclude that post-translational modulation of SREBPs may be involved in the observed improvement of hepatic cholesterol metabolism, which could be subject of future studies. In addition, we observed a trend towards increased hepatic TG secretion from the liver as constituent of VLDL, which would be in line with published data [42], but this effect was not significant. Furthermore, we showed that choline reduces hepatic inflammation, which is consistent with previous studies showing that choline inhibits liver damage [43]. The anti-inflammatory effect of choline is possibly a concomitant effect of the reduced hepatic lipids, confirming a previous study showing that choline alleviated liver injury by normalizing hepatic lipid metabolism [43].

Finally, we demonstrate that choline reduces plasma cholesterol, as shown by a reduction of non-HDL-C rather than HDL-C. This data is in agreement with human studies showing that increased intake of choline-enriched food (i.e., eggs) is associated with an improved plasma lipid profile [25, 27]. Our mechanistic studies revealed that choline both reduced hepatic cholesterol secretion and enhanced lipolytic conversion of VLDL by activated BAT accompanied by increased clearance of cholesterol by the liver. Therefore, the reduction of cholesterol is probably the combined effect of reduced hepatic cholesterol secretion and enhanced hepatic cholesterol clearance via the APOE-

LDLR pathway that is fully functional in APOE*3-Leiden.CETP mice. On the other hand, BAT activation for instance via cold exposure, lowers plasma TG [32], an effect that we did not observe in our study. This may imply that the nonsignificant mild increase in hepatic VLDL-TG secretion may in the long term contribute to higher hepatic TG output which counteracts a potential TG reduction induced by BAT activation.

In conclusion, our present study uncovers beneficial effects of choline on adiposity and plasma cholesterol. Mechanistically, choline reduces body fat accompanied by activating BAT, resulting in accelerated hepatic uptake of cholesterol-enriched lipoprotein remnants, which in combination with lower hepatic VLDL-cholesterol secretion and reduces plasma cholesterol.

3

Author contributions
CL designed the study, carried out the research, analyzed and interpreted the results, and wrote and revised the manuscript. ZS carried out the research, interpreted the results, reviewed and revised the manuscript. ZL carried out the research, interpreted the results, reviewed and revised the manuscript, and obtained funding. MRB advised the study and reviewed the manuscript. MS interpreted the results, reviewed and revised the manuscript. PCNR designed and advised the study, interpreted the results, edited, reviewed and revised the manuscript and obtained funding. YW designed and advised the study, interpreted the results, reviewed and revised the manuscript and obtained funding.

REFERENCES

1. Zeisel, S.H. and K.A. da Costa, *Choline: an essential nutrient for public health.* Nutr Rev, 2009. **67**(11): p. 615-23.

2. Krueger, E.S., T.S. Lloyd, and J.S. Tessem, *The Accumulation and Molecular Effects of Trimethylamine N-Oxide on Metabolic Tissues: It's Not All Bad.* Nutrients, 2021. **13**(8).

3. Wang, Z., et al., *Gut flora metabolism of phosphatidylcholine promotes cardiovascular disease.* Nature, 2011. **472**(7341): p. 57-63.

4. Koeth, R.A., et al., *Intestinal microbiota metabolism of L-carnitine, a nutrient in red meat, promotes atherosclerosis.* Nat Med, 2013. **19**(5): p. 576-85.

5. Seldin, M.M., et al., *Trimethylamine N-Oxide Promotes Vascular Inflammation Through Signaling of Mitogen-Activated Protein Kinase and Nuclear Factor-kappaB.* J Am Heart Assoc, 2016. **5**(2).

6. Collins, H.L., et al., *L-Carnitine intake and high trimethylamine N-oxide plasma levels correlate with low aortic lesions in ApoE(-/-) transgenic mice expressing CETP.* Atherosclerosis, 2016. **244**: p. 29-37.

7. Aldana-Hernandez, P., et al., *Dietary phosphatidylcholine supplementation reduces atherosclerosis in Ldlr(-/-) male mice(2).* J Nutr Biochem, 2021. **92**: p. 108617.

8. Aldana-Hernandez, P., et al., *Dietary Choline or Trimethylamine N-oxide Supplementation Does Not Influence Atherosclerosis Development in Ldlr-/- and Apoe-/- Male Mice.* J Nutr, 2020. **150**(2): p. 249-255.

9. Liu, C., et al., *Choline and butyrate beneficially modulate the gut microbiome without affecting atherosclerosis in APOE*3-Leiden.CETP mice.* Atherosclerosis, 2022. **362**: p. 47-55.

10. Gao, X., et al., *Dietary trimethylamine N-oxide exacerbates impaired glucose tolerance in mice fed a high fat diet.* J Biosci Bioeng, 2014. **118**(4): p. 476-81.

11. Schugar, R.C., et al., *The TMAO-Producing Enzyme Flavin-Containing Monooxygenase 3 Regulates Obesity and the Beiging of White Adipose Tissue.* Cell Rep, 2017. **19**(12): p. 2451-2461.

12. Chen, S., et al., *Trimethylamine N-Oxide Binds and Activates PERK to Promote Metabolic Dysfunction.* Cell Metab, 2019. **30**(6): p. 1141-1151 e5.

13. Schugar, R.C., et al., *Gut microbe-targeted choline trimethylamine lyase inhibition improves obesity via rewiring of host circadian rhythms.* Elife, 2022. **11**.

14. Golzarand, M., P. Mirmiran, and F. Azizi, *Association between dietary choline and betaine intake and 10.6-year cardiovascular disease in adults.* Nutrition Journal, 2022. **21**(1).

15. Meyer, K.A., et al., *Microbiota-Dependent Metabolite Trimethylamine N-Oxide and Coronary Artery Calcium in the Coronary Artery Risk Development in Young Adults Study (CARDIA).* J Am Heart Assoc, 2016. **5**(10).

16. Zhu, C., et al., *Whole egg consumption increases plasma choline and betaine without affecting TMAO levels or gut microbiome in overweight postmenopausal women.* Nutr Res, 2020. **78**: p. 36-41.

17. Taesuwan, S., et al., *Associations of choline intake with hypertension and blood pressure among older adults in cross-sectional 2011-2014 National Health and Nutrition Examination Survey (NHANES) differ by BMI and comorbidity status.* British Journal of Nutrition, 2022. **128**(1): p. 145-153.

18. Skagen, K., et al., *The Carnitine-butyrobetaine-trimethylamine-N-oxide pathway and its association with cardiovascular mortality in patients with carotid atherosclerosis.* Atherosclerosis, 2016. **247**: p. 64-9.

19. Koay, Y.C., et al., *Plasma levels of trimethylamine-N-oxide can be increased with 'healthy' and 'unhealthy' diets and do not correlate with the extent of atherosclerosis but with plaque instability.* Cardiovasc Res, 2021. **117**(2): p. 435-449.

20. Lemos, B.S., et al., *Effects of Egg Consumption and Choline Supplementation on Plasma Choline and Trimethylamine-N-Oxide in a Young Population.* J Am Coll Nutr, 2018. **37**(8): p. 716-723.

21. DiMarco, D.M., et al., *Intake of up to 3 Eggs/Day Increases HDL Cholesterol and Plasma Choline While Plasma Trimethylamine-N-oxide is Unchanged in a Healthy Population.* Lipids, 2017. **52**(3): p. 255-263.

22. *Whole egg consumption increases plasma choline and betaine without affecting TMAO levels or gut microbiome in overweight postmenopausal women.*

23. Thomas, M.S., et al., *Comparison between Egg Intake versus Choline Supplementation on Gut Microbiota and Plasma Carotenoids in Subjects with Metabolic Syndrome.* Nutrients, 2022. **14**(6).

24. Mlodzik-Czyzewska, M.A., et al., *Associations of plasma betaine, plasma choline, choline intake, and MTHFR polymorphism (rs1801133) with anthropometric parameters of healthy adults are sex-dependent.* J Hum Nutr Diet, 2022. **35**(4): p. 701-712.

25. Thomas, M.S., et al., *Eggs Improve Plasma Biomarkers in Patients with Metabolic Syndrome Following a Plant-Based Diet-A Randomized Crossover Study.* Nutrients, 2022. **14**(10).

26. Gao, X., Y.B. Wang, and G. Sun, *High dietary choline and betaine intake is associated with low insulin resistance in the Newfoundland population.* Nutrition, 2017. **33**: p. 28-34.

27. Lemos, B.S., et al., *Intake of 3 Eggs per Day When Compared to a Choline Bitartrate Supplement, Downregulates Cholesterol Synthesis without Changing the LDL/HDL Ratio.* Nutrients, 2018. **10**(2).

28. Garlid, K.D., M. Jaburek, and P. Jezek, *The mechanism of proton transport mediated by mitochondrial uncoupling proteins.* FEBS Lett, 1998. **438**(1-2): p. 10-4.

29. Nedergaard, J., et al., *UCP1: the only protein able to mediate adaptive non-shivering thermogenesis and metabolic inefficiency.* Biochim Biophys Acta, 2001. **1504**(1): p. 82-106.

30. Westerterp, M., et al., *Cholesteryl ester transfer protein decreases high-density lipoprotein and severely aggravates atherosclerosis in APOE*3-Leiden mice.* Arterioscler Thromb Vasc Biol, 2006. **26**(11): p. 2552-9.

31. van Eenige, R., et al., *RandoMice, a novel, user-friendly randomization tool in animal research.* PLoS One, 2020. **15**(8): p. e0237096.

32. Berbee, J.F., et al., *Brown fat activation reduces hypercholesterolaemia and protects from atherosclerosis development.* Nat Commun, 2015. **6**: p. 6356.

33. Rensen, P.C., et al., *Selective liver targeting of antivirals by recombinant chylomicrons--a new therapeutic approach to hepatitis B.* Nat Med, 1995. **1**(3): p. 221-5.

34. Liu, C., et al., *Pharmacological treatment with FGF21 strongly improves plasma cholesterol metabolism to reduce atherosclerosis.* Cardiovasc Res, 2022. **118**(2): p. 489-502.

35. Bligh, E.G. and W.J. Dyer, *A rapid method of total lipid extraction and purification.* Can J Biochem Physiol, 1959. **37**(8): p. 911-7.

36. Liu, C., et al., *Choline and butyrate beneficially modulate the gut microbiome without affecting atherosclerosis in APOE*3-Leiden.CETP mice.* Atherosclerosis, 2022.

37. Collins, H.L., et al., *Choline Supplementation Does Not Promote Atherosclerosis in CETP-Expressing Male Apolipoprotein E Knockout Mice.* Nutrients, 2022. **14**(8).

38. Wang, G.X., X.Y. Zhao, and J.D. Lin, *The brown fat secretome: metabolic functions beyond thermogenesis.* Trends Endocrinol Metab, 2015. **26**(5): p. 231-7.

3

39. Harms, M. and P. Seale, *Brown and beige fat: development, function and therapeutic potential.* Nat Med, 2013. **19**(10): p. 1252-63.

40. Polyzos, S.A., J. Kountouras, and C.S. Mantzoros, *Obesity and nonalcoholic fatty liver disease: From pathophysiology to therapeutics.* Metabolism, 2019. **92**: p. 82-97.

41. Zhu, J., et al., *The effects of choline on hepatic lipid metabolism, mitochondrial function and antioxidative status in human hepatic C3A cells exposed to excessive energy substrates.* Nutrients, 2014. **6**(7): p. 2552-71.

42. Corbin, K.D. and S.H. Zeisel, *Choline metabolism provides novel insights into nonalcoholic fatty liver disease and its progression.* Current Opinion in Gastroenterology, 2012. **28**(2): p. 159-165.

43. Al Rajabi, A., et al., *Choline supplementation protects against liver damage by normalizing cholesterol metabolism in Pemt/Ldlr knockout mice fed a high-fat diet.* J Nutr, 2014. **144**(3): p. 252-7.

SUPPLEMENT

Supporting table 1. List of polymerase chain reaction primer sequences used in mRNA expression analysis.

Gene	Forward primer (5'-3')	Reverse Primer (5'-3')
Actb	AACCGTGAAAAGATGACCCAGAT	CACAGCCTGGATGGCTACGTA
Adgre1	CTTTGGCTATGGGCTTCCAGTC	GCAAGGAGGACAGAGTTTATCGTG
Adipoq	CTCCACCCAAGGGAACTTGT	TAGGACCAAGAAGACCTGCATC
Apob	GCCCATTGTGGACAAGTTGATC	CCAGGACTTGGAGGTCTTGGA
Rplp0	GGACCCGAGAAGACCTCCTT	GCACATCACTCAGAATTTCAATGG
Ccl2	GCATCTGCCCTAAGGTCTTCA	TTCACTGTCACACTGGTCACTCCTA
Cd36	GCAAAGAACAGCAGCAAAATC	CAGTGAAGGCTCAAAGATGG
Cd68	ATCCCCACCTGTCTCTCTCA	TTGCATTTCCACAGCAGAAG
Cd163	CTCAGGAAACCAATCCCAGA	CAAGAGCCCTCGTGGTAGAC
Cpt1a	GAGACTTCCAACGCATGACA	ATGGGTTGGGGTGATGTAGA
Hmgcr	CCGGCAACAACAAGATCTGTG	ATGTACAGGATGGCGATGCA
Il1b	GCAACTGTTCCTGAACTCAACT	ATCTTTTGGGGTCCGTCAACT
iNos	CGGGCATCTGGTAGCCAGCG	TGGCAACATCAGGTCGGCCAT
Mrc1	GAGAGCCAAGCCATGAGAAC	GTCTGCACCCTCCGGTACTA
Mvk	GCCTTGAACTTGAGAACTTTCC	CACCTGCTTAATACCGATGTTG
Mttp	CTCTTGGCAGTGCTTTTTCTCT	GAGCTTGTATAGCCGCTCATT
Ppara	ATGCCAGTACTGCCGTTTTC	GGCCTTGACCTTGTTCATGT
Srebp1c	AGCCGTGGTGAGAAGCGCAC	ACACCAGGTCCTTCAGTGATTTGCT
Srebp2	TGAAGCTGGCCAATCAGAAAA	ACATCACTGTCCACCAGACTGC
Tnfa	AGCCCACGTCGTAGCAAACCAC	TCGGGGCAGCCTTGTCCCTT
Vsig4	GGATCCCACCCCACCCTAAAAACA	CTCGAGTCAGCAGGCAGGAATAGA

Actb, β-actin; *Adgre1*, adhesion G protein-coupled receptor E1; *Adipoq*, Adiponectin; *Apob*, apolipoprotein B; *Ccl2*, C-C motif chemokine ligand 2; *Cd36*, cluster of differentiation 36; *Cd68*, cluster of differentiation 68; *Cd163*, cluster of differentiation 163; *Cpt1a*, carnitine palmitoyl transferase 1α; *Hmgcr*, 3-hydroxy-3-methylglutaryl-CoA reductase; *Il1b*, interleukin-1β; *iNos*, inducible nitric oxide synthase; *Mrc1*, mannose receptor C-type 1; *Mvk*, mevalonate kinase; *Mttp*, microsomal triglyceride transfer protein; *Ppara*, peroxisome proliferator-activated receptor α; *Srebp*, sterol regulatory element-binding protein; *Rplp0*, ribosomal protein lateral stalk subunit p0; *Tnfa*, tumor necrosis factor α; *Vsig4*, V-set immunoglobulin-domain-containing 4.
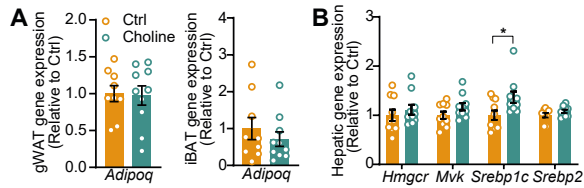
Fig. S1. Choline does not affect adipose tissue expression of adiponectin and has minor effects on hepatic expression of cholesterol synthesis genes. *APOE*3-Leiden.CETP* mice were fed a Western-type diet without and with choline for 16 weeks. (**A**) At the end of the study, gonadal white adipose tissue (gWAT) and interscapular brown adipose tissue (iBAT) was collected, and gene expression of adiponectin was determined in these adipose tissue depots. (**B**) In addition, the liver was also collected, and the expression of genes involved in cholesterol synthesis was measured in the liver. Data were obtained from study 2 and are represented as mean±SEM (n=8-10 per group). Differences were assessed using unpaired two-tailed Student's *t*-test. *$P<0.05$.
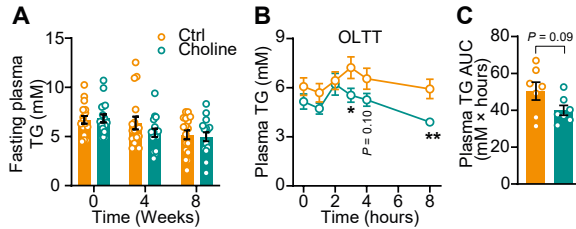
Fig. S2. Choline tends to improve lipid intolerance. *APOE*3-Leiden.CETP* mice were fed a Western-type diet without and with choline for 9 weeks. (**A**) At 0, 4 and 8 weeks, plasma triglyceride (TG) levels were measured. At week 6, (**B**) an oral lipid tolerance test (OLTT) was performed, and the area under the curve (AUC) of plasma TG during OLTT was calculated. Data were obtained from study 1 and are represented as mean±SEM (**A**, n=15-16 per group; **B**, n=6-8 per group). Differences were assessed using (**A** and **B** line graph) two-way ANOVA followed by Fisher's LSD test or (**B** bar graph) unpaired two-tailed Student's *t*-test. **$P<0.01$.
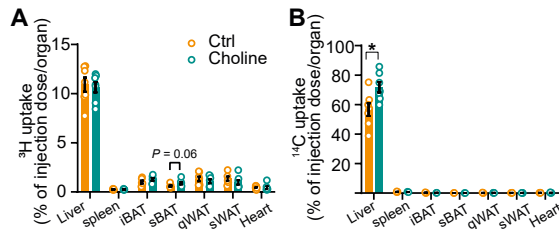
Fig. S3. Choline increases cholesterol-enriched remnant uptake by the liver. *APOE*3-Leiden.CETP* mice were fed a Western-type diet without and with choline for 9 weeks. At week 9, uptake of (**A**) ^{3}H and (**B**) ^{14}C by indicated organs was evaluated. Data were obtained from study 1 and are represented as mean±SEM (n=6-8 per group). Differences were assessed using unpaired two-tailed Student's *t*-test. *$P<0.05$. iBAT, interscapular brown adipose tissue; sBAT, subscapular brown adipose tissue; subcutaneous white adipose tissue (sWAT), gonadal white adipose tissue (gWAT).

4

γ-hydroxybutyric acid attenuates diet-induced metabolic dysfunction in developing and existing obesity

Cong Liu[1,2], Mik Zwaan[1,2], Aswin Verhoeven[3], Mink S. Schinkelshoek[4], Rolf Fronczek[4], Gert Jan Lammers[4], Yanan Wang[1,2,5], Martin Giera[3], Mariëtte R. Boon[1,2], Patrick C.N. Rensen[1,2,5], Milena Schönke[1,2]

[1] Department of Medicine, Division of Endocrinology, Leiden University Medical Center, Leiden, 2333 ZA, The Netherlands.
[2] Einthoven Laboratory for Experimental Vascular Medicine, Leiden University Medical Center, Leiden, 2333 ZA, The Netherlands.
[3] Center for Proteomics and Metabolomics, Leiden University Medical Center, Leiden, 2333 ZA, The Netherlands.
[4] Department of Neurology, Division of Endocrinology, Leiden University Medical Center, Leiden, 2333 ZA, The Netherlands.
[5] Med-X institute, Center for Immunological and Metabolic Diseases, and Department of Endocrinology, First Affiliated Hospital of Xi'an Jiaotong University, Xi'an Jiaotong University, Xi'an, 710061, China.

ABSTRACT
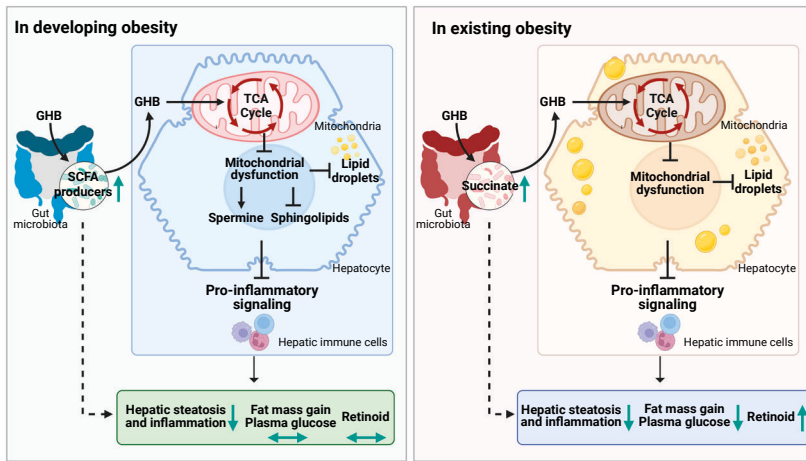
The narcolepsy drug γ-hydroxybutyric acid (GHB) promotes weight loss via unknown mechanisms. Here, we aimed to unveil the metabolic mechanisms underlying GHB-induced weight reduction in obesity. Furthermore, we aimed to examine whether GHB administration also confers weight loss during the development of obesity. We investigated the role of oral GHB treatment in body weight control in high fat diet (HFD)-induced developing and existing obesity in C57BL/6J mice. In existing obesity, but not in developing obesity, GHB attenuated HFD-induced fat mass gain, glucose intolerance and insulin resistance. However, in both metabolic conditions, GHB alleviated HFD-induced hepatic steatosis and inflammation. This was accompanied by improved hepatic mitochondrial dysfunction, as evidenced by upregulated hepatic genes encoding mitochondrial respiratory complexes. In line with this, in developing obesity, GHB alleviated the accumulation of toxic sphingolipids in the liver and in the circulation. In existing obesity, GHB prevented hepatic loss of retinoids and increased circulating acyl-carnitine, a substrate for brown fat combustion. Consistently, GHB alleviated HFD-induced adipose tissue dysfunction in obese mice, as evidenced by increased UCP-1 abundance in brown fat and decreased white adipocyte size and white fat inflammation. Moreover, GHB beneficially influenced the gut microbial composition, as shown by enrichment of short chain fatty acid producers in developing obesity, and anti-inflammatory and succinate-producers in existing obesity. Collectively, GHB promotes metabolic health in developing and existing obesity, which is associated with improved hepatic mitochondrial function, and likely involves beneficial modulation of the gut microbial composition. Our findings thus uncover previously unknown metabolic effects of GHB related to body weight management, and provide novel insights for new therapeutic handles for treating obesity and its related diseases.

INTRODUCTION

Obesity, one of the most prevalent public health concerns worldwide, is recognized as a major risk factor for the development of metabolic complications, such as type 2 diabetes (T2D) [1] and non-alcoholic fatty liver disease (NAFLD) [2]. Although lifestyle changes, medications and bariatric surgery are adopted in the clinic for body weight management [3, 4], the prevalence of obesity and its associated metabolic diseases continues to increase [4-6]. Therefore, additional therapeutics and strategies for the treatment of obesity are still needed.

Clinical studies have reported that γ-hydroxybutyric acid (GHB) treatment exerts weight loss-promoting effects [7-9]. GHB is naturally present in the mammalian brain where it acts as a neurotransmitter and neuromodulator, but it is also registered as a drug for treating the sleep disorder narcolepsy [10]. Narcolepsy commonly causes an increase in body weight after disease onset, frequently leading to obesity [11-13]. Despite being clinically used in the treatment of narcolepsy, GHB is unlikely to be prescribed as anti-obesity drug due to its central effects and its misuse-associated adverse effects (e.g. severe respiratory depression) [14]. However, elucidating the underlying mechanisms by which GHB reduces body weight may reveal therapeutic handles for the development of effective body weight control medications.

Although binding of GHB to brain-specific sites is well established and proposed to explain its neuro-biologic [10, 15] and neuro-pharmacologic properties [14, 16], the metabolic effects of GHB are speculated to be mediated by peripheral organs [17-19]. In particular, the liver is the primary organ involved in GHB metabolism [17, 20-22], as evidenced by studies showing that approximately 95-98% of administered GHB is metabolized in the liver [22, 23]. Within the liver, the major route of exogenous GHB metabolism is oxidation in the mitochondria of hepatocytes, where GHB can either directly undergo β-oxidation or can be oxidized via succinic semialdehyde to succinate. Consequently, GHB is transformed to carbon dioxide and water through the tricarboxylic acid (TCA) cycle [22].

Accumulating evidence has shown that the dysregulation of TCA cycle activity and mitochondrial function in the liver are associated with aberrant hepatocyte lipid accumulation [25, 26]. Given that the degree of liver lipid overload is directly linked to the severity of insulin resistance [27] and aberrant fat expansion [28-30], we hypothesized that GHB treatment may improve hepatic mitochondrial function to reduce hepatic lipid overload, thereby promoting weight loss. In addition, GHB is a short chain fatty acid (SCFA), and administration of the SCFAs butyrate and propionate

4

alleviates obesity-associated metabolic diseases at least partially through the beneficial modulation of the gut microbiota [31, 32]. Therefore, GHB treatment may also alter the gut microbial composition to exert weight loss-promoting effects.

In the present study, we tested the hypothesis that GHB administration beneficially modulates the function of the liver and/or the gut microbiota to improve obesity and its related disorders.

MATERIALS AND METHODS

Please see the **Supporting Information** for a detailed description of experimental procedures.

Animals and treatments

Male C57BL/6J mice were purchased from The Jackson Laboratory. Mice were group-housed under standard conditions (22℃; 12/12-hour light/dark cycle) with *ad libitum* access to water and rodent chow diet (Standard Rodent Diet 801203, Special Diets Services, United Kingdom), unless indicated otherwise. All animal experiments were carried out according to the Institute for Laboratory Animal Research Guide for the Care and Use of Laboratory Animals, and were approved by the National Committee for Animal Experiments (Protocol No. AVD1160020173305) and by the Ethics Committee on Animal Care and Experimentation of the Leiden University Medical Center (Protocol No. PE.18.034.042). All animal procedures were conform with the guidelines from Directive 2010/63/EU of the European Parliament on the protection of animals used for scientific purposes.

To evaluate the effects of GHB treatment on body weight control in existing obesity, we conducted a first therapeutic (T) experiment, in which 8-weeks-old mice were fed a high fat diet (HFD; 45% fat; ssniff, Soest, Germany) for 8 weeks to induce obesity. Then, based on body weight, body composition and 4-hour fasted plasma glucose and lipids, these mice were randomized into 2 groups (n = 8 per group) using RandoMice [33] to receive either GHB treatment ('T-GHB'; 150 mg/kg body weight via daily oral gavage, according to a pilot dose-finding study showing that this dosage did not cause a catatonic state in mice) or sterile-filtered water ('T-Vehicle') for 8 weeks. Moreover, to explore whether GHB administration confers weight loss effects in developing obesity, in a second preventive (P) experiment, mice at the age of 8 weeks were randomized into 2 groups (n = 8 per group). Then, they were fed a HFD while being administered with either GHB ('P-GHB'; 150 mg/kg body weight via daily oral gavage) or sterile-filtered water ('P-Vehicle') for 8 weeks.

Statistical analyses

Comparisons between two groups were performed using unpaired two-tailed Student's *t*-tests or two-way analysis of variance (ANOVA), unless indicated otherwise. Data are presented as mean ± SEM, and a *P* value less than 0.05 is considered statistically significant. All statistical analyses were performed with GraphPad Prism 9 (GraphPad Software Inc., CA, USA).

RESULTS

Oral administration of GHB attenuates fat mass gain and improves glucose control in existing obesity

To elucidate the mechanisms underlying GHB-mediated weight loss in obesity, we fed 8-week-old male wild-type C57BL/6J mice a HFD for 8 weeks to induce obesity, after which these mice continued to eat the same HFD and were treated with either vehicle or GHB for another 8 weeks (**Fig. 1A**). GHB did neither affect cumulative food intake over 8 weeks (**Fig. S1A**) nor voluntary locomotor activity (**Fig. S1B**). Nonetheless, GHB attenuated body weight gain (**Fig. 1B**), as explained by reduced gain of fat mass (**Fig. 1C**) rather than lean mass (**Fig. S1C**). Consistently, GHB reduced gonadal white adipose tissue (gWAT) and interscapular brown adipose tissue (iBAT) mass (**Fig. 1D-E**). In gWAT, GHB attenuated adipocyte enlargement (**Fig. 1F**) and reduced gene expression of the inflammatory markers adhesion G protein-coupled receptor E1 (*Adgre1*), encoding the macrophage surface marker F4/80, and tumor necrosis factor α (*Tnfa*), encoding a pro-inflammatory cytokine (**Fig. 1G**). In iBAT, GHB decreased the lipid content (**Fig. 1H**) and increased uncoupling protein-1 (UCP-1) protein abundance (**Fig. 1I**).

We next examined the modulatory role of GHB treatment in lipid and glucose metabolism. GHB had no impact on fasting plasma levels of triglycerides (TG) (**Fig. S1D**), non-esterified fatty acids (NEFA) (**Fig. S1E**) or free glycerol (**Fig. S1F**). Nonetheless, GHB did reduce fasting plasma glucose levels from four weeks of treatment onwards (**Fig. 1J**). Moreover, GHB improved glucose clearance during an intraperitoneal glucose tolerance test (**Fig. 1K**), and lowered fasting plasma insulin levels at week 6 (**Fig. 1L**). Consistently, GHB decreased the Homeostatic Model Assessment for Insulin Resistance (HOMA-IR) index (**Fig. 1M**). Collectively, these findings demonstrate that GHB attenuates diet-induced fat mass gain and improves glucose homeostasis in obesity.
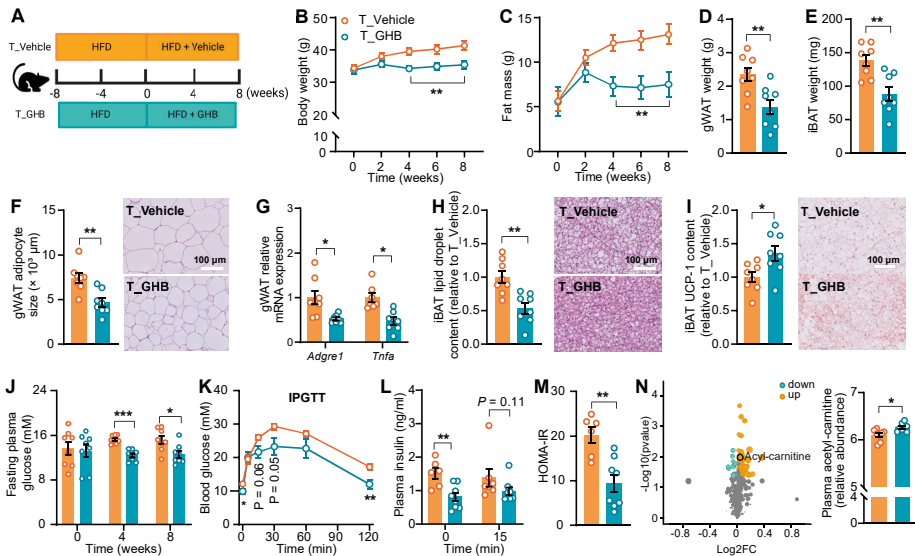
Fig. 1. Oral administration of GHB attenuates fat mass gain and improves glucose control in existing obesity. (**A**) Experimental setup. (**B**) Body weight and (**C**) fat mass were monitored throughout the experimental period. (**D-E**) At the end of the study, gonadal white adipose tissue (gWAT) and interscapular brown adipose tissue (iBAT) were collected and weighed. (**F**) White adipocyte size was assessed by hematoxylin-eosin (H&E) staining. (**G**) gWAT inflammation was assessed by quantifying proinflammatory gene expression. (**H**) Lipid droplet content and (**I**) uncoupling protein-1 (UCP-1) protein abundance in iBAT were evaluated by H&E staining and UCP-1 immunostaining, respectively. (**J**) Fasting plasma glucose levels were determined throughout the study. (**K**) At week 6, an intraperitoneal glucose tolerance test (IPGTT) was performed. (**L**) Fasting plasma insulin was measured during IPGTT. (**M**) Homeostasis model assessment of insulin resistance (HOMA-IR) was determined from fasting glucose and insulin at baseline. (**N**) At week 8, plasma metabolomics profiling was conducted, and acetyl-carnitine levels were determined by plasma metabolomics. Data are represented as means±SEM (n=8 per group). Differences were assessed using unpaired two-tailed Student's *t*-test or two-way ANOVA followed by Fisher's LSD test (**K and L**). *$P<0.05$, **$P<0.01$, ***$P<0.001$. *Adgre1*, adhesion G protein-coupled receptor E1; gWAT, gonadal white adipose tissue; HFD, high fat diet; iBAT, interscapular brown adipose tissue; *Tnfa*, tumor necrosis factor α.

GHB alleviates liver steatosis and inflammation, accompanied by improved retinol metabolism in existing obesity

To unravel the molecular impact of GHB treatment on peripheral tissues, untargeted metabolomics profiling of plasma from vehicle- and GHB-treated mice was performed and revealed that GHB treatment decreased 13 metabolites and increased 75 metabolites. For example, GHB treatment increased levels of acyl-carnitine (**Fig. 1N**), which is primarily generated in the liver through enhanced fatty acid (FA) oxidation [43]. In line with the body fat-lowering effect, GHB treatment reduced liver weight (**Fig. 2A**) and largely attenuated liver steatosis, as shown by reduced lipid droplets (**Fig. 2B**) and decreased TG levels (**Fig. 2C**). Untargeted metabolomic profiling of the liver identified 75 differentially regulated metabolites, including 34 downregulated
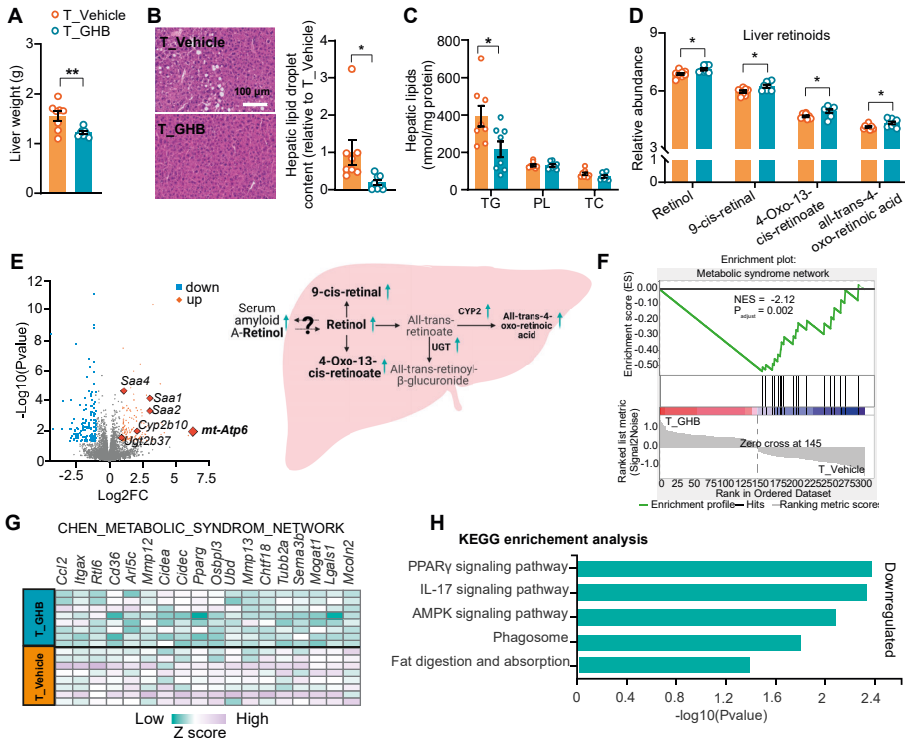
Fig. 2. GHB alleviates liver steatosis and inflammation, accompanied by improved retinol metabolism in existing obesity. (**A**) Liver weight, (**B**) liver lipid droplet content, (**C**) hepatic triglycerides (TG), phospholipids (PL) and total cholesterol (TC) were determined. (**D**) Liver retinoid levels were detected by liver metabolomics. Liver RNA sequencing was conducted, and differentially expressed genes (DEGs) were identified (**E**), and (**F-G**) gene set enrichment analysis (GSEA) and (**H**) KEGG pathway enrichment analysis were performed. Data are represented as means±SEM (n=8 per group). Differences were assessed using unpaired two-tailed Student's *t*-test. *P<0.05, **P<0.01.

and 41 upregulated metabolites, with GHB treatment. In agreement with the hepatic lipid reduction, GHB treatment decreased hepatic fatty acids and their conjugates (**Fig. S2A**). Intriguingly, GHB increased hepatic retinoids (**Fig. S2B**), as shown by increased hepatic retinol, 9-cis-retinal, 4-oxo-13-cis-retinoate and all-trans-4-oxo-retinoic acid levels (**Fig. 2D**). Coincidingly, RNA sequencing in livers from vehicle- or GHB-treated mice revealed that GHB upregulated the hepatic expression of genes involved in retinol transport, including serum amyloid A (SAA) 1 (*Saa1*), *Saa2* and *Saa4* [45-47], and retinol metabolism, including cytochrome P450 2B10 (*Cyp2b10*) [48] and UDP-glucuronosyltransferase 2B37 (*Ugt2b37*) [49] (**Fig. 2E**).

We identified mitochondrially encoded adenosine triphosphate (ATP) synthase membrane subunit 6 (*mt-ATP6*), a gene encoding mitochondrial ATP synthase, as the most upregulated gene (**Fig. 2E**), suggesting that GHB increased mitochondrial ATP synthesis [50]. Next, we conducted gene set enrichment analysis (GSEA) and identified that GHB reduced a gene set, CHEN_METABOLIC_SYNDROM_NETWORK, which is associated with the metabolic syndrome (**Fig. 2F-G**). The Molecular Signatures Database described genes within this gene set as 'genes that form the macrophage-enriched metabolic network (MEMN) and are claimed to have a causal relationship with the metabolic syndrome traits' (**Fig. 2F-2G**) [51]. Furthermore, we showed that these downregulated genes are mainly involved in lipogenic pathway peroxisome proliferator-activated receptor γ (PPARγ) signaling and pro-inflammatory pathway interleukin 17 (IL-17) signaling, and we also observed downregulation of pathways associated with the maintenance of energy balance (i.e. AMPK signaling and fat digestion and absorption) and regulation of immune responses (i.e. phagosome) (**Fig. 2H**). Altogether, the present study indicates that in existing obesity, GHB may alleviate HFD-induced liver damage as associated with improved liver mitochondrial function.

GHB beneficially modulates the gut microbiota composition and increases succinate concentrations in the caecal content in existing obesity

As GHB is a SCFA, and the SCFAs butyrate and propionate have been shown to attenuate obesity and associated metabolic disorders by modulating the gut microbiota composition, we then performed 16S rRNA gene sequencing to evaluate the impact of GHB on the gut microbiota. GHB treatment did not affect α diversity (**Fig. 3A**), while altering β diversity (**Fig. 3B**), indicative of altered gut microbial structure. Most commensal gut microbes in the caecal content of both vehicle- and GHB-treated mice belonged to the phyla *Firmicutes* and *Bacteroidota* which, along with *Desulfobacterota* and *Actinobacteriota*, represented approximately 95% of the total microbial community (**Fig. 3C**). Moreover, *Blautia*, *Faecalibaculum* and *Colidextribacter* were the most abundant genera in both groups (**Fig. S3B**). LEfSe analysis showed that GHB treatment reduced the abundance of pro-inflammatory genera, such as *Rikenellaceae R9 gut group* (*R. R9 gut group*)[52], *Alistipes* [53], *Colidextribacter* [54] and *Escherichia Shigella* (*E. Shigella*) [55], while increasing the abundance of *Harryflintia* [56] and *Bacillus* [57], both genera with anti-inflammatory properties (**Fig. 3D**). These findings indicate that GHB beneficially modulates the gut microbiota composition. Moreover, we determined gut microbial metabolites in the cecal content, and we observed that GHB tended to increase butyrate and propionate concentrations (**Fig. 3E-F and Fig. S3B**) and significantly increased succinate concentrations (**Fig. 3G**). Thus, we demonstrate that in obesity, GHB beneficially modulates the gut microbiota composition, accompanied by increased succinate concentrations in the caecal content.
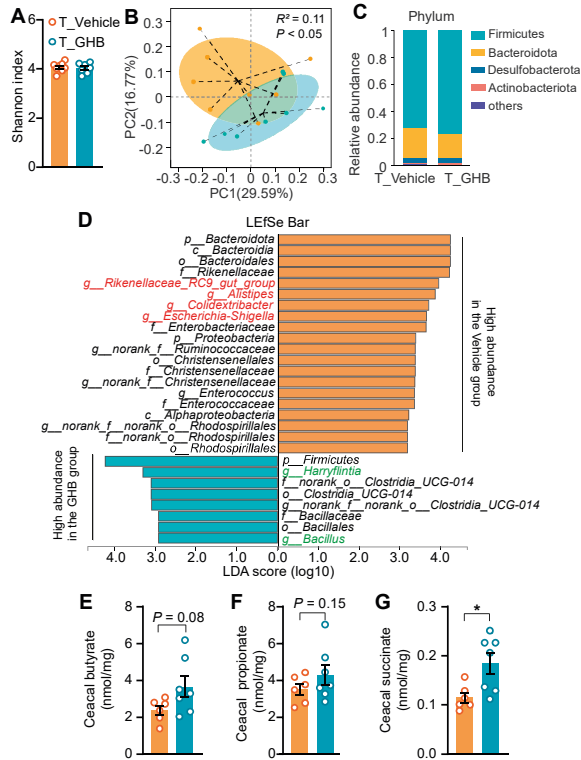
Fig. 3. GHB beneficially modulates the gut microbiota composition and increases succinate concentrations in the cecal content in existing obesity. At the end of the study, the cecal content was collected and sequenced (n=8 per group). (**A**) The Shannon index. (**B**) and Principal component analysis (PCA) were performed. (**C**) The abundance of microbial phyla. (**D**) Linear discrimination analysis (LDA) effect size analysis (LEfSe) was performed, and LDA scores calculated between groups. (**E-G**) Butyrate, and succinate levels in the caecal content were measured. Data are represented as means ± SEM (n=8 per group). Differences were assessed using unpaired two-tailed Student's t-test. *P<0.05.

GHB has no impact on body weight and glucose metabolism in developing obesity

The profound effects of GHB on body weight and glucose metabolism in obesity prompted us to also examine potential preventive effects of GHB during the development of diet-induced obesity. To this end, we fed mice a HFD while simultaneously orally administering GHB or vehicle for 8 weeks (**Fig. 4A**). GHB had no impact on food intake (**Fig. S4A**) but increased voluntary locomotor activity in the mice (**Fig. S4B**). However, GHB did neither affect body weight (**Fig. 4B**) nor body composition (**Fig. 4C** and **S4C**). Likewise, GHB had no impact on gWAT and iBAT (**Fig. 4D-G**) or plasma levels of lipids (**Fig. S4D-F**) and glucose (**Fig. 4H**). By performing plasma metabolomics analysis, we identified that GHB treatment downregulated 32 metabolites and upregulated only 6 metabolites. In developing obesity, GHB did not affect plasma acyl-carnitine levels, while GHB decreased plasma levels of the sphingosine derivative C16 sphinganine (**Fig. 4I**), which is a sphingolipid associated with NAFLD development [58].
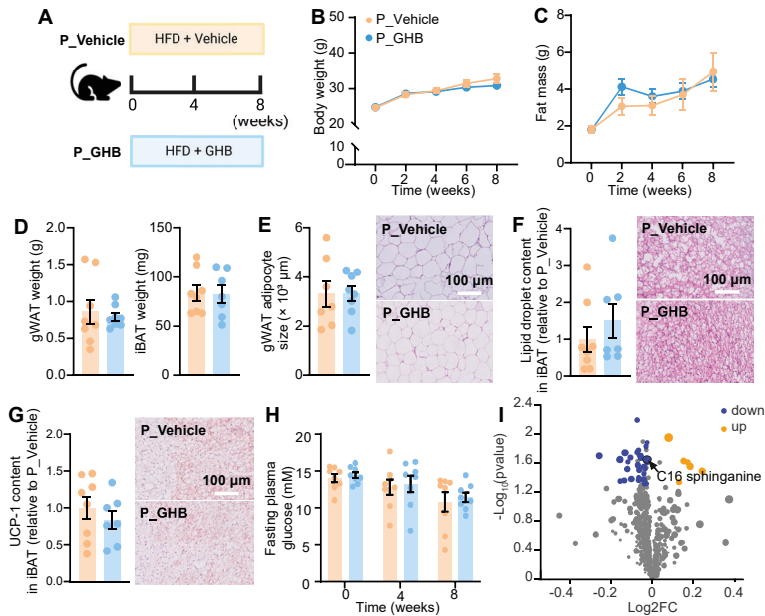
Fig. 4. GHB does not impact body weight and glucose metabolism in developing obesity. (**A**) Experimental setup. (**B**) Body weight and (**C**) body fat mass were measured throughout the experimental period. At the end of the study, (**D**) gWAT and iBAT were collected and weighed. (**E**) White adipocyte size and (**F**) iBAT lipid overload were assessed by H&E staining. (**G**) UCP-1 protein abundance was assessed in iBAT. (**H**) Fasting plasma glucose was measured throughout the study. (**I**) Plasma metabolites were determined by untargeted metabolomics. Data are represented as means±SEM (n=8 per group). Differences were assessed using unpaired two-tailed Student's *t*-test.

GHB prevents accumulation of hepatic sphingolipids, accompanied by downregulated pro-inflammatory signaling in developing obesity

While GHB treatment did not affect body weight and overall adiposity in developing obesity, GHB did decrease liver weight (**Fig. 5A**) and lowered hepatic lipid droplet content (**Fig. 5B**). GHB treatment did not significantly reduce hepatic TG, phospholipids (PL) and total cholesterol (TC) content (**Fig. 5C**), but decreased many hepatic lipids species as revealed by untargeted metabolomics profiling, including glycerophosphocholines (**Fig. S5A**), levels of which are increased in individuals with nonalcoholic steatohepatitis (NASH) [59]. Moreover, GHB increased hepatic amino acids, peptides and their analogues (**Fig. S5B**). In line with this, GHB-treated mice had increased hepatic levels of spermine (**Fig. 5D**), an amino acid metabolite with anti-oxidative and anti-inflammatory properties [60, 61]. Further analysis showed that GHB downregulated the sphingolipid signaling pathway, as deducted from reduced sphinganine and sphingosine levels in the liver (**Fig. 5D-E**). RNA sequencing in the liver also identified downregulated hepatic gene expression levels of sphingomyelin phosphodiesterase 3 (SMPD3), an enzyme

catalyzing the hydrolysis of sphingomyelin to form ceramide, with GHB treatment (**Fig. 5F**). Notably, we found cytochrome c oxidase III (*mt-Co3*), the mitochondrial gene encoding subunit IV of the respiratory complex, to be most upregulated upon GHB treatment in developing obesity (**Fig. 5F**), which suggests that GHB increases
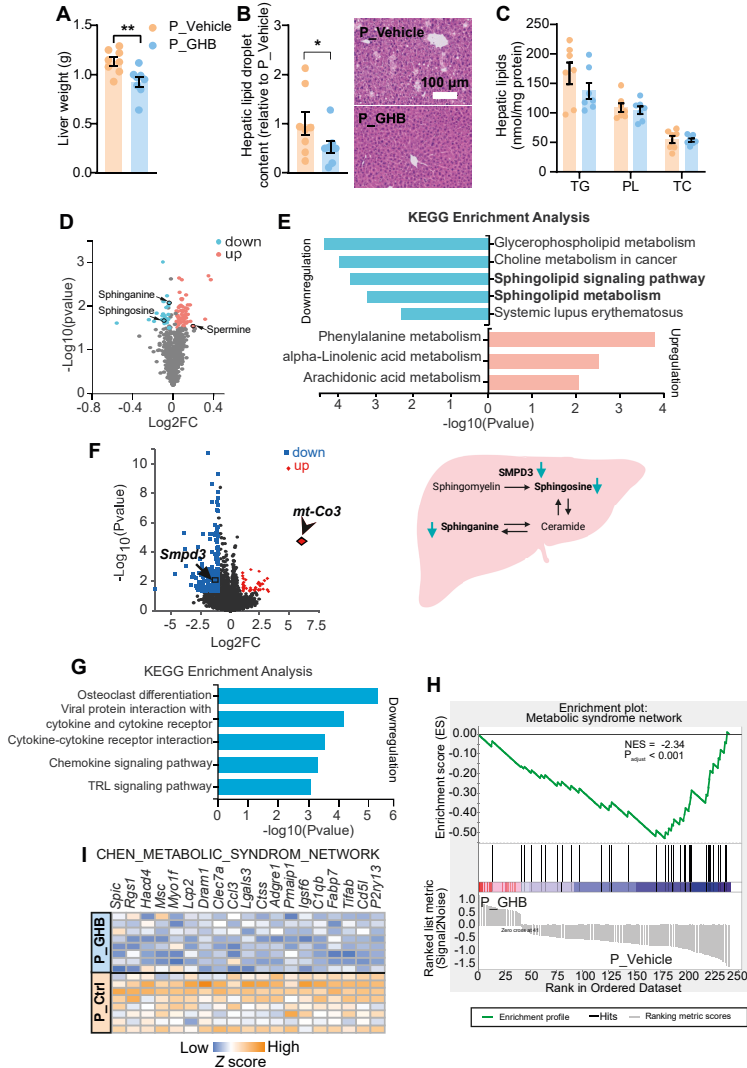
Fig. 5. GHB reduces the abundance of hepatic sphingolipids, accompanied by downregulated pro-inflammatory signaling in developing obesity. At week 8, (**A**) the liver was weighed and (**B** and **C**) hepatic lipid levels were assessed. (**D**) Hepatic metabolites were determined by untargeted metabolomics, and (**E**) KEGG pathway enrichment analysis was conducted. (**F**) Liver DEGs were identified by liver RNA sequencing and (**G**) KEGG pathway enrichment analysis and (**H-I**) GSEA were conducted. Data are represented as means ± SEM (n=8 per group). Differences were assessed using unpaired two-tailed Student's t-test. *P<0.05, **P<0.01.

hepatic electron transport chain (ETC) activity. Then, focusing particularly on the downregulated genes, we identified that GHB downregulated genes enriched in immune responses, including osteoclast differentiation, viral protein interaction with cytokine and cytokine receptor, cytokine-cytokine receptor interaction, chemokine signaling and Toll-like receptor signaling (**Fig. 5G**). Consistently, GSEA analysis showed that GHB downregulated a gene set involved in macrophage-mediated metabolic syndrome development (**Fig. 5H-I**). Collectively, these data indicate that GHB, also in developing obesity, ameliorates hepatic steatosis and attenuates hepatic inflammation, accompanied by upregulation of markers of improved hepatic mitochondrial function.
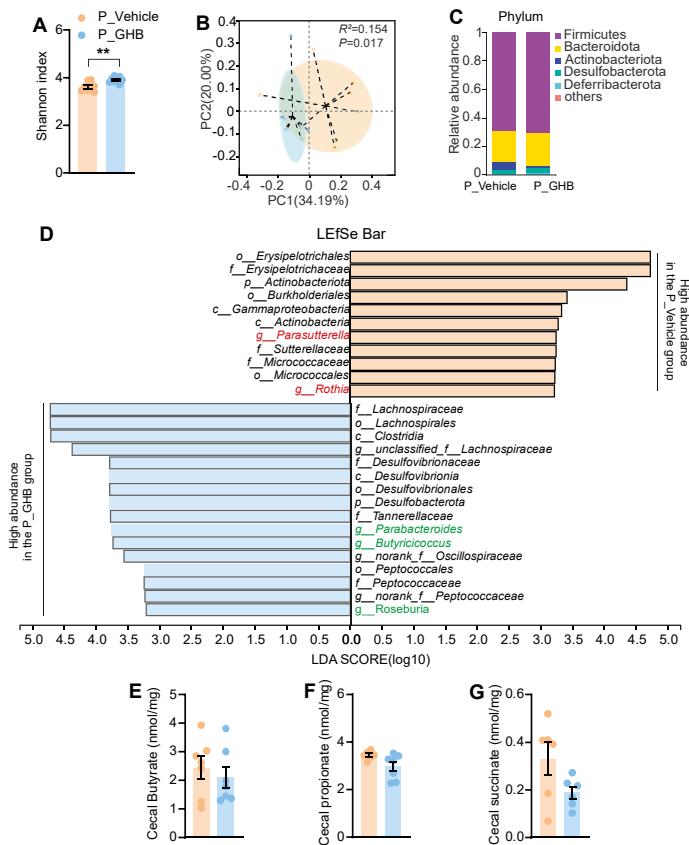
Fig. 6. GHB beneficially modulates the gut microbiota composition in developing obesity. After 8 weeks of GHB intervention, the caecal content was collected and bacterial 16S sequenced was performed (n=8 per group). (**A**) The Shannon index and (**B**) Principal component analysis (PCA) were evaluated. (**C**) The abundance of microbial phyla were detected. (**D**) LEfSe was analyzed, and LDA scores calculated between groups. (**E-G**) Butyrate, propionate and succinate levels in the caecal content were measured. Data are represented as means ± SEM (n=8 per group). Differences were assessed using unpaired two-tailed Student's t-test. **$P<0.01$.

GHB beneficially modulates gut microbiota composition in developing obesity

In the setting of developing obesity, GHB increased the α diversity of the gut microbiota (**Fig. 6A**) and principal component analysis revealed a pronounced difference in β diversity (i.e. gut microbiota structure) between vehicle- and GHB-treated mice (**Fig. 6B**). Moreover, we observed that in developing obesity, *Firmicutes* and *Bacteroidota* were the most abundant phyla in both treatment groups (**Fig. S6A**), and the *Blautia* and *Faecalibaculum* (**Fig. S6B**) were abundant genera in both vehicle and GHB groups. While pro-inflammatory microbes such as *Parasutterella* and *Rothia* were more abundant in vehicle-treated mice, GHB-treated mice showed increased abundance of the SCFA-producers *Parabacteroides*, *Butyricicoccus* and *Roseburia* (**Fig. 6D**). However, no differences in the concentrations of microbial metabolites were detectable in cecum content (**Fig. 6E-G** and **Fig. S6B**), Taken together, these data suggest that GHB beneficially modulates the gut microbiota composition not only in existing obesity, but also in developing obesity.

4

DISCUSSION

Clinical studies have reported a weight loss-promoting effect of the narcolepsy drug GHB [7-9], but the underlying metabolic mechanisms remained unclear. To understand how GHB reduces body weight and thereby reveal potential therapeutic targets for obesity and its associated metabolic diseases, we set out to explore the role of GHB in body weight control under obesogenic and obese conditions. We demonstrated that GHB alleviates HFD-induced hepatic lipid accumulation and inflammation in developing and existing obesity, but only exerts weight loss-promoting and glucose-lowering effects in existing obesity. We proposed that GHB-mediated beneficial hepatic effects in both settings are associated with improved hepatic mitochondrial function. Despite the differential effects of GHB on body weight and glucose metabolism in developing and existing obesity being still unclear, a possible explanation may be the degree of hepatic lipid overload that governs hepatic mitochondrial function and systemic insulin sensitivity. In addition, we observed that GHB beneficially modulates the gut microbiota composition under both metabolic conditions, which might be also linked to the improvement of metabolic health mediated by GHB administration.

Interestingly, while GHB did not affect fat mass gain and plasma glucose levels in developing obesity, GHB did reduce liver weight and prevented HFD-induced sphingolipid accumulation and inflammation in the liver. The early onset of obesity is characterized by aberrant lipid accumulation and impaired mitochondrial function

in non-adipose tissues, particularly in the liver. In developing obesity, FA disposal through β-oxidation and TG formation is overwhelmed in non-adipose tissues. As a result, excess FAs can form lipotoxic species, such as sphingolipids, that dampen mitochondrial function and induce local and systemic inflammation. This consequently leads to the development of obesity and its associated diseases, such as NAFLD [62-65]. GHB likely improves hepatic mitochondrial function in developing obesity, as shown by a profound upregulation of hepatic *mt-Co3*, a gene encoding mitochondrial complex IV which catalyzes the last step of the mitochondrial ETC and drives oxidative phosphorylation [66]. A recent study showed that HFD feeding promotes hepatocyte lipid overload and inhibits hepatic mitochondrial complex IV, resulting in increased hepatic oxidative stress and consequently liver damage which was attenuated by restoring mitochondrial complex IV activity [67]. Therefore, upregulation of complex IV may well explain the beneficial GHB-mediated effects on the liver. Since oral GHB is mainly metabolized in the liver, and primarily in hepatocytes, through the mitochondrial TCA cycle [22], the upregulated expression of hepatic *mt-Co3* upon GHB treatment may be driven by increased TCA activity of hepatocytes. Studies have shown that mitochondrial TCA activity is essential for modulating amino acid metabolism [68]. This may well explain why levels of amino acids are increased in livers of GHB-treated mice during HFD feeding. Consistently, we found that GHB increased hepatic levels of the amino acid metabolite spermine, which is crucial for maintaining TCA cycle activity [69-72]. These findings possibly identify *mt-Co3* and spermine as potential therapeutic targets to prevent obesity and its associated metabolic disorders.

In existing obesity, GHB not only improved liver function but also reduced body weight, as explained by reduced fat mass coinciding with improved adipose tissue function and insulin sensitivity. These beneficial systemic effects are likely also linked to the improvement of mitochondrial function in hepatocytes, since GHB increased systemic levels of acyl-carnitine, a liver-derived fuel source for BAT thermogenesis [43]. Previous studies showed that upon cold exposure, WAT-derived FAs activate hepatic carnitilation to generate acyl-carnitines within hepatocyte mitochondria, and once in the circulation, acyl-carnitines can be transported to BAT while the uptake into WAT and the liver are blocked [43]. We, however, did not observe any effects of GHB on circulating NEFA and free glycerol levels in developing and existing obesity, which possibly suggests that GHB does not directly affect adipose tissue function. Instead, GHB may directly act on the liver to modulate hepatic mitochondrial function. Indeed, in existing obesity, GHB increased hepatic expression of *mt-ATP6*, a gene encoding ATP synthase, which is also known as mitochondrial complex V and responsible for the final step of oxidative phosphorylation [73, 74]. The upregulation of *mt-ATP6* may also be driven by the GHB-induced increase in TCA activity in the liver, as TCA activity

governs respiratory efficiency [75]. Obesity-driven NAFLD is associated with disturbed TCA cycle activity, impaired mitochondrial ATP synthesis and reduced mitochondrial oxidative phosphorylation activity [67, 76, 77]. In agreement with improved hepatocyte mitochondrial function, we showed a profound reduction of hepatic steatosis and inflammation in obese mice treated with GHB. The differential modulation of mitochondrial gene expression by GHB in developing and existing obesity possibly can be explained by the differences in metabolic status, the degree of hepatic lipid levels and thus hepatocyte mitochondrial dynamics. Indeed, the morphology and dynamics of mitochondria change rapidly in response to various challenges, e.g. metabolic cues, and their structure and function varies at different stages of obesity and its related diseases [78, 79].

Notably, in existing obesity, we further reported that GHB protected against HFD-induced loss of hepatic retinoids. In healthy liver, hepatic stellate cells (HSCs) are considered "quiescent", and these quiescent HSCs represent the major storage site for retinoids in the whole body, as 90-95% of retinoids in the body are stored in HSCs [44]. However, during progressive NAFLD, hepatic inflammation leads to HSC activation, resulting in loss of retinoids. The loss of retinoids can induce the production of excessive amounts of extracellular matrix proteins and consequently promote fibrogenesis in the liver [80, 81]. Accordingly, our results may indicate that GHB protects against HSC activation, which may be the consequence of increased *mt-ATP6* expression in the liver (e.g. within the hepatocytes and HSCs). In agreement, deprivation of HSCs from retinol reduces mitochondrial ATP synthesis, and restoring retinol increased energy output [81, 82]. Furthermore, previous studies showed that within the liver, the transcription level of *mt-ATP6* correlates with retinol levels [50], indicating that GHB improves mitochondrial function to alleviate liver damage. This also highlights that hepatic *mt-ATP6* is a potential therapeutic target for obesity-driven NAFLD, including liver fibrosis.

Moreover, we reported that GHB administration beneficially modulates the gut microbiota composition in developing obesity and existing obesity. In developing obesity, GHB increased the abundance of SCFA producers (i.e. acetate-producer *Parabacteroides* [83-86] and butyrate-producers *Butyricicocus* [87] and *Roseburi*a [88]). These gut microbes have been shown to exert anti-inflammatory effects and confer metabolic benefits by increasing the production of SCFAs. By serving as the primary energy source of enterocytes, SCFAs can improve the gut barrier integrity, which is associated with alleviation of systemic inflammation [83-86, 89-91]. They also can act as a signaling molecules to maintain whole-body energy balance by reducing food intake and increasing thermogenesis [92, 93]. However, we did not observe any effects on gut

4

microbial metabolites, including SCFAs, in the cecal content upon GHB administration under obesogenic conditions. Reasons may be that these metabolites are quickly taken up by the body of the host or that they are produced at low concentrations which hampers detection of potential elevations. Also, we did not observe any effects of GHB on food intake and adipose tissue function (i.e. WAT inflammation and BAT activation) in developing obesity. However, our group previously reported that oral butyrate supplementation exerts beneficial effects in developing obesity but not in existing obesity (Li Z, et al.; JCI Insight, in press. Based on these findings, we speculate that GHB may not directly affect the gut microbiota; instead, beneficial effects on the gut microbiota possibly resulted from direct beneficial effects of GHB on hepatocyte mitochondrial function, causing overall improvement of health.

In existing obesity, we observed increased succinate levels in the cecum content of GHB-treated mice. The succinate was likely generated by the gut microbiota instead of being a metabolic product of GHB, as we did not observe increased succinate levels in the cecum content of GHB-treated mice with developing obesity. Also, it is unclear whether GHB can even reach the cecum upon oral administration. Accordingly, *Bacillus,* a microbe that we found enriched with GHB treatment in established obesity [94, 95], is able to produce succinate [96]. Recently, gut microbiota-derived succinate and succinate-producing bacteria were reported to exert anti-obesity and glucose-lowering effects [86, 97], since succinate in the gut can upregulate the intestinal glucogenesis pathway and, as a consequence, reduce hepatic glucose production. However, GHB did not change the hepatic expression of genes involved in glucose production. This may indicates that the increased gut microbiota-derived succinate was also the consequence of improved whole-body metabolism upon GHB treatment. Despite this, further studies are need to confirm the impact of GHB treatment on intestinal gluconeogenesis and hepatic glucose production in existing obesity. Likewise, the present study cannot exclude a contribution of the GHB-mediated beneficial effects on the gut microbiota on maintaining metabolic health, and further studies are thus still needed to evaluate potential causal effects between the gut microbiota changes and metabolic health improvement.

In conclusion, GHB improves HFD-induced mitochondrial dysfunction of the liver in both developing and existing obesity in mice. Provided these effects can be translated to humans, the beneficial effects of GHB on metabolic health that is observed in patients receiving GHB as narcolepsy treatment may be explained via primary beneficial effects on the liver. We propose that mitochondrial TCA cycle activity and ETC function, spermine and retinoids are potential therapeutic targets to combat obesity-associated metabolic diseases. Collectively, our findings provide additional

evidence that mitochondria-directed therapeutic strategies hold great promise for combating a wide variety of metabolic diseases, including obesity and NAFLD.

Acknowledgments

Author contributions

CL designed the study, carried out the research, analyzed and interpreted the results, and wrote and revised the manuscript. MZ carried out the research, interpreted the results, reviewed the manuscript. MSS, RF and GJL provided GHB and reviewed the manuscript. AV and MG performed cecum content metabolomics profiling and reviewed the manuscript. YW advised the study and reviewed the manuscript. MRB advised the study, reviewed the manuscript and obtained the funding. PCNR designed and advised the study, interpreted the results, edited, reviewed and revised the manuscript and obtained funding. MS advised the study, interpreted the results, reviewed and revised the manuscript and obtained the funding.

4

REFERENCES

1.   Kahn, S.E., R.L. Hull, and K.M. Utzschneider, Mechanisms linking obesity to insulin resistance and type 2 diabetes. Nature, 2006. **444**(7121): p. 840-6.

2.   Polyzos, S.A., J. Kountouras, and C.S. Mantzoros, Obesity and nonalcoholic fatty liver disease: From pathophysiology to therapeutics. Metabolism, 2019. **92**: p. 82-97.

3.   Dombrowski, S.U., et al., Long term maintenance of weight loss with non-surgical interventions in obese adults: systematic review and meta-analyses of randomised controlled trials. BMJ, 2014. **348**: p. g2646.

4.   Jastreboff, A.M., et al., Tirzepatide Once Weekly for the Treatment of Obesity. New England Journal of Medicine, 2022. **387**(3): p. 205-216.

5.   Saxon, D.R., et al., Antiobesity Medication Use in 2.2 Million Adults Across Eight Large Health Care Organizations: 2009-2015. Obesity, 2019. **27**(12): p. 1975-1981.

6.   Bessesen, D.H. and L.F. Van Gaal, Progress and challenges in anti-obesity pharmacotherapy. Lancet Diabetes Endocrinol, 2018. **6**(3): p. 237-248.

7.   Husain, A.M., R.K. Ristanovic, and R.K. Bogan, Weight loss in narcolepsy patients treated with sodium oxybate. Sleep Med, 2009. **10**(6): p. 661-3.

8.   Ponziani, V., et al., BMI changes in pediatric type 1 narcolepsy under sodium oxybate treatment. Sleep, 2021. **44**(7).

9.   Noujaim, M.G., A. Mourad, and J.D. Clough, Sodium Oxybate: A Cause of Extreme Involuntary Weight Loss in a Young Lady. Case Rep Med, 2019. **2019**: p. 6537815.

10. Snead, O.C., 3rd and K.M. Gibson, Gamma-hydroxybutyric acid. N Engl J Med, 2005. **352**(26): p. 2721-32.

11. Kok, S.W., et al., Hypocretin deficiency in narcoleptic humans is associated with abdominal obesity. Obesity Research, 2003. **11**(9): p. 1147-1154.

12. Poli, F., et al., Body mass index-independent metabolic alterations in narcolepsy with cataplexy. Sleep, 2009. **32**(11): p. 1491-7.

13. Ponziani, V., et al., Growing Up with Type 1 Narcolepsy: Its Anthropometric and Endocrine Features. J Clin Sleep Med, 2016. **12**(12): p. 1649-1657.

14. Felmlee, M.A., B.L. Morse, and M.E. Morris, gamma-Hydroxybutyric Acid: Pharmacokinetics, Pharmacodynamics, and Toxicology. AAPS J, 2021. **23**(1): p. 22.

15. Maitre, M., C. Klein, and A.G. Mensah-Nyagan, Mechanisms for the Specific Properties of gamma-Hydroxybutyrate in Brain. Med Res Rev, 2016. **36**(3): p. 363-88.

16. Buchele, F., et al., Sodium Oxybate for Excessive Daytime Sleepiness and Sleep Disturbance in Parkinson Disease: A Randomized Clinical Trial. JAMA Neurol, 2018. **75**(1): p. 114-118.

17. Schep, L.J., et al., The clinical toxicology of gamma-hydroxybutyrate, gamma-butyrolactone and 1,4-butanediol. Clin Toxicol (Phila), 2012. **50**(6): p. 458-70.

18. Donjacour, C.E., et al., Glucose and fat metabolism in narcolepsy and the effect of sodium oxybate: a hyperinsulinemic-euglycemic clamp study. Sleep, 2014. **37**(4): p. 795-801.

19. Donjacour, C.E., et al., Plasma total ghrelin and leptin levels in human narcolepsy and matched healthy controls: basal concentrations and response to sodium oxybate. J Clin Sleep Med, 2013. **9**(8): p. 797-803.

20. Zhang, G.F., et al., Metabolism of gamma-hydroxybutyrate in perfused rat livers. Biochem J, 2012. **444**(2): p. 333-41.

21. Luca, G., et al., Central and peripheral metabolic changes induced by gamma-hydroxybutyrate. Sleep, 2015. **38**(2): p. 305-13.

22. Busardo, F.P. and A.W. Jones, GHB pharmacology and toxicology: acute intoxication, concentrations in blood and urine in forensic cases and treatment of the withdrawal syndrome. Curr Neuropharmacol, 2015. **13**(1): p. 47-70.

23. Dave, R.A., K.E. Follman, and M.E. Morris, gamma-Hydroxybutyric Acid (GHB) Pharmacokinetics and Pharmacodynamics: Semi-Mechanistic and Physiologically Relevant PK/PD Model. AAPS J, 2017. **19**(5): p. 1449-1460.

24. Martinez-Reyes, I. and N.S. Chandel, Mitochondrial TCA cycle metabolites control physiology and disease. Nat Commun, 2020. **11**(1): p. 102.

25. Luukkonen, P.K., et al., Distinct contributions of metabolic dysfunction and genetic risk factors in the pathogenesis of non-alcoholic fatty liver disease. J Hepatol, 2022. **76**(3): p. 526-535.

26. Wolff, G., et al., Hepatocyte-specific activity of TSC22D4 triggers progressive NAFLD by impairing mitochondrial function. Mol Metab, 2022. **60**: p. 101487.

27. Meex, R.C.R. and M.J. Watt, Hepatokines: linking nonalcoholic fatty liver disease and insulin resistance. Nat Rev Endocrinol, 2017. **13**(9): p. 509-520.

28. Strissel, K.J., et al., Adipocyte death, adipose tissue remodeling, and obesity complications. Diabetes, 2007. **56**(12): p. 2910-8.

29. Turner, N., et al., Distinct patterns of tissue-specific lipid accumulation during the induction of insulin resistance in mice by high-fat feeding. Diabetologia, 2013. **56**(7): p. 1638-48.

30. Zhao, Y., et al., Liver governs adipose remodelling via extracellular vesicles in response to lipid overload. Nat Commun, 2020. **11**(1): p. 719.

31. Canfora, E.E., J.W. Jocken, and E.E. Blaak, Short-chain fatty acids in control of body weight and insulin sensitivity. Nat Rev Endocrinol, 2015. **11**(10): p. 577-91.

32. Lu, Y., et al., Short Chain Fatty Acids Prevent High-fat-diet-induced Obesity in Mice by Regulating G Protein-coupled Receptors and Gut Microbiota. Sci Rep, 2016. **6**: p. 37589.

33. van Eenige, R., et al., RandoMice, a novel, user-friendly randomization tool in animal research. PLoS One, 2020. **15**(8): p. e0237096.

34. Bligh, E.G. and W.J. Dyer, A rapid method of total lipid extraction and purification. Can J Biochem Physiol, 1959. **37**(8): p. 911-7.

35. Chen, S., et al., fastp: an ultra-fast all-in-one FASTQ preprocessor. Bioinformatics, 2018. **34**(17): p. i884-i890.

36. Kim, D., B. Langmead, and S.L. Salzberg, HISAT: a fast spliced aligner with low memory requirements. Nat Methods, 2015. **12**(4): p. 357-60.

37. Pertea, M., et al., StringTie enables improved reconstruction of a transcriptome from RNA-seq reads. Nat Biotechnol, 2015. **33**(3): p. 290-5.

38. Li, B. and C.N. Dewey, RSEM: accurate transcript quantification from RNA-Seq data with or without a reference genome. BMC Bioinformatics, 2011. **12**: p. 323.

39. Love, M.I., W. Huber, and S. Anders, Moderated estimation of fold change and dispersion for RNA-seq data with DESeq2. Genome Biol, 2014. **15**(12): p. 550.

4

40. Xie, C., et al., KOBAS 2.0: a web server for annotation and identification of enriched pathways and diseases. Nucleic Acids Res, 2011. **39**(Web Server issue): p. W316-22.

41. Subramanian, A., et al., Gene set enrichment analysis: a knowledge-based approach for interpreting genome-wide expression profiles. Proc Natl Acad Sci U S A, 2005. **102**(43): p. 15545-50.

42. Kim, H.K., S. Kostidis, and Y.H. Choi, NMR Analysis of Fecal Samples. Methods Mol Biol, 2018. **1730**: p. 317-328.

43. Simcox, J., et al., Global Analysis of Plasma Lipids Identifies Liver-Derived Acylcarnitines as a Fuel Source for Brown Fat Thermogenesis. Cell Metabolism, 2017. **26**(3): p. 509-+.

44. Tsuchida, T. and S.L. Friedman, Mechanisms of hepatic stellate cell activation. Nat Rev Gastroenterol Hepatol, 2017. **14**(7): p. 397-411.

45. Derebe, M.G., et al., Serum amyloid A is a retinol binding protein that transports retinol during bacterial infection. Elife, 2014. **3**.

46. Ganal, S.C. and A.J. MacPherson, An ambulance for retinol. Elife, 2014. **3**: p. e04246.

47. Esterhazy, D. and D. Mucida, Serum amyloid A proteins take retinol for a ride. Trends Immunol, 2014. **35**(11): p. 505-6.

48. Shmarakov, I.O., Retinoid-xenobiotic interactions: the Ying and the Yang. Hepatobiliary Surg Nutr, 2015. **4**(4): p. 243-67.

49. Akimoto, Y., et al., Retinoic Acid-Induced Epidermal Transdifferentiation in Skin. Journal of Developmental Biology, 2014. **2**(3): p. 158-173.

50. Berdanier, C.D., et al., Role of vitamin A in mitochondrial gene expression. Diabetes Res Clin Pract, 2001. **54 Suppl 2**: p. S11-27.

51. Chen, Y.Q., et al., Variations in DNA elucidate molecular networks that cause disease. Nature, 2008. **452**(7186): p. 429-435.

52. Sun, L., et al., Cecal Gut Microbiota and Metabolites Might Contribute to the Severity of Acute Myocardial Ischemia by Impacting the Intestinal Permeability, Oxidative Stress, and Energy Metabolism. Frontiers in Microbiology, 2019. **10**.

53. Parker, B.J., et al., The Genus Alistipes: Gut Bacteria With Emerging Implications to Inflammation, Cancer, and Mental Health. Front Immunol, 2020. **11**: p. 906.

54. Kang, G.U., et al., Exploration of Potential Gut Microbiota-Derived Biomarkers to Predict the Success of Fecal Microbiota Transplantation in Ulcerative Colitis: A Prospective Cohort in Korea. Gut Liver, 2022. **16**(5): p. 775-785.

55. Paciello, I., et al., Intracellular Shigella remodels its LPS to dampen the innate immune recognition and evade inflammasome activation. Proc Natl Acad Sci U S A, 2013. **110**(46): p. E4345-54.

56. Li, L., et al., Crude Polysaccharide Extracted From Moringa oleifera Leaves Prevents Obesity in Association With Modulating Gut Microbiota in High-Fat Diet-Fed Mice. Front Nutr, 2022. **9**: p. 861588.

57. Paynich, M.L., S.E. Jones-Burrage, and K.L. Knight, Exopolysaccharide from Bacillus subtilis Induces Anti-Inflammatory M2 Macrophages That Prevent T Cell-Mediated Disease. Journal of Immunology, 2017. **198**(7): p. 2689-2698.

58. Montefusco, D., et al., Analysis of the Sphingolipidome in NAFLD. Methods Mol Biol, 2022. **2455**: p. 279-303.

59. Anjani, K., et al., Circulating phospholipid profiling identifies portal contribution to NASH signature in obesity. J Hepatol, 2015. **62**(4): p. 905-12.

60.   Zhou, S., et al., Spermine Alleviates Acute Liver Injury by Inhibiting Liver-Resident Macrophage Pro-Inflammatory Response Through ATG5-Dependent Autophagy. Frontiers in Immunology, 2018. **9**.

61.   Holbert, C.E., et al., Polyamines in cancer: integrating organismal metabolism and antitumour immunity. Nat Rev Cancer, 2022. **22**(8): p. 467-480.

62.   Green, C.D., et al., Sphingolipids in metabolic disease: The good, the bad, and the unknown. Cell Metab, 2021. **33**(7): p. 1293-1306.

63.   Apostolopoulou, M., et al., Specific Hepatic Sphingolipids Relate to Insulin Resistance, Oxidative Stress, and Inflammation in Nonalcoholic Steatohepatitis. Diabetes Care, 2018. **41**(6): p. 1235-1243.

64.   Hammerschmidt, P., et al., CerS6-Derived Sphingolipids Interact with Mff and Promote Mitochondrial Fragmentation in Obesity. Cell, 2019. **177**(6): p. 1536-1552 e23.

65.   Friedman, S.L., et al., Mechanisms of NAFLD development and therapeutic strategies. Nat Med, 2018. **24**(7): p. 908-922.

66.   Li, Y.F., et al., Cytochrome c oxidase subunit IV is essential for assembly and respiratory function of the enzyme complex. Journal of Bioenergetics and Biomembranes, 2006. **38**(5-6): p. 283-291.

67.   Verbeek, J., et al., Roux-en-y gastric bypass attenuates hepatic mitochondrial dysfunction in mice with non-alcoholic steatohepatitis. Gut, 2015. **64**(4): p. 673-83.

68.   Ryan, D.G., et al., Disruption of the TCA cycle reveals an ATF4-dependent integration of redox and amino acid metabolism. Elife, 2021. **10**.

69.   Puleston, D.J., et al., Polyamine metabolism is a central determinant of helper T cell lineage fidelity. Cell, 2021. **184**(16): p. 4186-+.

70.   Puleston, D.J., et al., Polyamines and eIF5A Hypusination Modulate Mitochondrial Respiration and Macrophage Activation. Cell Metab, 2019. **30**(2): p. 352-363 e8.

71.   Madeo, F., et al., Spermidine in health and disease. Science, 2018. **359**(6374).

72.   Vrijsen, S., et al., ATP13A2-mediated endo-lysosomal polyamine export counters mitochondrial oxidative stress. Proc Natl Acad Sci U S A, 2020. **117**(49): p. 31198-31207.

73.   Ganetzky, R.D., et al., MT-ATP6 mitochondrial disease variants: Phenotypic and biochemical features analysis in 218 published cases and cohort of 14 new cases. Hum Mutat, 2019. **40**(5): p. 499-515.

74.   Ng, Y.S., et al., Pathogenic variants in MT-ATP6: A United Kingdom-based mitochondrial disease cohort study. Ann Neurol, 2019. **86**(2): p. 310-315.

75.   Satapati, S., et al., Elevated TCA cycle function in the pathology of diet-induced hepatic insulin resistance and fatty liver. J Lipid Res, 2012. **53**(6): p. 1080-92.

76.   Longo, M., et al., Mitochondrial dynamics and nonalcoholic fatty liver disease (NAFLD): new perspectives for a fairy-tale ending? Metabolism, 2021. **117**: p. 154708.

77.   Lee, K., et al., Hepatic Mitochondrial Defects in a Nonalcoholic Fatty Liver Disease Mouse Model Are Associated with Increased Degradation of Oxidative Phosphorylation Subunits. Mol Cell Proteomics, 2018. **17**(12): p. 2371-2386.

78.   Fromenty, B. and M. Roden, Mitochondrial alterations in fatty liver diseases. J Hepatol, 2022.

79.   Wai, T. and T. Langer, Mitochondrial Dynamics and Metabolic Regulation. Trends Endocrinol Metab, 2016. **27**(2): p. 105-117.

4

80. Okuno, M., et al., Retinoids exacerbate rat liver fibrosis by inducing the activation of latent TGF-beta in liver stellate cells. Hepatology, 1997. **26**(4): p. 913-21.

81. Trivedi, P., S. Wang, and S.L. Friedman, The Power of Plasticity-Metabolic Regulation of Hepatic Stellate Cells. Cell Metab, 2021. **33**(2): p. 242-257.

82. Chiu, H.J., D.A. Fischman, and U. Hammerling, Vitamin A depletion causes oxidative stress, mitochondrial dysfunction, and PARP-1-dependent energy deprivation. FASEB J, 2008. **22**(11): p. 3878-87.

83. Ezeji, J.C., et al., Parabacteroides distasonis: intriguing aerotolerant gut anaerobe with emerging antimicrobial resistance and pathogenic and probiotic roles in human health. Gut Microbes, 2021. **13**(1): p. 1922241.

84. Lei, Y.Y., et al., Parabacteroides produces acetate to alleviate heparanase-exacerbated acute pancreatitis through reducing neutrophil infiltration. Microbiome, 2021. **9**(1).

85. Wu, T.R., et al., Gut commensal Parabacteroides goldsteinii plays a predominant role in the anti-obesity effects of polysaccharides isolated from Hirsutella sinensis. Gut, 2019. **68**(2): p. 248-262.

86. Wang, K., et al., Parabacteroides distasonis Alleviates Obesity and Metabolic Dysfunctions via Production of Succinate and Secondary Bile Acids. Cell Rep, 2019. **26**(1): p. 222-235 e5.

87. Trachsel, J., S. Humphrey, and H.K. Allen, Butyricicoccus porcorum sp. nov., a butyrate-producing bacterium from swine intestinal tract. Int J Syst Evol Microbiol, 2018. **68**(5): p. 1737-1742.

88. Kasahara, K., et al., Interactions between Roseburia intestinalis and diet modulate atherogenesis in a murine model. Nature Microbiology, 2018. **3**(12): p. 1461-1471.

89. Seo, B., et al., Roseburia spp. Abundance Associates with Alcohol Consumption in Humans and Its Administration Ameliorates Alcoholic Fatty Liver in Mice. Cell Host Microbe, 2020. **27**(1): p. 25-40 e6.

90. Eeckhaut, V., et al., Butyricicoccus pullicaecorum in inflammatory bowel disease. Gut, 2013. **62**(12): p. 1745-1752.

91. Rodriguez, J., et al., Discovery of the gut microbial signature driving the efficacy of prebiotic intervention in obese patients. Gut, 2020. **69**(11): p. 1975-1987.

92. Li, Z., et al., Butyrate reduces appetite and activates brown adipose tissue via the gut-brain neural circuit. Gut, 2018. **67**(7): p. 1269-1279.

93. Gao, Z., et al., Butyrate improves insulin sensitivity and increases energy expenditure in mice. Diabetes, 2009. **58**(7): p. 1509-17.

94. Huang, J., et al., Enterococcus faecium R0026 Combined with Bacillus subtilis R0179 Prevent Obesity-Associated Hyperlipidemia and Modulate Gut Microbiota in C57BL/6 Mice. J Microbiol Biotechnol, 2021. **31**(2): p. 181-188.

95. Cao, G.T., et al., Bacillus licheniformis, a potential probiotic, inhibits obesity by modulating colonic microflora in C57BL/6J mice model. J Appl Microbiol, 2019. **127**(3): p. 880-888.

96. Hederstedt, L., Succinate:quinone oxidoreductase in the bacteria Paracoccus denitrificans and Bacillus subtilis. Biochim Biophys Acta, 2002. **1553**(1-2): p. 74-83.

97. De Vadder, F., et al., Microbiota-Produced Succinate Improves Glucose Homeostasis via Intestinal Gluconeogenesis. Cell Metab, 2016. **24**(1): p. 151-7.

SUPPLEMENT

Expanded methods

Measurement of body weight and body composition

Body weight was measured weekly with a scale, and body composition of conscious mice was measured every 2 weeks using an EchoMRI-100 analyzer (EchoMRI, Houston, TX, USA).

Locomotor activity measurement

After 2 weeks of GHB treatment, mice (n=8 per group) were single housed in fully automated metabolic cages (Promethion line, Sable Systems International, Las Vegas, NV, USA). These mice were first acclimatized to the system for 48 hours, then further monitored for another 48 hours (2 light/dark cycles), during which the locomotor activity was continuously measured.

Plasma parameters

Every 4 weeks, after 4-hour fasting, tail vein blood (n=8 per group) was collected into paraoxon-coated glass capillaries. Plasma was collected and measured for glucose, triglycerides (TG), non-esterified fatty acids (NEFAs) and free glycerol using commercial kits (Roche Diagnostics, Mannheim, Germany).

Glucose tolerance test

In the first experiment, at week 6, an intraperitoneal glucose tolerance test (IPGTT) was conducted with an injection of D-glucose (2 g/kg body weight) after 4-hour fasting (n=8 per group). Plasma glucose was measured before (0 min), and 15, 30, 60 and 120 min after D-glucose injection with a OneTouch Ultra glucometer (AccuCheck Sensor, Roche Diagnostics, Almere, The Netherlands) in a drop of tail vein blood. Extra blood was collected at t=0 and 15 min, spun down, and the serum samples were stored at -20℃ for glucose measurement (t=0) using a commercial enzymatic kit and insulin measurement (t=1 and 15 min) using the Ultra Sensitive Mouse Insulin ELISA kit (Crystal Chem, Zaandam, The Netherlands).

Adipose tissue histology

At the end of both experiments, various adipose tissue depots were collected. Formalin-fixed paraffin-embedded interscapular brown adipose tissue (iBAT) and gonadal white adipose tissue (gWAT) sections (5 µm thickness) were prepared for hematoxylin-eosin (H&E) staining. In addition, iBAT was processed for uncoupling protein-1 (UCP-1) staining. Using Image J software (version 1.52a; National Institutes of Health, Bethesda,

Maryland), the areas occupied by intracellular lipid vacuoles and UCP-1, as well as the size of adipocytes of gWAT were assessed.

Liver histology and lipid measurements

Formalin-fixed paraffin-embedded liver samples (n=8 per group) were stained with H&E. The unstained areas occupied by intracellular lipid vacuoles were quantified using Image J software. Hepatic lipids were extracted from frozen liver samples (n=8 per group) using a modified protocol from Bligh and Dyer [1]. Commercial kits were used for the measurement of hepatic TG, total cholesterol (TC), phospholipids (PL) and protein (Pierce, Thermo Fisher Scientific, Waltham, MA, USA). Hepatic lipids were expressed as nmol lipid per mg protein.

RNA sequencing analysis

Total RNA was extracted from frozen livers (n=8 per group), and RNA sequencing was performed by BGI Genomic Services (Hong Kong) and analyzed by Majorbio BioTech Co., Ltd (Shanghai, China). The Illumina HiSeq 2500 platform was used to construct RNA libraries and generate 2×150 bp long paired-end reads (Illumina, San Diego, CA, USA). The raw data end reads were trimmed and quality controlled by FASTQ with default parameters (https://github.com/OpenGene/fastp) [2], and the clean reads were separately aligned to the reference genome (GRCm38) with orientation mode (5′ to 3′ orientation) using the HISAT2 software (http://ccb.jhu.edu/software/hisat2/index.shtml) [3]. The mapped reads of each sample were assembled by StringTie in a reference-based approach (https://ccb.jhu.edu/software/stringtie/) [4]. To identify differentially expressed genes (DEGs) between the vehicle and GHB groups, the expression levels of each gene were calculated according to the transcripts per million reads (TPM) method. RSEM (http://deweylab.biostat.wisc.edu/rsem/) was used to quantify gene abundance [5]. Analysis of differential gene expression was performed using DESeq2 [6], and DEGs are defined as fold changes >2 and $P<0.05$. Volcano plots were generated using the EnhancedVolcano feature (https://github.com/kevinblighe/EnhancedVolcano). Kyoto Encyclopedia of Genes and Genomes (KEGG) pathway enrichment analysis was carried out by KOBAS (http://kobas.cbi.pku.edu.cn/home.do) [7]. Gene Set Enrichment analysis (GSEA) was also conducted to identify gene sets that share common biological function and significantly regulated gene sets were annotated based on the Molecular Signatures Database [8].

Quantitative reverse transcriptase-PCR

Using Tripure RNA isolation reagent (Roche, Mijdrecht, The Netherlands), total RNA was extracted from snap-frozen tissues (n=8 per group). Using Moloney Murine Leukemia Virus Reverse Transcriptase (Promega, Leiden, The Netherlands),

complementary DNA for quantitative reverse transcriptase-PCR was generated by reverse transcription of total RNA. Then, mRNA expression was normalized to *b-actin* and *Rplp0* mRNA levels and expressed as fold change compared with the Vehicle group. Primer sequences are listed in the **Supporting table 1.**

Plasma and liver untargeted metabolomics analysis

Lipids were extracted from plasma (~50 µL; n=8 per group) using 400 µL methanol: acetonitrile (1:1; v/v) solution. The mixture was then sonicated at 40 kHz for 30 min at 4℃ and placed at -20℃ for 30 min to precipitate proteins. After centrifugation at 13,000 rpm at 4℃ for 15 min, the supernatant was carefully transferred into new microtubes and dried under a gentle stream of nitrogen. Then, samples were reconstituted in 100 µL loading solution of acetonitrile: water (1:1; v/v) by brief sonication in a 5℃ water bath. The extracted metabolites were spun for 15 min at 13,000 g at 4℃ and the supernatant was transferred to new microtubes for LC-MS/MS analysis. Liver samples (~50 mg) were weighed, and the metabolites were extracted using 400 µL methanol:water (4:1, v/v) solution with 0.02 mg/mL L-2-chorophenylalanin as internal standard. The mixture was allowed to settle at -10℃ and treated in the high throughput tissue crusher Wonbio-96c at 50 Hz for 6 min followed by ultrasound at 40 kHz for 30 min at 5℃. The samples were placed at -20℃ for 30 min to precipitate proteins. After centrifugation at 13,000 at 4℃ for 15 min, the supernatant was carefully transferred to sample vials for LC-MS/MS analysis. As a part of the system conditioning and quality control process, a pooled quality control (QC) was prepared by mixing equal volumes of all samples. The QC samples were disposed and tested in the same manner as the samples.

The UHPLC-Q Exactive system was used for LC-MS analysis. Samples (~2 µL) were separated by HSS T3 column and then detected by mass spectrometry. The mobile phases contained 0.1% formic acid in water : acetonitrile (95:5, v/v) (solvent A) and 0.1% formic acid in acetonitrile : isopropanol : water (47.5:47.5:5, v/v) (solvent B). The solvent gradient changed according to the following conditions: 0-0.1 min, 0% B to 5% B; 0.1-2 min, 5% B to 25% B; 2- 9 min, 25% B to 100% B; 9-13 min, 100% B to 100% B; 13-13.1 min, 100% B to 0% B ; 13.1-16 min, 0% B to 0% B for equilibrating the systems. The injection volume of samples was 2 µL, and the sample flow rate was set to 0.4 mL/min. The column temperature was maintained at 40℃. The mass spectrometric detection were then conducted using a UHPLC-Q Exactive Mass Spectrometer equipped with an electrospray ionization (ESI) source which can handle metabolites in either a positive or a negative ion mode. The optimal conditions of the detection were set as following: heater temperature, 400℃; capillary temperature, 320℃; sheath gas flow rate, 40 arb; aux gas flow rate, 10 arb; ion-spray voltage floating (ISVF), -2800 V in negative mode and 3500 V in positive mode, respectively; Normalized collision energy, 20-40-60 V rolling

4

for MS/MS. Full MS resolution was 70,000, and MS/MS resolution was 17,500. Data was collected using the Data Dependent Acquisition (DDA) mode. The detection was carried out over a mass range of 70-1050 m/z. After completing the mass spectrometry detection, the raw data was proceeded by Progenesis QI software (Waters Corporation, Milford, USA), and a three-dimensional data matrix in CSV format was acquired. In order to reduce the errors caused by sample preparation and instrument instability, the response intensity of the sample mass spectrum peaks was normalized by the sum normalization method, and the normalized data matrix was obtained. At the same time, variables with relative standard deviation (RSD) > 30% of quality control (QC) samples were removed, and log10 logarithmization was performed to obtain the final data matrix for subsequent analysis.

The metabolites were searched and identified, and the main database was the HMDB (http://www.hmdb.ca/). Orthogonal least partial squares discriminant analysis (OPLS-DA) was performed using the R package ropls (Version 1.6.2), and 7-cycle interactive validation was used to evaluate the stability of the model. In addition, Student's t-test and fold difference analysis were performed. The selection of significantly different metabolites was determined based on the Variable importance in the projection (VIP) obtained by the OPLS-DA model and the P-value of Student's t-test. The metabolites with VIP>1, $P<0.05$ were defined as significantly different metabolites. Differential metabolites among two groups were summarized, and mapped into their biochemical pathways through metabolic enrichment and pathway analysis based on database search (KEGG, http://www. genome.jp/kegg/). These metabolites can be classified according to the pathways they are involved in or the functions they perform. Enrichment analysis was conducted using Python packages (https://docs.scipy.org/doc/scipy/).

Gut microbial metabolites measurement

The method for the NMR analysis of cecum content samples was adapted from the protocol developed for human fecal samples with a few changes [9]. The mass of each cecal content sample (~50 mg) was carefully weighed prior to the sample preparation. To each sample tube, 50 μL of 0.5 mm zirconium oxide beads (Next Advance, Inc. USA, New York), ceramic beads and 300 μL of pH 7.4 potassium phosphate buffer (0.15 M) containing 0.2 mM NaN_3 were added. Then, these tubes were subjected to bead beating for 30 seconds. The tubes were subsequently centrifuged at 18,000 g at 4℃ for 15 minutes. 250 μL of supernatant was transferred to new 1.5 mL Eppendorf tubes. These tubes were centrifuged at 18,000 g at 4℃ for 1 hour. 225 μL of supernatant was added to 25 μL of 100% D_2O containing 4 mM TSP-d4, and 6 mM dimethylsulfone. A

customized Gilson 215 liquid handler was used to transfer the samples to a 3.0 mm Bruker NMR tube rack.

^{1}H NMR data were collected using a Bruker 600 MHz Avance Neo/IVDr spectrometer equipped with a 5 mm TCI cryogenic probe head and a z-gradient system. A Bruker SampleJet sample changer was used for sample insertion and removal. All experiments were recorded at 300 K. A standard sample 99.8% methanol-d4 was used for temperature calibration before each batch of measurements [10]. One-dimensional (1D) ^{1}H NMR spectra were recorded using the first increment of a NOESY pulse sequence [11] with presaturation (γB1=50 Hz) during a relaxation delay of 4 s and a mixing time of 10 ms for efficient water suppression [12]. Initial shimming was performed using the TopShim tool on a random mix of urine samples from the study, and subsequently the axial shims were optimized automatically before every measurement. Duration of 90° pulses were automatically calibrated for each individual sample using a homonuclear-gated mutation experiment on the locked and shimmed samples after automatic tuning and matching of the probe head [13]. 16 scans of 65,536 points covering 12,335 Hz were recorded. The Free Induction Decay of the 1D experiment was zero-filled to 65,536 complex points prior to Fourier transformation. An exponential window function was applied with a line-broadening factor of 0.3 Hz. The spectra were automatically phase and baseline corrected and automatically referenced to an internal standard (TSP=0.0 ppm). Metabolites were quantified in a select number of spectra using the Chenomx NMR Suite (version 8.6), and by fitting the remaining spectra automatically in the KIMBLE environment [14]. The areas were converted to concentrations using the dimethylsulfone internal standard.

16S rRNA gene sequencing

After 8 weeks of GHB intervention, cecal contents (n=8 per group) were collected, and genomic bacterial DNA was isolated with the fast DNA stool mini kit (QIAamp, Manheim, Germany) following the manufacturer's instructions. Then, these DNA samples were used for 16S rRNA sequencing at BGI Genomics and analyzed by Majorbio BioTech Co., Ltd. Briefly, microbial DNA was amplified using a set of barcoded dual-index primers encoding the V3-V4 region of the 16S rRNA gene. A high-sensitive DNA analysis kit (Agilent, San Diego, CA, USA) was used to confirm the size of the amplicon library (~399 bp). The pooled amplicon library was then sequenced on the Illumina MiSeq platform using the 500 cycle MiSeq V2 Reagent kit (Illumina, San Diego, CA, USA) according to the manufacturer's instructions. The "Preparing Libraries for Sequencing on the MiSeq" protocol was used to prepare libraries with a final load concentration of 5.5 p.m., spiked with 15% PhiX to create diversity within the run. FASTQ files are generated when the 2x250 bp sequencing completes. Following

4

sequencing, microbiome bioinformatics were run using QIIME 2 2020.2. Briefly, non-singleton amplicon sequence variants (ASVs, 100% operational taxonomic units; OTUs) were generated from raw sequences after trimming with the cut-adapt plugin and denoising with the Dada2 plugin. Taxonomy was then assigned to ASVs using the classify-sklearn alignment algorithm against the GreenGenes database of 99% OTUs reference sequences. The α diversity (Shannon) and β diversity were calculated using the diversity plugin. Linear discriminant analysis (LDA) effect size (LEfSe) was computed to identify significantly different microbes in abundance between groups at different taxonomic levels.

Supporting table 1. List of polymerase chain reaction primer sequences used in mRNA expression analysis.

Gene	Forward primer (5'-3')	Reverse Primer (5'-3')
Acta2	CCTGACGGGCAGGTGATC	ATGAAAGATGGCTGGAAGAGAGTCT
Actb	AACCGTGAAAAGATGACCCAGAT	CACAGCCTGGATGGCTACGTA
Adgre1	CTTTGGCTATGGGCTTCCAGTC	GCAAGGAGGACAGAGTTTATCGTG
Rplp0	GGACCCGAGAAGACCTCCTT	GCACATCACTCAGAATTTCAATGG
Tnf	AGCCCACGTCGTAGCAAACCAC	TCGGGGCAGCCTTGTCCCTT

Acta2, actin α 2; *Actb*, β-actin *Adgre1*, adhesion G protein-coupled receptor E1; *Rplp0*, ribosomal protein lateral stalk subunit p0; *Tnf*, tumor necrosis factor α.

REFERENCES

1. Bligh, E.G. and W.J. Dyer, *A rapid method of total lipid extraction and purification.* Can J Biochem Physiol, 1959. **37**(8): p. 911-7.

2. Chen, S., et al., *fastp: an ultra-fast all-in-one FASTQ preprocessor.* Bioinformatics, 2018. **34**(17): p. i884-i890.

3. Kim, D., B. Langmead, and S.L. Salzberg, *HISAT: a fast spliced aligner with low memory requirements.* Nat Methods, 2015. **12**(4): p. 357-60.

4. Pertea, M., et al., *StringTie enables improved reconstruction of a transcriptome from RNA-seq reads.* Nat Biotechnol, 2015. **33**(3): p. 290-5.

5. Li, B. and C.N. Dewey, *RSEM: accurate transcript quantification from RNA-Seq data with or without a reference genome.* BMC Bioinformatics, 2011. **12**: p. 323.

6. Love, M.I., W. Huber, and S. Anders, *Moderated estimation of fold change and dispersion for RNA-seq data with DESeq2.* Genome Biol, 2014. **15**(12): p. 550.

7. Xie, C., et al., *KOBAS 2.0: a web server for annotation and identification of enriched pathways and diseases.* Nucleic Acids Res, 2011. **39**(Web Server issue): p. W316-22.

8. Subramanian, A., et al., *Gene set enrichment analysis: a knowledge-based approach for interpreting genome-wide expression profiles.* Proc Natl Acad Sci U S A, 2005. **102**(43): p. 15545-50.

9. Kim, H.K., S. Kostidis, and Y.H. Choi, *NMR Analysis of Fecal Samples.* Methods Mol Biol, 2018. **1730**: p. 317-328.

10. Findeisen, M., T. Brand, and S. Berger, *A 1H-NMR thermometer suitable for cryoprobes.* Magn Reson Chem, 2007. **45**(2): p. 175-8.

11. Kumar, A., R.R. Ernst, and K. Wuthrich, *A two-dimensional nuclear Overhauser enhancement (2D NOE) experiment for the elucidation of complete proton-proton cross-relaxation networks in biological macromolecules.* Biochem Biophys Res Commun, 1980. **95**(1): p. 1-6.

12. Vilen, E.M., M. Klinger, and C. Sandstrom, *Application of diffusion-edited NMR spectroscopy for selective suppression of water signal in the determination of monomer composition in alginates.* Magn Reson Chem, 2011. **49**(9): p. 584-91.

13. Wu, P.S. and G. Otting, *Rapid pulse length determination in high-resolution NMR.* J Magn Reson, 2005. **176**(1): p. 115-9.

14. Verhoeven, A., M. Giera, and O.A. Mayboroda, *KIMBLE: A versatile visual NMR metabolomics workbench in KNIME.* Anal Chim Acta, 2018. **1044**: p. 66-76.

4
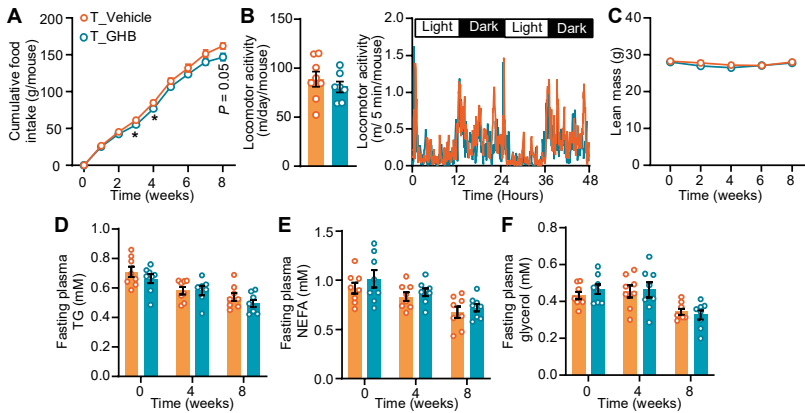
Fig. S1. GHB has no impact on food intake, locomotor activity, body lean mass and fasting plasma lipids in existing obesity. (**A**) Food intake, (**C**) body lean mass, (**D**) fasting plasma levels of triglyceride (TG), (**E**) non-esterified fatty acids (NEFA) and (**F**) free glycerol were monitored throughout the experimental period. (**B**) At week 2, locomotor activity was measured. Data are represented as means ± SEM (n=7-8 per group). Differences were assessed using unpaired two-tailed Student's *t*-test. *$P<0.05$.
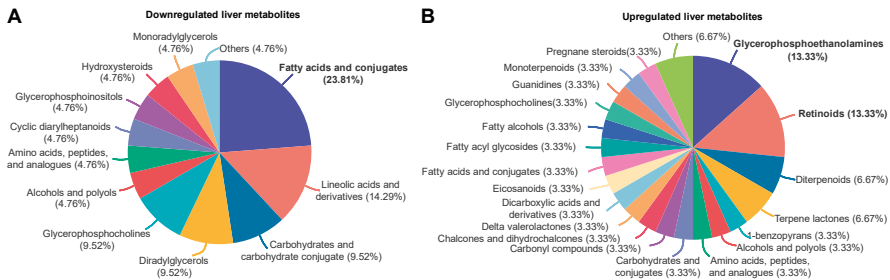
Fig. S2. GHB increases hepatic retinoids in existing obesity. After 8 weeks of GHB treatment, liver samples (n=8 per group) were collected and used for untargeted metabolomics. Differentially modulated hepatic metabolites were detected and analyzed, and the percentage of each metabolite species is depicted as pie chart.
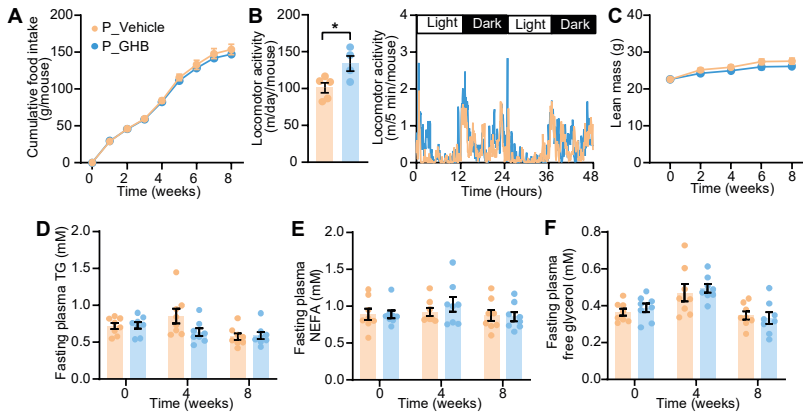
Fig. S4. GHB increases locomotor activity in developing obesity. (**A**) Food intake, (**C**) body lean mass, (**D**) fasting plasma levels of triglyceride (TG), (**E**) non-esterified fatty acids (NEFA) and (**F**) free glycerol were monitored throughout the experimental period. (**B**) At week 2, locomotor activity was measured. Data are represented as means±SEM (n=7-8 per group). Differences were assessed using unpaired two-tailed Student's *t*-test. *$P<0.05$.
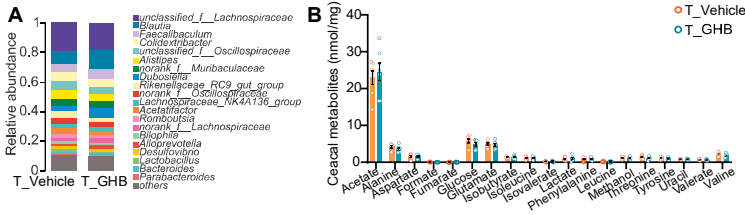
Fig. S3. GHB has no impact on gut microbial metabolites in existing obesity. At the end of the study, the cecal content was collected and the bacterial DNA sequenced (n=8 per group). (**A**) The abundance of microbial genera was evaluated. (**B**) Gut microbial metabolites were determined by performing metabolomics using cecum content samples from vehicle- and GHB-treated mice. Data are represented as means±SEM (n=8 per group).
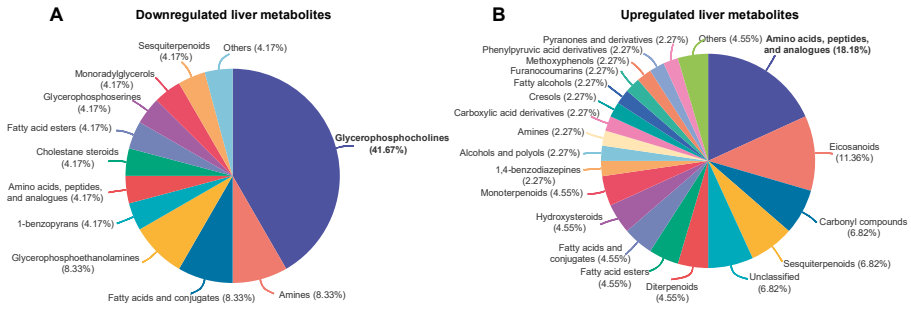
Fig. S5. GHB decreases glycerophosphocholine and increases hepatic amino acids, peptides and analogues in developing obesity. After 8 weeks of GHB interventions, liver samples (n=8 per group) were collected and used for untargeted metabolomics. Differentially modulated hepatic metabolites were detected and analyzed, and the percentage of each metabolite species was depicted as pie chart.
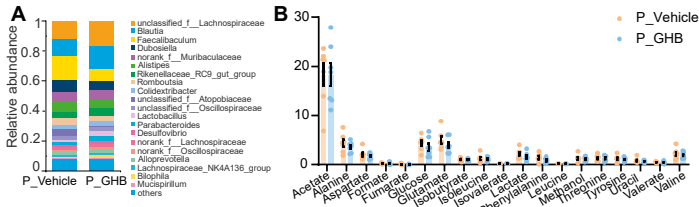
Fig. S6. GHB has no impact on gut microbial metabolites in developing obesity. At the end of the study, the cecal content was collected and the bacterial DNA sequenced (n=8 per group). (**A**) The abundance of microbial genera was evaluated. (**B**) Gut microbial metabolites were determined by performing metabolomics using cecum content samples from vehicle- and GHB-treated mice. Data are represented as means±SEM (n=8 per group).

Table S1 Plasma Metabolomics

ID	Metab ID	Formula	Metabolite	Significant	Regulate
neg_74	metab_20264	C10H19NO3	Capryloylglycine	yes	up
neg_105	metab_20295	C18H28O2	9,12-Octadecadiynoic Acid	yes	up
neg_137	metab_20327	C14H28O3	2-Hydroxymyristic Acid	yes	up
neg_327	metab_20513	C12H22O6	Phaseolic acid	yes	up
neg_575	metab_20756	C20H26O5	3-Epinobilin	yes	up
neg_702	metab_20880	C21H32O5	3a,11b,21-Trihydroxy-20-oxo-5b-pregnan-18-al	yes	up
neg_1157	metab_21327	C18H30O3	9(S)-HOTrE	yes	up
neg_2485	metab_22557	C14H24O8	Valproic acid glucuronide	yes	up
neg_3165	metab_23160	C12H18O4	3,4-Methylenesebacic acid	yes	up
neg_4216	metab_24124	C14H26O5	3-Hydroxytetradecanedioic acid	yes	up
neg_6186	metab_25932	C23H46NO8P	GPEtn(16:0/2:0)	yes	up
neg_8216	metab_27918	C17H34O3	12-hydroxyheptadecanoic acid	yes	up
neg_9559	metab_29168	C21H36O9	Glucosyl (2E,6E,10x)-10,11-dihydroxy-2,6-farnesadienoate	yes	up
neg_9806	metab_29396	C16H24O4	Methyl (3b,11x)-3-Hydroxy-8-oxo-6-eremophilen-12-oate	yes	up
neg_12049	metab_31443	C12H20O4	Traumatic Acid	yes	up
neg_12757	metab_32084	C26H30O13	6-{2-[3-(2,4-dihydroxyphenyl)propanoyl]-6-[(3,3-dimethyloxiran-2-yl)methyl]-3,5-dihydroxyphenoxy}-3,4,5-trihydroxyoxane-2-carboxylic acid	yes	up
neg_12992	metab_32302	C9H12O6S	(4-ethyl-2-hydroxy-6-methoxyphenyl) oxidanesulfonic acid	yes	up
neg_3258	metab_23240	C15H16O5	Ursinic acid	yes	down
neg_4585	metab_24459	C11H16O6S	[4-(3-hydroxybutyl)-2-methoxyphenyl] oxidanesulfonic acid	yes	down
neg_6423	metab_26159	C28H54NO7P	LysoPC(20:2(11Z,14Z))	yes	down
neg_8199	metab_27901	C28H52NO7P	LysoPC(20:3(5Z,8Z,11Z))	yes	down
neg_8543	metab_28219	C27H44O7	Crustecdysone	yes	down
neg_10903	metab_30393	C24H40O6	1b-Hydroxycholic acid	yes	down
neg_12065	metab_31458	C10H9NO3	5-Phenyl-1,3-oxazinane-2,4-dione	yes	down
pos_26	metab_25	C8H15NO3	Hexanoylglycine	yes	up
pos_49	metab_48	C15H24O2	Capsidiol	yes	up
pos_78	metab_77	C18H34O2	Petroselinic acid	yes	up
pos_100	metab_99	C13H22O2	Propyl 2,4-decadienoate	yes	up
pos_101	metab_100	C10H20O3	3-Hydroxycapric acid	yes	up
pos_102	metab_101	C20H28O4	5,6-epoxy,18R-HEPE	yes	up
pos_150	metab_149	C15H24O2	Dihydro-alpha-santalic acid	yes	up
pos_286	metab_285	C16H32O3	16-Hydroxy hexadecanoic acid	yes	up

4

Table S1 Plasma Metabolomics (continued)

ID	Metab ID	Formula	Metabolite	Significant	Regulate
pos_508	metab_504	C20H28O5	Bakkenolide C	yes	up
pos_547	metab_543	C14H24O2	8-Tetradecynoic acid	yes	up
pos_713	metab_709	C24H50NO6P	PC(P-16:0/0:0)	yes	up
pos_726	metab_722	C17H34O3	Avocadene	yes	up
pos_747	metab_742	C16H30O2	11Z-hexadecenoic acid	yes	up
pos_773	metab_768	C20H30O3	8(S)-HEPE	yes	up
pos_794	metab_788	C20H28O3	Phytocassane E	yes	up
pos_801	metab_795	C11H18O2	(2E,6Z)-2,6-Nonadien-1-Yl acetate	yes	up
pos_814	metab_807	C15H26O3	8-Hydroxy-4(6)-lactarene-5,14-diol	yes	up
pos_844	metab_837	C13H22O3	4,5-Dihydrovomifoliol	yes	up
pos_1714	metab_1700	C10H19NO4	O-propanoyl-carnitine	yes	up
pos_1898	metab_1884	C9H16O2	4-hydroxy Nonenal	yes	up
pos_2066	metab_2048	C15H24O3	Zedoarondiol	yes	up
pos_2090	metab_2072	C20H30O4	Prostaglandin-c2	yes	up
pos_2315	metab_2295	C20H20O3	3-(5-hydroxy-2,2-dimethyl-2H-chromen-6-yl)-1-phenylpropan-1-one	yes	up
pos_2430	metab_2410	C41H78NO8P	PC(15:0/18:2(9Z,12Z))	yes	up
pos_2452	metab_2432	C44H80NO7P	PC(P-16:0/20:4)	yes	up
pos_2741	metab_2721	C19H28O3S	S-Japonin	yes	up
pos_3065	metab_3041	C16H32O3	3-hydroxy-hexadecanoic acid	yes	up
pos_3090	metab_3066	C17H34O4	MG(14:0/0:0/0:0)	yes	up
pos_3469	metab_3442	C13H25NO4	(+/-)-Hexanoylcarnitine	yes	up
pos_3542	metab_3512	C4H9N3O2	Creatine	yes	up
pos_4131	metab_4063	C11H21NO5	(R)-3-hydroxybutyrylcarnitine	yes	up
pos_7287	metab_7124	C12H20O2	8-Dodecynoic acid	yes	up
pos_7691	metab_7525	C11H18O2	Methyl 4,8-decadienoate	yes	up
pos_7754	metab_7588	C12H18O3	Jasmonic acid	yes	up
pos_8214	metab_8046	C14H24O2	Alepric acid	yes	up
pos_8249	metab_8080	C10H18O	2-decenal	yes	up
pos_12338	metab_12083	C20H30O7	Cinncassiol A	yes	up
pos_12881	metab_12595	C27H44O3	23S,25-dihydroxyvitamin D3	yes	up
pos_13098	metab_12808	C14H22	3,5,7-Trimethyl-2E,4E,6E,8E-undecatetraene	yes	up
pos_13600	metab_13298	C12H20O	3,6,8-dodecatrien-1-ol	yes	up
pos_13753	metab_13449	C19H26O3	Acitretin(Ro 23-3571)	yes	up
pos_13827	metab_13522	C31H45NO5	Scyphostatin A	yes	up
pos_14037	metab_13730	C8H8O	Phenylacetaldehyde	yes	up
pos_14166	metab_13857	C11H18O2	Methyl geranate	yes	up

Table S1 Plasma Metabolomics (continued)

ID	Metab ID	Formula	Metabolite	Significant	Regulate
pos_14180	metab_13871	C22H28O4	Nitenin	yes	up
pos_14393	metab_14082	C13H14O	(E)-2-Tridecene-4,6,8-triyn-1-ol	yes	up
pos_14420	metab_14109	C18H26O4	Compactin diol lactone	yes	up
pos_14575	metab_14261	C17H33NO4	Decanoyl-L-carnitine	yes	up
pos_14771	metab_14455	C12H16O2	C12:4n-2,4,8,10	yes	up
pos_15520	metab_15200	C17H28O4	(1(10)E,4a,5E)-1(10),5-Germacradiene-12-acetoxy-4,11-diol	yes	up
pos_15795	metab_15459	C11H12O4	Dimethylcaffeic acid	yes	up
pos_16702	metab_16345	C15H24O4	Bisacurone epoxide	yes	up
pos_18520	metab_18142	C14H18N2O4	L-phenylalanyl-L-hydroxyproline	yes	up
pos_19521	metab_19109	C6H11NO4	Acetylhomoserine	yes	up
pos_19712	metab_19294	C4H6O2	Oxolan-3-one	yes	up
pos_19899	metab_19464	C9H17NO4	Acetylcarnitine	yes	up
pos_20160	metab_19698	C7H15NO3	L-Carnitine	yes	up
pos_809	metab_20185	C19H30O2	Epiandrosterone	yes	up
pos_607	metab_603	C46H84NO8P	PC(18:1(11Z)/20:3(5Z,8Z,11Z))	yes	down
pos_1129	metab_1118	C7H8N2O2	N-Methyl-4-pyridone-3-carboxamide	yes	down
pos_2429	metab_2409	C48H82NO8P	PC(20:3(5Z,8Z,11Z)/20:4(8Z,11Z,14Z,17Z))	yes	down
pos_2887	metab_2866	C28H52NO7P	PC(20:3/0:0)	yes	down
pos_3055	metab_3031	C14H22O3	(9R,13R)-1a,1b-dihomo-jasmonic acid	yes	down
pos_13673	metab_13371	C18H35NO2	Lepadin D	yes	down

4

Table S2 Liver Metabolomics

ID	Metab ID	Formula	Metabolite	Significant	Regulate
neg_18	metab_17855	C20H34O7	10,11-dihydro-20-trihydroxy-leukotriene B4	yes	up
neg_529	metab_18351	C21H36O9	Glucosyl (2E,6E,10x)-10,11-dihydroxy-2,6-farnesadienoate	yes	up
neg_1548	metab_19358	C4H9N3O2	3-Guanidinopropanoate	yes	up
neg_2440	metab_20195	C10H16O4	Alpha-Carboxy-delta-nonalactone	yes	up
neg_2515	metab_20264	C16H25NO9	Simmondsin	yes	up
neg_2825	metab_20571	C14H18N2O5	Tyrosyl-Hydroxyproline	yes	up
neg_2840	metab_20586	C11H20O6	Prenyl glucoside	yes	up
neg_3190	metab_20933	C9H12O2	2,6,6-Trimethyl-2-cyclohexene-1,4-dione	yes	up
neg_4246	metab_21976	C14H26O5	3-Hydroxytetradecanedioic acid	yes	up
neg_4867	metab_22587	C25H38O6	Erinacine C	yes	up
neg_5721	metab_23421	C25H42NO7P	PE(20:5/0:0)	yes	up
neg_7931	metab_25570	C21H44NO6P	PE(P-16:0e/0:0)	yes	up
neg_8088	metab_25712	C27H48NO7P	PE(22:4/0:0)	yes	up
neg_8231	metab_25842	C27H46NO7P	PE(22:5/0:0)	yes	up
neg_8448	metab_26046	C23H44NO7P	PE(18:2/0:0)	yes	up
neg_8800	metab_26383	C23H42NO7P	LysoPE(0:0/18:3(9Z,12Z,15Z))	yes	up
neg_9201	metab_26771	C25H36O6	Erinacine B	yes	up
neg_10841	metab_28379	C7H12O	Xi-3-Methyl-3-cyclohexen-1-ol	yes	up
neg_11179	metab_28716	C14H24O3	L-Menthyl acetoacetate	yes	up
neg_11264	metab_28801	C15H22O4	Arlatin	yes	up
neg_12588	metab_30114	C16H23N3O10	3'-Amino-3'-deoxythimidine glucuronide	yes	up
neg_12610	metab_30136	C21H22O5	3-[2-(hydroxymethyl)-5-methoxy-2-methyl-2H-chromen-6-yl]-1-(4-hydroxyphenyl)propan-1-one	yes	up
neg_76	metab_17911	C20H34O5	13,14-dihydro-15-keto-PGE1	yes	down
neg_139	metab_17974	C20H30O2	5,6-dehydro Arachidonic Acid	yes	down
neg_1270	metab_19083	C20H36O4	Prostaglandin D1 Alcohol	yes	down
neg_8334	metab_25939	C26H40N4O6	Neuromedin N (1-4)	yes	down
neg_8337	metab_25942	C21H32O4	3b,15b,17a-Trihydroxy-pregnenone	yes	down
neg_9081	metab_26657	C20H34O3	8(S)-HETrE	yes	down
neg_9140	metab_26713	C21H34O5	Cortolone	yes	down
neg_9592	metab_27148	C24H40O6	1b-Hydroxycholic acid	yes	down
neg_10008	metab_27556	C22H34O5	8-iso-16-cyclohexyl-tetranor Prostaglandin E2	yes	down
pos_104	metab_103	C12H20O2	3,7-Dimethyl-2E,6-octadienyl acetate	yes	up
pos_163	metab_162	C20H28O	9-cis-retinal	yes	up
pos_276	metab_274	C19H28O4	Oryzalide B	yes	up
pos_306	metab_304	C27H44NO7P	PE(22:6/0:0)	yes	up
pos_442	metab_438	C20H28O4	7'-Carboxy-gamma-tocotrienol	yes	up
pos_671	metab_665	C21H44NO6P	PE(P-16:0/0:0)	yes	up

Table S2 Liver Metabolomics (continued)

ID	Metab ID	Formula	Metabolite	Significant	Regulate
pos_1092	metab_1077	C21H30O4	21-Deoxycortisol	yes	up
pos_1104	metab_1089	C21H32O4	15(R)-15-methyl Prostaglandin A2	yes	up
pos_1718	metab_1690	C20H26O3	4-Oxo-13-cis-retinoate	yes	up
pos_2151	metab_2122	C41H76NO8P	GPEtn(18:1/18:2)	yes	up
pos_2189	metab_2160	C43H78NO7P	PE(P-18:0/20:4)	yes	up
pos_2388	metab_2358	C44H80NO7P	PC(P-16:0/20:4)	yes	up
pos_2861	metab_2826	C23H42NO7P	PE(18:3/0:0)	yes	up
pos_4896	metab_4794	C6H10O4S	3,3'-Thiobispropanoic acid	yes	up
pos_6730	metab_6621	C20H26O3	All-trans-4-oxoretinoic acid	yes	up
pos_8589	metab_8451	C45H76NO8P	GPEtn(18:1/22:6)	yes	up
pos_13153	metab_12910	C14H24O3	(1S,2S)-3-oxo-2-pentyl-cyclopentanebutanoic acid	yes	up
pos_13222	metab_12979	C20H28O4	5,6-epoxy,18R-HEPE	yes	up
pos_8014	metab_17836	C20H30O	Retinol	yes	up
pos_19	metab_18	C19H36O4	MG(16:1(9Z)/0:0/0:0)	yes	down
pos_46	metab_45	C18H36O4	(+)-15,16-Dihydroxyoctadecanoic acid	yes	down
pos_134	metab_133	C37H66O5	DG(16:1(9Z)/18:2(9Z,12Z)/0:0)	yes	down
pos_136	metab_135	C37H68O5	DG(18:2(9Z,12Z)/16:0/0:0)	yes	down
pos_165	metab_164	C22H32O3	(+/-)13-HDoHE	yes	down
pos_166	metab_165	C18H34O3	Ricinoleic acid	yes	down
pos_172	metab_171	C20H30O2	Eicosapentaenoic Acid	yes	down
pos_177	metab_176	C29H49O12P	PI(20:4(5Z,8Z,11Z,14Z)/0:0)	yes	down
pos_182	metab_181	C16H26O2	SCLAREOLIDE	yes	down
pos_336	metab_334	C15H26O3	8-Hydroxy-4(6)-lactarene-5,14-diol	yes	down
pos_548	metab_542	C35H64O5	DG(14:1(9Z)/18:1(11Z)/0:0)	yes	down
pos_1598	metab_1574	C8H15NO6	N-Acetylmannosamine	yes	down
pos_2179	metab_2150	C35H66O5	DG(16:0/16:1(9Z)/0:0)	yes	down
pos_2188	metab_2159	C46H86NO8P	PC(18:0/20:3(5Z,8Z,11Z))	yes	down
pos_2432	metab_2400	C50H82NO8P	PC(20:3(5Z,8Z,11Z)/22:6(4Z,7Z,10Z,13Z,16Z,19Z))	yes	down
pos_6451	metab_6344	C15H26N2O2	Aphyllic acid	yes	down
pos_6538	metab_6430	C21H24N2O4	Horhammericine	yes	down
pos_7587	metab_7473	C19H32O2	Methyl linolenate	yes	down
pos_9239	metab_9090	C18H34O2	Vaccenic acid	yes	down
pos_9964	metab_9800	C39H66O5	DG(18:2(9Z,12Z)/18:3(9Z,12Z,15Z)/0:0)	yes	down
pos_11192	metab_10981	C21H24O4	5-Deoxymyricanone	yes	down
pos_11943	metab_11706	C22H36O3	Carbocyclic Thromboxane A2	yes	down
pos_11972	metab_11735	C20H34O3	15-OxoEDE	yes	down
pos_12032	metab_11794	C22H32O3	1alpha-hydroxy-22-oxo-23,24,25,26,27-pentanorvitamin D3	yes	down
pos_1429	metab_17831	C12H22O11	Inulobiose	yes	down

Table S3 RNA-seq

Gene id	Gene name	Gene description	T_Ctrl_ vs_T_GHB
306			
ENSMUSG00000053219	Raet1e	retinoic acid early transcript 1E	Down
ENSMUSG00000009633	G0s2	G0/G1 switch gene 2	Down
ENSMUSG00000042195	Slc35f2	solute carrier family 35, member F2	Down
ENSMUSG00000073835	Mup-ps12	major urinary protein, pseudogene 12	Down
ENSMUSG00000050860	Phospho1	phosphatase, orphan 1	Down
ENSMUSG00000089929	Bcl2a1b	B cell leukemia/lymphoma 2 related protein A1b	Down
ENSMUSG00000049685	Cyp2g1	cytochrome P450, family 2, subfamily g, polypeptide 1	Down
ENSMUSG00000079242	C730034F03Rik	RIKEN cDNA C730034F03 gene	Down
ENSMUSG00000000440	Pparg	peroxisome proliferator activated receptor gamma	Down
ENSMUSG00000109141	Gm30692	predicted gene, 30692	Down
ENSMUSG00000030364	Clec2h	C-type lectin domain family 2, member h	Down
ENSMUSG00000030762	Aqp8	aquaporin 8	Down
ENSMUSG00000081094	Rpl19-ps11	ribosomal protein L19, pseudogene 11	Down
ENSMUSG00000092323	BB365896	expressed sequence BB365896	Down
ENSMUSG00000110597	Gm8798	predicted gene 8798	Down
ENSMUSG00000087404	Gm11752	predicted gene 11752	Down
ENSMUSG00000092517	Art2a	ADP-ribosyltransferase 2a	Down
ENSMUSG00000019214	Chtf18	CTF18, chromosome transmission fidelity factor 18	Down
ENSMUSG00000030468	Siglecg	sialic acid binding Ig-like lectin G	Down
ENSMUSG00000083171	Gm12321	predicted gene 12321	Down
ENSMUSG00000078735	Il11ra2	interleukin 11 receptor, alpha chain 2	Down
ENSMUSG00000090622	A930033H14Rik	RIKEN cDNA A930033H14 gene	Down
ENSMUSG00000029822	Osbpl3	oxysterol binding protein-like 3	Down
ENSMUSG00000106224	Gm43823	predicted gene 43823	Down
ENSMUSG00000094437	Gm9830	predicted gene 9830	Down
ENSMUSG00000032643	Fhl3	four and a half LIM domains 3	Down
ENSMUSG00000112384	Gm34921	predicted gene, 34921	Down
ENSMUSG00000035186	Ubd	ubiquitin D	Down
ENSMUSG00000029254	Stap1	signal transducing adaptor family member 1	Down
ENSMUSG00000097352	C920009B18Rik	RIKEN cDNA C920009B18 gene	Down
ENSMUSG00000004654	Ghrhr	growth hormone releasing hormone receptor	Down
ENSMUSG00000050578	Mmp13	matrix metallopeptidase 13	Down
ENSMUSG00000068220	Lgals1	lectin, galactose binding, soluble 1	Down
ENSMUSG00000041653	Pnpla3	patatin-like phospholipase domain containing 3	Down
ENSMUSG00000096458	Moap1	modulator of apoptosis 1	Down

Table S3 RNA-seq (continued)

Gene id	Gene name	Gene description	T_Ctrl_ vs_T_GHB
ENSMUSG00000046415	B430212C06Rik	RIKEN cDNA B430212C06 gene	Down
ENSMUSG00000118011	Gm50266	predicted gene, 50266	Down
ENSMUSG00000031636	Pdlim3	PDZ and LIM domain 3	Down
ENSMUSG00000044017	Adgrd1	adhesion G protein-coupled receptor D1	Down
ENSMUSG00000093930	Hmgcs1	3-hydroxy-3-methylglutaryl-Coenzyme A synthase 1	Down
ENSMUSG00000068601	Gm10244	predicted gene 10244	Down
ENSMUSG00000061086	Myl4	myosin, light polypeptide 4	Down
ENSMUSG00000100157	2310034O05Rik	RIKEN cDNA 2310034O05 gene	Down
ENSMUSG00000100254	Trpc2	transient receptor potential cation channel, subfamily C, member 2	Down
ENSMUSG00000099889	Mrgprb11-ps	MAS-related GPR, member B11, pseudogene	Down
ENSMUSG00000040592	Cd79b	CD79B antigen	Down
ENSMUSG00000028773	Fabp3	fatty acid binding protein 3	Down
ENSMUSG00000070713	Gm10282	predicted pseudogene 10282	Down
ENSMUSG00000049723	Mmp12	matrix metallopeptidase 12	Down
ENSMUSG00000028871	Rspo1	R-spondin 1	Down
ENSMUSG00000055809	Dnaaf3	dynein, axonemal assembly factor 3	Down
ENSMUSG00000041538	H2-Ob	histocompatibility 2, O region beta locus	Down
ENSMUSG00000001739	Cldn15	claudin 15	Down
ENSMUSG00000069170	Adgrv1	adhesion G protein-coupled receptor V1	Down
ENSMUSG00000102615	Gm37844	predicted gene, 37844	Down
ENSMUSG00000062170	Fmr1nb	Fmr1 neighbor	Down
ENSMUSG00000110838	Gm47789	predicted gene, 47789	Down
ENSMUSG00000107198	Gm19619	predicted gene, 19619	Down
ENSMUSG00000091462	Gm17084	predicted gene 17084	Down
ENSMUSG00000028671	Gale	galactose-4-epimerase, UDP	Down
ENSMUSG00000114247	Gm32063	predicted gene, 32063	Down
ENSMUSG00000030724	Cd19	CD19 antigen	Down
ENSMUSG00000063011	Msln	mesothelin	Down
ENSMUSG00000001131	Timp1	tissue inhibitor of metalloproteinase 1	Down
ENSMUSG00000116656	Gm49708	predicted gene, 49708	Down
ENSMUSG00000022696	Sidt1	SID1 transmembrane family, member 1	Down
ENSMUSG00000027574	Nkain4	Na+/K+ transporting ATPase interacting 4	Down
ENSMUSG00000027577	Chrna4	cholinergic receptor, nicotinic, alpha polypeptide 4	Down
ENSMUSG00000040985	Sun3	Sad1 and UNC84 domain containing 3	Down
ENSMUSG00000110774	Gm39318	predicted gene, 39318	Down

4

Table S3 RNA-seq (continued)

Gene id	Gene name	Gene description	T_Ctrl_ vs_T_GHB
ENSMUSG00000112110	Gm15608	predicted gene 15608	Down
ENSMUSG00000001349	Cnn1	calponin 1	Down
ENSMUSG00000086015	4833417C18Rik	RIKEN cDNA 4833417C18 gene	Down
ENSMUSG00000038508	Gdf15	growth differentiation factor 15	Down
ENSMUSG00000061780	Cfd	complement factor D (adipsin)	Down
ENSMUSG00000026650	Meig1	meiosis expressed gene 1	Down
ENSMUSG00000113811	Gm47882	predicted gene, 47882	Down
ENSMUSG00000004341	Gpx6	glutathione peroxidase 6	Down
ENSMUSG00000073460	Pnldc1	poly(A)-specific ribonuclease (PARN)-like domain containing 1	Down
ENSMUSG00000097253	Gm26770	predicted gene, 26770	Down
ENSMUSG00000028664	Ephb2	Eph receptor B2	Down
ENSMUSG00000057969	Sema3b	sema domain, immunoglobulin domain (Ig), short basic domain, secreted, (semaphorin) 3B	Down
ENSMUSG00000002944	Cd36	CD36 molecule	Down
ENSMUSG00000114469	C730002L08Rik	RIKEN cDNA C730002L08 gene	Down
ENSMUSG00000025726	Slc28a1	solute carrier family 28 (sodium-coupled nucleoside transporter), member 1	Down
ENSMUSG00000090002	Gm16006	predicted gene 16006	Down
ENSMUSG00000021950	Anxa8	annexin A8	Down
ENSMUSG00000032254	Kif23	kinesin family member 23	Down
ENSMUSG00000006398	Cdc20	cell division cycle 20	Down
ENSMUSG00000110755	BC049987	cDNA sequence BC049987	Down
ENSMUSG00000114664	Gm48639	predicted gene, 48639	Down
ENSMUSG00000115509	Gm49012	predicted gene, 49012	Down
ENSMUSG00000058794	Nfe2	nuclear factor, erythroid derived 2	Down
ENSMUSG00000030278	Cidec	cell death-inducing DFFA-like effector c	Down
ENSMUSG00000006517	Mvd	mevalonate (diphospho) decarboxylase	Down
ENSMUSG00000103144	Pcdhga1	protocadherin gamma subfamily A, 1	Down
ENSMUSG00000032080	Apoa4	apolipoprotein A-IV	Down
ENSMUSG00000012187	Mogat1	monoacylglycerol O-acyltransferase 1	Down
ENSMUSG00000034634	Ly6d	lymphocyte antigen 6 complex, locus D	Down
ENSMUSG00000044854	1700056E22Rik	RIKEN cDNA 1700056E22 gene	Down
ENSMUSG00000048489	Depp1	DEPP1 autophagy regulator	Down
ENSMUSG00000011008	Mcoln2	mucolipin 2	Down
ENSMUSG00000018868	Pnpla5	patatin-like phospholipase domain containing 5	Down
ENSMUSG00000038768	9130409I23Rik	RIKEN cDNA 9130409I23 gene	Down
ENSMUSG00000112762	4930459C07Rik	RIKEN cDNA 4930459C07 gene	Down

Table S3 RNA-seq (continued)

Gene id	Gene name	Gene description	T_Ctrl_vs_T_GHB
ENSMUSG00000005883	Spo11	SPO11 initiator of meiotic double stranded breaks	Down
ENSMUSG00000030789	Itgax	integrin alpha X	Down
ENSMUSG00000058672	Tubb2a	tubulin, beta 2A class IIA	Down
ENSMUSG00000005540	Fcer2a	Fc receptor, IgE, low affinity II, alpha polypeptide	Down
ENSMUSG00000044678	Ly6k	lymphocyte antigen 6 complex, locus K	Down
ENSMUSG00000091867	Cyp2a22	cytochrome P450, family 2, subfamily a, polypeptide 22	Down
ENSMUSG00000083812	Gm5054	predicted gene 5054	Down
ENSMUSG00000021872	Rnase10	ribonuclease, RNase A family, 10 (non-active)	Down
ENSMUSG00000110611	Gm20163	predicted gene, 20163	Down
ENSMUSG00000107019	Gm43682	predicted gene 43682 [Source:MGI Symbol	Down
ENSMUSG00000021974	Fgf9	fibroblast growth factor 9	Down
ENSMUSG00000111282	Gm47528	predicted gene, 47528	Down
ENSMUSG00000001403	Ube2c	ubiquitin-conjugating enzyme E2C	Down
ENSMUSG00000038352	Arl5c	ADP-ribosylation factor-like 5C	Down
ENSMUSG00000108472	Gm45212	predicted gene 45212	Down
ENSMUSG00000055745	Rtl6	retrotransposon Gag like 6	Down
ENSMUSG00000089665	Fcor	Foxo1 corepressor	Down
ENSMUSG00000087669	Gm11724	predicted gene 11724	Down
ENSMUSG00000038540	Tmc3	transmembrane channel-like gene family 3	Down
ENSMUSG00000020419	Hormad2	HORMA domain containing 2	Down
ENSMUSG00000020651	Slc26a4	solute carrier family 26, member 4	Down
ENSMUSG00000097533	Gm26590	predicted gene, 26590	Down
ENSMUSG00000075025	Gm10804	predicted gene 10804	Down
ENSMUSG00000022033	Pbk	PDZ binding kinase	Down
ENSMUSG00000049109	Themis	thymocyte selection associated	Down
ENSMUSG00000008153	Clstn3	calsyntenin 3	Down
ENSMUSG00000087611	4930458D05Rik	RIKEN cDNA 4930458D05 gene	Down
ENSMUSG00000098140	Gm26938	predicted gene, 26938	Down
ENSMUSG00000043259	Fam13c	family with sequence similarity 13, member C	Down
ENSMUSG00000024526	Cidea	cell death-inducing DNA fragmentation factor, alpha subunit-like effector A	Down
ENSMUSG00000104213	Ighd	immunoglobulin heavy constant delta	Down
ENSMUSG00000078452	Raet1d	retinoic acid early transcript delta	Down
ENSMUSG00000021200	Asb2	ankyrin repeat and SOCS box-containing 2	Down
ENSMUSG00000075044	Slc22a29	solute carrier family 22. member 29	Down
ENSMUSG00000111013	Gm32468	predicted gene, 32468	Down

4

Table S3 RNA-seq (continued)

Gene id	Gene name	Gene description	T_Ctrl_vs_T_GHB
ENSMUSG00000038725	Pkhd1l1	polycystic kidney and hepatic disease 1-like 1	Down
ENSMUSG00000086136	Gm12718	predicted gene 12718	Down
ENSMUSG00000042985	Upk3b	uroplakin 3B	Down
ENSMUSG00000097762	4732463B04Rik	RIKEN cDNA 4732463B04 gene	Down
ENSMUSG00000099570	Gm29000	predicted gene 29000	Down
ENSMUSG00000118383	Gm50321	predicted gene, 50321	Down
ENSMUSG00000097482	Gm17634	predicted gene, 17634	Down
ENSMUSG00000116295	Gm32885	predicted gene, 32885	Down
ENSMUSG00000082920	Gm13864	predicted gene 13864	Down
ENSMUSG00000062309	Rpp25	ribonuclease P/MRP 25 subunit	Down
ENSMUSG00000107252	Gm5767	predicted gene 5767	Down
ENSMUSG00000052485	Tmem171	transmembrane protein 171	Down
ENSMUSG00000037953	A4gnt	alpha-1,4-N-acetylglucosaminyltransferase	Down
ENSMUSG00000033450	Tagap	T cell activation Rho GTPase activating protein	Down
ENSMUSG00000074570	Cass4	Cas scaffolding protein family member 4	Down
ENSMUSG00000116478	Gm18890	predicted gene, 18890	Down
ENSMUSG00000035385	Ccl2	chemokine (C-C motif) ligand 2	Down
ENSMUSG00000067818	Myl9	myosin, light polypeptide 9, regulatory	Down
ENSMUSG00000074183	Gsta1	glutathione S-transferase, alpha 1 (Ya)	Down
ENSMUSG00000070425	Xntrpc	Xndc1-transient receptor potential cation channel, subfamily C, member 2 readthrough	Up
ENSMUSG00000097140	Gm26779	predicted gene, 26779	Up
ENSMUSG00000049892	Rasd1	RAS, dexamethasone-induced 1	Up
ENSMUSG00000083012	Fam220a	family with sequence similarity 220, member A	Up
ENSMUSG00000101596	Gm28182	predicted gene 28182	Up
ENSMUSG00000110440	Gm45894	predicted gene 45894	Up
ENSMUSG00000064357	mt-Atp6	mitochondrially encoded ATP synthase 6	Up
ENSMUSG00000104159	Gm38099	predicted gene, 38099	Up
ENSMUSG00000047511	Olfr1396	olfactory receptor 1396	Up
ENSMUSG00000017146	Brca1	breast cancer 1, early onset	Up
ENSMUSG00000113898	Gm19144	predicted gene, 19144	Up
ENSMUSG00000115272	Gm49965	predicted gene, 49965	Up
ENSMUSG00000074115	Saa1	serum amyloid A 1	Up
ENSMUSG00000029683	Lmod2	leiomodin 2 (cardiac)	Up
ENSMUSG00000105891	A230001M10Rik	RIKEN cDNA A230001M10 gene	Up
ENSMUSG00000001672	Marveld3	MARVEL (membrane-associating) domain containing 3	Up

Table S3 RNA-seq (continued)

Gene id	Gene name	Gene description	T_Ctrl_ vs_T_GHB
ENSMUSG00000040017	Saa4	serum amyloid A 4	Up
ENSMUSG00000061322	Dnai1	dynein axonemal intermediate chain 1	Up
ENSMUSG00000044927	H1f10	H1.10 linker histone	Up
ENSMUSG00000110384	Gm45301	predicted gene 45301	Up
ENSMUSG00000092009	Myh15	myosin, heavy chain 15	Up
ENSMUSG00000085615	A330035P11Rik	RIKEN cDNA A330035P11 gene	Up
ENSMUSG00000032482	Cspg5	chondroitin sulfate proteoglycan 5	Up
ENSMUSG00000108884	Gm45792	predicted gene 45792	Up
ENSMUSG00000083170	Gm14405	predicted gene 14405	Up
ENSMUSG00000021466	Ptch1	patched 1	Up
ENSMUSG00000074269	Rec114	REC114 meiotic recombination protein	Up
ENSMUSG00000091971	Hspa1a	heat shock protein 1A	Up
ENSMUSG00000117001	Gm49858	predicted gene, 49858	Up
ENSMUSG00000048794	Cfap100	cilia and flagella associated protein 100	Up
ENSMUSG00000029380	Cxcl1	chemokine (C-X-C motif) ligand 1	Up
ENSMUSG00000024222	Fkbp5	FK506 binding protein 5	Up
ENSMUSG00000092470	Gm20518	predicted gene 20518	Up
ENSMUSG00000117250	Gm49871	predicted gene, 49871	Up
ENSMUSG00000113399	Gm48199	predicted gene, 48199	Up
ENSMUSG00000001095	Slc13a2	solute carrier family 13 (sodium-dependent dicarboxylate transporter), member 2	Up
ENSMUSG00000104113	Gm37292	predicted gene, 37292	Up
ENSMUSG00000094098	Vmn2r44	vomeronasal 2, receptor 44	Up
ENSMUSG00000084917	Gm17477	predicted gene, 17477	Up
ENSMUSG00000104918	Gm42944	predicted gene 42944	Up
ENSMUSG00000039903	Eva1c	eva-1 homolog C (C. elegans)	Up
ENSMUSG00000037443	Cep85	centrosomal protein 85	Up
ENSMUSG00000037447	Arid5a	AT rich interactive domain 5A (MRF1-like)	Up
ENSMUSG00000107877	Gm43951	predicted gene, 43951	Up
ENSMUSG00000100150	Gm19585	predicted gene, 19585	Up
ENSMUSG00000084383	Gm13370	predicted gene 13370	Up
ENSMUSG00000038415	Foxq1	forkhead box Q1	Up
ENSMUSG00000099556	Gm28857	predicted gene 28857	Up
ENSMUSG00000113261	Gm47404	predicted gene, 47404	Up
ENSMUSG00000097443	Gm17529	predicted gene, 17529	Up
ENSMUSG00000115220	Gm49768	predicted gene, 49768	Up

4

Table S3 RNA-seq (continued)

Gene id	Gene name	Gene description	T_Ctrl_ vs_T_GHB
ENSMUSG00000066361	Serpina3c	serine (or cysteine) peptidase inhibitor, clade A, member 3C	Up
ENSMUSG00000020000	Moxd1	monooxygenase, DBH-like 1	Up
ENSMUSG00000057465	Saa2	serum amyloid A 2	Up
ENSMUSG00000104222	Gm7292	predicted gene 7292	Up
ENSMUSG00000020218	Wif1	Wnt inhibitory factor 1	Up
ENSMUSG00000051639	Fbl-ps2	fibrillarin, pseudogene 2	Up
ENSMUSG00000060716	Plekhh1	pleckstrin homology domain containing, family H (with MyTH4 domain) member 1	Up
ENSMUSG00000109863	Gm45643	predicted gene 45643	Up
ENSMUSG00000028354	Fmn2	formin 2	Up
ENSMUSG00000109807	Gm45244	predicted gene 45244	Up
ENSMUSG00000025582	Nptx1	neuronal pentraxin 1	Up
ENSMUSG00000047462	Gpr141b	G protein-coupled receptor 141B	Up
ENSMUSG00000020805	Slc13a5	solute carrier family 13 (sodium-dependent citrate transporter), member 5	Up
ENSMUSG00000037341	Slc9a7	solute carrier family 9 (sodium/hydrogen exchanger), member 7	Up
ENSMUSG00000050440	Hamp	hepcidin antimicrobial peptide	Up
ENSMUSG00000056966	Gjc3	gap junction protein, gamma 3	Up
ENSMUSG00000027070	Lrp2	low density lipoprotein receptor-related protein 2	Up
ENSMUSG00000042846	Lrrtm3	leucine rich repeat transmembrane neuronal 3	Up
ENSMUSG00000026072	Il1r1	interleukin 1 receptor, type I	Up
ENSMUSG00000116765	Gm49762	predicted gene, 49762	Up
ENSMUSG00000029752	Asns	asparagine synthetase	Up
ENSMUSG00000072849	Serpina1e	serine (or cysteine) peptidase inhibitor, clade A, member 1E	Up
ENSMUSG00000030219	Erp27	endoplasmic reticulum protein 27	Up
ENSMUSG00000103560	Gm38070	predicted gene, 38070	Up
ENSMUSG00000024873	Cnih2	cornichon family AMPA receptor auxiliary protein 2	Up
ENSMUSG00000105703	Gm43305	predicted gene 43305	Up
ENSMUSG00000026415	Fcamr	Fc receptor, IgA, IgM, high affinity	Up
ENSMUSG00000105708	Gm36070	predicted gene, 36070	Up
ENSMUSG00000024274	Zscan30	zinc finger and SCAN domain containing 30	Up
ENSMUSG00000108878	Gm49493	predicted gene, 49493	Up
ENSMUSG00000070501	Ifi214	interferon activated gene 214	Up
ENSMUSG00000053113	Socs3	suppressor of cytokine signaling 3	Up
ENSMUSG00000091680	Klhdc7b	kelch domain containing 7B	Up
ENSMUSG00000105338	Gm43802	predicted gene 43802	Up
ENSMUSG00000076576	Igkv6-32	immunoglobulin kappa variable 6-32	Up

Table S3 RNA-seq (continued)

Gene id	Gene name	Gene description	T_Ctrl_ vs_T_GHB
ENSMUSG00000087367	Gm15491	predicted gene 15491	Up
ENSMUSG00000020185	E2f7	E2F transcription factor 7	Up
ENSMUSG00000101106	Gm28819	predicted gene 28819	Up
ENSMUSG00000001103	Sebox	SEBOX homeobox	Up
ENSMUSG00000005952	Trpv1	transient receptor potential cation channel, subfamily V, member 1	Up
ENSMUSG00000038599	Capn8	calpain 8	Up
ENSMUSG00000049281	Scn3b	sodium channel, voltage-gated, type III, beta	Up
ENSMUSG00000100162	Gm20687	predicted gene 20687	Up
ENSMUSG00000058579	Cela2a	chymotrypsin-like elastase family, member 2A	Up
ENSMUSG00000085445	Gm16348	predicted gene 16348	Up
ENSMUSG00000022388	Ttll8	tubulin tyrosine ligase-like family, member 8	Up
ENSMUSG00000096883	Shisa8	shisa family member 8	Up
ENSMUSG00000021209	Ppp4r4	protein phosphatase 4, regulatory subunit 4	Up
ENSMUSG00000113663	Gm48504	predicted gene, 48504	Up
ENSMUSG00000100968	Gm2098	predicted gene 2098	Up
ENSMUSG00000020205	Phlda1	pleckstrin homology like domain, family A, member 1	Up
ENSMUSG00000086765	Gm11827	predicted gene 11827	Up
ENSMUSG00000116946	Gm41442	predicted gene, 41442	Up
ENSMUSG00000026442	Nfasc	neurofascin	Up
ENSMUSG00000057425	Ugt2b37	UDP glucuronosyltransferase 2 family, polypeptide B37	Up
ENSMUSG00000028862	Map3k6	mitogen-activated protein kinase kinase kinase 6	Up
ENSMUSG00000024029	Tff3	trefoil factor 3, intestinal	Up
ENSMUSG00000037386	Rims2	regulating synaptic membrane exocytosis 2	Up
ENSMUSG00000116145	5730521K06Rik	RIKEN cDNA 5730521K06 gene	Up
ENSMUSG00000021750	Fam107a	family with sequence similarity 107, member A	Up
ENSMUSG00000021453	Gadd45g	growth arrest and DNA-damage-inducible 45 gamma	Up
ENSMUSG00000066687	Zbtb16	zinc finger and BTB domain containing 16	Up
ENSMUSG00000041930	Fam222a	family with sequence similarity 222, member A	Up
ENSMUSG00000030650	Tmc5	transmembrane channel-like gene family 5	Up
ENSMUSG00000083287	Idi1-ps1	isopentenyl-diphosphate delta isomerase, pseudogene 1	Up
ENSMUSG00000040125	Gpr26	G protein-coupled receptor 26	Up
ENSMUSG00000098678	Mroh6	maestro heat-like repeat family member 6	Up
ENSMUSG00000109198	D7Bwg0826e	DNA segment, Chr 7, Brigham & Women's Genetics 0826 expressed	Up
ENSMUSG00000090021	Gm6493	predicted gene 6493	Up
ENSMUSG00000095061	E030018B13Rik	RIKEN cDNA E030018B13 gene	Up

4

Table S3 RNA-seq (continued)

Gene id	Gene name	Gene description	T_Ctrl_ vs_T_GHB
ENSMUSG00000049414	Gm5417	predicted gene 5417	Up
ENSMUSG00000090264	Eif4ebp3	eukaryotic translation initiation factor 4E binding protein 3	Up
ENSMUSG00000048534	Jaml	junction adhesion molecule like	Up
ENSMUSG00000052415	Tchh	trichohyalin	Up
ENSMUSG00000022032	Scara5	scavenger receptor class A, member 5	Up
ENSMUSG00000091393	5330438I03Rik	RIKEN cDNA 5330438I03 gene	Up
ENSMUSG00000030483	Cyp2b10	cytochrome P450, family 2, subfamily b, polypeptide 10	Up
ENSMUSG00000042918	Mamstr	MEF2 activating motif and SAP domain containing transcriptional regulator	Up
ENSMUSG00000071036	Gm10309	predicted gene 10309	Up
ENSMUSG00000117901		novel transcript, antisense to Macrod1	Up
ENSMUSG00000090069	E430024P14Rik	RIKEN cDNA E430024P14 gene	Up
ENSMUSG00000058921	Slc10a5	solute carrier family 10 (sodium/bile acid cotransporter family), member 5	Up
ENSMUSG00000028445	Enho	energy homeostasis associated	Up
ENSMUSG00000022346	Myc	myelocytomatosis oncogene	Up
ENSMUSG00000038037	Socs1	suppressor of cytokine signaling 1	Up
ENSMUSG00000087684	1200007C13Rik	RIKEN cDNA 1200007C13 gene	Up
ENSMUSG00000072919	Noxred1	NADP+ dependent oxidoreductase domain containing 1	Up
ENSMUSG00000015533	Itga2	integrin alpha 2	Up
ENSMUSG00000066170	E230001N04Rik	RIKEN cDNA E230001N04 gene	Up
ENSMUSG00000057182	Scn3a	sodium channel, voltage-gated, type III, alpha	Up
ENSMUSG00000118670		mucin 19	Up
ENSMUSG00000056870	Gulp1	GULP, engulfment adaptor PTB domain containing 1	Up
ENSMUSG00000096221	1500002C15Rik	RIKEN cDNA 1500002C15 gene	Up
ENSMUSG00000092534	Pagr1b	PAXIP1 associated glutamate rich protein 1B	Up
ENSMUSG00000099389	Gm29603	predicted gene 29603	Up
ENSMUSG00000083992	Gm11478	predicted gene 11478	Up

Table S4 Plasma Metabolomics

Metabolites ID	Metabolite	Formula	Metab ID	Regulate
neg_1590	Erythronic acid	C4H8O5	metab_21744	down
neg_8994	Annoglabasin E	C20H32O3	metab_28653	down
neg_12734	9-Oxo-nonanoic acid	C9H16O3	metab_32064	down
neg_14055	2-O-(6-Phospho-alpha-mannosyl)-D-glycerate	C9H17O12P	metab_33271	down
pos_41	Linoleamide	C18H33NO	metab_40	down
pos_44	17,18-DiHETE	C20H32O4	metab_43	down
pos_59	(R)-(+)-2-Pyrrolidone-5-carboxylic acid	C5H7NO3	metab_58	down
pos_516	2,6-nonadienoic acid	C9H14O2	metab_512	down
pos_814	8-Hydroxy-4(6)-lactarene-5,14-diol	C15H26O3	metab_807	down
pos_830	(1S,2S)-3-oxo-2-pentyl-cyclopentanebutanoic acid	C14H24O3	metab_823	down
pos_839	7-oxo-11E,13-Tetradecadienoic acid	C14H22O3	metab_832	down
pos_840	3-Hydroxy-beta-ionone	C13H20O2	metab_833	down
pos_844	4,5-Dihydrovomifoliol	C13H22O3	metab_837	down
pos_852	7(14)-Bisabolene-2,3,10,11-tetrol	C15H28O4	metab_845	down
pos_2066	Zedoarondiol	C15H24O3	metab_2048	down
pos_2090	Prostaglandin-c2	C20H30O4	metab_2072	down
pos_2283	Farnesyl acetone	C18H30O	metab_2263	down
pos_3169	4-Hydroxyvalsartan	C24H29N5O4	metab_3143	down
pos_3641	Uric acid	C5H4N4O3	metab_3608	down
pos_5696	3-hydroxyhexanoyl carnitine	C14H27NO5	metab_5572	down
pos_5761	DL-2-Aminooctanoic acid	C8H17NO2	metab_5633	down
pos_8085	C16 Sphinganine	C16H35NO2	metab_7917	down
pos_13753	Acitretin(Ro 23-3571)	C19H26O3	metab_13449	down
pos_13971	Bremazocine	C20H29NO2	metab_13664	down
pos_14016	Vulgarone A	C15H22O	metab_13709	down
pos_14166	Methyl geranate	C11H18O2	metab_13857	down
pos_14180	Nitenin	C22H28O4	metab_13871	down
pos_14420	Compactin diol lactone	C18H26O4	metab_14109	down
pos_15116	8-Hydroxycarvotanacetone	C10H16O2	metab_14798	down
pos_16824	Dihydronepetalactone	C10H16O2	metab_16467	down
pos_16963	10-oxo-5,8-decadienoic acid	C10H14O3	metab_16606	down
pos_20073	L-Glutamine	C5H10N2O3	metab_19621	down
neg_1620	Butyl (S)-3-hydroxybutyrate [arabinosyl-(1->6)-glucoside]	C19H34O12	metab_21774	up
neg_2506	4-Nitrophenyl sulfate	C6H5NO6S	metab_22576	up
neg_4001	Goshonoside F4	C32H54O12	metab_23938	up
neg_5353	Saponin D	C48H78O17	metab_25160	up
neg_8621	Polyoxyethylene (600) monoricinoleate	C21H40O3	metab_28293	up
neg_11409	{[3-(2-hydroxy-4-methoxyphenyl)prop-2-en-1-yl]oxy} sulfonic acid	C10H12O6S	metab_30858	up

4

Table S5 Liver Metabolomics

ID	Metabolite	Metab ID	Formula	Regulate
neg_5987	9'-Carboxy-gamma-chromanol	metab_23678	C23H36O4	down
neg_6377	LysoPC(P-18:0)	metab_24041	C26H54NO6P	down
neg_9545	3'-Hydroxy-T2 Toxin	metab_27101	C24H34O10	down
neg_11996	5-[3-methoxy-4-(sulfooxy)phenyl]pentanoic acid	metab_29526	C12H16O7S	down
pos_126	Oleic Acid ethyl ester	metab_125	C20H38O2	down
pos_132	Arachidonic acid ethyl ester	metab_131	C22H36O2	down
pos_145	Arachidonic Acid methyl ester	metab_144	C21H34O2	down
pos_522	GPCho(20:4/22:6)	metab_516	C50H80NO8P	down
pos_529	GPCho(22:6/22:6)	metab_523	C52H80NO8P	down
pos_595	Cis-12-Octadecenoic Acid methyl ester	metab_589	C19H36O2	down
pos_1772	Sphinganine	metab_1744	C18H39NO2	down
pos_1810	N,N-dimethyl-Safingol	metab_1782	C20H43NO2	down
pos_2047	PC(20:0/0:0)	metab_2019	C28H58NO7P	down
pos_2089	PC(18:3(6Z,9Z,12Z)/22:6(4Z,7Z,10Z,13Z,16Z,19Z))	metab_2061	C48H78NO8P	down
pos_2097	GPEtn(20:4/22:6)	metab_2069	C47H74NO8P	down
pos_2102	PS(18:0/22:6(4Z,7Z,10Z,13Z,16Z,19Z))	metab_2074	C46H78NO10P	down
pos_2115	1alpha-hydroxy-25,26,27-trinorvitamin D3 24-carboxylic acid	metab_2087	C24H36O4	down
pos_2158	PC(P-18:0/18:3)	metab_2129	C44H82NO7P	down
pos_2429	PC(18:1(11Z)/18:3(9Z,12Z,15Z))	metab_2397	C44H80NO8P	down
pos_2432	PC(20:3(5Z,8Z,11Z)/22:6(4Z,7Z,10Z,13Z,16Z,19Z))	metab_2400	C50H82NO8P	down
pos_2437	GPEtn(18:2/22:6)	metab_2405	C45H74NO8P	down
pos_2438	PC(18:2(9Z,12Z)/22:6(4Z,7Z,10Z,13Z,16Z,19Z))	metab_2406	C48H80NO8P	down
pos_2611	PC(P-18:0/0:0)	metab_2579	C26H54NO6P	down
pos_3006	Sphingosine	metab_2969	C18H37NO2	down
pos_8789	PC(16:0/P-18:0)	metab_8643	C42H84NO7P	down
pos_10025	Lathosterol	metab_9856	C27H46O	down
pos_12379	Cerebronic acid	metab_12140	C24H48O3	down
pos_12591	MG(a-21:0/0:0/0:0)[rac]	metab_12352	C24H48O4	down
pos_15173	DL-2-Aminooctanoic acid	metab_14921	C8H17NO2	down
neg_55	Leucyl-phenylalanine	metab_17890	C15H22N2O3	up
neg_147	(+/-)4-HDoHE	metab_17982	C22H32O3	up
neg_194	N-Acetyl-D-phenylalanine	metab_18029	C11H13NO3	up
neg_642	(+/-)9-HpODE	metab_18463	C18H32O4	up
neg_2191	ALANYL-dl-LEUCINE	metab_19957	C9H18N2O3	up
neg_2292	8-(2-hydroxypropan-2-yl)-2-oxo-2H,8H,9H-furo[2,3-h]chromen-9-yl 3-methylbut-2-enoate	metab_20049	C19H20O6	up

Table S5 Liver Metabolomics (continued)

ID	Metabolite	Metab ID	Formula	Regulate
neg_2671	9-Oxo-nonanoic acid	metab_20420	C9H16O3	up
neg_2965	2,2'-(3-methylcyclohexane-1,1-diyl)diacetic acid	metab_20710	C11H18O4	up
neg_3355	(4S,8R)-8,9-Dihydroxy-p-menth-1(6)-en-2-one	metab_21095	C10H16O3	up
neg_3938	3-keto-Digoxigenin	metab_21674	C23H32O5	up
neg_3958	Atractyligenin	metab_21694	C20H30O3	up
neg_4801	5-cis-15(R)-Iloprost	metab_22521	C22H32O4	up
neg_5069	PGA1	metab_22788	C20H32O4	up
neg_5285	17-keto-4(Z),7(Z),10(Z),13(Z),15(E),19(Z)-Docosahexaenoic Acid	metab_22997	C22H30O3	up
neg_10016	Annoglabasin F	metab_27564	C22H34O5	up
neg_10258	Panaquinquecol 1	metab_27799	C18H28O3	up
neg_10972	Arginyl-Tryptophan	metab_28510	C17H24N6O3	up
neg_11214	Annuolide E	metab_28751	C15H20O3	up
neg_11648	6-Pentyl-2H-pyran-2-one	metab_29184	C10H14O2	up
neg_11767	Trans-4,5-epoxy-2(E)-Decenal	metab_29301	C10H16O2	up
neg_11943	Phenylpyruvic acid	metab_29474	C9H8O3	up
neg_12458	Pseudoecgonine	metab_29984	C9H15NO3	up
neg_12732	Isoleucyl-Tyrosine	metab_30257	C15H22N2O4	up
neg_12944	Glycyl-Phenylalanine	metab_30466	C11H14N2O3	up
neg_13029	Leucyl-Arginine	metab_30546	C12H25N5O3	up
neg_13075	Acetyl-DL-Valine	metab_30589	C7H13NO3	up
neg_11757	Dehydrovomifoliol	metab_31296	C13H18O3	up
pos_10	N-Acetyl-DL-methionine	metab_9	C7H13NO3S	up
pos_33	N-Acetyl-L-phenylalanine	metab_32	C11H13NO3	up
pos_54	3-Hydroxy-beta-ionone	metab_53	C13H20O2	up
pos_230	Acetyl-L-tyrosine	metab_229	C11H13NO4	up
pos_275	6E-nonenoic acid	metab_273	C9H16O2	up
pos_281	PC(20:5/0:0)	metab_279	C28H48NO7P	up
pos_1085	2-Pentyl-3-phenyl-2-propenal	metab_1070	C14H18O	up
pos_1716	Glechomafuran	metab_1688	C15H20O3	up
pos_1721	(-)-Leucothol C	metab_1693	C20H30O4	up
pos_1722	5(S),14(R)-Lipoxin B4	metab_1694	C20H32O5	up
pos_2987	5,6-Ep-15S-HETE	metab_2950	C20H30O4	up
pos_3010	Pseudoionone	metab_2973	C13H20O	up
pos_3014	13(S)-HpOTrE	metab_2977	C18H30O4	up
pos_3246	Spermine	metab_3207	C10H26N4	up
pos_4360	ALANYL-dl-PHENYLALANINE	metab_4265	C12H16N2O3	up

Table S5 Liver Metabolomics (continued)

ID	Metabolite	Metab ID	Formula	Regulate
pos_4812	Jasmolone	metab_4711	C11H16O2	up
pos_4891	O-Adipoylcarnitine	metab_4789	C13H23NO6	up
pos_4990	(S)-Neolyratyl acetate	metab_4888	C12H18O2	up
pos_5077	10beta-12,13-Dinor-8-oxo-6-eremophilen-11-al	metab_4975	C13H18O2	up
pos_6717	Thromboxane B3	metab_6608	C20H32O6	up
pos_7059	6alpha-methylprednisolone	metab_6948	C22H30O5	up
pos_7302	Tetrahydrodeoxycortisol	metab_7189	C21H34O4	up
pos_7376	PGD2 ethanolamide	metab_7263	C22H37NO5	up
pos_11803	25-Cinnamoyl-vulgaroside	metab_11567	C34H46O7	up
pos_12232	6,8,10,12-pentadecatetraenal	metab_11993	C15H22O	up
pos_12332	(10)-Gingerol	metab_12093	C21H34O4	up
pos_12850	PGE3 1,15-lactone	metab_12609	C20H28O4	up
pos_13209	12,13-Epoxy-9,15-octadecadienoic acid	metab_12966	C18H30O3	up
pos_13327	Bicyclo-PGE2	metab_13083	C20H30O4	up
pos_13517	5,6,15-trihydroxy-7,9,13-Eicosatrien-11-ynoic acid	metab_13273	C20H30O5	up
pos_13520	16-phenoxy tetranor PGF2alpha	metab_13276	C22H30O6	up
pos_13869	1,2,4-Trimethylbenzene	metab_13624	C9H12	up
pos_13926	2-Phenylethyl octanoate	metab_13681	C16H24O2	up
pos_14272	2-Hydroxyacorenone	metab_14024	C15H24O2	up
pos_14289	20-COOH-leukotriene E4	metab_14041	C23H35NO7S	up
pos_16218	M-Cresol	metab_17833	C7H8O	up

Table S6 RNA-seq

Gene ID	Gene name	Gene description	P_Ctrl_ vs_P_GHB
242			
ENSMUSG00000059089	Fcgr4	Fc receptor, IgG, low affinity IV	down
ENSMUSG00000114133	Gm20075	predicted gene, 20075	down
ENSMUSG00000043740	B430306N03Rik	RIKEN cDNA B430306N03 gene	down
ENSMUSG00000027398	Il1b	interleukin 1 beta	down
ENSMUSG00000009092	Derl3	Der1-like domain family, member 3	down
ENSMUSG00000015854	Cd5l	CD5 antigen-like	down
ENSMUSG00000051736	Fam229b	family with sequence similarity 229	down
ENSMUSG00000044938	Klhl31	kelch-like 31	down
ENSMUSG00000028931	Kcnab2	potassium voltage-gated channel, shaker-related subfamily, beta member 2	down
ENSMUSG00000059994	Fcrl1	Fc receptor-like 1	down
ENSMUSG00000043263	Ifi209	interferon activated gene 209	down
ENSMUSG00000019874	Fabp7	fatty acid binding protein 7	down
ENSMUSG00000023078	Cxcl13	chemokine (C-X-C motif) ligand 13	down
ENSMUSG00000058981	Olfr1406	olfactory receptor 1406	down
ENSMUSG00000045868	Gvin1	GTPase, very large interferon inducible 1	down
ENSMUSG00000031906	Smpd3	sphingomyelin phosphodiesterase 3, neutral	down
ENSMUSG00000029752	Asns	asparagine synthetase	down
ENSMUSG00000115902	D730005E14Rik	RIKEN cDNA D730005E14 gene	down
ENSMUSG00000117079	Gm41611	predicted gene, 41611	down
ENSMUSG00000026390	Marco	macrophage receptor with collagenous structure	down
ENSMUSG00000076612	Ighg2c	immunoglobulin heavy constant gamma 2C	down
ENSMUSG00000076613	Ighg2b	immunoglobulin heavy constant gamma 2B	down
ENSMUSG00000089942	Pira2	paired-Ig-like receptor A2	down
ENSMUSG00000101264	Gm28347	predicted gene 28347	down
ENSMUSG00000096950	Gm9530	predicted gene 9530	down
ENSMUSG00000072761	Gm6712	predicted gene 6712	down
ENSMUSG00000096715	Igkv3-4	immunoglobulin kappa variable 3-4	down
ENSMUSG00000117545	Gm30794	predicted gene, 30794	down
ENSMUSG00000030474	Siglece	sialic acid binding Ig-like lectin E	down
ENSMUSG00000050994	Adgb	androglobin	down
ENSMUSG00000055546	Timd4	T cell immunoglobulin and mucin domain containing 4	down
ENSMUSG00000050022	Amz1	archaelysin family metallopeptidase 1	down

Table S6 RNA-seq (continued)

Gene ID	Gene name	Gene description	P_Ctrl_ vs_P_GHB
ENSMUSG00000062593	Gm49339	predicted gene, 49339	down
ENSMUSG00000037318	Traf3ip3	TRAF3 interacting protein 3	down
ENSMUSG00000087623	Gm12404	predicted gene 12404	down
ENSMUSG00000030054	Gp9	glycoprotein 9 (platelet)	down
ENSMUSG00000022489	Pde1b	phosphodiesterase 1B, Ca2+-calmodulin dependent	down
ENSMUSG00000031304	Il2rg	interleukin 2 receptor, gamma chain	down
ENSMUSG00000103998	Gm38025	predicted gene, 38025	down
ENSMUSG00000031093	Dock11	dedicator of cytokinesis 11	down
ENSMUSG00000056071	S100a9	S100 calcium binding protein A9 (calgranulin B)	down
ENSMUSG00000032254	Kif23	kinesin family member 23	down
ENSMUSG00000112332	4930466K18Rik	RIKEN cDNA 4930466K18 gene	down
ENSMUSG00000034438	Gbp8	guanylate-binding protein 8	down
ENSMUSG00000039533	Mmd2	monocyte to macrophage differentiation-associated 2	down
ENSMUSG00000051439	Cd14	CD14 antigen	down
ENSMUSG00000076609	Igkc	immunoglobulin kappa constant	down
ENSMUSG00000024679	Ms4a6d	membrane-spanning 4-domains, subfamily A, member 6D	down
ENSMUSG00000031506	Ptpn7	protein tyrosine phosphatase, non-receptor type 7	down
ENSMUSG00000078763	Slfn1	schlafen 1	down
ENSMUSG00000035004	Igsf6	immunoglobulin superfamily, member 6	down
ENSMUSG00000098290	Obox4-ps1	oocyte specific homeobox 4, pseudogene 1	down
ENSMUSG00000025930	Msc	musculin	down
ENSMUSG00000078154	Gm12184	predicted gene 12184	down
ENSMUSG00000030278	Cidec	cell death-inducing DFFA-like effector c	down
ENSMUSG00000087273	Gm13203	predicted gene 13203	down
ENSMUSG00000021322	Aoah	acyloxyacyl hydrolase	down
ENSMUSG00000023067	Cdkn1a	cyclin-dependent kinase inhibitor 1A (P21)	down
ENSMUSG00000032484	Ngp	neutrophilic granule protein	down
ENSMUSG00000073207	Ccdc160	coiled-coil domain containing 160	down
ENSMUSG00000076937	Iglc2	immunoglobulin lambda constant 2	down
ENSMUSG00000076934	Iglv1	immunoglobulin lambda variable 1	down
ENSMUSG00000089829	Gm16565	predicted gene 16565	down
ENSMUSG00000059108	Ifitm6	interferon induced transmembrane protein 6	down
ENSMUSG00000038543	BC028528	cDNA sequence BC028528	down

Table S6 RNA-seq (continued)

Gene ID	Gene name	Gene description	P_Ctrl_ vs_P_GHB
ENSMUSG00000024353	Mzb1	marginal zone B and B1 cell-specific protein 1	down
ENSMUSG00000026536	Ifi211	interferon activated gene 211	down
ENSMUSG00000069792	Wfdc17	WAP four-disulfide core domain 17	down
ENSMUSG00000044912	Syt16	synaptotagmin XVI	down
ENSMUSG00000037868	Egr2	early growth response 2	down
ENSMUSG00000040026	Saa3	serum amyloid A 3	down
ENSMUSG00000000392	Fap	fibroblast activation protein	down
ENSMUSG00000036905	C1qb	complement component 1, q subcomponent, beta polypeptide	down
ENSMUSG00000106380	Gm3519	predicted gene 3519	down
ENSMUSG00000030144	Clec4d	C-type lectin domain family 4, member d	down
ENSMUSG00000109209	Gm45104	predicted gene 45104	down
ENSMUSG00000067547	Gm7666	predicted pseudogene 7666	down
ENSMUSG00000020057	Dram1	DNA-damage regulated autophagy modulator 1	down
ENSMUSG00000033777	Tlr13	toll-like receptor 13	down
ENSMUSG00000046182	Gsg1l	GSG1-like	down
ENSMUSG00000030148	Clec4a2	C-type lectin domain family 4, member a2	down
ENSMUSG00000058174	Gm5148	predicted gene 5148	down
ENSMUSG00000064246	Chil1	chitinase-like 1	down
ENSMUSG00000025020	Slit1	slit guidance ligand 1	down
ENSMUSG00000097113	Gm19705	predicted gene, 19705	down
ENSMUSG00000092083	Kcnb2	potassium voltage gated channel, Shab-related subfamily, member 2	down
ENSMUSG00000022432	Smc1b	structural maintenance of chromosomes 1B	down
ENSMUSG00000005667	Mthfd2	methylenetetrahydrofolate dehydrogenase (NAD+ dependent), methenyltetrahydrofolate cyclohydrolase	down
ENSMUSG00000089859	Olfr1565	olfactory receptor 1565	down
ENSMUSG00000052270	Fpr2	formyl peptide receptor 2	down
ENSMUSG00000070806	Zmynd12	zinc finger, MYND domain containing 12	down
ENSMUSG00000055202	Zfp811	zinc finger protein 811	down
ENSMUSG00000048794	Cfap100	cilia and flagella associated protein 100	down
ENSMUSG00000102014	2900009J06Rik	RIKEN cDNA 2900009J06 gene	down
ENSMUSG00000106709	Gm30270	predicted gene, 30270	down
ENSMUSG00000034987	Hrh2	histamine receptor H2	down
ENSMUSG00000036362	P2ry13	purinergic receptor P2Y, G-protein coupled 13	down

4

Table S6 RNA-seq (continued)

Gene ID	Gene name	Gene description	P_Ctrl_ vs_P_GHB
ENSMUSG00000057425	Ugt2b37	UDP glucuronosyltransferase 2 family, polypeptide B37	down
ENSMUSG00000076552	Igkv4-61	immunoglobulin kappa chain variable 4-61	down
ENSMUSG00000020642	Rnf144a	ring finger protein 144A	down
ENSMUSG00000048498	Cd300e	CD300E molecule	down
ENSMUSG00000034059	Ypel4	yippee like 4	down
ENSMUSG00000028497	Hacd4	3-hydroxyacyl-CoA dehydratase 4	down
ENSMUSG00000113152	Gm48422	predicted gene, 48422	down
ENSMUSG00000029816	Gpnmb	glycoprotein (transmembrane) nmb	down
ENSMUSG00000023992	Trem2	triggering receptor expressed on myeloid cells 2	down
ENSMUSG00000061540	Orm2	orosomucoid 2	down
ENSMUSG00000110047	A230085B16Rik	RIKEN cDNA A230085B16 gene	down
ENSMUSG00000025163	Cd7	CD7 antigen	down
ENSMUSG00000111282	Gm47528	predicted gene, 47528	down
ENSMUSG00000106628	Gm43558	predicted gene 43558	down
ENSMUSG00000066682	Pilrb2	paired immunoglobin-like type 2 receptor beta 2	down
ENSMUSG00000113088	Gm36757	predicted gene, 36757	down
ENSMUSG00000042244	Pglyrp3	peptidoglycan recognition protein 3	down
ENSMUSG00000020798	Spns3	spinster homolog 3	down
ENSMUSG00000087390	Gm7598	predicted gene 7598	down
ENSMUSG00000002699	Lcp2	lymphocyte cytosolic protein 2	down
ENSMUSG00000032224	Fam81a	family with sequence similarity 81, member A	down
ENSMUSG00000030651	Art2b	ADP-ribosyltransferase 2b	down
ENSMUSG00000062488	Ifit3b	interferon-induced protein with tetratricopeptide repeats 3B	down
ENSMUSG00000047798	Cd300lf	CD300 molecule like family member F	down
ENSMUSG00000063838	Cdc42ep5	CDC42 effector protein (Rho GTPase binding) 5	down
ENSMUSG00000026358	Rgs1	regulator of G-protein signaling 1	down
ENSMUSG00000000982	Ccl3	chemokine (C-C motif) ligand 3	down
ENSMUSG00000082776	Gm7061	predicted gene 7061	down
ENSMUSG00000113790	Gm17872	predicted gene, 17872	down
ENSMUSG00000059775	Rps26-ps1	ribosomal protein S26, pseudogene 1	down
ENSMUSG00000030708	Dnajb13	DnaJ heat shock protein family (Hsp40) member B13	down
ENSMUSG00000020431	Adcy1	adenylate cyclase 1	down

Table S6 RNA-seq (continued)

Gene ID	Gene name	Gene description	P_Ctrl_ vs_P_GHB
ENSMUSG00000021904	Sema3g	sema domain, immunoglobulin domain (Ig), short basic domain, secreted, (semaphorin) 3G	down
ENSMUSG00000049107	Ntf3	neurotrophin 3	down
ENSMUSG00000032816	Igdcc4	immunoglobulin superfamily, DCC subclass, member 4	down
ENSMUSG00000024056	Ndc80	NDC80 kinetochore complex component	down
ENSMUSG00000022876	Samsn1	SAM domain, SH3 domain and nuclear localization signals, 1	down
ENSMUSG00000035373	Ccl7	chemokine (C-C motif) ligand 7	down
ENSMUSG00000072620	Slfn2	schlafen 2	down
ENSMUSG00000052013	Btla	B and T lymphocyte associated	down
ENSMUSG00000057182	Scn3a	sodium channel, voltage-gated, type III, alpha	down
ENSMUSG00000038085	Cnbd2	cyclic nucleotide binding domain containing 2	down
ENSMUSG00000060402	Chst8	carbohydrate sulfotransferase 8	down
ENSMUSG00000087611	4930458D05Rik	RIKEN cDNA 4930458D05 gene	down
ENSMUSG00000079293	Clec7a	C-type lectin domain family 7, member a	down
ENSMUSG00000090164	BC035044	cDNA sequence BC035044	down
ENSMUSG00000064147	Rab44	RAB44, member RAS oncogene family	down
ENSMUSG00000110316	Gm45311	predicted gene 45311	down
ENSMUSG00000038917	3930402G23Rik	RIKEN cDNA 3930402G23 gene	down
ENSMUSG00000030650	Tmc5	transmembrane channel-like gene family 5	down
ENSMUSG00000010461	Eya4	EYA transcriptional coactivator and phosphatase 4	down
ENSMUSG00000024521	Pmaip1	phorbol-12-myristate-13-acetate-induced protein 1	down
ENSMUSG00000084319	Tpt1-ps3	tumor protein, translationally-controlled, pseudogene 3	down
ENSMUSG00000024008	Cpne5	copine V	down
ENSMUSG00000015950	Ncf1	neutrophil cytosolic factor 1	down
ENSMUSG00000105504	Gbp5	guanylate binding protein 5	down
ENSMUSG00000020892	Aloxe3	arachidonate lipoxygenase 3	down
ENSMUSG00000051627	H1f4	H1.4 linker histone, cluster member	down
ENSMUSG00000024013	Fgd2	FYVE, RhoGEF and PH domain containing 2	down
ENSMUSG00000024399	Ltb	lymphotoxin B	down
ENSMUSG00000040264	Gbp2b	guanylate binding protein 2b	down
ENSMUSG00000004359	Spic	Spi-C transcription factor (Spi-1/PU.1 related)	down
ENSMUSG00000105055	Gm43079	predicted gene 43079	down
ENSMUSG00000028555	Ttc39a	tetratricopeptide repeat domain 39A	down

4

Table S6 RNA-seq (continued)

Gene ID	Gene name	Gene description	P_Ctrl_ vs_P_GHB
ENSMUSG00000020573	Pik3cg	phosphatidylinositol-4,5-bisphosphate 3-kinase catalytic subunit gamma	down
ENSMUSG00000044708	Kcnj10	potassium inwardly-rectifying channel, subfamily J, member 10	down
ENSMUSG00000071661	Zbtb3	zinc finger and BTB domain containing 3	down
ENSMUSG00000017652	Cd40	CD40 antigen	down
ENSMUSG00000046167	Gldn	gliomedin	down
ENSMUSG00000086481	Gm11707	predicted gene 11707	down
ENSMUSG00000085014	Gm13490	predicted gene 13490	down
ENSMUSG00000023349	Clec4n	C-type lectin domain family 4, member n	down
ENSMUSG00000050335	Lgals3	lectin, galactose binding, soluble 3	down
ENSMUSG00000072596	Ear2	eosinophil-associated, ribonuclease A family, member 2	down
ENSMUSG00000020218	Wif1	Wnt inhibitory factor 1	down
ENSMUSG00000044811	Cd300c2	CD300C molecule 2	down
ENSMUSG00000060044	Tmem26	transmembrane protein 26	down
ENSMUSG00000069516	Lyz2	lysozyme 2	down
ENSMUSG00000004730	Adgre1	adhesion G protein-coupled receptor E1	down
ENSMUSG00000003545	Fosb	FBJ osteosarcoma oncogene B	down
ENSMUSG00000026068	Il18rap	interleukin 18 receptor accessory protein	down
ENSMUSG00000076614	Ighg1	immunoglobulin heavy constant gamma 1 (G1m marker)	down
ENSMUSG00000036353	P2ry12	purinergic receptor P2Y, G-protein coupled 12	down
ENSMUSG00000038642	Ctss	cathepsin S	down
ENSMUSG00000104077	Gm37027	predicted gene, 37027	down
ENSMUSG00000060176	Kif27	kinesin family member 27	down
ENSMUSG00000095351	Igkv3-2	immunoglobulin kappa variable 3-2	down
ENSMUSG00000018927	Ccl6	chemokine (C-C motif) ligand 6	down
ENSMUSG00000074342	I830077J02Rik	RIKEN cDNA I830077J02 gene	down
ENSMUSG00000044229	Nxpe4	neurexophilin and PC-esterase domain family, member 4	down
ENSMUSG00000097391	Mirg	miRNA containing gene	down
ENSMUSG00000103037	Pcdhgb1	protocadherin gamma subfamily B, 1	down
ENSMUSG00000030200	Bcl2l14	BCL2-like 14 (apoptosis facilitator)	down
ENSMUSG00000025165	Sectm1a	secreted and transmembrane 1A	down
ENSMUSG00000022148	Fyb	FYN binding protein	down

Table S6 RNA-seq (continued)

Gene ID	Gene name	Gene description	P_Ctrl_ vs_P_GHB
ENSMUSG00000049625	Tifab	TRAF-interacting protein with forkhead-associated domain, family member B	down
ENSMUSG00000020808	Pimreg	PICALM interacting mitotic regulator	down
ENSMUSG00000044827	Tlr1	toll-like receptor 1	down
ENSMUSG00000032739	Pram1	PML-RAR alpha-regulated adaptor molecule 1	down
ENSMUSG00000074183	Gsta1	glutathione S-transferase, alpha 1 (Ya)	down
ENSMUSG00000024300	Myo1f	myosin IF	down
ENSMUSG00000039013	Siglecf	sialic acid binding Ig-like lectin F	down
ENSMUSG00000110498	A630001O12Rik	RIKEN cDNA A630001O12 gene	down
ENSMUSG00000062007	Hsh2d	hematopoietic SH2 domain containing	down
ENSMUSG00000064358	mt-Co3	mitochondrially encoded cytochrome c oxidase III	up
ENSMUSG00000096497	Olfr787	olfactory receptor 787	up
ENSMUSG00000110099	Gm45344	predicted gene 45344	up
ENSMUSG00000031517	Gpm6a	glycoprotein m6a	up
ENSMUSG00000043753	Dmrta1	doublesex and mab-3 related transcription factor like family A1	up
ENSMUSG00000095486	Vmn2r22	vomeronasal 2, receptor 22	up
ENSMUSG00000106447	Gm42957	predicted gene 42957	up
ENSMUSG00000082762	Gm12366	predicted gene 12366	up
ENSMUSG00000055271	9330161L09Rik	RIKEN cDNA 9330161L09 gene	up
ENSMUSG00000085101	Platr16	pluripotency associated transcript 16	up
ENSMUSG00000109953	5430430B14Rik	RIKEN cDNA 5430430B14 gene	up
ENSMUSG00000037096	Gm9762	predicted pseudogene 9762	up
ENSMUSG00000112008	Gm47218	predicted gene, 47218	up
ENSMUSG00000081671	Gm13167	predicted gene 13167	up
ENSMUSG00000028546	Elavl4	ELAV like RNA binding protein 4	up
ENSMUSG00000106767	Gm42727	predicted gene 42727	up
ENSMUSG00000051022	Hs3st1	heparan sulfate (glucosamine) 3-O-sulfotransferase 1	up
ENSMUSG00000040537	Adam22	a disintegrin and metallopeptidase domain 22	up
ENSMUSG00000109564	Muc16	mucin 16	up
ENSMUSG00000023039	Krt7	keratin 7	up
ENSMUSG00000115782	Gm49116	predicted gene, 49116	up
ENSMUSG00000105912	Gm10440	predicted gene 10440	up
ENSMUSG00000024274	Zscan30	zinc finger and SCAN domain containing 30	up

4

Table S6 RNA-seq (continued)

Gene ID	Gene name	Gene description	P_Ctrl_ vs_P_GHB
ENSMUSG00000047155	Cyp4x1	cytochrome P450, family 4, subfamily x, polypeptide 1	up
ENSMUSG00000074796	Slc4a11	solute carrier family 4, sodium bicarbonate transporter-like, member 11	up
ENSMUSG00000041730	Prrxl1	paired related homeobox protein-like 1	up
ENSMUSG00000086916	Gm15903	predicted gene 15903	up
ENSMUSG00000042985	Upk3b	uroplakin 3B	up
ENSMUSG00000112516	Gm47968	predicted gene, 47968	up
ENSMUSG00000097760	6030442K20Rik	RIKEN cDNA 6030442K20 gene	up
ENSMUSG00000063011	Msln	mesothelin	up
ENSMUSG00000071347	C1qtnf9	C1q and tumor necrosis factor related protein 9	up
ENSMUSG00000087367	Gm15491	predicted gene 15491	up
ENSMUSG00000049436	Upk1b	uroplakin 1B	up
ENSMUSG00000081855	Rpl17-ps5	ribosomal protein L17, pseudogene 5	up
ENSMUSG00000023935	Spats1	spermatogenesis associated, serine-rich 1	up
ENSMUSG00000111539	Gm48372	predicted gene, 48372	up
ENSMUSG00000107227	Gm42559	predicted gene 42559	up
ENSMUSG00000103400	Gm15853	predicted gene 15853	up
ENSMUSG00000023046	Igfbp6	insulin-like growth factor binding protein 6	up
ENSMUSG00000005237	Dnah2	dynein, axonemal, heavy chain 2	up

5

FGF21 protects against hepatic lipotoxicity and macrophage activation to attenuate fibrogenesis in nonalcoholic steatohepatitis

Cong Liu[1, 2], Milena Schönke[1, 2], Borah Spoorenberg[1, 2], Joost M. Lambooij[3, 4], Hendrik J.P. van der Zande[3], Enchen Zhou[1, 2], Maarten E. Tushuizen[5], Anne-Christine Andréasson[6], Andrew Park[7], Stephanie Oldham[8], Martin Uhrbom[6], Ingela Ahlstedt[6], Yasuhiro Ikeda[7], Kristina Wallenius[6], Xiao-Rong Peng[6], Bruno Guigas[3], Mariëtte R. Boon[1, 2], Yanan Wang[,1, 2, 9], Patrick C.N. Rensen[1, 2, 9]

[1] Department of Medicine, Division of Endocrinology, Leiden University Medical Center, Leiden, The Netherlands.
[2] Einthoven Laboratory for Experimental Vascular Medicine, Leiden University Medical Center, Leiden, The Netherlands.
[3] Department of Parasitology, Leiden University Medical Center, Leiden, The Netherlands.
[4] Department of Cell and Chemical Biology, Leiden University Medical Center, Leiden, The Netherlands.
[5] Department of Gastroenterology and Hepatology, Leiden University Medical Center, Leiden, The Netherlands.
[6] Bioscience Metabolism, Research and Early Development, Cardiovascular, Renal and Metabolism (CVRM), BioPharmaceuticals R&D, AstraZeneca, Gothenburg, Sweden.
[7] Biologics Engineering and Targeted Delivery, Oncology R&D, AstraZeneca, Gaithersburg, USA.
[8] Bioscience Metabolism, Research and Early Development, Cardiovascular, Renal and Metabolism (CVRM), BioPharmaceuticals R&D, AstraZeneca, Gaithersburg, USA.
[9] Med-X institute, Center for Immunological and Metabolic Diseases, and Department of Endocrinology, First Affiliated Hospital of Xi'an Jiaotong University, Xi'an Jiaotong University, Xi'an, China.

ABSTRACT
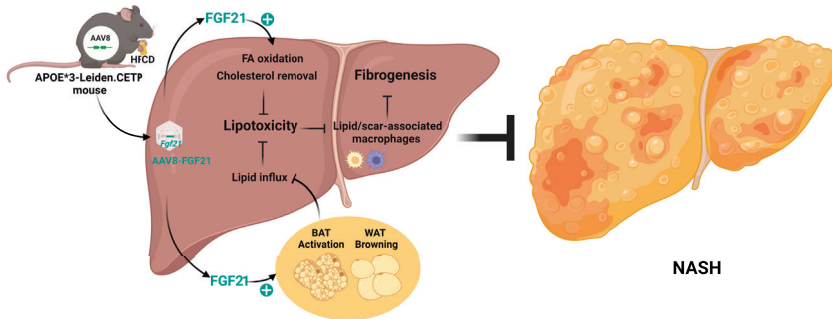
Analogues of the hepatokine FGF21 are in clinical development for type 2 diabetes and nonalcoholic steatohepatitis (NASH) treatment. Although their glucose-lowering and insulin-sensitizing effects have been largely unraveled, the mechanisms by which they alleviate liver injury have only been scarcely addressed. Here, we aimed to unveil the mechanisms underlying the protective effects of FGF21 on NASH using APOE*3-Leiden. CETP mice, a well-established model for human-like metabolic diseases. Liver-specific FGF21 overexpression was achieved in mice, followed by administration of a high-fat high-cholesterol diet for 23 weeks. FGF21 prevented hepatic lipotoxicity, accompanied by activation of thermogenic tissues and attenuation of adipose tissue inflammation, improvement of hyperglycemia and hypertriglyceridemia, and upregulation of hepatic programs involved in fatty acid oxidation and cholesterol removal. Furthermore, FGF21 inhibited hepatic inflammation, as evidenced by reduced Kupffer cell (KC) activation, diminished monocyte infiltration and lowered accumulation of monocyte-derived macrophages. Moreover, FGF21 decreased lipid- and scar-associated macrophages, which correlated with less hepatic fibrosis as demonstrated by reduced collagen accumulation. Collectively, hepatic FGF21 overexpression limits hepatic lipotoxicity, inflammation and fibrogenesis. Mechanistically, FGF21 blocks hepatic lipid influx and accumulation through combined endocrine and autocrine signaling, respectively, which prevents KC activation and lowers the presence of lipid- and scar-associated macrophages to inhibit fibrogenesis.

INTRODUCTION

The liver is the nexus of many metabolic pathways, including those of glucose, fatty acids (FAs) and cholesterol. In health, these metabolites are distributed to peripheral tissues while preventing long-lasting accumulation in the liver. In a pathological state, however, lipids may accrue in the liver, thereby impairing liver function and carving the path towards the development of nonalcoholic fatty liver disease (NAFLD) [1]. NAFLD is considered a spectrum of liver diseases ranging from liver steatosis, characterized by lipid accumulation in hepatocytes, to nonalcoholic steatohepatitis (NASH) with hepatic steatosis, lobular inflammation, hepatocyte ballooning and varying degrees of fibrosis [2, 3]. Patients diagnosed with NASH are predisposed to developing cirrhosis and hepatocellular carcinoma, among whom patients with severe liver fibrosis are at greatest risk of overall- and liver-related mortality [4]. Despite this, there are currently no approved pharmaceutical therapeutics for NASH. Instead, lifestyle modifications remain the first-line treatment for NASH, although this is rarely attainable in the long term, and liver transplantation is still the sole intervention to treat the end-stage of NASH [2, 5]. Thus, there is an unmet need for therapeutic strategies that control the progression of NASH, in particular of liver fibrosis, and reverse the underlying pathophysiology.

Current hypotheses suggest that adipose tissue dysfunction and lipid spillover leads to hepatic lipotoxicity, and thereby the initiation of NASH [6, 7], which further progresses through the inflammatory response triggered by hepatic lipotoxicity [7]. This inflammatory response and subsequent fibrogenesis are primarily initiated by liver macrophages [8]. Hepatic macrophages mainly consist of embryonically-derived macrophages, termed resident Kupffer cells (ResKCs), and monocyte-derived macrophages (MoDMacs) that are recruited from the circulation [9]. In the steady state, ResKCs serve as sentinels for liver homeostasis. In NASH, liver injury caused by excess lipids and hepatocyte damage/death, triggers ResKC activation, leading to pro-inflammatory cytokine and chemokine release [10]. This fosters the infiltration of newly-recruited monocytes into the liver, which gives rise to various pro-inflammatory and pro-fibrotic macrophage subsets [8, 10]. Interestingly, recent preclinical and clinical studies have reported that modulation of ResKC activation, monocyte recruitment or macrophage differentiation, to some extent, can attenuate NASH [8, 11]. In light of these findings, FGF21, a hepatokine with both lipid-lowering and anti-inflammatory properties [12, 13], has been brought to the foreground as a promising potential therapeutic to treat NASH.

5

The specificity of FGF21 action for various metabolic tissues is determined by the FGF receptor (FGFR) which forms a heterodimer with the transmembrane co-receptor β-Klotho (KLB) [14, 15]. While the FGFR is ubiquitously expressed, KLB is primarily expressed in the liver and adipose tissue [14, 15], therefore possibly limiting FGF21 action to these tissues. Physiologically, FGF21 is considered a stress-induced hormone whose levels rise in metabolically compromised states, such as obesity [16] and NASH [17]. The increased FGF21 in these pathologies is likely induced by an accumulation of lipids in the liver [18]. As such, plasma FGF21 also positively correlates with the severity of steatohepatitis and fibrosis in patients with NASH [17]. Induction of FGF21 is thought to mediate a compensatory response to limit metabolic dysregulation [19], although this level is not sufficient. Interestingly, two phase 2a clinical trials reported that pharmacological FGF21 treatment improves liver steatosis in NASH patients [20, 21]. While an *in vivo* study testing the therapeutic potency of FGF21 in choline-deficient and high-fat diet-induced NASH has previously reported both anti-inflammatory and anti-fibrotic effects [22], detailed mechanistic understanding is still lacking.

In the present study, we aimed to elucidate the mechanisms underlying FGF21-mediated improvement of NASH, in particular of steatohepatitis and fibrogenesis. To this end, we used *APOE*3-Leiden.CETP* mice, a well-established model for human cardiometabolic diseases. These mice exhibit human-like lipoprotein metabolism, develop hyperlipidemia, obesity and inflammation when fed a high-fat high-cholesterol diet (HFCD), and develop fibrotic NASH closely resembling clinical features that accompany NASH in humans [23, 24]. Moreover, these mice show human-like responses to both lipid-lowering and anti-inflammatory therapeutics during the development of metabolic syndrome [25-28]. Here, we show that specific overexpression of FGF21 in the liver, resulting in increases circulating FGF21 levels, activates hepatic signaling associated with FA oxidation and cholesterol removal. In parallel, FGF21 activates thermogenic tissues and reduces adipose tissue inflammation, thereby protecting against adipose tissue dysfunction, hyperglycemia and hypertriglyceridemia. As a consequence, FGF21 largely limits lipid accumulation in the liver and potently blocks hepatic KC activation and monocyte recruitment, thereby preventing the accumulation of pro-inflammatory macrophages in the liver. In addition, FGF21 reduced the number of pro-fibrotic macrophages in the injured liver, potentially explaining why FGF21 counteracts all features of NASH, including hepatic steatosis, inflammation and fibrogenesis.
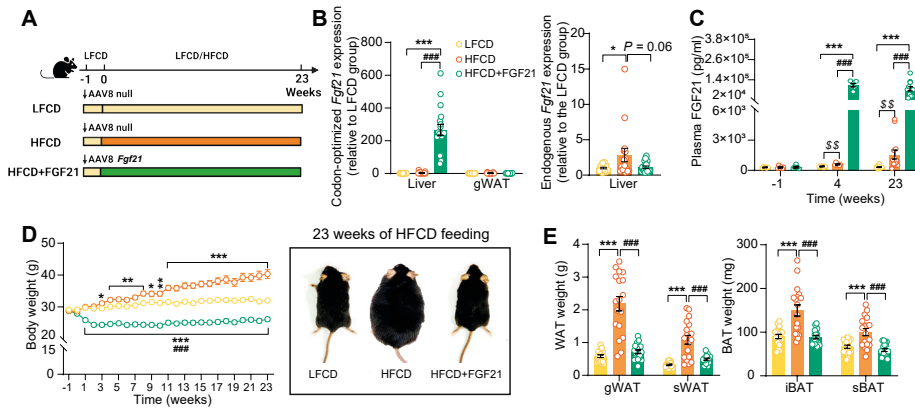
RESULTS

Liver-specific FGF21 overexpression increases circulating FGF21 levels and protects against HFCD-induced body fat mass gain

We aimed to elucidate the underlying mechanisms of FGF21-mediated hepatoprotective effects on NASH, by using *APOE*3-Leiden.CETP* mice fed with a HFCD, a model that induces all stages of NASH in a human-like fashion and recapitulates the ultrastructural changes observed in NASH patients [23, 24]. Since the liver is the main contributor to circulating FGF21 [14], we employed an adeno-associated virus vector 8 (AAV8) vector expressing codon-optimized murine *FgF21* to induce liver-specific FGF21 overexpression in APOE*3-Leiden.CETP mice. Mice treated with either AAV8-*Fgf21* or AAV8-null as controls were fed with a HFCD for 23 weeks (**Fig. 1A**). We confirmed liver-specific FGF21 overexpression by a large increase in codon-optimized *Fgf21* expression in the liver but not in adipose tissue (**Fig. 1B**), resulting in high circulating FGF21 levels that persisted throughout the study (**Fig. 1C**). In addition, we observed that HFCD feeding increased hepatic endogenous *Fgf21* expression (+184%), which, however, was prevented by AAV8-*Fgf21* administration (**Fig. 1B**). Furthermore, by performing a student *t*-test between the LFCD and HFCD groups, we did observe that as compared to the LFCD group, HFCD feeding increased plasma FGF21 levels at week 4 (+52%) and week 23 (+383%) (**Fig. 1C**).These results are in agreement with previous findings showing that FGF21 is a stress-induced hepatokine whose levels increases in metabolically compromised states, such as obesity [16] and NAFLD [17]. HFCD progressively and profoundly increased body weight over the experimental period, accompanied by increased white adipose tissue (WAT) and brown adipose tissue (BAT) weights relative to those of low fat low cholesterol (LFCD)-fed mice (**Fig. 1D,E**). In favorable contrast, FGF21 reduced body weight in the first 3 weeks, after which body weight stabilized and remained lower than that of LFCD- and HFCD-fed mice by the end of the study (-18% and -35%, respectively; **Fig. 1D**). Concomitantly, FGF21 decreased weights of gonadal WAT (gWAT; -67%), subcutaneous WAT (sWAT; -55%), interscapular BAT (iBAT; -41%) and subscapular BAT (-41%) to levels comparable to those observed in LFCD-fed mice (**Fig. 1E**). These findings thus highlight the potent effects of FGF21 on preventing fat mass gain under NASH-inducing dietary conditions.

Fig. 1. Liver-specific FGF21 overexpression increases circulating FGF21 levels and protects against HFCD-induced body fat mass gain. (**A**) Experimental set up. (**B**) At week 23, codon-optimizedFGF21 mRNA expression in the liver and gWAT was quantified (n=16-18), and endogenous*Fgf21* expression in the liver was also measured (n=16-18).(**C**) Plasma FGF21 levels were measured before (at week -1; pooled samples, n=6 per group) and after (at week 4, pooled samples, n=6 per group; week 23, n=12-16 per group) AAV8-*Fgf21* administration.(**D**) Body weight was monitored throughout the experimental period (n=17-18). (**E**) At week 23, brown adipose tissue (BAT) and white adipose tissue (WAT) depots were isolated and weighed (n=18). Data are shown as mean±SEM. Differences were assessed using one-way ANOVA followed by a Tukey post-test. *$P<0.05$; **$P<0.01$, ***$P<0.001$, compared with the LFCD group. ###$P<0.001$, compared with the HFCD group. (**C**) Differences between the LFCD and HFCD groups were assessed using student t test. $$P<0.01$, compared the LFCD group. AAV8, adeno-associated virus 8; FGF21, fibroblast growth factor 21; gWAT, gonadal WAT; HFCD, high fat and high cholesterol diet; iBAT, interscapular BAT; LFCD, low fat and low cholesterol diet; sBAT, subscapular BAT; sWAT, subcutaneous white adipose tissue.

FGF21 protects against HFCD-induced adipose tissue dysfunction

The profound fat mass-lowering effects of liver-derived FGF21 prompted us to examine its role in adipose tissue function. Since we and others have previously shown that FGF21 activates thermogenic adipose tissues [29, 30], we first performed histological analyses of BAT and sWAT, the adipose tissue that is most prone to browning [31]. We observed that FGF21 prevented the HFCD-induced lipid overload in BAT (-66%) and increased uncoupling protein-1 (UCP-1) expression compared with both the LFCD- and HFCD-fed groups (+15% and +26%, respectively) (**Fig. 2A**). In sWAT, FGF21 prevented HFCD-induced adipocyte hypertrophy (-41%), and increased the UCP-1 content (+94%) (**Fig. 2B**). Among the adipose tissue depots, gWAT is most prone to diet-induced inflammation, and surgical removal of inflamed gWAT attenuates NASH in obese mice [32]. Similar to sWAT, FGF21 protected against HFCD-induced adipocyte enlargement (-52%) in gWAT and in addition fully prevented the formation of crown-like structures (CLSs; -93%) (**Fig. 2C**). In agreement with these findings, FGF21 suppressed the HFCD-induced expression of adhesion G protein-coupled receptor E1 (*Adgre1*; -56%), encoding the macrophage surface marker F4/80, in addition to decreased expression of the pro-
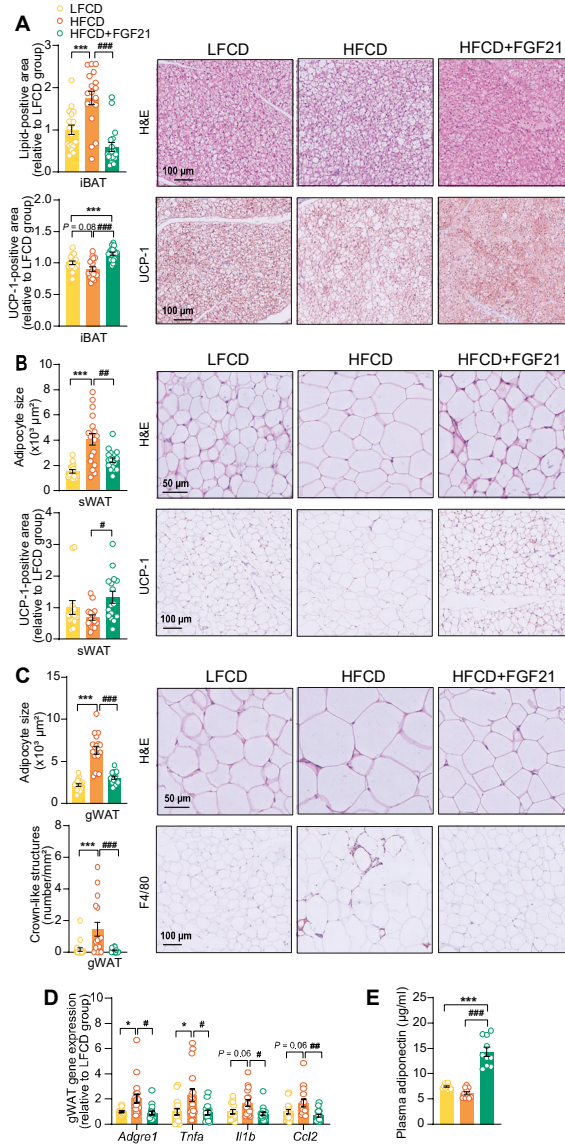
Fig. 2. FGF21 protects against HFCD-induced adipose tissue dysfunction. (**A**) In iBAT, the lipid content and expression of uncoupling protein-1 (UCP-1) were quantified after H&E staining and UCP-1 immunostaining, respectively. (**B**) In sWAT, the adipocyte enlargement was assessed by H&E staining, and the tissue browning was evaluated by UCP-1 immunostaining. (**C**) In gWAT, the adipocyte hypertrophy was detected, and the number of CLSs was assessed, and (**D**) mRNA expression of pro-inflammatory markers was quantified. (**E**) Plasma adiponectin concentration in fasted blood plasma was measured at week 22. (**A**)-(**D**), n=14-18 per group; (**E**), n=10 per group. Differences were assessed using one-way ANOVA followed by a Tukey post-test. *$P<0.05$, ***$P<0.001$, compared with the LFCD group. #$P<0.05$, ##$P < 0.01$, ###$P<0.001$, compared with the HFCD group. *Adgre1*, adhesion G protein-coupled receptor E1; *Tnfa*, tumor necrosis factor α; *Il1b*, interleukin-1β; *Ccl2*, chemokine C–C motif ligand 2.

inflammatory mediators tumor necrosis factor α (*Tnfa*; -60%), interleukin-1β (*Il1b*; -50%) and monocyte attractant chemokine C–C motif ligand 2 (*Ccl2*; -60%) (**Fig. 2D**). Besides, FGF21 tended to upregulate *Klb* (+33%) and *Fgfr1* (+ 30%) expression compared to HFCD-fed mice (**Fig. 2-fig. supplement 1**). Moreover, consistent with the critical role of adiponectin in mediating the therapeutic benefits of FGF21 in adipose tissue[22, 33], FGF21 increased plasma adiponectin levels compared to both LFCD- and HFCD-fed mice (+93% and +133%, respectively; **Fig. 2E**). These combined findings thus indicate that FGF21 prevents HFCD-induced adipose tissue dysfunction during NASH development.

FGF21 alleviates HFCD-induced hyperglycemia and hypertriglyceridemia

We next examined whether FGF21 confers its glucose and lipid lowering effects during NASH development. While HFCD induced hyperglycemia as compared to LFCD, FGF21 normalized fasting plasma glucose compared to LFCD, which was accompanied by lower glucose excursion after an intraperitoneal glucose tolerance test (**Fig. 3A,B**). In addition, FGF21 normalized the plasma insulin and Homeostatic Model Assessment for Insulin Resistance index (**Fig. 3C**), indicating that FGF21 restores insulin sensitivity to
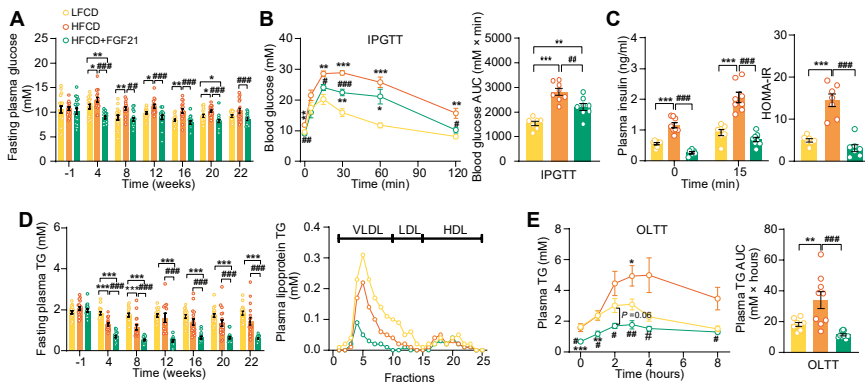
Fig. 3. FGF21 alleviates HFCD-induced hyperglycemia and hypertriglyceridemia. (**A**) Fasting plasma glucose levels were measured during the experimental period. (**B**) At week 16, an intraperitoneal glucose tolerance test (IPGTT) was initiated. (**B**) The area under the curve (AUC) of plasma glucose during the IPGTT and (**C**) plasma insulin concentration in response to the IPGTT was determined at the indicated timepoints. (**C**) Homeostasis model assessment of insulin resistance (HOMA-IR) was determined from fasting glucose and insulin levels. (**D**) Fasting plasma TG levels were measured throughout the study. The distribution of triglyceride over lipoproteins was determined (pooled samples; n=5 per group) from plasma of week 22. (**E**) At week 20, an oral lipid tolerance test (OLTT) was initiated, and AUC of plasma TG during the OLTT was calculated. (**A and D**), n=14-18 per group; (**B-C**), n=7-8 per group; (**E**), n=6-9 per group. Data are shown as mean±SEM. Differences were assessed using one-way ANOVA followed by a Tukey post-test. *$P<0.05$, **$P<0.01$, ***$P<0.001$, compared with the LFCD group. #$P<0.05$, ##$P<0.01$, ###$P<0.001$, compared with the HFCD group.

that observed in LFCD-fed mice. FGF21 did not prevent the HFCD-induced increase of plasma total cholesterol (TC) levels (**Fig. 3-fig. supplement 1A**), nor the distribution of cholesterol over the various lipoproteins (**Fig. 3-fig. supplement 1B**). Nonetheless, FGF21 strongly and consistently reduced fasting plasma triglyceride (TG) levels throughout the experimental period compared with LFCD- and HFCD-fed mice (-67% and -58%; at week 22), which was specific for very-low density lipoprotein (VLDL) and low density lipoprotein (LDL) (**Fig. 3D**). In addition, an oral lipid tolerance test revealed that FGF21 prevented HFCD-induced lipid intolerance (**Fig. 3E**). Taken together, FGF21 prevents the HFCD-induced increase in circulating glucose and reduces circulating TG levels beyond those observed in LFCD-fed mice.

FGF21 protects against HFCD-induced hepatic steatosis, inflammation, and fibrogenesis

Then, we investigated the effects of FGF21 on liver steatosis, inflammation and fibrosis. FGF21 not only prevented HFCD-induced liver weight gain (-58%), but even reduced liver weight to a level lower than that of LFCD-fed mice (-40%; **Fig. 4A,F**). Moreover, FGF21 abolished the HFCD-induced increase in steatosis, lobular inflammation and hepatocellular ballooning (**Fig. 4B, Fig. 4-fig. supplement 1A,B**). Therefore, FGF21 completely prevented the HFCD-induced large increase in the NAFLD activity score (-74%; **Fig. 4C,F**). Furthermore, FGF21 prevented collagen accumulation in the liver as assessed by Picrosirius Red staining (-58%; **Fig. 4D,F**). We then measured hepatic concentration of hydroxyproline, a major constituent of collagen and thus a marker of extracellular matrix accumulation. In line with the hepatic collagen content, HFCD feeding increased the hepatic hydroxyproline content, which was prevented by FGF21 (-49%; **Fig. 4E**). Taken together, our data demonstrate that FGF21 protects against HFCD-induced hepatosteatosis, steatohepatitis as well as fibrogenesis.

FGF21 abolishes liver lipotoxicity, accompanied by activation of hepatic signaling involved in FA oxidation and cholesterol removal

In the context of NASH, pro-inflammatory responses and fibrogenesis occur when hepatocytes are injured by lipotoxicity [7, 34]. Indeed, 23 weeks of HFCD feeding promoted aberrant accumulation of TG as well as TC in the liver (**Fig. 5A**). In agreement with the data presented in **Fig. 4**, FGF21 abrogated the HFCD-induced increase in hepatic TG levels (-62%) and tended to decrease hepatic TC levels (-22%), resulting in smaller lipid droplets (**Fig. 5A**). In addition to reduced lipid overflow from WAT, we reasoned that FGF21 may also directly act on the liver to prevent HFCD-induced liver lipotoxicity. In agreement, compared to both LFCD- and HFCD-fed mice, FGF21 profoundly upregulated the expression of *Klb* (+150% and +223%), *Fgfr1* (+57% and +79%), *Fgfr2* (+97% and +77%), and *Fgfr4* (+53% and +67%) (**Fig. 5-fig. supplement 1**). We next
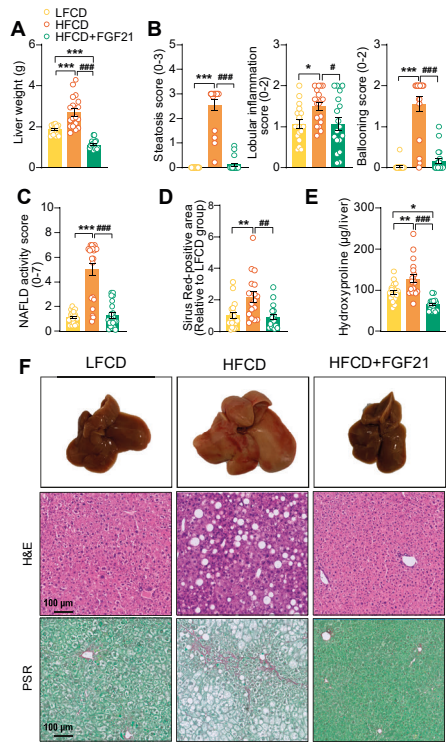
Fig. 4. FGF21 protects against HFCD-induced hepatic steatosis, inflammation and fibrosis. (A) At week 23, liver weight was determined, and (**B**) scoring of histological features of steatosis, lobular inflammation and ballooning as well as (**C**) NAFLD activity was evaluated by H&E staining. (**D**) Liver fibrosis was assessed by Picrosirius Red (PSR) staining, and (**E**) hepatic hydroxyproline levels were determined. (**F**) Representative macroscopic, H&E and PSR pictures are shown. Data are shown as mean±SEM (n=16-18 per group). Differences were assessed using one-way ANOVA followed by a Tukey post-test. *$P<0.05$; **$P<0.01$, ***$P<0.001$, compared with the LFCD group. ##$P<0.01$; ###$P<0.001$, compared with the HFCD group

quantified the hepatic expression of key genes involved in FA and cholesterol handling. FGF21 did not attenuate the HFCD-induced increased expression of FA translocase cluster of differentiation 36 (C*d36*) (**Fig. 5-supplement 2A**). In favorable contrast, compared to both LFCD- and HFCD-fed mice, FGF21 did increase the expression of carnitine palmitoyl transferase 1α (*Cpt1a*, +66% and +53%), peroxisome proliferator-activated receptor α (*Ppara*, +67% and +53%) and peroxisome proliferator-activated receptor γ coactivator 1α (*Pgc1a*; +188% and +225%), all of those genes being key players involved in FA oxidation (**Fig. 5B**). Moreover, compared to LFCD- and HFCD-fed mice, FGF21 increased the expression of apolipoprotein B (*Apob*, +26% and +38%), which is involved in VLDL secretion (**Fig. 5-fig. supplement 2B**). Furthermore, FGF21 upregulated the expression of ATP-binding cassette transporter G member 5 (*Abcg5*; 7-fold and 2-fold), crucial for biliary secretion of neutral sterols (**Fig. 5C**), increased the
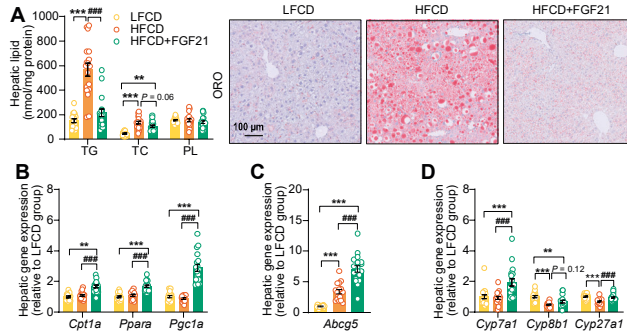
Fig. 5. FGF21 abolishes liver lipotoxicity, accompanied by activation of hepatic signaling involved in FA oxidation and cholesterol removal. (**A**) Triglyceride (TG), total cholesterol (TC) and phospholipid (PL) levels were determined in the liver (n=18 per group), and representative Oil Red O (ORO) pictures are shown. (**B**) The relative mRNA expression of genes involved in fatty acid oxidation and (**C and D**) cholesterol removal (n=15-18 per group) were determined in the liver. Data are shown as mean ± SEM. Differences were assessed using one-way ANOVA followed by a Tukey post-test. **$P<0.01$, ***$P<0.001$, compared with the LFCD group. ###$P<0.001$, compared with the HFCD group. *Abcg5*, ATP-binding cassette transporter G member 5; *Cpt1a*, carnitine palmitoyl transferase 1α; *Cyp7a1*, cholesterol 7α-hydroxylase; *Cyp8b1*, sterol 12α-hydroxylase; *Cyp27a1*, sterol 27-hydroxylase; *Pgc1a*, peroxisome proliferator-activated receptor gamma coactivator 1α; *Ppara*, peroxisome proliferator-activated receptor α.

expression of cholesterol 7α-hydroxylase (*Cyp7a1*; +94% and +109%), a key gene involved in the classic bile acid synthesis pathway (**Fig. 5D**), and restored the expression of sterol 27-hydroxylase (+38%), involved in the alternative bile acid pathway (**Fig. 5D**). Considering that bile acid synthesis is a major pathway for hepatic cholesterol disposal [35], FGF21 likely regulates bile acid metabolism to prevent HFCD-induced cholesterol accumulation in the liver. Collectively, our data indicate that FGF21 increases the hepatic expression of key genes involved in β-oxidation and cholesterol removal, which together with reduced lipid overload from WAT may explain FGF21-induced alleviation of liver lipotoxicity under NASH-inducing dietary conditions.

FGF21 prevents activation of various KC subsets

Then, we performed an in-depth phenotyping of hepatic immune cells using spectral flow cytometry. For this, we developed a panel that identifies most major immune cell subsets (for gating strategy see **Fig. 6-fig. supplement 1A**). As compared to LFCD, HFCD tended to reduce total CD45$^+$ leukocytes, which were increased by FGF21 (**Fig. 6-fig. supplement 1B**). Combining conventional gating and dimension-reduction analysis through uniform manifold approximation and projection allowed to identify FGF21-induced changes in cell subset abundance (**Fig. 6A**). FGF21 prevented HFCD-induced loss of eosinophils, neutrophils and B cells, and increased numbers of dendritic cells and T cells compared with those observed in both LFCD- and HFCD-fed mice (**Fig. 6-fig. supplement 1B**). More importantly, FGF21 increased the

number of total KCs compared with that of both LFCD- and HFCD-fed mice (+63% and +156; **Fig. 6-fig. supplement 1B**), attenuated HFCD-induced monocyte recruitment (-18%), and tended to repress the HFCD-induced increase in hepatic MoDMacs (-42%; **Fig. 6-fig. supplement 1B**).

During the development of NASH, MoDMacs can gradually seed in KC pool by acquiring ResKCs identity and replacing the dying ResKCs [36]. These recruited MoKCs can have both detrimental and supportive roles, contributing to increase in pathology during fibrosis onset, but hastening recovery when the damage-evoking agent is attenuated/removed [37]. In light of this, we assessed the abundance and phenotype of ResKCs and monocyte-derived KCs (MoKCs). We observed that FGF21 completely abolished the HFCD-induced reduction of the number of ResKCs (+319%) and potently protected against HFCD-induced ResKC activation as shown by decreased proportion of CD11c+ ResKCs (-53%; **Fig. 6B**). FGF21 also completely abolished the HFCD-induced upregulation of CD36 in ResKCs, to levels that are even lower than those in LFCD-fed mice (-88% *vs.* LFCD; -94% *vs.* HFCD; **Fig. 6B**). In addition, FGF21 increased the number of MoKCs compared with that of both LFCD- and HFCD-fed mice (+92% and +123%), and prevented the HFCD-induced increase in the abundance of CD11c+ MoKCs (-42%) (**Fig. 6C**). Strikingly, compared to both LFCD- and HFCD-fed mice, FGF21 downregulated CD9 (-32% and -49%) and CD36 (-98% and -100%) in MoKCs (**Fig. 6C**). Furthermore, FGF21 profoundly repressed HFCD-induced upregulation of hepatic *Tnfa* (-37%), *Il1b* (-41%) and *Ccl2* (-54%) expression to levels comparable to those in LFCD-fed mice (**Fig. 6D)**, which is in line with the observation that FGF21 prevents KC activation. Given that CD36hi ResKCs and CD36hi/ CD9hi MoKCs are involved in the formation of hepatic CLSs[10, 37-39], we next assessed CLSs and observed that FGF21 completely prevented the HFCD-induced formation of CLSs in the liver (-93%; **Fig. 6D**). These data demonstrate that FGF21 inhibits the activation of ResKCs and MoKCs and prevents the accumulation of CD36hi ResKCs and CD36hi/ CD9hi MoKCs under dietary conditions that result in NASH, which likely contribute to the beneficial effects of FGF21 on hepatic inflammation and fibrosis.

FGF21 protects against COL1A1 accumulation, as predicted by the reduction of CD36hi KCs and CD9hi KCs

To further evaluate whether FGF21-induced reductions of lipid-associated macrophages (i.e., CD36hi ResKCs and CD36hi MoKCs) [38] and scar-associated macrophages (i.e., CD9hi MoKCs) [40], are implicated in fibrogenesis, we performed multiple univariate regression analyses. These revealed that both NAFLD activity and liver fibrosis were associated with both CD36hi ResKCs, CD36hi MoKCs and CD9hi MoKCs (**Fig. 6-fig. supplement 2A-D**), indicating that FGF21 likely improves liver fibrosis by reducing these lipid-

and scar-associated macrophages. To further understand the underlying mechanisms by which FGF21 prevents liver fibrosis, we measured hepatic expression of key genes involved in fibrogenesis (**Fig. 6D**). FGF21 tended to decrease the expression of connective tissue growth factor (*Ctgf*; -27%), a major fibrogenic factor, and normalized the HFCD-induced increased expression of its downstream target collagen type Iα 1 (*Col1a1*; -61%; **Fig. 6D**). This finding was confirmed by immunohistochemistry, revealing that FGF21 reduced hepatic COL1A1 accumulation (-46%; **Fig. 6D**). Furthermore, univariate regression analysis revealed that COL1A1 expression is predicted by CD36^{hi} ResKCs, CD36^{hi} MoKCs and CD9^{hi} MoKCs (**Fig. 6E, Fig. 6-fig. supplement 2E**). Taken together, these data indicate that FGF21 reduces lipid- and scar-associated macrophages to inhibit COL1A1 synthesis and prevent fibrogenesis.

5

151
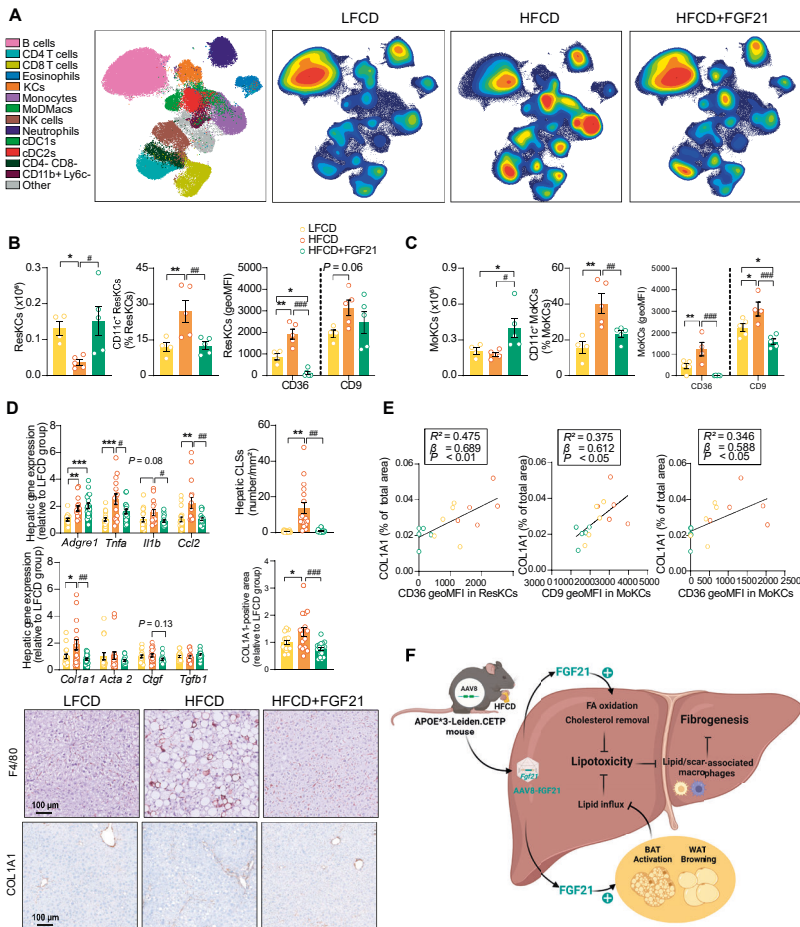
DISCUSSION

Several FGF21 analogues are currently being evaluated in clinical trials for the treatment of NASH [20, 21]. While the protective effect of pharmacological intervention with long-acting FGF21 on human liver steatosis has been uncovered [20, 21, 41], mechanisms underlying attenuated steatosis as well all the anti-inflammatory and anti-fibrotic effects of FGF21 on NASH are still largely unexplored. Therefore, we set out to elucidate mechanisms by which FGF21 beneficially modulates these various aspects of NASH in HFCD-fed *APOE*3-Leiden.CETP* mice, a well-established model for diet-induced NASH [23, 24]. Based on our findings, we propose that FGF21 attenuates liver lipotoxicity via endocrine signaling to adipose tissue to induce thermogenesis, thereby preventing adipose tissue dysfunction to reduce lipid overflow to the liver, as well as autocrine signaling to the liver to increase FA oxidation and cholesterol removal. In addition, FGF21 prevents KC activation, monocyte recruitment and the formation of lipid- and scar-associated macrophages, thereby likely inhibiting collagen accumulation and alleviating liver fibrogenesis.

Hepatic lipotoxicity is one of the major risk factors determining the progression of liver steatosis into NASH, as shown in multiple clinical studies with obese patients [42-44]. By feeding *APOE*3-Leiden.CETP* mice a diet rich in fat and cholesterol, we mimicked a situation in which a positive energy balance induces many aspects of the metabolic syndrome, including insulin resistance, obesity with increased fat accumulation, and hepatic lipotoxicity indicated by hepatomegaly with aberrant accumulation of TG as well as TC. Hepatic lipotoxicity likely results from lipid overflow from insulin-resistant adipose tissue towards the liver in combination with hepatic insulin resistance that prevents insulin-stimulated outflow of lipids [45]. Within this dietary context, we applied a single administration of an AAV8 vector encoding codon-optimized FGF21, which resulted in liver-specific FGF21 overexpression. Since the codon-optimized FGF21 mitigates the poor pharmacokinetic properties of native FGF21, including its short plasma half-life (0.5-2 hours) by reducing proteolytic degradation [45], an elevated level of circulating FGF21 was reached throughout the dietary intervention period. By this strategy, we mimicked the situation in which circulating FGF21 predominantly derives from the liver [46]. Indeed, circulating FGF21 correlates well with the hepatic expression of FGF21 [47]. Interestingly, hepatic expression of FGF21 fully prevented the diet-induced increase in liver weight, liver lipids (i.e., TG and TC) and steatosis score.

These lipotoxicity-protective effects of FGF21 can partially be explained by endocrine effects of liver-derived FGF21 on adipose tissue, which besides the liver has high expression of β-Klotho, the co-receptor of the FGFR [14, 15]. Indeed, FGF21 fully

prevented the HFCD-induced increase in weights of WAT and BAT, with decreased lipid accumulation in these adipose tissue depots as well as induction of BAT activation and WAT browning. These data imply that FGF21 induces thermogenesis which increases energy expenditure, consistent with the thermogenic responses observed for recombinant FGF21 in C57BL/6 mice fed with an obesogenic diet [29]. Likewise, by using *APOE*3-Leiden.CETP* mice, we previously reported that FGF21 treatment highly increased energy expenditure without affecting food intake [30]. Activation of thermogenic tissues by classical β-adrenergic receptor largely increases the uptake of circulating lipoprotein-derived FAs by BAT and beige WAT [48], which we recently also demonstrated for recombinant FGF21 [30]. This can thus at least partly explain the marked TG-lowering effect of FGF21 observed in the current study. Thermogenic activation also increases the uptake and combustion of glucose, although the glucose-lowering and insulin-sensitizing effects of FGF21 can also be explained by attenuated WAT inflammation in combination with increased adiponectin expression as well as improved liver insulin sensitivity [30, 33, 49].

Besides endocrine FGF21 signaling in adipose tissue, liver lipotoxicity is likely further prevented by autocrine FGF21 signaling. Indeed, we showed that liver-specific FGF21 overexpression increased hepatic expression of genes involved in FA oxidation (*Cpt1a*, *Ppara*, *Pgc1a*), biliary cholesterol secretion (*Abcg5*), bile acids synthesis (*Cyp7a1*) and VLDL production (*Apob*). Of note, these observations are in line with previous reports showing increased FA oxidation [50] and upregulated *Abcg5* [51], *Cyp7a1* [51, 52] and *Apob* [30] in the liver upon FGF21 treatment. Altogether, the marked protective effects of FGF21 on HFCD-induced hepatic lipotoxicity likely results from combined endocrine and autocrine signaling, leading to reduced lipid influx from adipose tissue to the liver coupled to the activation of hepatic FA oxidation and cholesterol elimination pathways. Our observations may likely explain the recent clinical findings that treatment with FGF21 analogues in patients with NASH not only reduced hepatic steatosis [20, 21] but also increased hepatic bile acid synthesis and further promoted cholesterol removal, lowering the risk for further hepatic lipotoxicity [53].

While NASH is initiated by hepatic lipotoxicity, NASH progression is mainly driven by impaired KC homeostasis and subsequent liver inflammation [54]. Therefore, we investigated in depth the inflammatory response in the liver through a combination of immunohistochemistry, flow cytometry and gene expression analyses. HFCD feeding induced an array of inflammatory effects, including increased lobular inflammation, hepatocyte ballooning and NAFLD activity scores as well as increased inflammatory foci and CLSs, accompanied by a reduction in ResKCs with a relative increase in CD11c+ ResKCs, and an increase in MoDMacs and CD11c+ MoKCs. These observations

are likely explained by lipotoxicity-related damage to ResKCs, and release of TNFα, IL-1β and MCP-1 (*Ccl2*), both activating various downstream pro-inflammatory mediators as well as promoting monocyte recruitment to remodel the KC pool[36, 55] and further exacerbating hepatic inflammation [10, 38, 54, 56, 57]. Importantly, FGF21 prevented most of these HFCD-induced inflammatory responses, as it normalized lobular inflammation, hepatocyte ballooning and NAFLD activity scores and CLSs, and reduced pro-inflammatory activation of various KC subsets.

Fibrosis has been identified as the most important predictor of prognosis in NAFLD patients, and therefore a main target in experimental pharmacological approaches [58]. HFCD feeding during 23 weeks induced early signs of fibrosis, as evident from an increased *Col1a1* expression and COL1A1 content, accompanied by an increased content of the hydroxyproline. Importantly, FGF21 blocked liver fibrogenesis, and decreased the hydroxyproline content. These alterations were accompanied with reductions in lipid-associated macrophages (i.e., CD36^{hi} ResKCs/MoKCs) [38] and scar-associated macrophages (i.e., CD9^{hi} MoKCs) [40]. In fact, when analysing the mouse groups together, CD36^{hi} ResKCs/MoKCs and CD9^{hi} MoKCs positively correlated with liver fibrosis as reflected by hydroxyproline content and COL1A-positive area, suggesting that these lipid- and scar-associated macrophages are involved in fibrogenesis in our model. Indeed, high numbers of CD9^{hi} macrophages have been found in fibrotic regions of the liver [37, 39, 40, 55], and these cells are able to prime quiescent primary murine hepatic stellate cells to upregulate the expression of fibrillar collagen through CTGF [40], thereby promoting and exacerbating liver fibrosis. Therefore, we speculate that FGF21 protects against early liver fibrosis likely through preventing the accumulation of CD36^{hi}/CD9^{hi} KCs, thereby inhibiting activation of hepatic stellate cells to produce collagen.

This study is not without limitations. In this work, we used a gene therapy approach to examine the effects of liver-derived FGF21 on NASH based on the use of a single injection of an AAV8 vector encoding codon-optimized murine FGF21. Although AAV8 is hepatocyte trophic, we have not excluded potential contribution of other hepatic cells to total FGF21 expression. Also, while AAV8-*Fgf21* was non-toxic, sustained supra-pharmacological plasma levels of FGF21 were achieved, which do not necessarily reflect effects of current pharmacological strategies with long-acting FGF21. Interestingly, AAV-mediated gene therapy has already been tested in the clinic for life-threatening diseases such as hemophilia B, and has demonstrated stable expression of factor IX following AAV-mediated delivery [59]. Therefore, it is reasonable to speculate that liver-targeted gene therapy as an approach to induce stable overexpression of FGF21 may ultimately have potential to reach to the clinic.

In conclusion, hepatic overexpression of FGF21 in *APOE*3-Leiden.CETP* mice limits diet-induced hepatic lipotoxicity, inflammation and fibrogenesis. Through a combination of endocrine and autocrine signaling, FGF21 reduces hepatic lipid influx and accumulation, respectively. This results in reduced macrophage activation and monocyte recruitment with less presence of lipid- and scar-associated macrophages, limiting activation of hepatic stellate cells to produce collagen (for graphic summary see **Figure 6F**). As such, our studies provide a mechanistic explanation for the hepatoprotective effects of FGF21 analogues in recent clinical trials including reduction in steatosis [20, 21, 53] as well as the fibrotic marker N-terminal type III collagen pro-peptide [20, 21], and further highlight the potential of FGF21 for clinical implementation as a therapeutic in the treatment of advanced NASH.

MATERIALS AND METHODS

Please see the **Supplemental Materials** for a detailed description of all experimental procedures.

Animals and treatments

Male *APOE*3-Leiden.CETP* mice (on a C57BL/6J background) were generated as previously described [60]. Mice at the age of 10-12 weeks were group-housed (2-4 mice per cage) under standard conditions (22℃, 12/12-hour light/dark cycle) with *ad libitum* access to water and a LFCD (Standard Rodent Diet 801203, Special Diets Services, United Kingdom), unless indicated otherwise. Then, based on body weight and 4-hour (9.00-13.00) fasted plasma glucose, TG and TC levels, these mice were randomized into three treatment groups (n=18 per group), after which they received either AAV8-*Fgf21*, a liver-tropic AAV8 capsid vector expressing codon-optimized murine *Fgf21* under the control of a liver specific apolipoprotein E (*Apoe*)/alpha-1-antitrypsin (*Aat*) promoter (HFCD+FGF21 group; $2×10^{10}$ genome copies per mouse), or with the same genome copy number of AAV8-null (HFCD and LFCD groups) via a single intravenous injection. After one week of recovery, mice in the HFCD+FGF21 and HFCD groups were switched to a HFCD (60% fat and 1% cholesterol; C1090-60, Altromin, Germany) and maintained on the diet for 23 weeks, at which APOE*3-Leiden.CETP mice have developed both steatosis, hepatic inflammation and early fibrosis [23, 61]. An intraperitoneal glucose tolerance test (n=8 per group) and an oral lipid tolerance test (n=10 per group) were performed at week 16 and week 20, respectively. Flow cytometry (n=5 per group) was conducted at week 23.

Statistics

Comparisons among three groups were analyzed using one-way ANOVA followed by a Tukey post-test, unless indicated otherwise. Data are presented as mean±SEM, and a P value of less than 0.05 was considered statistically significant. All statistical analyses were performed with GraphPad Prism 9.01 for Windows (GraphPad Software Inc., California, CA, USA).

Study approval

All animal experiments were carried out according to the Institute for Laboratory Animal Research Guide for the Care and Use of Laboratory Animals, and were approved by the National Committee for Animal Experiments (Protocol No. AVD1160020173305) and by the Ethics Committee on Animal Care and Experimentation of the Leiden University Medical Center (Protocol No. PE.18.034.041).

Acknowledgments

Author contributions

CL designed the study, carried out the research, analyzed and interpreted the results, and wrote and revised the manuscript. MS interpreted the results, reviewed and revised the manuscript and obtained the funding. BS and EZ carried out the research and reviewed the manuscript. JML, HJPZ and BG designed and advised the study, interpreted the results and reviewed the manuscript. MET advised the study and reviewed the manuscript. ACA, SO and KW advised the study, interpreted the results and reviewed the manuscript. AP designed AAV8-FGF21 vectors and edited the manuscript. MU and IA analyzed and interpreted the results and reviewed the manuscript. YI and X-RP provided AAV8-FGF21 vectors, advised the study, interpreted the results and reviewed the manuscript. MRB advised the study and reviewed the manuscript. YW designed and advised the study, interpreted the results, reviewed and revised the manuscript. PCNR designed and advised the study, interpreted the results, edited, reviewed and revised the manuscript and obtained the funding.

REFERENCES

1. Cusi, K., *Role of obesity and lipotoxicity in the development of nonalcoholic steatohepatitis: pathophysiology and clinical implications.* Gastroenterology, 2012. **142**(4): p. 711-725 e6.

2. Friedman, S.L., et al., *Mechanisms of NAFLD development and therapeutic strategies.* Nat Med, 2018. **24**(7): p. 908-922.

3. Arab, J.P., M. Arrese, and M. Trauner, *Recent Insights into the Pathogenesis of Nonalcoholic Fatty Liver Disease.* Annual Review of Pathology: Mechanisms of Disease, Vol 13, 2018. **13**: p. 321-350.

4. Taylor, R.S., et al., *Association Between Fibrosis Stage and Outcomes of Patients With Nonalcoholic Fatty Liver Disease: A Systematic Review and Meta -Analysis.* Gastroenterology, 2020. **158**(6): p. 1611-+.

5. Stefan, N., H.U. Haring, and K. Cusi, *Non-alcoholic fatty liver disease: causes, diagnosis, cardiometabolic consequences, and treatment strategies.* Lancet Diabetes Endocrinol, 2019. **7**(4): p. 313-324.

6. Musso, G., R. Gambino, and M. Cassader, *Recent insights into hepatic lipid metabolism in non-alcoholic fatty liver disease (NAFLD).* Progress in Lipid Research, 2009. **48**(1): p. 1-26.

7. Neuschwander-Tetri, B.A., *Hepatic lipotoxicity and the pathogenesis of nonalcoholic steatohepatitis: the central role of nontriglyceride fatty acid metabolites.* Hepatology, 2010. **52**(2): p. 774-88.

8. Tacke, F., *Targeting hepatic macrophages to treat liver diseases.* J Hepatol, 2017. **66**(6): p. 1300-1312.

9. Krenkel, O. and F. Tacke, *Liver macrophages in tissue homeostasis and disease.* Nat Rev Immunol, 2017. **17**(5): p. 306-321.

10. Tran, S., et al., *Impaired Kupffer Cell Self-Renewal Alters the Liver Response to Lipid Overload during Non-alcoholic Steatohepatitis.* Immunity, 2020. **53**(3): p. 627-640 e5.

11. Krenkel, O., et al., *Therapeutic inhibition of inflammatory monocyte recruitment reduces steatohepatitis and liver fibrosis.* Hepatology, 2018. **67**(4): p. 1270-1283.

12. Meng, W., et al., *The miR-182-5p/FGF21/acetylcholine axis mediates the crosstalk between adipocytes and macrophages to promote beige fat thermogenesis.* Jci Insight, 2021. **6**(17).

13. Guo, Y., et al., *Fibroblast growth factor 21 potentially inhibits microRNA-33 expression to affect macrophage actions.* Lipids Health Dis, 2016. **15**(1): p. 208.

14. Fisher, F.M. and E. Maratos-Flier, *Understanding the Physiology of FGF21.* Annu Rev Physiol, 2016. **78**: p. 223-41.

15. Geng, L., K.S.L. Lam, and A. Xu, *The therapeutic potential of FGF21 in metabolic diseases: from bench to clinic.* Nat Rev Endocrinol, 2020. **16**(11): p. 654-667.

16. Zhang, X., et al., *Serum FGF21 levels are increased in obesity and are independently associated with the metabolic syndrome in humans.* Diabetes, 2008. **57**(5): p. 1246-53.

17. Barb, D., et al., *Plasma Fibroblast Growth Factor 21 Is Associated With Severity of Nonalcoholic Steatohepatitis in Patients With Obesity and Type 2 Diabetes.* J Clin Endocrinol Metab, 2019. **104**(8): p. 3327-3336.

18. Li, H., et al., *Fibroblast growth factor 21 levels are increased in nonalcoholic fatty liver disease patients and are correlated with hepatic triglyceride.* J Hepatol, 2010. **53**(5): p. 934-40.

19. Flippo, K.H. and M.J. Potthoff, *Metabolic Messengers: FGF21.* Nat Metab, 2021. **3**(3): p. 309-317.

20. Sanyal, A., et al., *Pegbelfermin (BMS-986036), a PEGylated fibroblast growth factor 21 analogue, in patients with non-alcoholic steatohepatitis: a randomised, double-blind, placebo-controlled, phase 2a trial.* Lancet, 2019. **392**(10165): p. 2705-2717.

5

21. Harrison, S.A., et al., *Efruxifermin in non-alcoholic steatohepatitis: a randomized, double-blind, placebo-controlled, phase 2a trial.* Nat Med, 2021. **27**(7): p. 1262-1271.

22. Bao, L.C., et al., *A long-acting FGF21 alleviates hepatic steatosis and inflammation in a mouse model of non-alcoholic steatohepatitis partly through an FGF21-adiponectin-IL17A pathway.* British Journal of Pharmacology, 2018. **175**(16): p. 3379-3393.

23. Morrison, M.C., et al., *Mirtoselect, an anthocyanin-rich bilberry extract, attenuates non-alcoholic steatohepatitis and associated fibrosis in ApoE(*)3Leiden mice.* J Hepatol, 2015. **62**(5): p. 1180-6.

24. Liang, W., et al., *Establishment of a general NAFLD scoring system for rodent models and comparison to human liver pathology.* PLoS One, 2014. **9**(12): p. e115922.

25. van den Hoek, A.M., *APOE*3Leiden.CETP transgenic mice as model for pharmaceutical treatment of the metabolic syndrome.* Diabetes, 2013. **16**: p. 537–544.

26. van der Hoorn, J.W., et al., *The dual PPARalpha/gamma agonist tesaglitazar blocks progression of pre-existing atherosclerosis in APOE*3Leiden.CETP transgenic mice.* Br J Pharmacol, 2009. **156**(7): p. 1067-75.

27. Li, Z., et al., *Butyrate reduces appetite and activates brown adipose tissue via the gut-brain neural circuit.* Gut, 2018. **67**(7): p. 1269-1279.

28. Duivenvoorden, I., et al., *Dietary sphingolipids lower plasma cholesterol and triacylglycerol and prevent liver steatosis in APOE*3Leiden mice.* Am J Clin Nutr, 2006. **84**(2): p. 312-21.

29. Schlein, C., et al., *FGF21 Lowers Plasma Triglycerides by Accelerating Lipoprotein Catabolism in White and Brown Adipose Tissues.* Cell Metab, 2016. **23**(3): p. 441-53.

30. Liu, C., et al., *Pharmacological treatment with FGF21 strongly improves plasma cholesterol metabolism to reduce atherosclerosis.* Cardiovasc Res, 2021.

31. Zhang, F., et al., *An Adipose Tissue Atlas: An Image-Guided Identification of Human-like BAT and Beige Depots in Rodents.* Cell Metab, 2018. **27**(1): p. 252-262 e3.

32. Mulder, P., et al., *Surgical removal of inflamed epididymal white adipose tissue attenuates the development of non-alcoholic steatohepatitis in obesity.* Int J Obes (Lond), 2016. **40**(4): p. 675-84.

33. Lin, Z., et al., *Adiponectin mediates the metabolic effects of FGF21 on glucose homeostasis and insulin sensitivity in mice.* Cell Metab, 2013. **17**(5): p. 779-89.

34. Machado, M.V. and A.M. Diehl, *Pathogenesis of Nonalcoholic Steatohepatitis.* Gastroenterology, 2016. **150**(8): p. 1769-77.

35. Tu, H., *FXR, a Bile Acid Receptor and Biological Sensor.* Trends in Cardiovascular Medicine, 2000. **10**(1): p. 30-35.

36. Tran, S., et al., *Impaired Kupffer Cell Self-Renewal Alters the Liver Response to Lipid Overload during Non-alcoholic Steatohepatitis.* Immunity, 2020. **53**(3): p. 627-+.

37. Seidman, J.S., et al., *Niche-Specific Reprogramming of Epigenetic Landscapes Drives Myeloid Cell Diversity in Nonalcoholic Steatohepatitis.* Immunity, 2020. **52**(6): p. 1057-1074 e7.

38. Bleriot, C., et al., *A subset of Kupffer cells regulates metabolism through the expression of CD36.* Immunity, 2021. **54**(9): p. 2101-+.

39. Daemen, S., et al., *Dynamic Shifts in the Composition of Resident and Recruited Macrophages Influence Tissue Remodeling in NASH.* Cell Rep, 2021. **34**(2): p. 108626.

40. Ramachandran, P., et al., *Resolving the fibrotic niche of human liver cirrhosis at single-cell level.* Nature, 2019. **575**(7783): p. 512-+.

41. Aggarwal, P., et al., *Nonalcoholic steatohepatitis (NASH) cirrhosis: a snapshot of therapeutic agents in clinical development and the optimal design for clinical trials.* Expert Opinion on Investigational Drugs, 2022.

42. Bril, F., et al., *Metabolic and histological implications of intrahepatic triglyceride content in nonalcoholic fatty liver disease.* Hepatology, 2017. **65**(4): p. 1132-1144.

43. Armstrong, M.J., et al., *Glucagon-like peptide 1 decreases lipotoxicity in non-alcoholic steatohepatitis.* J Hepatol, 2016. **64**(2): p. 399-408.

44. Ratziu, V., et al., *Aramchol in patients with nonalcoholic steatohepatitis: a randomized, double-blind, placebo-controlled phase 2b trial.* Nat Med, 2021. **27**(10): p. 1825-1835.

45. Zarei, M., et al., *Targeting FGF21 for the Treatment of Nonalcoholic Steatohepatitis.* Trends Pharmacol Sci, 2020. **41**(3): p. 199-208.

46. Nishimura, T., et al., *Identification of a novel FGF, FGF-21, preferentially expressed in the liver.* Biochim Biophys Acta, 2000. **1492**(1): p. 203-6.

47. Markan, K.R., et al., *Circulating FGF21 Is Liver Derived and Enhances Glucose Uptake During Refeeding and Overfeeding.* Diabetes, 2014. **63**(12): p. 4057-4063.

48. Berbee, J.F., et al., *Brown fat activation reduces hypercholesterolaemia and protects from atherosclerosis development.* Nat Commun, 2015. **6**: p. 6356.

49. Yang, Q., A. Vijayakumar, and B.B. Kahn, *Metabolites as regulators of insulin sensitivity and metabolism.* Nat Rev Mol Cell Biol, 2018. **19**(10): p. 654-672.

50. Fisher, F.M., et al., *Fibroblast growth factor 21 limits lipotoxicity by promoting hepatic fatty acid activation in mice on methionine and choline-deficient diets.* Gastroenterology, 2014. **147**(5): p. 1073-83 e6.

51. Keinicke, H., et al., *FGF21 regulates hepatic metabolic pathways to improve steatosis and inflammation.* Endocr Connect, 2020. **9**(8): p. 755-768.

52. Zhang, J., et al., *Chronic Over-expression of Fibroblast Growth Factor 21 Increases Bile Acid Biosynthesis by Opposing FGF15/19 Action.* EBioMedicine, 2017. **15**: p. 173-183.

53. Luo, Y., et al., *Pegbelfermin selectively reduces secondary bile acid concentrations in patients with non-alcoholic steatohepatitis.* JHEP Rep, 2022. **4**(1): p. 100392.

54. Cai, J., X.J. Zhang, and H. Li, *The Role of Innate Immune Cells in Nonalcoholic Steatohepatitis.* Hepatology, 2019. **70**(3): p. 1026-1037.

55. Remmerie, A., et al., *Osteopontin Expression Identifies a Subset of Recruited Macrophages Distinct from Kupffer Cells in the Fatty Liver.* Immunity, 2020. **53**(3): p. 641-+.

56. Schwabe, R.F., I. Tabas, and U.B. Pajvani, *Mechanisms of Fibrosis Development in Nonalcoholic Steatohepatitis.* Gastroenterology, 2020. **158**(7): p. 1913-1928.

57. Yu, Y., et al., *STING-mediated inflammation in Kupffer cells contributes to progression of nonalcoholic steatohepatitis.* J Clin Invest, 2019. **129**(2): p. 546-555.

58. Heyens, L.J.M., et al., *Liver Fibrosis in Non-alcoholic Fatty Liver Disease: From Liver Biopsy to Non-invasive Biomarkers in Diagnosis and Treatment.* Frontiers in Medicine, 2021. **8**.

59. Nathwani, A.C., et al., *Adeno-Associated Mediated Gene Transfer for Hemophilia B:8 Year Follow up and Impact of Removing "Empty Viral Particles" on Safety and Efficacy of Gene Transfer.* Blood, 2018. **132**.

5

60. Westerterp, M., et al., *Cholesteryl ester transfer protein decreases high-density lipoprotein and severely aggravates atherosclerosis in APOE*3-Leiden mice.* Arterioscler Thromb Vasc Biol, 2006. **26**(11): p. 2552-9.

61. Hui, S.T., et al., *The Genetic Architecture of Diet-Induced Hepatic Fibrosis in Mice.* Hepatology, 2018. **68**(6): p. 2182-2196.

SUPPLEMENT

Expanded methods

Generation of recombinant adeno-associated virus (AAV) vectors

AD-293 cells (Agilent, Santa Clara, CA, USA) were plated in a five layered chamber in Gibco™ DMEM supplemented with 10% Gibco™ FBS and 1% Gibco™ penicillin-streptomycin (Thermo Fisher Scientific, Waltham, MA, USA). When these cells reached at 60-85% confluency under the microscope, they were transfected by polyethylenimine (Polyscience, Torrance, CA, USA) with triple plasmids, including pHelper containing adenoviral E2A and E4 genes, pRep2Cap8 encoding AAV2 Rep proteins and AAV8 serotype capsid, and either pAAV-apolipoprotein E (*Apoe*)/alpha-1-antitrypsin (*Aat*) promoter-driven codon-optimized murine *Fgf21* or pAAV-*Apoe*/no plasmid, in a ratio of 2:1.4:1, respectively. After 72 hours of the post-transfection, cells were harvested and lysed via three freeze-thaw cycles followed by 1 hour of benzonase treatment at 37℃. Supernatants were then further purified using iodixanol gradient based ultracentrifugation. Titers of all AAV vectors used for *in vivo* study were quantitated by quantitative reverse transcriptase-PCR. Given that the AAV8 vector is naturally mouse hepatocyte trophic, the AAT promoter is highly active in hepatocytes, and hepatocytes have a slow turnover, this approach results in sustained hepatocyte-selective expression of murine *Fgf21* in the long-term. Since the recombinant AAV8 vector was generated by a standard and helper-free 3 plasmid transfection system, this vector does not express AAV8 and adenoviral helper proteins, and cannot replicate in transduced hepatocytes. Pilot data in C57BL/6 mice showed that the AAV8-*Fgf21* vector (3×10^{10}, 1×10^{11} and 1×10^{12} genome copies/mouse) did not cause liver injury, as judged from unaffected alanine transaminase (ALT) and aspartate transaminase (AST) levels in plasma at 8 days after injection.

Body weight and plasma glucose, triglycerides (TG) and total cholesterol (TC)

Body weight (n=18 per group) was recorded weekly of all mice throughout the study. Every 4 weeks, mice were fasted for 4 hours (9.00-13.00), and subsequently, tail vein blood was collected into paraoxon-coated glass capillaries. Plasma (n=18 per group) was collected and measured for glucose, TG and TC using commercial enzymatic kits (Roche Diagnostics, Mannheim, Germany).

Plasma FGF21, adiponectin and lipoprotein profile

Plasma FGF21 concentrations were determined at week -1 (pooled samples, n=6 per group), week 4 (pooled samples, n=6 per group) and week 23 (n=12-16 per group) using Mouse/Rat FGF21 Quantikine ELISA Kit (R&D Systems, Minneapolis, NE, USA).

5

Plasma adiponectin levels were measured at week 22 (n=10 per group) using Mouse Adiponectin/Acrp30 Quantikine ELISA Kit (R&D Systems, Minneapolis, NE, USA). At week 22, 4 μL of 4-hour fasting plasma per mouse (n=18 per group) were pooled in each treatment group to measure the distribution of TG and TC over lipoproteins by fast-performance liquid chromatography using Super 6 column (GE Healthcare, Piscataway, NJ, USA).

Glucose tolerance test and lipid tolerance test

At week 16, an intraperitoneal glucose tolerance test (IPGTT) was performed with an injection of D-glucose (2 g/kg body weight) after 4 hours fasting (9.00-13.00; n=8 per group). Blood was collected via tail vein at 0, 5, 15, 30, 60 and 120 min for each test. The glucose was measured with a OneTouch Ultra glucometer (AccuCheck Sensor, Roche Diagnostics, Almere, The Netherlands), and the area under the curve (AUC) was calculated. During IPGTT, extra blood was collected at 0 and 15 min, spun down, and the serum samples were stored at -20℃ for glucose measurement using a commercial enzymatic kit (Roche Diagnostics; Mannheim, Germany) and insulin measurement using an Ultra Sensitive Mouse Insulin ELISA kit (Crystal Chem, Zaandam, The Netherlands). HOMA-IR was calculated with the following formula: [fasting serum glucose (mM) × fasting serum insulin (μU/mL)]/22.5 [1]. At week 20, oral lipid tolerance test was conducted. To this end, mice (n=10 per group) were fasted for 4 hours (9.00-13.00h), and received olive oil (10 mL/kg body weight) via oral gavage. Blood was collected into paraoxon-coated glass capillaries at 0, 2, 4, 6 and 8 hours, spun down, and the plasma samples were stored at -20℃ for TG measurement using commercial enzymatic kits (Roche Diagnostics, Mannheim, Germany).

Hepatic lipids and hydroxyproline

Hepatic lipids were extracted from snap-frozen liver samples (n=18 per group) using a modified protocol from Bligh and Dyer [2]. Liver TG, TC and phospholipid (PL; Instruchemie, Delfzijl, The Netherlands) and protein (Pierce, Thermo Fisher Scientific, Waltham, MA, USA) concentrations were measured. Hepatic lipids were expressed as nmol per mg protein. Hepatic hydroxyproline concentrations (n=18 per group) were determined using a Mouse Hydroxyproline Assay Kit (QuickZyme Biosciences, Leiden, The Netherlands).

Adipose tissue Histology

Formalin-fixed paraffin-embedded interscapular brown adipose tissue (iBAT), subcutaneous white adipose tissue (sWAT) and gonadal white adipose tissue (gWAT) sections (5 μm thickness) were prepared for hematoxylin-eosin (H&E) staining[3]. Moreover, iBAT and sWAT sections were processed for uncoupling protein-1 (UCP-1)

staining [4], and gWAT sections were used for F4/80 staining [5]. The areas occupied by intracellular lipid vacuoles (n=18 per group) and UCP-1 (n=18 per group) were quantified using Image J software (version 1.52a; National Institutes of Health, Bethesda, Maryland). Using Image J software, the size of adipocyte of gWAT (n=18 per group) and sWAT (n=18 per group) and the number of crown-like structures (CLSs) within the gWAT (n=18 per group) were assessed. The number of CLSs in the gWAT was expressed as the number of CLS per mm2.

Liver histology and histological grading of NAFLD activity score

Liver tissue (n=18 per group) was fixed, embedded and sectioned (5 µm thickness) for H&E, oil red O (ORO), F4/80, Picrosirius Red (PSR) and COL1A1 staining. The number of CLS in the liver was counted using Image J software and expressed as the number of CLS per mm2. In addition, hepatic collagen accumulation was evaluated by quantifying Picrosirius Red- and COL1A1-positive areas in the liver using Image J software. For NAFLD activity score determination, a clinically utilized scoring system was adapted for the current study based on liver section H&E staining [6]. The scoring system is ranged from 0-7, and is evaluated semi-quantitatively through three criterions: steatosis (0-3), lobular inflammation (0-2), and hepatocellular ballooning (0-2). Values in figures for each staining present means of 6-9 different and randomly analyzed fields (~1.5 mm2) of each mouse, and were used for statistical analysis.

Gene expression analysis

Total RNA was isolated from snap-frozen tissues (n=18 per group for each tissue) using TriPure RNA Isolation Reagent (Roche Diagnostics, Mijdrecht, The Netherlands). Thereafter, complementary DNA for quantitative reverse transcriptase-PCR was generated using Moloney Murine Leukemia Virus Reverse Transcriptase (Promega, Leiden, the Netherlands). Then, mRNA expression was normalized to *Actb* and *Rplp0* mRNA levels and expressed as fold change compared with the LFCD group. The primer sequences are listed in the **Appendix-table 1**.

Isolation of hepatic leukocytes

At the end of the study, livers (n=5 per group) were collected in ice-cold RPMI 1640+Glutamax (Thermo Fisher Scientific, Waltham, MA, USA). The tissues were subsequently minced and digested for 45 min at 37℃ in RPMI 1640+Glutamax supplemented with 1 mg/mL collagenase type IV from Clostridium histolyticum (Sigma-Aldrich, St. Louis, MO, USA), 2000 U/mL DNase (Sigma-Aldrich, St. Louis, MO, USA) and 1 mM CaCl2 as previously described [7]. The digested liver tissues were passed through a 100 µm cell strainer and washed with PBS supplemented with 0.5% BSA and 2 mM EDTA (PBS/BSA/EDTA). The samples were spun down (530 x g, 10 min at 4℃) after

which the pellet was resuspended in PBS/BSA/EDTA and centrifuged at 50 x g to pellet the hepatocytes (3 min at 4℃). The supernatant was next collected and centrifuged (530 x g, 10 min at 4℃) after which the pellet was treated with erythrocyte lysis buffer (0.15 M NH4Cl; 1 mM KHCO3; 0.1 mM Na2EDTA) for 2 min at room temperature. After washing with PBS/BSA/EDTA, total leukocytes were isolated by means of Magnetic-activated cell sorting (MACS) using LS columns and CD45 MicroBeads (35 μL beads per liver; Miltenyi Biotec, Bergisch Gladbach, Germany) according to the manufacturer's protocol. Isolated CD45+ cells were counted and stained with Zombie NIR (Biolegend, San Diego, CA, USA) for 20 min at room temperature followed by fixation with 1.9% paraformaldehyde (Sigma-Aldrich, St. Louis, MO, USA) for 15 min at room temperature after which the fixed leukocytes were further processed for flow cytometry.

Flow cytometry

For analysis of hepatic leukocyte subsets, isolated CD45^{+} cells were incubated with a cocktail of antibodies directed against XCR1, CD11c, CD19, Ly6G, F4/80, MHC-II, CD45, CLEC2, Siglec-F, CD64, CD8, NK1.1, CD11b, CD4, CD90.2, Ly6C, CD3, CD36, CD9 and TIM4 in PBS/BSA/EDTA supplemented with True-Stain monocyte blocker (Biolegend, San Diego, CA, USA) and Brilliant Stain Buffer Plus (BD Biosciences, Franklin Lakes, NJ, USA) for 30 min at 4℃. The stained samples (n=5 per group) were measured by spectral flow cytometry using a Cytek Aurora spectral flow cytometer (Cytek Biosciences, Fremont, CA, USA). Spectral unmixing of the flow cytometry data was performed using SpectroFlo v3.0 (Cytek Biosciences, Fremont, CA, USA). Gating of flow cytometry data was performed using FlowJo[TM] v10.8 Software (BD Biosciences, Franklin Lakes, NJ, USA). Dimensionality reduction by means of Uniform Manifold Approximation and Projection (UMAP) was performed using OMIQ data analysis software (Omiq inc, Santa Clara, CA, USA). Statistical analysis was performed using GraphPad version 9.01 for Windows (GraphPad Software, La Jolla, CA, USA). Representative gating strategies are shown in **Fig. S5A** and information regarding the antibodies used is listed in **Appendix-table 2**.

REFERENCES

1. Fraulob, J.C., et al., *A Mouse Model of Metabolic Syndrome: Insulin Resistance, Fatty Liver and Non-Alcoholic Fatty Pancreas Disease (NAFPD) in C57BL/6 Mice Fed a High Fat Diet.* J Clin Biochem Nutr, 2010. **46**(3): p. 212-23.

2. Bligh, E.G. and W.J. Dyer, *A rapid method of total lipid extraction and purification.* Can J Biochem Physiol, 1959. **37**(8): p. 911-7.

3. Cardiff, R.D., C.H. Miller, and R.J. Munn, *Manual hematoxylin and eosin staining of mouse tissue sections.* Cold Spring Harb Protoc, 2014. **2014**(6): p. 655-8.

4. Kooijman, S., et al., *Central GLP-1 receptor signalling accelerates plasma clearance of triacylglycerol and glucose by activating brown adipose tissue in mice.* Diabetologia, 2015. **58**(11): p. 2637-46.

5. Lanthier, N., et al., *Kupffer cell activation is a causal factor for hepatic insulin resistance.* American Journal of Physiology-Gastrointestinal and Liver Physiology, 2010. **298**(1): p. G107-G116.

6. Bedossa, P., et al., *Histopathological algorithm and scoring system for evaluation of liver lesions in morbidly obese patients.* Hepatology, 2012. **56**(5): p. 1751-9.

7. van der Zande, H.J.P., et al., *The helminth glycoprotein omega-1 improves metabolic homeostasis in obese mice through type 2 immunity-independent inhibition of food intake.* Faseb Journal, 2021. **35**(2).

5

Appendix-table 1. List of polymerase chain reaction primer sequences used in mRNA expression analysis.

Gene	Forward primer (5'-3')	Reverse Primer (5'-3')
Abcg5	GAGCTGCAGAGGATGATTGCT	AGCCACCCTGGTCTTGGA
Acta2	CCTGACGGGCAGGTGATC	ATGAAAGATGGCTGGAAGAGAGTCT
Actb	AACCGTGAAAAGATGACCCAGAT	CACAGCCTGGATGGCTACGTA
Adgre1	CTTTGGCTATGGGCTTCCAGTC	GCAAGGAGGACAGAGTTTATCGTG
Adipoq	CTCCACCCAAGGGAACTTGT	TAGGACCAAGAAGACCTGCATC
Apob	GCCCATTGTGGACAAGTTGATC	CCAGGACTTGGAGGTCTTGGA
Ccl2	GCATCTGCCCTAAGGTCTTCA	TTCACTGTCACACTGGTCACTCCTA
Cd36	GCAAAGAACAGCAGCAAAATC	CAGTGAAGGCTCAAAGATGG
Col1a1	GAGAGAGCATGACCGATGGATT	TGTAGGCTACGCTGTTCTTGCA
Cpt1a	GAGACTTCCAACGCATGACA	ATGGGTTGGGGTGATGTAGA
Ctgf	GGCCTCTTCTGCGATTTCG	CCATCTTTGGCAGTGCACACT
Cyp7a1	CAGGGAGATGCTCTGTGTTCA	AGGCATACATCCCTTCCGTGA
Cyp8b1	GGACAGCCTATCCTTGGTGA	CGGAACTTCCTGAACAGCTC
Cyp27a1	TCTGGCTACCTGCACTTCCT	CTGGATCTCTGGGCTCTTTG
Codon-optimized Fgf21	GCCCACCTGGAGATCAGGGAGGA	GGCAGGAAGCGCACAGGTCCCCAG
Fgf21	GGGGTCATTCAAATCCTGGGTGTCA	ACACATTGTAACCGTCCTCCAGCAG
Fgfr1	AGAGTCCAAGAGTAAAAGCAGC	CTTCCGAGGTTCAGCTCTCC
Fgfr2	GCTATAAGGTACGAAACCAGCAC	GGTTGATGGACCCGTATTCATTC
Fgfr4	TCCATGACCGTCGTACACAAT	ATTTGACAGTATTCCCGGCAG
Il1b	GCAACTGTTCCTGAACTCAACT	ATCTTTTGGGGTCCGTCAACT
Klb	TGTTCTGCTGCGAGCTGTTAC	TACCGGACTCACGTACTGTTT
Mttp	CTCTTGGCAGTGCTTTTTCTCT	GAGCTTGTATAGCCGCTCATT
Pgc1a	TGCTAGCGGTTCTCACAGAG	AGTGCTAAGACCGCTGCATT
Ppara	ATGCCAGTACTGCCGTTTTC	GGCCTTGACCTTGTTCATGT
Rplp0	GGACCCGAGAAGACCTCCTT	GCACATCACTCAGAATTTCAATGG
Tgfb1	TTGCCCTCTACAACCAACACAA	GGCTTGCGACCCACGTAGTA
Tnfa	AGCCCACGTCGTAGCAAACCAC	TCGGGGCAGCCTTGTCCCTT

Abcg5, ATP-binding cassette transporter G member 5; *Acta2*, actin α 2; *Actb*, β-actin *Adgre1*, adhesion G protein-coupled receptor E1; *Adipoq*, adiponectin; *Apob*, apolipoprotein B; *Ccl2*, C-C motif chemokine ligand 2; *Cd36*, cluster of differentiation 36; *Col1a1*, collagen type 1α1; *Cpt1a*, carnitine palmitoyl transferase 1α; *Ctgf*, connective tissue growth factor; *Cyp7a1*, cholesterol 7α-hydroxylase; *Cyp8b1*, sterol 12α-hydroxylase; *Cyp27a1*, sterol 27-hydroxylase; *Fgf21*, exogenous fibroblast growth factor; *Fgfr*, fibroblast growth factor receptor; *Il1b*, interleukin-1β; *Klb*, β-Klotho; *Pgc1a*, peroxisome proliferator-activated receptor gamma coactivator 1α; *Ppara*, peroxisome proliferator-activated receptor α; *Rplp0*, ribosomal protein lateral stalk subunit p0; *Tgfb1*, transforming growth factor-β; *Tnfa*, tumor necrosis factor α.

Appendix-table 2. List of antibodies and other reagents used for flow cytometry analyses

| Target	Clone	Conjugate	Source	Catalog number
CD3	17A2	APC/Fire-810	Biolegend	100267
CD4	RM4-5	APC	eBioscience	17-0042-83
CD8	RPA-T8	PE-Cy5	BD Biosciences	561951
CD9	MZ3	PerCP-Cy5.5	Biolegend	124817
CD11b	M1/70	PE-Cy7	eBioscience	25-0112-82
CD11c	HL3	V450	BD Biosciences	560521
CD19	1D3	BV480	BD Biosciences	566107
CD36	HM36	PE	Biolegend	102606
CD45	30-F11	BV785	Biolegend	103149
CD64	X54-5/7.1	PE-DAZZLE594	Biolegend	139320
CD90.2	30-H12	Alexa Fluor 700	Biolegend	105319
CLEC2	17D9	FITC	Bio-Rad	MCA5700
F4/80	BM8	BV711	Biolegend	123147
Ly6C	HK1.4	APC-Cy7	Biolegend	128025
Ly6G	1A8	BV650	Biolegend	127641
MHC-II	M5/114.15.2	BV750	BD Biosciences	747458
MHC-II	M5/114.15.2	Alexa Fluor 700	Thermo Fisher	56-5321-82
NK1.1	PK136	PerCP-Cy5.5	Biolegend	108727
Siglec-F	E50-2440	PE	BD Biosciences	552126
Siglec-F	E50-2440	BV605	BD Biosciences	740388
TIM4	54 (RMT4-54)	PerCP-eFluor710	Thermo Fisher	46-5866-82
XCR1	ZET	BV421	Biolegend	148216
Other reagents				
Zombie NIR™ Fixable Viability Kit			Biolegend	423106
True-Stain Monocyte Blocker			Biolegend	426103
Brilliant Stain Buffer Plus			BD Biosciences	566385
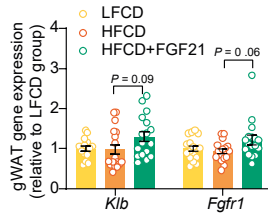
Fig. 2-fig. supplement 1. Liver-specific FGF21 overexpression tends to upregulate mRNA expression of FGF21 receptor 1 (FGFR1) and co-receptor β-Klotho (KLB) in white adipose tissue (WAT). The mRNA expression of KLB and FGFR1 in gonadal WAT (gWAT). Data are shown as mean ± SEM (n=16-18 per group). Differences were assessed using one-way ANOVA followed by a Tukey post-test.
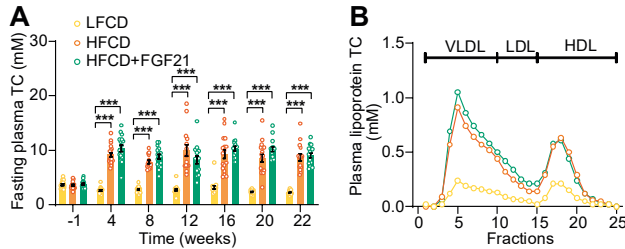
Fig. 3-fig. supplement 1. HFCD increases fasting cholesterol levels. (**A**) Fasting plasma total cholesterol (TC) levels were measured over a 23-week intervention period (n=14-18 per group), and (**B**) the distribution of the cholesterol over circulating lipoproteins was assessed at week 22 (pooled samples; n=18 per group). Data are shown as mean±SEM. Differences were assessed using one-way ANOVA followed by a Tukey post-test. ***$P<0.001$, compared with the LFCD group. VLDL, very low-density lipoprotein; LDL, low-density lipoprotein; HDL, high-density lipoprotein.
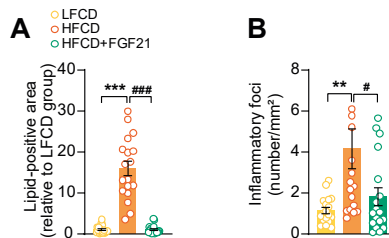
Fig. 4-fig. supplement 1. FGF21 abolishes HFCD-induced increase of hepatic lipid-positive area and the number of inflammatory foci. At week 23, (**A**) hepatic lipid droplet content and (**B**) inflammatory foci numbers were assessed by H&E staining. Data are shown as mean±SEM (n=18 per group). Differences were assessed using one-way ANOVA followed by a Tukey post-test. **$P < 0.01$, ***$P < 0.001$, compared with the LFCD group. #$P<0.01$ ###$P<0.001$, compared with the HFCD group.
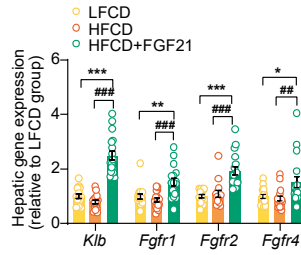
**Fig. 5-fig. supplement 1. Liver-specific FGF21 overexpression upregulates hepatic mRNA expression of FGF21 receptors (FGFRs) and co-receptor β-Klotho (KLB).** The mRNA levels of KLB and FGFRs in the liver. Data are shown as mean±SEM (n=14-18 per group). Differences were assessed using one-way ANOVA followed by a Tukey post-test. *$P<0.05$, **$P<0.01$, ***$P<0.001$, compared with the LFCD group. ##$P<0.01$, ###$P<0.001$, compared with the HFCD group.
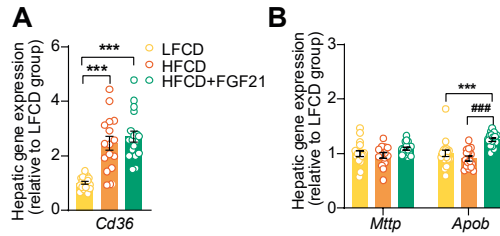
Fig. 5-fig. supplement 2. FGF21 increases apolipoprotein B mRNA (*Apob*) expression in the liver. At end of the study, hepatic expression of genes involved in (**A**) fatty acid uptake and (**B**) VLDL production was quantified (n=15-18 per group). Data are shown as mean±SEM. Differences were assessed using one-way ANOVA followed by a Tukey post-test. ***$P<0.001$, compared with the LFCD group. ###$P<0.001$, compared with the HFCD group. *Apob*, apolipoprotein B; *Cd36*, cluster of differentiation 36; *Mttp*, microsomal triglyceride transfer protein.
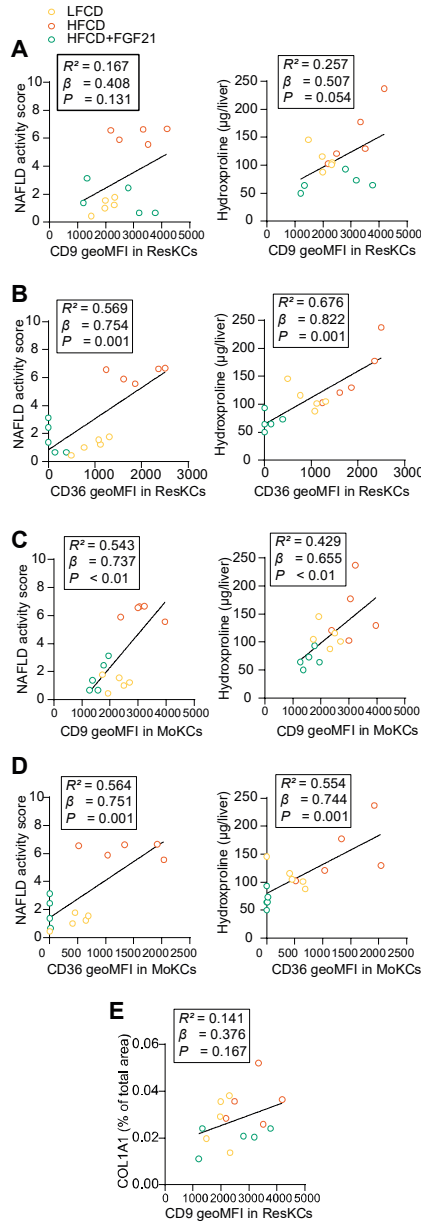
Fig. 6-fig. supplement 1. FGF21 modulates the hepatic immune cell pool. (**A**) Flow cytometry gating strategy. (**B**) After 23 weeks of treatment, CD45⁺ cells were isolated from the liver, and the number of CD45⁺ cells, eosinophils, neutrophils, B cells, dendritic cells (DCs), T cells, natural killer (NK) cells, total Kupffer cells (KCs), Ly6C^{hi} monocytes and monocyte-derived macrophages (MoDMacs) was assessed. Data are shown as mean±SEM (n=4-5 per group). Differences were assessed using one-way ANOVA followed by a Fisher's LSD test. *P<0.05, **P<0.01, compared with the LFCD group. #P<0.05, ##P<0.01, compared with the HFCD group.
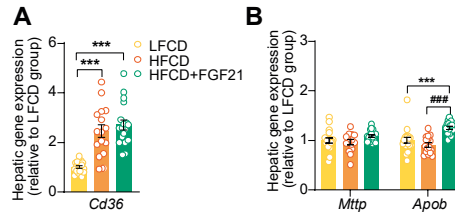
Fig. 6-fig. supplement 2. CD36^hi ResKCs as well as CD36^hi/CD9^hi MoKCs positively correlate with NAFLD activity score and liver fibrosis. NAFLD activity scores and liver hydroxyproline levels were plotted against the expression of (**A**) CD9 and (**B**) CD36 in ResKCs as well as (**C**) CD9 and (**D**) CD36 in MoKCs. (**E**) Hepatic expression of collagen type 1α 1 (COL1A1) was plotted against the expression of CD9 in ResKCs. Linear regression analyses were performed. Data are represented as mean ± SEM (n=5 per group).

6

Pharmacological treatment with FGF21 strongly improves plasma cholesterol metabolism to reduce atherosclerosis

Cong Liu[1,2], Milena Schönke[1,2], Enchen Zhou[1,2], Zhuang Li[1,2], Sander Kooijman[1,2], Mariëtte R. Boon[1,2], Mikael Larsson[3], Kristina Wallenius[3], Niek Dekker[4], Louise Barlind[4], Xiao-Rong Peng[3], Yanan Wang[1,2,5], Patrick C.N. Rensen[1,2,5]

[1] Department of Medicine, Division of Endocrinology, Leiden University Medical Center, Leiden, The Netherlands.
[2] Einthoven Laboratory for Experimental Vascular Medicine, Leiden University Medical Center, Leiden, The Netherlands.
[3] Cardiovascular, Renal and Metabolism, AstraZeneca BioPharmaceutical R&D, Gothenburg, Sweden.
[4] Discovery Sciences, AstraZeneca BioPharmaceutical R&D, Gothenburg, Sweden.
[5] Department of Endocrinology, First Affiliated Hospital of Xi'an Jiaotong University, Xi'an Jiaotong University, Xi'an, China.

ABSTRACT
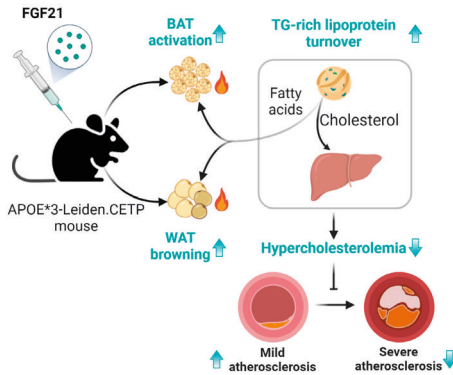
Fibroblast growth factor (FGF) 21, a key regulator of energy metabolism, is currently evaluated in humans for treatment of type 2 diabetes and nonalcoholic steatohepatitis. However, the effects of FGF21 on cardiovascular benefit, particularly on lipoprotein metabolism in relation to atherogenesis, remain elusive. Here, the role of FGF21 in lipoprotein metabolism in relation to atherosclerosis development was investigated by pharmacological administration of a half-life extended recombinant FGF21 protein to hypercholesterolemic APOE*3-Leiden.CETP mice, a well-established model mimicking atherosclerosis initiation and development in humans. FGF21 reduced plasma total cholesterol, explained by a reduction in non-HDL-cholesterol. Mechanistically, FGF21 promoted brown adipose tissue (BAT) activation and white adipose tissue (WAT) browning, thereby enhancing the selective uptake of fatty acids from triglyceride-rich lipoproteins into BAT and into browned WAT, consequently accelerating the clearance of the cholesterol-enriched remnants by the liver. In addition, FGF21 reduced body fat, ameliorated glucose tolerance and markedly reduced hepatic steatosis, related to upregulated hepatic expression of genes involved in fatty acid oxidation and increased hepatic VLDL-triglyceride secretion. Ultimately, FGF21 largely decreased atherosclerotic lesion area, which was mainly explained by the reduction in non-HDL-cholesterol as shown by linear regression analysis, decreased lesion severity and increased atherosclerotic plaque stability index. FGF21 improves hypercholesterolemia by accelerating triglyceride-rich lipoprotein turnover as a result of activating BAT and browning of WAT, thereby reducing atherosclerotic lesion severity and increasing atherosclerotic lesion stability index. We have thus provided additional support for the clinical use of FGF21 in the treatment of atherosclerotic cardiovascular disease.

INTRODUCTION

Atherosclerosis, which underlies life-threatening cardiovascular diseases, is driven by hypercholesterolemia [1]. Apolipoprotein (Apo) B-containing cholesterol-rich lipoproteins enter the arterial intima to trigger or propagate a complex inflammatory cascade accompanied by cholesterol-laden foam cell accumulation, fatty streak formation and subsequently the progressive development of atherosclerotic plaques [1]. Cholesterol homeostasis in the circulation thus modulates the initiation and severity of atherosclerosis. The attenuation of hypercholesterolemia potently reduces morbidity and mortality of atherosclerotic cardiovascular diseases as consistently observed in extensive clinical studies [2]. However, many at-risk patients either fail to reach their target cholesterol levels with current therapeutics such as statins or are intolerant to statins due to their adverse effects [3]. This leaves many patients with obvious residual risks, indicating that additional effective therapeutics including novel cholesterol-lowering agents are needed.

FGF21, an endocrine hormone, has received increasing attention for its ability to regulate energy homeostasis and counteract obesity-related disorders [4, 5]. Physiologically, FGF21 is induced by a diverse range of stressors such as cold exposure, fasting/starvation and ketogenic diet consumption, and in turn aids the adaptation to the stressor by increasing adaptive thermogenesis, lipolysis, ketogenesis and fatty acid (FA) oxidation, respectively [6-8]. Moreover, patients with obesity [9], type 2 diabetes [10] and non-alcoholic fatty liver diseases [11] show higher serum FGF21 levels, demonstrating a compensatory FGF21 response in an attempt to overcome FGF21 resistance or maintain metabolic homeostasis. FGF21 treatment has multiple therapeutic benefits for cardiometabolic disorders in rodents and humans, including alleviation of insulin resistance [5] and attenuation of nonalcoholic steatohepatitis [12].

FGF21 exerts its metabolic actions through cell-surface receptors comprised of the conventional FGF receptor 1 in complex with β-klotho, which is abundantly expressed in fat tissue [13]. Despite adipose tissue being its primary target organ [14], FGF21 also acts on the hypothalamus [15], hindbrain [16] and liver [8] to sustain metabolic homeostasis. FGF21 was recently shown to directly and indirectly (via the sympathetic nervous system) act on adipose tissue to promote brown fat activation and white fat browning, thereby increasing energy expenditure and promoting weight loss [17, 18].

Studies on the role of FGF21 in atherosclerosis development are still scarce and mainly derived from genetic studies, showing that FGF21-deficiency in ApoE-knockout mice increases atherosclerosis [19]. Strikingly, FGF21 administration improves

hypercholesterolemia in obese non-human primates[20] and humans [21], implying that beneficial effects of FGF21 on lipoprotein metabolism may attenuate atherosclerosis progression. Indeed, increased circulating FGF21 levels in atherosclerosis patients are proposed to be a compensatory mechanism to prevent vascular damage [22]. A single study has evaluated the pharmacological effect of FGF21 on atherosclerosis in FGF21 and ApoE double-knockout mice [19]. However, since ApoE is essential for mediating uptake of triglyceride (TG)-rich lipoprotein remnants by the liver, ApoE-knockout mice may not be the preferred model to study potential effects of FGF21 on atherosclerosis development through modulation of plasma lipid metabolism.

The main objective of the current study was to evaluate the role of lipoprotein metabolism in the effects of pharmacological FGF21 treatment on atherosclerosis development. To that end, we used APOE*3-Leiden.CETP mice, a translational model for human-like lipoprotein metabolism that, in favorable contrast to ApoE or low-density lipoprotein receptor (LDLR)-knockout mice, respond to the cholesterol-lowering effects of lipid-lowering agents [23]. Here, we report that FGF21 decreases hypercholesterolemia by accelerating TG-rich lipoprotein turnover as a result of activating BAT and browning of WAT, thereby reducing atherosclerotic lesion severity and increasing the atherosclerotic lesion stability index.

METHODS

Animals

Female *APOE*3-Leiden.CETP* mice were obtained as previously described [24]. Mice at the age of 8-12 weeks were housed under standard conditions (22℃; 12/12-hour light/dark cycle) with *ad libitum* access to water and a cholesterol-containing Western-type diet (WTD; 0.15% cholesterol and 16% fat; Altromin, Lage, Germany). All mice were acclimatized to housing and WTD for 3 weeks prior to the pharmacological intervention, to raise plasma cholesterol from approx. 2 mM up to stable levels of approx. 15 mM that are sufficient to induce atherosclerosis development. Then, based on 4-hour fasted plasma lipid levels, body weight and body composition, these mice were randomized to 2 treatment groups receiving either recombinant FGF21 (AstraZeneca, 1 mg/kg body weight, according to previous studies [20, 25]) or vehicle (0.1% BSA in sterile-filtered PBS) via subcutaneous injection, 3 times per week (i.e. Monday, Wednesday and Friday at approx. 1 pm). In a first study, mice were treated for 16 weeks, in which indirect calorimetry was assessed at week 8 and atherosclerosis development at week 16 (n=16 mice per group). In a second study, mice were treated for 12 weeks, in which an intraperitoneal glucose tolerance test (IPGTT) was performed at week 6

and very low-density lipoprotein (VLDL) production was assessed at week 12 (n=8 per group). Unless indicated otherwise, mice were group housed (3-5 per cage) during the treatment period to avoid stress caused by single housing. All animal experiments were carried out according to the Institute for Laboratory Animal Research Guide for the Care and Use of Laboratory Animals, and were approved by the National Committee for Animal Experiments (Protocol No. AVD1160020173305) and by the Ethics Committee on Animal Care and Experimentation of the Leiden University Medical Center (Protocol No. PE.18.034.014 and No. PE.18.034.044). All animal procedures were conform the guidelines from Directive 2010/63/EU of the European Parliament on the protection of animal used for scientific purposes.

Recombinant FGF21 protein

FGF21 has a short half-life *in vivo*, and a Fc-fusion was designed to increase circulation levels for longer duration of action [26]. Recombinant FGF21 protein was generated as described under Expanded Methods in the **Supplementary Materials.**

Measurement of body weight and body composition

Body weight was determined weekly with a scale, and body composition was determined biweekly in conscious mice using an EchoMRI-100 analyzer (EchoMRI, Houston, TX, USA).

Indirect calorimetry

In the first experiment, indirect calorimetry was carried out in fully automated metabolic cages (Promethion line, Sable Systems International, Las Vegas, NV, USA) after 8 weeks of treatment. Mice (n=8 per group) were single housed and acclimatized to the system for 48 hours, then further monitored for 72 hours (3 light/dark cycles). Food intake, physical activity, O_2 consumption (mL/h/kg body weight) and CO_2 production (mL/h/kg body weight) were continuously monitored. Mice had *ad libitum* access to food and water and received either FGF21 or vehicle every other day. Energy expenditure, fat oxidation rate and carbohydrate oxidation rate were calculated [27] and expressed per mouse. Besides, these values were expressed per g lean mass.

Glucose tolerance test

In the second experiment, after 6 weeks of treatment, an IPGTT was conducted with an injection of D-glucose (2 g/kg body weight) after 4 hours fasting (9:00-13:00; n=8 per group). The IPGTT was performed as described under Expanded Methods in the **Supplementary Materials.** Homeostasis Model Assessment for Insulin Resistance (HOMA-IR) was calculated with the following formula: [fasting serum glucose (mM) × fasting serum insulin (μU/ml)]/22.5.

6

In vivo plasma decay and organ uptake of VLDL-mimicking particles

VLDL-mimicking particles (average size 80 nm) labeled with glycerol tri[³H]oleate ([³H] TO) and [¹⁴C]cholesteryl oleate ([¹⁴C]CO) were prepared using a previously published method[28]. After 16 weeks of treatment, 8 mice per group were selected and fasted for 4 hours (9:00-13:00) and intravenously injected (t=0 min) with the VLDL-mimicking particles (1.0 mg TG in 200 μL PBS). Blood samples were collected from the tail vein at 0 min (before injection) and 2, 5, 10 and 15 min after injection to measure the plasma decay of [³H]TO and [¹⁴C]CO. After 15 min, all mice were sacrificed by CO_2 inhalation and perfused with ice-cold PBS. Subsequently, tissues were isolated, and pieces from the mice treated with VLDL-mimicking particles were transferred into High Performance glass vials (PerkinElmer, Groningen, The Netherlands) and dissolved overnight at 56℃ in 0.5 mL Solvable (PerkinElmer, Groningen, The Netherlands). Dissolved organs were mixed with 5 mL Ultima Gold scintillation fluid (PerkinElmer, Groningen, The Netherlands), and vials were placed in a Tri-Carb 2910TR Low Activity Liquid Scintillation Analyzer (PerkinElmer, Groningen, The Netherlands) to assess ³H and ¹⁴C activity. Disintegrations per minute (dpm) of ³H and ¹⁴C were expressed as percentage of the injected dose per gram tissue. Other pieces of the tissues were either snap-frozen in liquid N_2 (for molecular analysis) or embedded in paraffin (for immunohistochemistry).

Plasma lipid profiles and adiponectin levels

Every 4 weeks, after 4-hour fasting (9:00-13:00), tail vein blood was collected into paraoxon-coated glass capillaries. Plasma was collected and measured for TG, free fatty acid (FFA) and total cholesterol (TC) levels using commercial enzymatic kits from Roche Diagnostics (Mannhein, Germany). Plasma high-density lipoprotein cholesterol (HDL-C) levels were measured using previously published approach [27]. Plasma adiponectin was measured before (week 0) and after (week 16) the treatment using Mouse Adiponectin/Acrp30 Quantikine ELISA Kit (R&D Systems, Minneapolis, NE, USA).

Adipose tissue histology

Formalin-fixed paraffin-embedded interscapular brown adipose tissue (iBAT) and subcutaneous white adipose tissue (sWAT) tissue sections (5 μm) were prepared for haematoxylin and eosin staining using standard protocols [29], and uncoupling protein-1 (UCP-1) immunostaining as described previously [30]. The areas occupied by intracellular lipid vacuoles and UCP-1 protein within the iBAT were quantified using Image J software (version 1.52a; National Institutes of Health, Bethesda, Maryland).

Liver histology and lipid measurements

Formalin-fixed paraffin-embedded liver samples were stained with haematoxylin and eosin staining. The areas occupied by intracellular lipid vacuoles were quantified using Image J software. Hepatic lipids were extracted from frozen liver samples using a modified protocol from Bligh and Dyer [31]. Using commercial kits, TG ,TC and phospholipid (PL) (Instruchemie, Delfzijl, The Netherlands) and protein (Pierce, Thermo Fisher Scientific, Waltham, MA, USA) concentrations were determined. Hepatic lipids were expressed as nmol lipid per mg protein.

Gene expression analysis

Using Tripure RNA isolation reagent (Roche, Mijdrecht, The Netherlands), total RNA was extracted from snap-frozen tissues. Using Moloney Murine Leukemia Virus Reverse Transcriptase (Promega, Leiden, The Netherlands), complementary DNA for quantitative reverse transcriptase-PCR was generated by reverse transcription of total RNA. Then, mRNA expression was normalized to *β-actin* and *Rplp0* mRNA levels and expressed as fold change compared with the vehicle group. Primer sequences are listed in the **Supplementary Materials**.

Hepatic VLDL production

In the second experiment, at week 12, mice (n=8) were fasted for 4 hours (9:00-13:00) and anesthetized by the intraperitoneal injection (once) of 6.25 mg/kg Acepromazine (Alfasan, Woerden, The Netherlands), 6.25 mg/kg Midazolam (Roche, Mijdrecht, The Netherlands), and 0.31 mg/kg Fentanyl (Janssen-Cilag, Tilburg, The Netherlands) [32]. Anesthesia was maintained by intraperitoneal injection (3 times; every 45 minutes) of 0.03 mg/kg Acepromazine, 0.03 mg/kg Midazolam and 0.001 mg/kg Fentanyl [32], and body temperature was monitored throughout the experimental procedure to ensure a proper deep plane of anesthesia. Hepatic VLDL production was assessed as described under Expanded Methods in the **Supplementary Materials.** Commercial kits were used for the measurement of VLDL-TG, -TC and -PL and -protein.

Atherosclerosis quantification

In the first experiment, at 16 weeks hearts were collected, prepared and cross-sectioned (5 μm) as described previously [27]. Four sections with 50 μm intervals were used per mouse for atherosclerosis measurements. Sections were stained with haematoxylin-phloxine-saffron for histological analysis using standard protocols [33]. Lesions were classified by severity according to the guidelines of the American Heart Association adapted for mice [34]. Various types of lesions were discerned: no lesions, mild lesions (types 1–3) and severe lesions (types 4–5). Lesion composition was assessed as described under Expanded Methods in the **Supplementary Materials**. Lesion area and

composition were measured using Image J software. By dividing the relative collagen and smooth muscle cell area by the relative area of macrophages within the same lesion, the stability index was calculated.

Statistical analyses

Comparisons between vehicle and FGF21 groups were performed using the unpaired two-tailed Student's *t-test*. The square root of the lesion area was taken to linearize the relationship with the plasma TC, non-HDL-C and HDL-C exposures and plasma adiponectin levels (at 16 week). To assess significant correlations between atherosclerotic lesion size and plasma TC, non-HDL-C and HDL-C exposures and plasma adiponectin levels, univariate regression analyses were performed. Then, to predict the contribution of plasma TC, non-HDL-C and HDL-C exposures and adiponectin to the atherosclerotic lesion size, multiple regression analysis was performed. Data are presented as mean ± SEM, and a *P* value less than 0.05 is considered statistically significant. All statistical analyses were performed with GraphPad Prism 8 (GraphPad Software Inc., California, CA, USA) except for univariate and multiple regression analyses which were performed with SPSS 20.0 (SPSS, Chicago, IL USA) for Windows.

RESULTS

FGF21 decreases body fat mass by increasing energy expenditure

We first examined whether FGF21 confers its beneficial effect on body weight under atherogenic conditions. In line with previous studies [4], FGF21 potently prevented weight gain (**Fig. 1A**). The body weight of FGF21-treated mice was reduced compared to vehicle-treated mice after only 2 weeks of treatment (-12%) and thereafter stabilized but remained significantly lower (-19% at week 16) than that of vehicle-treated mice. FGF21 only marginally but significantly reduced body lean mass (-6%) after 2 weeks of treatment, which stabilized during the remainder of the treatment period (**Fig. S1A**). In contrast, FGF21-treated mice showed resistance to gain body fat on the WTD, resulting in a lower fat mass (-46% at week 16) when compared to the vehicle counterparts (**Fig. 1B**). Therefore, the reduction of the body weight was mainly caused by fat mass loss. To understand how FGF21 potently reduces fat mass, next we housed mice in metabolic cages to measure whole-body energy metabolism. FGF21 treatment did not influence food intake (**Fig. 1C**), nor physical activity (**Fig. 1D**). Rather, FGF21 treatment induced a robust and consistent increase in energy expenditure (**Fig. 1E** and **S2A**), explained mainly by markedly increased fat oxidation (**Fig. 1F-1G** and **S2B-S2D**), which thus explains the potent effect of FGF21 treatment on preventing fat mass gain.
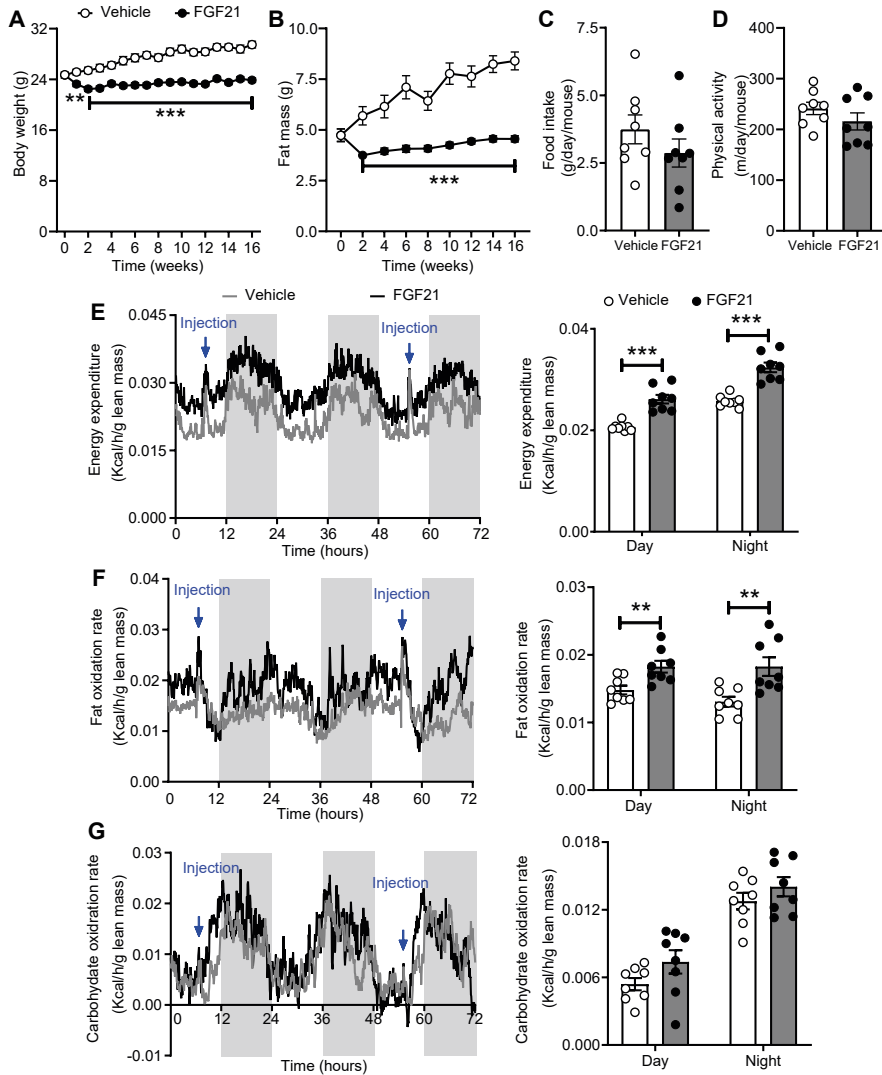
Fig. 1. FGF21 decreases body fat mass by increasing energy expenditure. Body weight **(A)** and fat mass **(B)** were measured throughout the study (n=15-16). In week 8, food intake **(C)**, physical activity **(D)**, energy expenditure **(E)**, fat oxidation rate **(F)** and carbohydrate oxidation rate **(G)** were monitored, and values shown **(E-G)** were corrected for body lean mass (n=8). **(A-D)**, data are represented as mean±SEM. **(E-G)**, for line graphs, data are shown as mean for each group (12-hour cycle; shaded area represents the dark cycle); for bar graphs, data are shown as mean±SEM. Differences were assessed using unpaired two-tailed Student's t-test. **P<0.01, ***P<0.001.

FGF21 promotes brown fat activation and white fat browning, and improves glucose metabolism

Since the markedly increased FA oxidation is consistent with BAT activation [27], we next quantified intracellular lipid vacuoles and UCP-1 abundance in both BAT and WAT. As compared to vehicle group, FGF21 administration reduced iBAT weight (-21%; **Fig. 2A**), lowered the lipid droplet content in iBAT (-56%; **Fig. 2B**) and increased UCP-1 content in iBAT (+32%; **Fig. 2C**), which is consistent with BAT activation. Likewise, FGF21 decreased gonadal WAT (-53%; **Fig. 2D**). Since browning predominantly occurs in sWAT [35], histological analysis was thus performed in sWAT. FGF21 markedly reduced lipid droplet size and increased the number of UCP-1 positive areas (**Fig. 2E**), which may suggest that FGF21 improves mitochondrial function in WAT. In line with this suggestion, FGF21 upregulated the expression of key genes involved in mitochondrial biogenesis and dynamics (**Fig. 2F**). Since mitochondrial dysfunction in adipocytes is the primary cause of adipose tissue inflammation [36], we hypothesized that FGF21 would reduce inflammation in WAT. Indeed, FGF21 decreased mRNA levels of tumor necrosis factor α (*Tnfα*; -60%) and Interleukin 1β (*Il1-β*; -57%) in sWAT (**Fig. 2G**).

Notably, FGF21 increased adiponectin (*Adipoq*) gene expression in iBAT (+35%) and sWAT (+66%) (**Fig. 2H**), accompanied by increased adiponectin levels in the circulation (+47%; **Fig. 2I**). Since increased adiponectin was shown to mediate the effect of FGF21 on glucose homeostasis and insulin sensitivity [37], an IPGTT was performed in mice in a second experiment after 6 weeks of treatment. FGF21 slightly but significantly reduced fasting blood glucose levels (**Fig. 2J**), decreased the glucose excursion during the IPGTT, and lowered plasma insulin levels (**Fig. 2K**). Consistently, FGF21 decreased the HOMA-IR index (**Fig. 2L**), indicating that FGF21 increases insulin sensitivity also under atherogenic conditions.

FGF21 promotes TG-derived FA uptake by both brown and white fat and accelerates cholesterol-enriched remnant clearance by the liver

To investigate the role of BAT activation and WAT browning in VLDL metabolism, we intravenously injected mice with VLDL-mimicking particles labeled with [^{3}H]TO and [^{14}C]CO at the end of the study. In vehicle-treated mice, the plasma decay of [^{3}H]TO ($t_{1/2}$ =5.0 min; **Fig. 3A**) was faster than of [^{14}C]CO ($t_{1/2}$ > 15 min; **Fig. 3C**), indicating that VLDL-TG-derived FA uptake precedes the clearance of VLDL remnants. While BAT was relatively the most active tissue responsible for the uptake of [^{3}H]TO-derived [^{3}H]oleate (**Fig. 3B**), [^{14}C]CO was mainly effectively taken up by the liver (**Fig. 3D**). FGF21 largely accelerated the clearance of [^{3}H]TO from plasma ($t_{1/2}$ =3.5 min; **Fig. 3A**) caused by a strongly increased uptake of [^{3}H]TO-derived [^{3}H]oleate by iBAT (+259%), subscapular BAT (+261%), and sWAT (+66%) (**Fig. 3B**). Concomitantly, FGF21 treatment
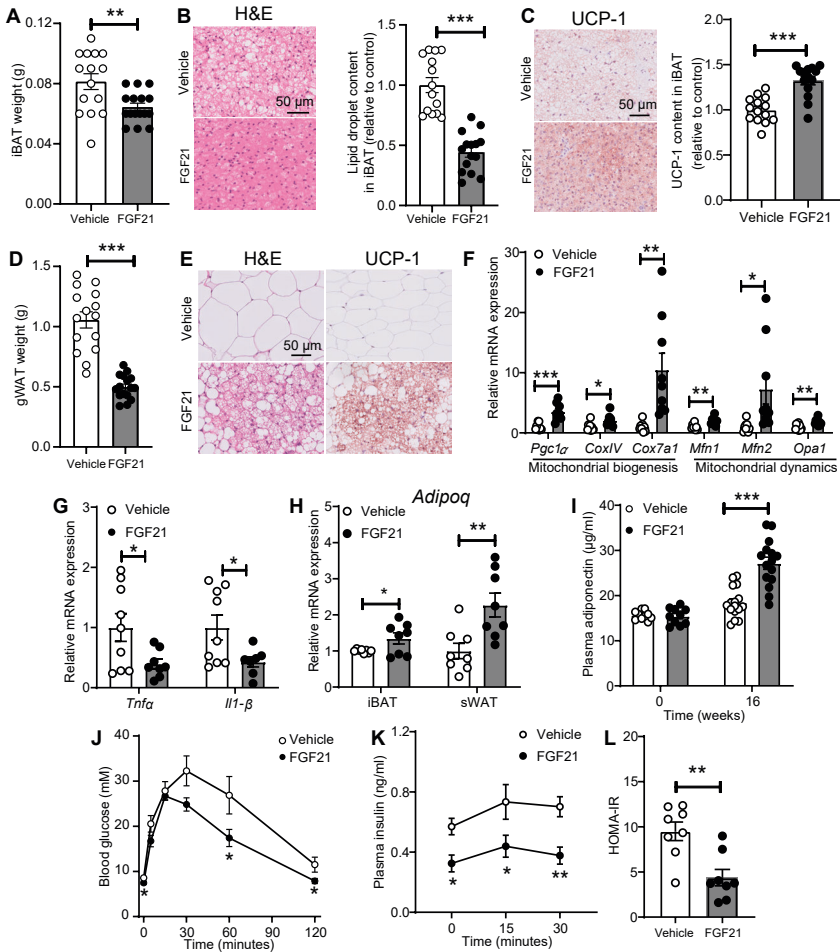
Fig. 2. FGF21 promotes brown fat activation and white fat browning, and improves glucose metabolism. After 16 weeks of treatment, interscapular BAT (iBAT) **(A)** and gonadal WAT (gWAT) **(D)** were weighed. In iBAT, the lipid content **(B)** and expression of uncoupling protein-1 (UCP-1) **(C)** were quantified after hematoxyline & eosin (H&E) staining and UCP-1 immunostaining, respectively. The browning of subcutaneous WAT (sWAT) was determined by H&E staining and UCP-1 immunostaining, and representative pictures are shown **(E)**. The relative expression of genes involved in mitochondrial function **(F)** and inflammation **(G)** in sWAT, and the relative mRNA levels of *adiponectin* in iBAT and sWAT **(H)** were measured. Fasting plasma adiponectin levels were measured at week 0 and week 16 **(I)**. The intraperitoneal glucose tolerance test (IPGTT) was performed after 6 weeks of the treatment, during which plasma glucose **(J)** and insulin **(K)** levels were measured. In addition, the homeostatic model assessment for insulin resistance (HOMA-IR) was calculated **(L)**. Data are represented as mean ± SEM (**A-E**, n=15-16; **F-H**, n=8-10; **I**, n=10 or 15-16; **J-L**, n=7-8). (**A-I**), data were obtained from the first experiment; (**J-L**), data were obtained from the second experiment. *$P<0.05$; **$P<0.01$, ***$P<0.001$ (unpaired two-tailed Student's *t*-test). *Adipoq*, adiponectin; *CoxIV*, mitochondrial cytochrome C oxidase subunit IV; *Cox7a1*, cytochrome C oxidase polypeptide 7A1; *Il1-β*, interleukin 1 β; *Mfn1/2*, mitofusin-1/2; *Mttp*, microsomal triglyceride transfer protein; *Opa1*, dynamin-like 120 kDa protein, mitochondrial; *Pgc1α*, peroxisome proliferator-activated receptor γ coactivator 1-α; *Tnfα*, tumor necrosis factor α.

accelerated the plasma clearance of [^{14}C]CO ($t_{1/2}$ = 8.5 min; **Fig. 3C**). This was mainly attributed to largely increased uptake of [^{14}C]CO by the liver (+128%), although higher [^{14}C]CO uptake was also observed in iBAT (+159%), subscapular BAT (+157%) and sWAT (+95%) **(Fig. 3D)**. These effects were accompanied by increased hepatic expression of the *Ldlr* **(Fig. S3A)** and proprotein convertase subtilisin/kexin 9 (*Pcsk9*) **(Fig. S3B)**.
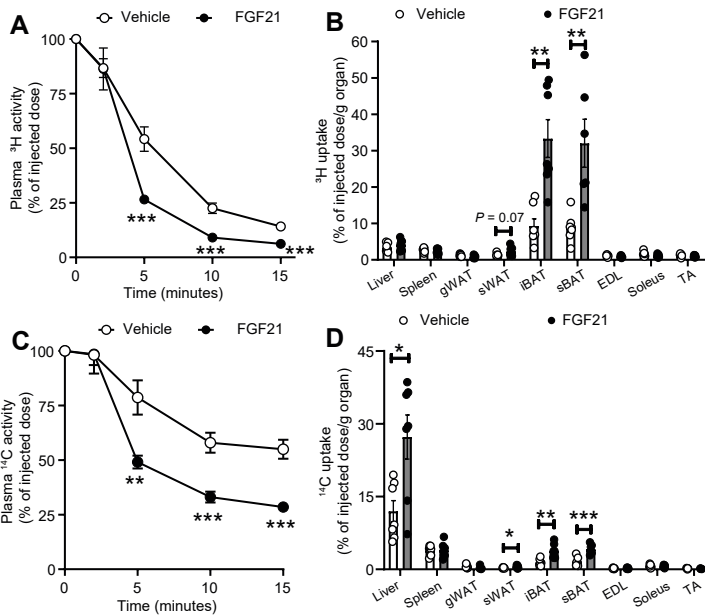

Fig. 3. FGF21 promotes TG-derived FA uptake by brown fat and white fat and accelerates cholesterol-enriched remnant clearance by the liver. The clearance of ^{3}H **(A)** and ^{14}C **(C)** from plasma and the uptake of ^{3}H **(B)** and ^{14}C **(D)** by various tissues were assessed. Data are represented as mean ± SEM (n = 6-7). *P<0.05, **P<0.01, ***P<0.001 (unpaired two-tailed Student's *t*-test). EDL, extensor digitorum longus; gWAT, gonadal white adipose tissue; iBAT, interscapular brown adipose tissue; sBAT, subscapular brown adipose tissue; sWAT, subcutaneous white adipose tissue; TA, tibialis anterior.

FGF21 reduces hypercholesterolemia

We next evaluated the effect of FGF21 on plasma lipid levels. FGF21 increased fasting plasma FFA levels during the first 8 weeks of treatment **(Fig. 4A)**, reflecting enhanced lipolysis in WAT, followed by an increase in fasting plasma TG levels from week 12 onwards **(Fig. 4B)**. In contrast, FGF21 consistently decreased fasting plasma TC **(Fig. 4C)** and non-HDL-C **(Fig. 4D)** levels, and increased fasting plasma HDL-C levels after 16 weeks **(Fig. 4E)**, indicating that FGF21 improves hypercholesterolemia under atherogenic conditions.
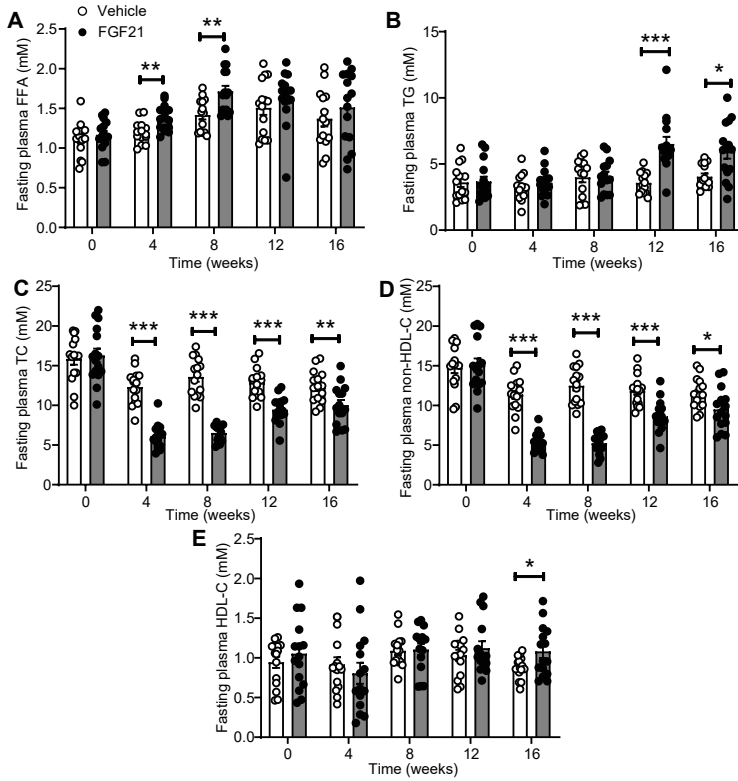
Fig. 4. FGF21 reduces hypercholesterolemia. Throughout the study, fasting plasma levels of free fatty acids (FFA) **(A)**, triglycerides (TG) **(B)**, total cholesterol (TC) **(C),** non-high density lipoprotein-cholesterol (non-HDL-C) **(D)** and high density lipoprotein-cholesterol (HDL-C) **(E)** were measured. Data are represented as mean ± SEM (n = 14-15). *$P < 0.05$, **$P < 0.01$, ***$P < 0.001$ (unpaired two-tailed Student's t-test).

FGF21 reduces hepatic steatosis accompanied by upregulated expression of genes involved in fatty acid oxidation and increased VLDL production

To elucidate the molecular mechanism responsible for FGF21-induced increase of plasma TG levels, we first quantified the hepatic expression of genes involved in lipid handling in livers obtained after 16 weeks. FGF21 upregulated mRNA expression of the fatty acid transporter, cluster of differentiation 36 (*Cd36*) **(Fig. 5A)**, accompanied by upregulated expression of genes involved in *de novo* lipogenesis, including acetyl-CoA carboxylase (*Acc1*), fatty acid synthase (*Fasn*) and diacylglycerol O-acyltransferase 2 (*Dgat2*) **(Fig. 5B)**. FGF21-treated mice also showed higher hepatic mRNA levels of carnitine palmitoyl transferase 1a (*Cpt1*) and peroxisome proliferator-activated receptor α (*Pparα*), both involved in hepatic FA oxidation (**Fig. 5C).**

Interestingly, FGF21 also increased hepatic expression of microsomal triglyceride transfer protein (*Mttp*) and *ApoB* (**Fig. 5D**), suggesting that FGF21 increases hepatic

VLDL production. Indeed, FGF21 increased both the production rate of VLDL-TG (**Fig. 5E**) and VLDL-ApoB (**Fig. 5F**). Moreover, FGF21 decreased the amount of TC per ApoB (**Fig. S4A**) and did not affect the amounts of TG, PL and protein per ApoB (**Fig. S4B-S4D**), suggesting that FGF21-induced increase in plasma TG is due to the increased hepatic VLDL particle production rather than enhanced VLDL lipidation.
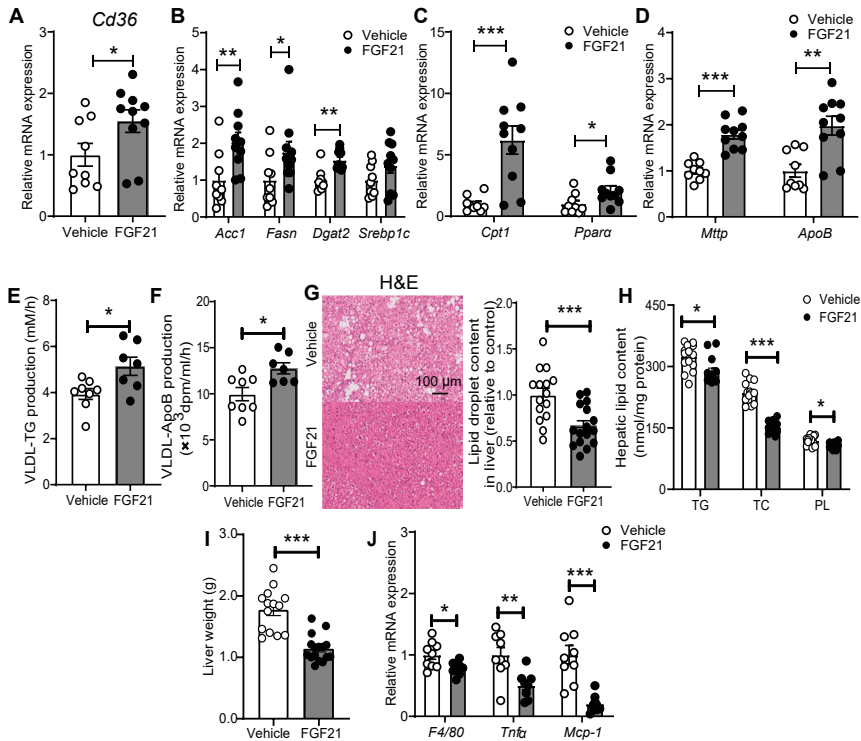

Fig. 5. FGF21 reduces hepatic steatosis accompanied by upregulated expression of genes involved in fatty acid oxidation and increased VLDL particle production. After 16 weeks of treatment, the relative mRNA expression levels of genes involved in fatty acid uptake (**A**), de novo lipogenesis (**B**) and fatty acid oxidation (**C**), very low density lipoprotein (VLDL) production and secretion (**D**) and inflammation (**J**) were determined in the liver. The hepatic VLDL-TG (**E**) and VLDL-ApoB (**F**) production rates were assessed after 12 weeks of the treatment. After 16 weeks of treatment, the hepatic lipid content was assessed by H&E staining (**G**), and triglyceride (TG), total cholesterol (TC) and phospholipid (PL) levels (**H**) were determined within the liver, and liver weight (**I**) was measured. Data are represented as mean ± SEM (**A-D** and **J**, n = 8-10; **E-F**, n = 7-8; **G-H**, n = 14-15). (**A-D**) and (**G-J**), data were obtained from the first experiment; (**E-F**), data were obtained from the second experiment. *$P < 0.05$, **$P < 0.01$, ***$P < 0.001$ (unpaired two-tailed Student's t-test). Acc1, acetyl-CoA carboxylase; ApoB, apolipoprotein B; Cd36, cluster of differentiation 36; Cpt1, carnitine palmitoyl transferase 1; Dgat2, diacylglycerol O-acyltransferase 2; Fasn, fatty acid synthase; Mcp-1, monocyte chemoattractant protein 1; Mttp, microsomal triglyceride transfer protein; Ppara, peroxisome proliferator-activated receptor α; Srebp1c, sterol regulatory element-binding transcription factor 1; Tnfα, tumor necrosis factor α.

Next, to evaluate the effects of FGF21 on hepatic lipid content, histological and biochemical analyses were performed. In line with previous work [5], FGF21 reduced hepatic steatosis as evidenced by reduced intracellular lipid vacuoles within the liver (-34%; **Fig. 5G)** and decreased levels of hepatic TG (-10%), TC (-32%) and PL (-7%) **(Fig. 5H)**. Consistently, FGF21 reduced liver weight (-36%; **Fig. 5I)**. Lipid homeostasis has been shown to play a pivotal role in regulating the inflammatory response in the liver [38]. In line, FGF21 reduced the hepatic mRNA levels of *F4/80*, *Tnfα* and monocyte chemoattractant protein-1 (*Mcp-1*) **(Fig. 5J)**. Collectively, these data suggest that FGF21 increases hepatic FA uptake coupled to enhanced FA oxidation, TG synthesis and VLDL-TG production, which may together explain the FGF21-induced reduction in steatosis.

FGF21 attenuates atherosclerosis progression as mainly predicted by the reduction of plasma non-HDL-C levels

Since FGF21 improved hypercholesteremia, the most important risk factor for atherosclerosis, we next investigated whether FGF21 alleviates atherosclerosis progression. To this end, in the first experiment, atherosclerotic lesion area, severity and composition were determined after 16 weeks of treatment. Histological evaluation showed that FGF21 markedly decreased atherosclerotic lesion area throughout the aortic root (**Fig. 6A and 6B**), leading to a much lower mean atherosclerotic lesion area (-73%; **Fig. 6C**). Moreover, FGF21 markedly improved lesion severity as evident from less severe lesions (-74%; **Fig. 6D**), more mild lesions (+68%; **Fig. 6D**), and more nondiseased segments **(**+440%; **Fig. 6E)**. Notably, FGF21 significantly improved atherosclerotic stability index (+46%; **Fig. 6G**) via reducing macrophage content (-24%; **Fig. 6F and 6H**) without influencing collagen and smooth muscle cell content within the plaques **(Fig. S5A and S5B and Fig. 6H)**. Consistently, although the gene expression in aorta tissue of vascular cell adhesion protein 1 (*Vcam-1*) was comparable between these two groups, FGF21-treated mice had lower mRNA levels of intercellular adhesion molecule-1 *(Icam-1*; -41%*)* and *Mcp-1* (-39%) than the control group (**Fig. 6I**).

Next, we evaluated the contribution of FGF21-induced TC and non-HDL-C lowering to the attenuation in atherosclerosis. Univariate regression analysis revealed that the lesion area was predicted by plasma TC (R^2 = 0.719) and non-HDL-C (R^2 = 0.706) but not HDL-C (P = 0.307; R^2 = 0.037) (**Figure 6J-6L**). Although a previous study showed that adiponectin can mediate the FGF21-induced reduction of atherosclerosis[19], we observed that plasma adiponectin levels predicted lesion area to only a modest extent (P = 0.005; R^2 = 0.259; **Figure 6M**). Taken together, in our experimental model FGF21 reduces atherosclerosis mainly by reducing non-HDL-C.
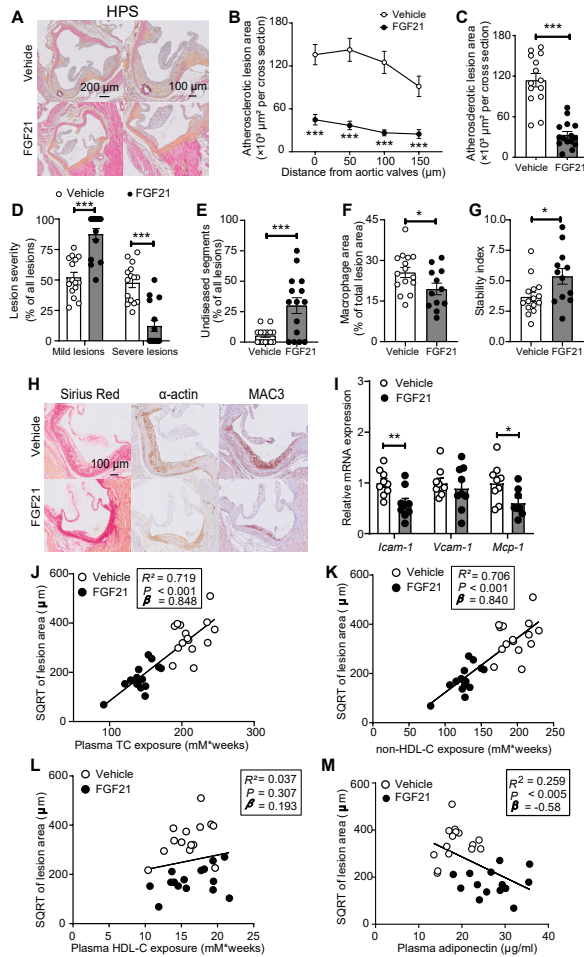
Fig. 6. FGF21 protects against atherosclerosis progression as largely predicted by the reduction of plasma non-HDL-C levels. At week 16, hearts were collected, the valve areas of their aortic roots were stained with haematoxylin-phloxine-saffron (HPS), and representative pictures are shown **(A)**. Lesion area as a function of distance from the aortic valves was determined by calculating the lesion area of four consecutive cross-sections starting from the appearance of open aortic valve leaflets **(B)**. From the four cross-sections, the mean atherosclerotic lesion area was determined **(C)**. Lesions were categorized according to lesion severity **(D)**, and the percentage of nondiseased segments was scored **(E)**. The valve area of aortic root was stained with Sirius Red, an anti-α-actin antibody and an anti-MAC3 antibody to quantify the content of collagen, smooth muscle cells and macrophages **(F)** within the lesions, respectively. Representative pictures are shown **(H)**. The stability index (collagen and smooth muscle cell content/macrophage content of the lesions) was calculated **(G)**. The relative expression of genes involved in inflammation was measured in aorta **(I)**. The square root (SQRT) of the atherosclerotic lesion area was plotted against the plasma TC **(J)**, non-HDL-C **(K)** and HDL-C **(L)** exposure during the 16-week treatment period and plasma adiponectin levels at week 16 **(M)**. Linear regression analyses were performed. Data are represented as mean ± SEM (**A-H and J-M**, n = 14-15; **I**, n = 9-10). *$P < 0.05$, ***$P < 0.001$ (unpaired two-tailed Student's *t*-test). *Icam-1*, intercellular adhesion molecule 1; *Mcp-1*, monocyte chemoattractant protein 1; *Vcam-1*, vascular cell adhesion molecule 1.

DISCUSSION

FGF21 has been proposed to be a physiological protector against metabolic stress, while pharmacological doses of FGF21 mimetics to animal models or human lead to profound effects on insulin sensitivity and lipid profile [39]. Although clinical trials are underway with long-acting analogs of FGF21 to combat obesity, type 2 diabetes and nonalcoholic steatohepatitis [40], the effect of pharmacological treatment with FGF21 on atherosclerosis development as well as underlying mechanisms are far from being elucidated. Here, we used APOE*3-Leiden.CETP mice to show that exogenous recombinant FGF21 primes adipose tissue to enhance VLDL-TG hydrolysis and uptake of liberated FA by BAT and WAT, followed by accelerated uptake of cholesterol-enriched remnants by the liver. Accordingly, FGF21 markedly reduces circulating atherogenic cholesterol levels, thereby potently attenuating atherosclerosis development.

First, we demonstrated that FGF21 also in an atherogenic setting enhances energy expenditure leading to prevention of body fat gain. FGF21-induced weight loss has been reported to be caused in part by the induction of energy expenditure in obese rodents and humans, achieved by the recruitment of thermogenic pathways in brown fat and the browning of white fat [25, 41]. Consistently, our histological and immunologic analyses showed that FGF21 treatment markedly increased BAT activation and WAT browning as determined by UCP-1 protein expression. We did not observe any effect of FGF21 on food consumption. In diabetic rhesus monkeys, FGF21 at high doses up to 50 mg/kg did decrease food intake up to 60%, contributing to body weight lowering [42]. However, FGF21 treatment at lower doses induced weight loss without affecting food intake in wild-type mic[4], diet-induced obese mice [5], and non-human primates [43], which is consistent with our data. Also, in our study FGF21 did not seem to affect physical activity, while FGF21 increased physical activity in diet-induced obese mice [5] and stimulated torpor in 24 hour-fasted wild-type mic[8]. These seemingly divergent results suggest a critical role of FGF21 in maintaining energy homeostasis. At least, in our lean APOE*3-Leiden.CETP mice treated with moderate pharmacological doses of FGF21 (1 mg/kg; 3 times per week), prevention of body fat gain is thus mainly attributed to enhanced energy expenditure. The fact that we observed enhanced oxidation of FAs versus carbohydrates is in line with selective classical BAT activation as induced by cold exposure or β3-adrenergic receptor activation in both mice and humans [27, 44-46]. Additionally, we observed that FGF21 slightly prevented lean body mass gain. Although we did not perform detailed studies to investigate the specific organs affected, this may be attributed to a generally increased catabolic state induced by FGF21.

6

We also showed that FGF21 improves glucose tolerance and insulin sensitivity under atherogenic conditions. A previous study showed that the metabolic effects of FGF21 on glucose homeostasis and insulin sensitivity is mediated by adiponectin [37]. Consistently, in our study FGF21 upregulated adiponectin expression in both BAT and WAT, accompanied by highly increased plasma adiponectin levels. We also showed that FGF21 reduced inflammation in WAT, through which insulin sensitivity may have improved [36]. In white adipocytes mitochondrial function has been reported to be essential for adiponectin synthesis[47, 48], and mitochondrial dysfunction has been postulated as the primary cause of adipose tissue inflammation [36]. Therefore, the beneficial effects of FGF21 on glucose metabolism may be attributed to an improvement of WAT mitochondrial function, which is in agreement with our findings.

Next, we reported that FGF21 alleviates WTD-induced hypercholesterolemia, with a marked initial reduction of non-HDL-C levels and increased HDL-C levels after prolonged intervention. This is in agreement with human studies showing that administering either FGF21 or FGF21 analogs improves the plasma lipid profile [21, 49]. Mechanistic studies revealed that FGF21 enhances lipolytic conversion of VLDL by BAT and by WAT. Consistently, a clinical trial has shown that FGF21 treatment upregulated gene/protein expression related to thermogenesis in human adipocyte [50]. Given that our data are in line with classical BAT activation, the increased uptake of liberated FAs by WAT is probably the direct consequence of browning [27]. The avid uptake of generated VLDL remnants resulting from lipolysis by BAT and browned WAT by the liver is likely mediated via the ApoE-LDLR pathway, since we previously observed that clearance of VLDL remnants generated by BAT and browned WAT is impaired in ApoE-deficient and LDLR-deficient mice[27]. Consistently, we found that FGF21 treatment markedly increased hepatic *Ldlr* expression, albeit that hepatic *Pcsk9* levels were also increased upon FGF21 treatment. Likely, the increase in hepatic *Ldlr* expression aims to compensate for the reduced hepatic cholesterol levels by increasing the uptake of cholesterol from the circulation, while *Pcsk9* regulates *Ldlr* expression to maintain the homeostasis of this process. However, in contrast to classical BAT activation, we did not observe a lowering in plasma TG, which was even increased by prolonged FGF21 treatment. Notably, while β3-adrenergic receptor activation did not increase plasma FFA [27], FGF21 increased FFA levels already after short-term treatment, which has been described as a compensatory mechanism to adapt to the highly increased energy expenditure [51, 52]. Therefore, it is likely that FGF21 induces more massive lipolysis in WAT as compared to classical BAT activation, which subsequently induces substrate-driven VLDL production in the liver. This would be in full agreement with the observed increased hepatic expression of genes involved in FA uptake, *de novo* lipogenesis and VLDL production and increased VLDL-TG production rate.

We also observed that FGF21 treatment reduces hepatic lipid levels. While a high FFA flux to the liver may lead to hepatic steatosis, e.g. as observed in CD36-deficient mice [53], both TG, TC and PL levels were lower in FGF21- vs vehicle-treated mice. Besides that FGF21 increases VLDL production, which already limits accumulation of TG in the liver, FGF21 probably also upregulates hepatic FA oxidation, further indicating a role of FGF21 in maintaining circulating FFA and hepatic lipid homeostasis. Interesting, a previous study demonstrated that FGF21 lowers plasma TG by reducing FFA and consequently hepatic VLDL lipidation [18]. This seeming discrepancy with our study is likely explained by different diets and different treatment periods. While our mice received WTD containing 16% fat and FGF21 treatment for 16 weeks, in the study of Schlein et al [18], mice were fed a high-fat diet (60% fat) and treated with FGF21 for only 10 days. During a short-term FGF21 intervention period on high-fat diet, the diet may provide sufficient chylomicron-TG to maintain the whole-body energy homeostasis. As compared to high-fat diet, WTD contains limited TG that may not meet the need for the increased whole-body metabolism, especially during prolonged FGF21 treatment. Moreover, we showed that FGF21 treatment reduces hepatic inflammation, which is consistent with previous studies showing that FGF21 inhibits inflammation during nonalcoholic steatohepatitis development [40, 54].

Finally, we observed that FGF21 treatment markedly reduces atherosclerosis development. Univariate regression analysis revealed that the reduction in atherosclerotic lesion area was mainly predicted by the reduction in non-HDL-C. In line with this, clinical trials have shown that early interventions to lower non-HDL-C levels can reverse and even eradicate earlier stages of atherosclerosis [1]. FGF21 also increased the atherosclerotic plaque stability index via decreasing the lesion macrophage content relative to the smooth muscle cell and collagen content. This may indicate that besides lowering cholesterol to reduce atherosclerosis initiation, FGF21 may also regulate inflammation which would be in agreement with our observation that FGF21 reduces spleen weight (-26.6%; **Fig. S1B**) and inhibits the expression of the *Icam-1* and *Mcp-1* in the aorta. In addition, FGF21 was shown to regulate foam cell formation and inflammatory responses in oxidized low-density lipoprotein-induced macrophages *in vitro* [55]. A preclinical study showed that adiponectin may mediate the anti-inflammatory effects of FGF21 in atherosclerosis[19]. In line, FGF21 increased adiponectin in our study and plasma adiponectin levels explained approx. 26% of the variation in atherosclerotic lesion area. However, adiponectin may not play a protective causal role in coronary heart diseases pathogenesis in humans [56]. From studies using FGF21 deficient ApoE-knockout mice, it was implied that endogenous FGF21 reduces hepatic cholesterol synthesis, thereby protecting against atherosclerosis [19]. In contrast, we found that FGF21 treatment upregulated the hepatic expression of genes

6

involved in cholesterol synthesis, including 3-hydroxy-3-methylglutaryl-CoA reductase (*Hmgcr*; **Fig. S3C**) and sterol regulatory element-binding protein-2 (*Srebp2*; **Fig. S3D**), likely as a compensatory response to decreased cholesterol levels. Since FGF21 has been proposed to play a key role in hepatic cholesterol clearance in wild-type mice [7], and ApoE-knockout mice have an abrogated hepatic uptake of remnant lipoproteins, these data obtained in ApoE-knockout mice probably have limited translational value for humans.

This study is not without limitations. First, we used recombinant lipoproteins that acquire all exchangeable apolipoproteins but do not have apoB [28]. Nevertheless, our previous studies have shown that they truly mimic TG-rich lipoprotein metabolism in mice, since ApoB is mainly required for their synthesis while ApoE is essential for their clearance. Second, the long-circulating recombinant FGF21 protein may not fully represent the wild type native protein. However, the *in vitro* activities are comparable between these two proteins (e.g. Erk phosphorylation and βKlotho binding activity) [26], and the main purpose of our study was to explore a pharmacological FGF21-based strategy, for which long-circulating recombinant FGF21 is evidently preferred over short-lived endogenous FGF21.

In conclusion, our present study uncovers that the anti-atherogenic effects of FGF21 are mainly mediated through reducing hypercholesterolemia. Mechanistically, FGF21 activates BAT and induces browning of WAT, resulting in accelerated catabolism of TG-rich lipoproteins followed by rapid uptake of their remnants by the liver. Given that chronic administration of a long-acting form of FGF21 in obese patients reduces plasma TC and non-HDL-C levels [21, 49], and FGF21 is a biomarker of subclinical atherosclerosis in humans [57], our study supports the development of FGF21 as a powerful therapeutic for the treatment of hypercholesterolemia and atherosclerosis.

Author contributions
CL designed the study, carried out the research, analyzed and interpreted the results, and wrote and revised the manuscript. MS carried out the research, interpreted the results, reviewed and revised the manuscript and obtained the funding. EZ, ZL, SK and MRB advised the study and reviewed the manuscript. ML and KW advised the study, interpreted the results and reviewed the manuscript. ND designed long-circulating

recombinant FGF21 and edited the manuscript. LB synthesized and purified long-circulating recombinant FGF21. X-RP provided long-circulating recombinant FGF21, advised the study, interpreted the results and reviewed the manuscript. YW designed and advised the study, interpreted the results, reviewed and revised the manuscript and obtained the funding. PCNR designed and advised the study, interpreted the results, edited, reviewed and revised the manuscript and obtained funding.

6

REFERENCES

1. Robinson, J.G., et al., *Eradicating the Burden of Atherosclerotic Cardiovascular Disease by Lowering Apolipoprotein B Lipoproteins Earlier in Life.* Journal of the American Heart Association, 2018. **7**(20).

2. Hegele, R.A., et al., *Nonstatin Low-Density Lipoprotein-Lowering Therapy and Cardiovascular Risk Reduction-Statement From ATVB Council.* Arterioscler Thromb Vasc Biol, 2015. **35**(11): p. 2269-80.

3. Reiner, Z., *Resistance and intolerance to statins.* Nutr Metab Cardiovasc Dis, 2014. **24**(10): p. 1057-66.

4. Coskun, T., et al., *Fibroblast growth factor 21 corrects obesity in mice.* Endocrinology, 2008. **149**(12): p. 6018-27.

5. Xu, J., et al., *Fibroblast Growth Factor 21 Reverses Hepatic Steatosis, Increases Energy Expenditure, and Improves Insulin Sensitivity in Diet-Induced Obese Mice.* Diabetes, 2009. **58**(1): p. 250-259.

6. Ameka, M., et al., *Liver Derived FGF21 Maintains Core Body Temperature During Acute Cold Exposure.* Sci Rep, 2019. **9**(1): p. 630.

7. Badman, M.K., et al., *Hepatic fibroblast growth factor 21 is regulated by PPARalpha and is a key mediator of hepatic lipid metabolism in ketotic states.* Cell Metab, 2007. **5**(6): p. 426-37.

8. Inagaki, T., et al., *Endocrine regulation of the fasting response by PPARalpha-mediated induction of fibroblast growth factor 21.* Cell Metab, 2007. **5**(6): p. 415-25.

9. Dushay, J., et al., *Increased Fibroblast Growth Factor 21 in Obesity and Nonalcoholic Fatty Liver Disease.* Gastroenterology, 2010. **139**(2): p. 456-463.

10. Cheng, X.B., et al., *Serum FGF-21 Levels in Type 2 Diabetic Patients.* Endocrine Research, 2011. **36**(4): p. 142-148.

11. Praktiknjo, M., et al., *Fibroblast growth factor 21 is independently associated with severe hepatic steatosis in non-obese HIV-infected patients.* Liver Int, 2019. **39**(8): p. 1514-1520.

12. Sanyal, A., et al., *Pegbelfermin (BMS-986036), a PEGylated fibroblast growth factor 21 analogue, in patients with non-alcoholic steatohepatitis: a randomised, double-blind, placebo-controlled, phase 2a trial.* Lancet, 2019. **392**(10165): p. 2705-2717.

13. Ding, X., et al., *betaKlotho is required for fibroblast growth factor 21 effects on growth and metabolism.* Cell Metab, 2012. **16**(3): p. 387-93.

14. Fisher, F.M. and E. Maratos-Flier, *Understanding the Physiology of FGF21.* Annu Rev Physiol, 2016. **78**: p. 223-41.

15. Geller, S., et al., *Tanycytes Regulate Lipid Homeostasis by Sensing Free Fatty Acids and Signaling to Key Hypothalamic Neuronal Populations via FGF21 Secretion.* Cell Metab, 2019. **30**(4): p. 833-844 e7.

16. Bookout, A.L., et al., *FGF21 regulates metabolism and circadian behavior by acting on the nervous system.* Nat Med, 2013. **19**(9): p. 1147-52.

17. Huang, Z., et al., *The FGF21-CCL11 Axis Mediates Beiging of White Adipose Tissues by Coupling Sympathetic Nervous System to Type 2 Immunity.* Cell Metab, 2017. **26**(3): p. 493-508 e4.

18. Schlein, C., et al., *FGF21 Lowers Plasma Triglycerides by Accelerating Lipoprotein Catabolism in White and Brown Adipose Tissues.* Cell Metab, 2016. **23**(3): p. 441-53.

19. Lin, Z., et al., *Fibroblast growth factor 21 prevents atherosclerosis by suppression of hepatic sterol regulatory element-binding protein-2 and induction of adiponectin in mice.* Circulation, 2015. **131**(21): p. 1861-71.

20. Kharitonenkov, A., et al., *The metabolic state of diabetic monkeys is regulated by fibroblast growth factor-21.* Endocrinology, 2007. **148**(2): p. 774-781.

21. Talukdar, S., et al., *A Long-Acting FGF21 Molecule, PF-05231023, Decreases Body Weight and Improves Lipid Profile in Non-human Primates and Type 2 Diabetic Subjects.* Cell Metabolism, 2016. **23**(3): p. 427-440.

22. Jin, L., Z. Lin, and A. Xu, *Fibroblast Growth Factor 21 Protects against Atherosclerosis via Fine-Tuning the Multiorgan Crosstalk.* Diabetes Metab J, 2016. **40**(1): p. 22-31.

23. van den Hoek, A.M., et al., *APOE*3Leiden.CETP transgenic mice as model for pharmaceutical treatment of the metabolic syndrome.* Diabetes Obes Metab, 2014. **16**(6): p. 537-44.

24. Westerterp, M., et al., *Cholesteryl ester transfer protein decreases high-density lipoprotein and severely aggravates atherosclerosis in APOE*3-Leiden mice.* Arterioscler Thromb Vasc Biol, 2006. **26**(11): p. 2552-9.

25. Samms, R.J., et al., *Discrete Aspects of FGF21 In Vivo Pharmacology Do Not Require UCP1.* Cell Rep, 2015. **11**(7): p. 991-9.

26. Hecht, R., et al., *Rationale-Based Engineering of a Potent Long-Acting FGF21 Analog for the Treatment of Type 2 Diabetes.* PLoS One, 2012. **7**(11): p. e49345.

27. Berbee, J.F., et al., *Brown fat activation reduces hypercholesterolaemia and protects from atherosclerosis development.* Nat Commun, 2015. **6**: p. 6356.

28. Rensen, P.C.N., et al., *Selective Liver Targeting of Antivirals by Recombinant Chylomicrons - a New Therapeutic Approach to Hepatitis-B.* Nature Medicine, 1995. **1**(3): p. 221-225.

29. Cardiff, R.D., C.H. Miller, and R.J. Munn, *Manual hematoxylin and eosin staining of mouse tissue sections.* Cold Spring Harb Protoc, 2014. **2014**(6): p. 655-8.

30. Kooijman, S., et al., *Central GLP-1 receptor signalling accelerates plasma clearance of triacylglycerol and glucose by activating brown adipose tissue in mice.* Diabetologia, 2015. **58**(11): p. 2637-46.

31. Bligh, E.G. and W.J. Dyer, *A rapid method of total lipid extraction and purification.* Can J Biochem Physiol, 1959. **37**(8): p. 911-7.

32. Wang, Y., et al., *CETP expression reverses the reconstituted HDL-induced increase in VLDL.* J Lipid Res, 2011. **52**(8): p. 1533-41.

33. Bencosme, S.A., *A Trichrome Staining Method for Routine Use.* American Journal of Clinical Pathology, 1954. **24**(11): p. 1324-1328.

34. Wong, M.C., et al., *Hepatocyte-specific IKKbeta expression aggravates atherosclerosis development in APOE*3-Leiden mice.* Atherosclerosis, 2012. **220**(2): p. 362-8.

35. Zhang, F., et al., *An Adipose Tissue Atlas: An Image-Guided Identification of Human-like BAT and Beige Depots in Rodents.* Cell Metabolism, 2018. **27**(1): p. 252-+.

36. Woo, C.Y., et al., *Mitochondrial Dysfunction in Adipocytes as a Primary Cause of Adipose Tissue Inflammation.* Diabetes Metab J, 2019. **43**(3): p. 247-256.

37. Lin, Z., et al., *Adiponectin mediates the metabolic effects of FGF21 on glucose homeostasis and insulin sensitivity in mice.* Cell Metab, 2013. **17**(5): p. 779-89.

38. Endo-Umeda, K. and M. Makishima, *Liver X Receptors Regulate Cholesterol Metabolism and Immunity in Hepatic Nonparenchymal Cells.* Int J Mol Sci, 2019. **20**(20).

39. Mindur, J.E. and F.K. Swirski, *Growth Factors as Immunotherapeutic Targets in Cardiovascular Disease.* Arteriosclerosis Thrombosis and Vascular Biology, 2019. **39**(7): p. 1275-1287.

6

40. Sonoda, J., M.Z. Chen, and A. Baruch, *FGF21-receptor agonists: an emerging therapeutic class for obesity-related diseases.* Horm Mol Biol Clin Investig, 2017. **30**(2).

41. Fisher, F.M., et al., *FGF21 regulates PGC-1alpha and browning of white adipose tissues in adaptive thermogenesis.* Genes Dev, 2012. **26**(3): p. 271-81.

42. Talukdar, S., et al., *A Long-Acting FGF21 Molecule, PF-05231023, Decreases Body Weight and Improves Lipid Profile in Non-human Primates and Type 2 Diabetic Subjects.* Cell Metab, 2016. **23**(3): p. 427-40.

43. Andersen, B., et al., *FGF21 decreases body weight without reducing food intake or bone mineral density in high-fat fed obese rhesus macaque monkeys.* Int J Obes (Lond), 2018. **42**(6): p. 1151-1160.

44. Bartelt, A., et al., *Brown adipose tissue activity controls triglyceride clearance.* Nat Med, 2011. **17**(2): p. 200-5.

45. Khedoe, P.P., et al., *Brown adipose tissue takes up plasma triglycerides mostly after lipolysis.* J Lipid Res, 2015. **56**(1): p. 51-9.

46. Bakker, L.E., et al., *Brown adipose tissue volume in healthy lean south Asian adults compared with white Caucasians: a prospective, case-controlled observational study.* Lancet Diabetes Endocrinol, 2014. **2**(3): p. 210-7.

47. Kusminski, C.M. and P.E. Scherer, *Mitochondrial dysfunction in white adipose tissue.* Trends in Endocrinology and Metabolism, 2012. **23**(9): p. 435-443.

48. Koh, E.H., et al., *Essential role of mitochondrial function in adiponectin synthesis in adipocytes.* Diabetes, 2007. **56**(12): p. 2973-81.

49. Gaich, G., et al., *The effects of LY2405319, an FGF21 analog, in obese human subjects with type 2 diabetes.* Cell Metab, 2013. **18**(3): p. 333-40.

50. Lee, P., et al., *Irisin and FGF21 are cold-induced endocrine activators of brown fat function in humans.* Cell Metab, 2014. **19**(2): p. 302-9.

51. Owen, B.M., et al., *FGF21 Acts Centrally to Induce Sympathetic Nerve Activity, Energy Expenditure, and Weight Loss.* Cell Metabolism, 2014. **20**(4): p. 670-677.

52. Ma, W., et al., *The Role of Kupffer Cells as Mediators of Adipose Tissue Lipolysis.* J Immunol, 2019. **203**(10): p. 2689-2700.

53. Goudriaan, J.R., et al., *CD36 deficiency increases insulin sensitivity in muscle, but induces insulin resistance in the liver in mice.* J Lipid Res, 2003. **44**(12): p. 2270-7.

54. Bao, L.C., et al., *A long-acting FGF21 alleviates hepatic steatosis and inflammation in a mouse model of non-alcoholic steatohepatitis partly through an FGF21-adiponectin-IL17A pathway.* British Journal of Pharmacology, 2018. **175**(16): p. 3379-3393.

55. Wang, N., et al., *Fibroblast growth factor 21 regulates foam cells formation and inflammatory response in Ox-LDL-induced THP-1 macrophages.* Biomed Pharmacother, 2018. **108**: p. 1825-1834.

56. Borges, M.C., et al., *Role of Adiponectin in Coronary Heart Disease Risk: A Mendelian Randomization Study.* Circ Res, 2016. **119**(3): p. 491-9.

57. Basurto, L., et al., *Monocyte chemoattractant protein-1 (MCP-1) and fibroblast growth factor-21 (FGF-21) as biomarkers of subclinical atherosclerosis in women.* Experimental Gerontology, 2019. **124**.

SUPPLEMENT

Expanded methods

Recombinant FGF21 protein

The Fc region of human immunoglobulin G1 [1] was codon optimized for mammalian expression and subcloned in pEBNAZ mammalian expression vector under control of a cytomegalovirus promotor. The Fc fusion protein was preceded by a mouse Igκ chain VIII P01661 signal sequence for secretion into the medium. The Fc sequence was followed by a 15 amino acid Gly-Ser rich linker followed by mature FGF21 sequence residues His29-Ser209 including two stabilizing mutations L98R/P171G (FGF21 numbering). Mutation L98R prevents aggregation of FGF21, whereas mutation P171G stabilizes FGF21 against proteolytic inactivation by FAPα [1]. Suspension grown Expi293F cells were polyethyleneimine transfected with expression plasmid and cell supernatant was harvested after 5 days. Fc-fusion protein was purified in PBS using protein A (MabSelect SuRe, GE Healthcare, Uppsala, Sweden) affinity purification under exotoxin-free conditions. The supernatant was incubated with the resin overnight at 4℃ and washed with 1x PBS, pH 7.4. The protein was eluted with 0.1 M glycine, pH 3.5. The eluate was mixed with 1 M Tris-HCl, pH 9.0 to neutralize the pH. Buffer exchange to 1x PBS, pH 7.4 was done by using PD-10 columns. Typical yields were over 10 mg purified fusion protein from 100 mL culture supernatant. Purified protein was aliquoted, flash frozen and stored at -80℃.

Glucose tolerance test

In the second experiment, at week 6, an IPGTT was conducted with an injection of D-glucose (2 g/kg body weight) to mice (n = 8 per group) after 4 hours fasting (9:00-13:00). Blood (0.6 µl) was collected via tail vein at 0, 5, 15, 30, 60 and 120 min for each test. The glucose was measured with a OneTouch Ultra glucometer (AccuCheck Sensor, Roche Diagonstics, Almere, The Netherlands). During IPGTT, extra blood was collected at 0,15 and 30 min, spun down, and the serum samples were stored at -20℃ for glucose measurement (blood collected at t=0 min) using a commercial enzymatic kit (Roche Diagnostics; Mannhein, Germany) and insulin measurement using an Ultra Sensitive Mouse Insulin ELISA kit (Crystal Chem, Zaandam, The Netherlands).

Hepatic VLDL production

In the second experiment, at week 12, mice (n=8 per group) were fasted for 4 hours (9:00-13:00) and anesthetized by the intraperitoneal injection (t=-75 min) of 6.25 mg/kg Acepromazine (Alfasan, Woerden, The Netherlands), 6.25 mg/kg Midazolam (Roche, Mijdrecht, The Netherlands), and 0.31 mg/kg Fentanyl (Janssen-Cilag, Tilburg, The

Netherlands) [2]. At t=-30 min, mice received an intravenous injection of 20 μCi Tran ^{35}S label (MP Biomedicals, Eindhoven, the Netherlands) via tail vein. Next, at t=0 min, these mice were intravenously injected with Triton WR 1339 (500 mg/kg body weight; Aldrich, Germany). Blood samples were collected via the tail vein at t=0 min and 15, 30, 60 and 90 min (after Triton WR 1339 injection) for serum TG measurement, and VLDL-TG production rate was calculated as mM/h from the slope of the curves. At t=120 min, mice were euthanized with an overdose of anesthetics and exsanguinated via the orbital sinus. VLDL was isolated from serum after density gradient ultracentrifugation, and ^{35}S-ApoB was measured in the VLDL fraction, and VLDL-AopB production rate was shown as dpm/ml/h.

Atherosclerotic lesion composition

To quantify the collagen, smooth muscle cell and macrophage content within the atherosclerotic lesions, Sirius Red, monoclonal mouse antibody M0851 (1:800; Dako, Heverlee, The Netherlands) against smooth muscle cell actin and rat monoclonal anti-mouse MAC-3 antibody (1:1000; BD Pharmingen, San Diego, CA, USA) were used, respectively. To amplify immunostainings, Vector Laboratories Elite ABC kit (Vector Laboratories Inc., Burlingame, CA, USA) was used, and the immune-peroxidase complex was visualized with Nova Red (Vector Laboratories Inc., Burlingame, CA, USA). Lesion composition were analyzed using Image J software.

REFERENCES

1. Hecht, R., et al., *Rationale-Based Engineering of a Potent Long-Acting FGF21 Analog for the Treatment of Type 2 Diabetes.* PLoS One, 2012. **7**(11): p. e49345.

2. Wang, Y., et al., *CETP expression reverses the reconstituted HDL-induced increase in VLDL.* J Lipid Res, 2011. **52**(8): p. 1533-41.

6

Supplemental Table 1: List of polymerase chain reaction primer sequences used in mRNA expression analysis.

| Gene	Species	Sequence (5'-3')
Acc1	Mice	Forward: AGAATCTCCTGGTGACAATGCTTATT Reverse: GCTCTGTGAGGATATTTAGCAGCTC
Adipoq	Mice	Forward: CTCCACCCAAGGGAACTTGT Reverse: TAGGACCAAGAAGACCTGCATC
Apob	Mice	Forward: ATGTCATAATTGCCATAGATAGTGCCA Reverse: TCGCGTATGTCTCAAGTTGAGAG
β-actin	Mice	Forward: AACCGTGAAAAGATGACCCAGAT Reverse: CACAGCCTGGATGGCTACGTA
Cd36	Mice	Forward: GTTCTTCCAGCCAATGCCTTT Reverse: ATGTCTAGCACACCATAAGATGTACAGTT
CoxIV	Mice	Forward: GAGAGCTTCGCCGAGATGAA Reverse: ATGGGGCCATACACATAGCTC
Cox7a1	Mice	Forward: AAAACCGTGTGGCAGAGAAG Reverse: CCAGCCCAAGCAGTATAAGC
Cpt1	Mice	Forward: CACTACGGAGTCCTGCAACTTTG Reverse: AGCTTGAACCTCTGCTCTGCC
Dgat2	Mice	Forward: GGTGCCCTGACAGAGCAGAT Reverse: CAGTAAGGCCACAGCTGCTG
Fasn	Mice	Forward: GGCATCATTGGGCACTCCTT Reverse: GCTGCAAGCACAGCCTCTCT
F4/80	Mice	Forward: CTTTGGCTATGGGCTTCCAGTC Reverse: GCAAGGAGGACAGAGTTTATCGTG
Hmgcr	Mice	Forward: CCGGCAACAACAAGATCTGTG Reverse: ATGTACAGGATGGCGATGCA
Icam-1	Mice	Forward: GGACCACGGAGCCAATTTC Reverse: CTCGGAGACATTAGAGAACAATGC
Il1-β	Mice	Forward: TGG TGT GTG ACG TTC CCA TTA Reverse: AGG TGG AGA GCT TTC AGC TCA TAT
Ldlr	Mice	Forward: GCATCAGCTTGGACAAGGTGT Reverse: GGGAACAGCCACCATTGTTG
Mcp-1	Mice	Forward: GCATCTGCCCTAAGGTCTTCA Reverse: TTCACTGTCACACTGGTCACTCCTA
Mfn-1	Mice	Forward: CCACAAGCTGTGTTCGGAT Reverse: CGATGATGCCCATGGAGGTT
Mfn-2	Mice	Forward: CCAGCTAGAAACTTCTCCTCTGT Reverse: TGACGGTGACGATGGAGTTG
Mttp	Mice	Forward: AGCTTTGTCACCGCTGTGC Reverse: TCCTGCTATGGTTTGTTGGAAGT
Opa1	Mice	Forward: CCTGTGCATCCAAGACGGAT Reverse: TGGGAAGAGCTTGCCTTCAA
Pcsk9	Mice	Forward: TGTGAGGTCCCACTCTGTG Reverse: GCTTCTGCTCCAGAGGTCA

Supplemental Table 1: List of polymerase chain reaction primer sequences used in mRNA expression analysis. (continued)

| Gene	Species	Sequence (5'-3')
Pgc1α	Mice	Forward: TGCTAGCGGTTCTCACAGAG Reverse: AGTGCTAAGACCGCTGCATT
Pparα	Mice	Forward: TGAACAAAGACGGGATG Reverse: TCAAACTTGGGTTCCATGAT
Rplp0	Mice	Forward: GGACCCGAGAAGACCTCCTT Reverse: GCACATCACTCAGAATTTCAATGG
Srebp1c	Mice	Forward: GGAGCCATGGATTGCACATT Reverse: CCTGTCTCACCCCCAGCATA
Srebp2	Mice	Forward: TGAAGCTGGCCAATCAGAAAA Reverse: ACATCACTGTCCACCAGACTGC
Tnfα	Mice	Forward: AGCCCACGTCGTAGCAAACCAC Reverse: TCGGGGCAGCCTTGTCCCTT
Vcam-1	Mice	Forward: ACAAAACGATCGCTCAAATCG Reverse: CGCGTTTAGTGGGCTGTCTATC

Acc1, acetyl-CoA carboxylase; *Adipoq*, adiponectin; *Apob*, apolipoprotein B; *Cd36*, cluster of differentiation 36; *CoxIV*, mitochondrial cytochrome C oxidase subunit IV; *Cox7a1*, cytochrome C oxidase polypeptide 7A1; *Cpt1*, carnitine palmitoyl transferase 1; *Dgat2*, diacylglycerol O-acyltransferase 2; *Fasn*, fatty acid synthase; *Hmgcr*, 3-hydroxy-3-methylglutaryl-CoA reductase; *Icam-1*, intercellular adhesion molecule 1; *Il1-β*, interleukin 1 β; *Ldlr*, low-density lipoprotein receptor; *Mcp-1*, monocyte chemoattractant protein 1; *Mfn1/2*, mitofusin-1/2; *Mttp*, microsomal triglyceride transfer protein; *Opa1*, dynamin-like 120 kDa protein, mitochondrial; *Pcsk9*, proprotein convertase subtilisin/kexin 9; *Pgc1α*, peroxisome proliferator-activated receptor γ coactivator 1-α; *Ppara*, peroxisome proliferator-activated receptor α; *Rplp0*, ribosomal protein lateral stalk subunit P0; *Srebp1c/2*, sterol regulatory element-binding transcription factor 1/2; *Tnfα*, tumor necrosis factor α; *Vcam-1*, vascular cell adhesion molecule 1.
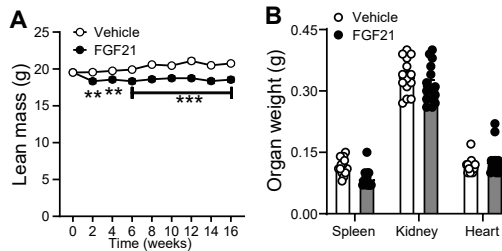

Supplementary Fig. 1. FGF21 reduces body lean mass and spleen weight. Body lean mass **(A)** was measured throughout the study. After 16 weeks of treatment, the weight of spleen, kidney and heart **(B)** were measured. Data are represented as mean ± SEM (n=15-16).**$P<0.01$, ***$P<0.001$ (unpaired two-tailed Student's *t*-test).
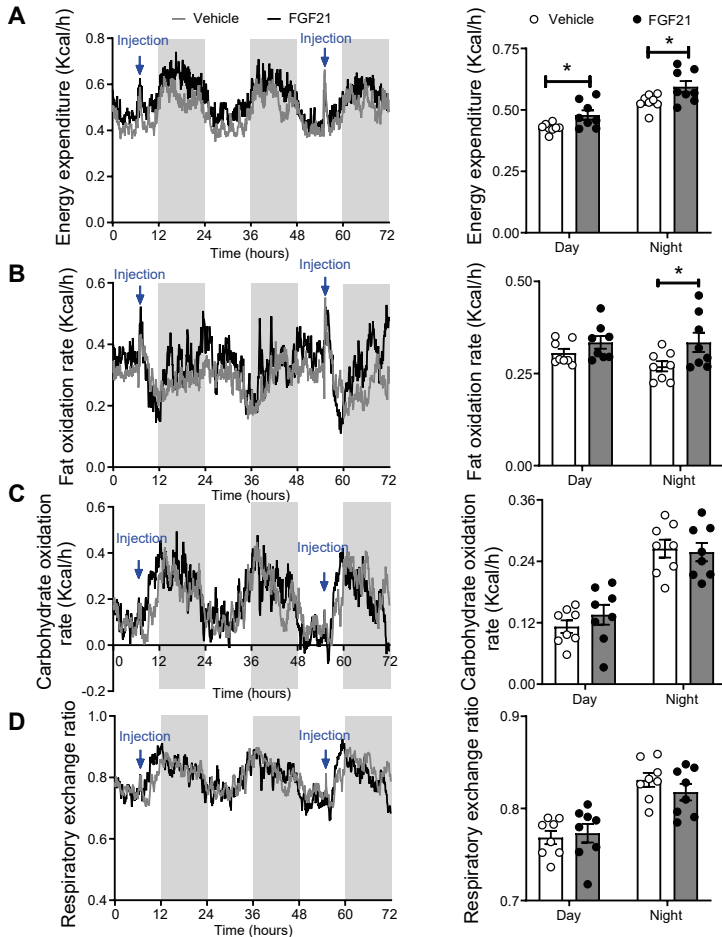
Supplementary Fig. 2. FGF21 increases energy expenditure and rate of fat oxidation. Following 8 weeks treatment, energy expenditure **(A)**, fat oxidation rate **(B)**, carbohydrate oxidation rate **(C)** and respiratory exchange ratio **(D)** were monitored (n=8 per group). **A-D**, for line graphs, data are shown as mean for each group (12-hour cycle; shaded area represents the dark cycle); for bar graphs, data are shown as mean±SEM. *$P<0.05$ (unpaired two-tailed Student's t-test).
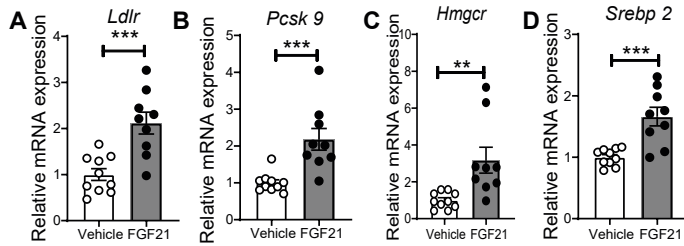
Supplementary Fig. 3. FGF21 increases hepatic expression of genes involved in cholesterol metabolism. After 16 weeks of treatment, the relative expression of genes involved in cholesterol uptake **(A and B)** and synthesis **(C and D)** were measured in the liver. Data are represented as mean ± SEM (n=9-10). **$P<0.01$, ***$P<0.001$ (unpaired two-tailed Student's t-test). *Hmgcr*, 3-hydroxy-3-methylglutaryl-CoA reductase; *Ldlr*, low-density lipoprotein receptor; *Pcsk9*, proprotein convertase subtilisin/kexin 9; *Srebp2*, sterol regulatory element-binding transcription factor 2.
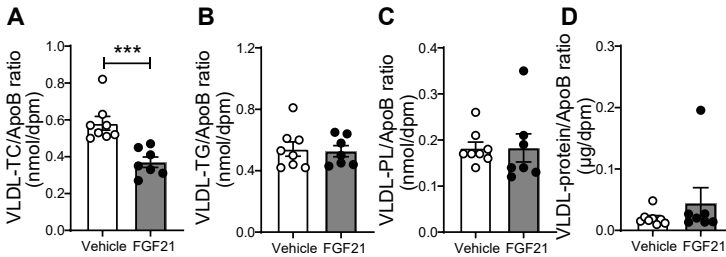
Supplementary Fig. 4. FGF21 reduces cholesterol content in the newly secreted VLDL particles. After 12 weeks of the treatment, hepatic very low-density lipoprotein (VLDL) production was evaluated by assessing serum TG accumulation after blocking lipoprotein lipase-mediated lipolysis while labeling apolipoprotein B (ApoB) with Tran[35]S. VLDL was isolated from serum, and the levels of total cholesterol (TC), triglyceride (TG), phospholipid (PL) and protein of VLDL particles were measured, and the amounts of TC **(A)**, TG **(B)**, PL **(C)** and protein **(D)** per ApoB were calculated. Data are represented as mean±SEM (n=7-8). ***$P < 0.001$ (unpaired two-tailed Student's t-test).
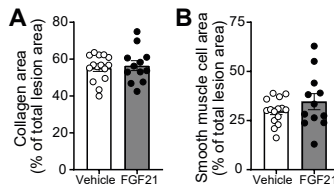
Supplementary Fig. 5. FGF21 does not influence collagen and smooth muscle content within atherosclerotic lesions. At week 16, hearts were collected, the valve areas of their aortic roots were stained with Sirius Red and an anti-α-actin antibody to quantify the content of collagen **(A)** and smooth muscle cells **(B)** within the lesions, respectively. Data are represented as mean±SEM (n=14-15). Differences were assessed using unpaired two-tailed Student's t-test.

7

General discussion and future perspectives

GENERAL DISCUSSION

Over the past few decades we have witnessed advances in understanding of how tissues communicate with one another in health and disease. Now, it is well-established that cardiometabolic diseases are far more than simple dysfunction within local tissues and organs. Rather, cardiometabolic health is regulated by highly controlled coordination between various metabolic organ systems. By generating signaling molecules, such as peptide/protein hormones, bioactive lipids and small molecules, these functional metabolic organ systems are able to work together to maintain cardiometabolic health. However, dysregulation of the inter-organ cross-talk by disturbing the production of these signaling molecules, for example, contributes to the development of obesity and its associated cardiometabolic diseases, such as non-alcoholic fatty liver disease (NAFLD) and atherosclerotic cardiovascular disease (asCVD).

In recent years, signaling molecules involved in the inter-organ communication have been proposed as potential targets for combating cardiometabolic diseases. These molecules are often easier to manipulate than other determinants of cardiometabolic diseases, such as genetic makeup and environmental factors. Therefore, approaches aiming to regulate local and/or systemic levels of these signaling molecules (e.g. organokines and metabolites) are currently being explored to alleviate cardiometabolic diseases. Despite some progress made in the treatment of these diseases, more can be done to tackle the risks of cardiometabolic diseases. In particular, cardiovascular diseases (CVDs) remain the leading cause of death worldwide, taking an estimated 18 million lives each year [1]. Therefore, there is still an unmet need for additional therapeutic targets and approaches that can effectively combat cardiometabolic diseases.

In this thesis, by using dietary and pharmacological interventions, the potential of targeting inter-organ cross-talk to combat cardiometabolic diseases has been further explored. Two main therapeutic targets have been investigated to treat cardiometabolic diseases, namely **1)** gut microbiota-centered inter-organ cross-talk and **2)** liver-centered inter-organ crosstalk. The promise and future of these therapeutic targets and potential approaches will be discussed in this chapter.

1. Drugging the gut microbiota to improve inter-organ crosstalk for combating cardiometabolic diseases

The vast community of micro-organisms that inhabit the gut, i.e. the gut microbiota, has influence far beyond food digestion. Recent studies uncovered a potential contribution of the gut microbiota to the development of certain cardiometabolic

7

diseases. The mechanisms by which the gut microbiota modulates etiopathogenesis of cardiometabolic diseases are just beginning to be dissected. The gut microbiota forms a bioreactor that is fueled by exogenous (e.g. dietary nutrients) and endogenous (e.g. glycoproteins of the intestinal mucus layer) compounds. Upon breaking down these molecules, the gut microbiota can generate various metabolites, such as short chain fatty acids (SCFAs) and trimethylamine (TMA). These fermentation processes may also cause increased intestinal permeability, thereby causing translocation of microbiota-associated molecules e.g. lipopolysaccharide (LPS), into the circulation of the host. Upon entering to the circulation, gut microbial metabolites and gut microbiota-associated bioactive molecules can signal to metabolic organs, like adipose tissue and the liver, of the host to affect the host cardiometabolic health. Therefore, intervention studies aiming to manipulate the gut microbiota to influence local and/or systemic levels of its associated signaling molecules are crucial next steps. The gut microbiota-centered inter-organ cross-talk has thus been regarded as a novel therapeutic target for cardiometabolic diseases. The section below describes the therapeutic potential of such approaches that have been investigated in this thesis.

1.1 Regulating the production of gut microbiota-associated signaling molecules by dietary interventions

The diet and gut microbiota interact in a mutualistic manner. On the one hand, dietary factors are among the most potent modulators of the gut microbiota. On the other hand, microorganisms in the gut in turn affect the utilization and storage of ingested dietary nutrients, with potentially profound impact on host health. To understand how the diet affects the gut microbiota to influence cardiometabolic health, and to search for suitable dietary regimens that can effectively alleviate cardiometabolic diseases, various dietary intervention strategies are being tested in preclinical and clinical research. The main strategies include manipulating specific dietary nutrient(s) and optimizing dietary patterns (e.g. Ketogenic, Mediterranean and Paleolithic diet). In this thesis, to uncover the regulatory role of dietary components in the gut microbiota-host cross-talk and the consequences of this cross-talk for cardiometabolic health, I chose to modify the content of specific dietary nutrient(s) (**Chapter 2** and **Chapter 3**). One limitation of this approach is that dietary nutrients are rarely consumed in isolation. Nevertheless, manipulation of specific dietary components is required to gain mechanistical insights into their roles of in the microbiota-host communication, and is necessary to develop effective dietary regimens that can limit cardiometabolic dysfunction, which have been elaborated on below.

Reducing dietary simple sugar and saturated fat intake*.* Diet rich in simple sugars and/or saturated fat has been shown to cause a rapid remodeling of the gut microbiota

and trigger the development of cardiometabolic diseases in both animals and humans [2-5]. One mechanism by which the gut microbiota impacts cardiometabolic health upon high consumption of these dietary components is the damage of the gut barrier [5, 6]. Preclinical studies show that high simple sugars and/or saturated fat consumption increases the abundance of mucus-degrading bacteria that compromise intestinal barrier integrity [7, 8]. As a result, LPS, a cell wall component of Gram-negative bacteria, is released into the circulation, binds to Toll-like 4 receptors that are expressed in various immune cells (e.g. macrophages) and tissues (e.g. hepatocytes and adipocytes), and elicits pro-inflammatory responses [8-10]. In line with this, clinical studies observed that circulating LPS levels correlate with the development of cardiometabolic diseases, such as obesity [11] and NAFLD [12]. To investigate whether limiting the consumption of dietary sugar and fat is able to reduce the incidence of cardiometabolic diseases, several dietary intervention strategies have been evaluated in experimental animal models and in the clinic. The ketogenic diet, for example, which is characterized by low carbohydrates (CHOs; ~5-10% of total caloric intake) and was originally developed as a treatment for epilepsy, has been optimized for dietary fat and protein quantity and quality, and adopted for body weight management. Animal studies have shown that a ketogenic diet protects against obesity, while contradictory findings have been reported for e.g. type 2 diabetes (T2D) and asCVD [13, 14]. Some human studies reported a negative impact of ketogenic diets on the gut microbiota and cardiometabolic health [15, 16]. However, these studies were performed in small populations, limiting generalization to larger cohorts. Recently, a meta-analysis of 5 clinical trials with 447 participants [17] and recent clinical study involving 311 women with obesity [18] indicated that a low-fat diet is a feasible alternative to a low-CHOs diet for inducing weight loss with beneficial cardiometabolic effects, which were associated with decreased abundance of Gram-negative bacteria in the gut [19]. Likewise, a Mediterranean diet with a small proportion of complex CHOs (i.e. dietary fiber) and a high proportion of monounsaturated fat elicited favorable microbiota profiles (e.g. lower ratios of *Firmicutes*: *Bacteroidetes*) and metabolite production (high fecal SCFAs) and exhibited cardiovascular benefits [20, 21].

These findings thus suggest that limiting simple sugars and/or saturated fat consumption holds great promise in combating cardiometabolic diseases. However, future studies are needed to find the most suitable dietary fat and/or sugar content that can safely maintain cardiometabolic health in the long-term. Also, evaluating the impact of different types and sources of fat and CHO on the gut microbiota and cardiometabolic diseases is required, which would be helpful in improving current existing dietary patterns and developing novel dietary patterns that can effectively protect against cardiometabolic diseases. Besides, as modified versions of ketogenic

7

and Mediterranean diet protocols are rapidly growing in popularity, it is important to examine their long-term impact and safety on the gut microbial community and cardiometabolic health.

Increasing dietary fiber intake. In contrast to unfavorable effects of dietary saturated fat and simple sugars, dietary fiber (i.e. complex CHO) has been shown to beneficially modulate the gut microbiota and consequently improve cardiometabolic diseases. Dietary fibers are indigestible by the human gut as human cells do not have the enzymatic capacity to break down complex CHOs. However, unique taxa of gut microbes utilize dietary fiber as an important energy source. Fermentation of dietary fibers by gut microbes results in the production of large amounts of SCFAs, which benefit the host by serving as both recovered energy from otherwise in accessible dietary fiber and potent regulatory molecules with broad physiological effects. SCFAs were first identified as a principal energy source for intestinal epithelial cells, and most of the gut microbiota-derived SCFAs, in particular butyrate, have been estimated to be consumed by these cells, resulting in maintained intestinal barrier function and protection from intestinal inflammation [22]. Recent evidence revealed that butyrate can exerts functions beyond the intestine in the brain and peripheral tissues. SCFAs signal via the vagal nerve and via several G protein-coupled receptors in the intestine to regulate whole-body metabolism [23, 24]. By using *APOE*3-Leiden.CETP* mice, a well-established mouse model for human-like cardiometabolic diseases, our group reported that dietary butyrate regulates the gut-brain axis to improve energy metabolism through decreasing food intake and increasing fat oxidation by activating thermogenic tissues. As a result, dietary butyrate potently prevented the development of high-fat diet (HFD)-induced obesity and its associated metabolic disorders, including dyslipidemia, insulin resistance and hepatic steatosis [25]. Consistently, plant-rich and vegan/vegetarian diets rich in fiber, have been shown to promote weight loss through modulating the gut microbiota [26]. However, it should be noted that despite the observed protective effects of dietary fiber and SCFAs on obesity-associated disorders, humans with obesity were shown to have high fecal and cecal levels of SCFAs, indicating that SCFAs may also contribute to increased energy harvest [27]. Therefore, the individual's status of energy homeostasis may determine whether the beneficial effects of SCFAs on metabolism outweigh the extra calories obtained.

In addition to the beneficial effects of dietary fiber and SCFAs on body weight control, recent studies showed that butyrate can reduce atherosclerosis in inflammation-driven atherosclerotic mouse models (i.e. *Apoe* $^{-/-}$ and *Ldlr*$^{/-}$ mice) partially via improving the gut barrier function [28]. Butyrate can inhibit the overgrowth of Gram-negative bacteria in the gut, thereby alleviating intestinal barrier permeability and systemic

inflammation. As a result, butyrate can block macrophage infiltration into plaques and protect against atherosclerosis progression. Given that hypercholesteremia is another key driver of atherosclerosis development, in **Chapter 2,** we examined whether butyrate confers its antiatherogenic effects in human-like *APOE*3-Leiden.CETP* mice. We demonstrated that while butyrate beneficially modulates the gut microbiota composition and function, we found no influence of butyrate on atherosclerotic plaque size, severity and composition, including the macrophage-positive areas within the lesions. Our data indicate that increased SCFA levels *per se* may not be sufficient to protect against asCVD. However, future studies are still needed to evaluate the therapeutic effects of dietary fibers themselves on asCVD in humanized animal models (e.g. *APOE*3-Leiden.CETP* mice) and in humans.

Optimizing dietary protein quantity and quality. Dietary protein provides gut microorganisms with essential nitrogen and carbon. Amino acid catabolism generates various functional molecules, most of which can influence cardiometabolic health [19]. For example, amines, phenols and indoles can combine with nitric oxide to form genotoxic N-nitroso compounds that increases the risk of carcinogenesis in humans populations [29]. In contrast, indole-propionic acid, a gut microbiota-associated metabolite of tryptophan, can protect against asCVD by promoting reverse cholesterol transport [30, 31]. The source of dietary protein also regulates gut microbiota-dependent metabolic output. This is best exemplified by the production of trimethylamine N-oxide (TMAO) from L-carnitine and its derivative choline, which are abundant in animal protein such as red meat, eggs and fish [32-34]. Studies in mice (e.g. $Apoe^{-/-}$, $Ldlr^{-/-}$, diet-induced obese (DIO) and *ob/ob* mice), have linked high dietary L-carnitine and choline consumption to the pathogenesis of cardiometabolic diseases, as caused by the generation of TMAO through the communication between the gut microbiota and liver [34]. The gut microbiota can convert dietary choline into trimethylamine (TMA) that is delivered via the portal vein to the liver where hepatocytes rapidly oxidize TMA into TMAO. TMAO was reported to aggravate atherosclerosis via several pathways, such as promoting foam cell formation and activating proinflammatory responses [34, 35]. However, in **Chapter 2**, by using humanized *APOE*3-Leiden.CETP* mice, we surprisingly demonstrated that diet rich in choline beneficially modulates the gut microbiota without affecting atherosclerosis. In **Chapter 3**, we further reported that dietary choline activates brown adipose tissue (BAT) to alleviate adiposity. In line with our findings, human studies showed a profound body weight reduction upon high dietary choline intervention [36]. Moreover, we demonstrated that increased plasma TMAO levels did not associate with the development of atherosclerosis (**Chapter 2**). The fact that TMAO induces atherosclerosis in $Apoe^{-/-}$ and $Ldlr^{-/-}$ mice but not in humanized *APOE*3-Leiden.CETP* mice, may suggest that TMAO lacks atherogenic

7

properties in humans. Similarly, many clinical trials did not find any association between plasma TMAO and CVD risk [37-39]. Multiple systematic reviews and cohort studies have shown that the high intake of eggs, rich in TMAO precursors, is not associated with asCVD risk and mortality [40, 41]. Notably, a very recent study reported that TMAO even promotes anti-tumor immunity in triple negative breast cancer. This study reported that TMAO inhibits tumor growth by activating CD8^{+} T cell-mediated anti-tumor immunity [42]. Also, the TMAO precursor choline enhances response to immunotherapy in triple negative breast cancer [42]. It would be interesting to investigate the role of dietary choline in other aspects of cardiometabolic diseases, such as obesity-associated cancers in the future. The current results highlight that vast effects of amino acid metabolites that are generated by the gut microbiota on host physiology are now just beginning to emerge and represent an area ripe for future research.

Optimizing dietary micronutrients. Besides macronutrients, dietary micronutrients also modulate the gut microbiota and affect cardiometabolic health. Vitamin D, for example, was shown to mitigate obesity-associated metabolic dysfunction in part by beneficially shaping the gut microbiota composition [43]. Like vitamins, metals can dramatically alter the composition and function of the gut microbiota, with profound impact on the host's cardiometabolic health. A recent study reported that high dietary iron consumption promotes NAFLD development in the context of obesity. By performing fecal microbiota transplantation, this study demonstrated that iron-induced liver damage is mediated by the gut microbiota [44]. Moreover, the high-salt diet can induce hypertension, as caused by decreased abundance of *Lactobacillus* and increased proportion of proinflammatory T helper 17 cells [45]. Overall, the interactions observed thus far between micronutrients and the gut microbiota, as well as a myriad of other interactions that undoubtedly still await discovery, represent a promising avenue for future research. These findings also emphasize the critical role of determining micronutrient composition in gut microbiota-based dietary intervention studies and warrant the need for clinical research in people at high risk of inadequate or excessive micronutrient intake.

Collectively, currently available data have shown that modulation of the dietary content of macro- and micro-nutrients has profound impact on the gut microbiota-centered inter-organ cross-talk and holds great promise for combating cardiometabolic diseases. Herein, we have further added novel insights into the role of dietary fiber and protein interventions in regulating cardiometabolic health. We have shown that while dietary supplementation with butyrate can effectively promote weight loss, it may not be able to protect against asCVD (**Chapter 2**). Future studies are required to examine

the protective effects of dietary fiber itself on asCVD in various animal models and in humans. Besides, we demonstrated that dietary choline, which is highly present in animal proteins (e.g. red meat, eggs, fish and sea food) has favorable effects on the gut microbiome and body composition, without affecting atherosclerosis (**Chapters 2** and **3**). Furthermore, plasma TMAO levels did not correlate with atherosclerosis (**Chapter 2**). Given that alternative voices regarding the effect of choline/TMAO on health and disease are getting louder, future studies are needed to examine whether high intake of (specific) animal proteins is in fact detrimental or not. Taken together, the plasticity of the gut microbiota makes their dietary modification an attractive approach for cardiometabolic disease prevention and treatment. However, one main factor that complicates the implementation of dietary interventions is the heterogeneity of gut microbiota composition among individuals which is caused by e.g. their different genetic backgrounds. In this regard, a main challenge for the future will be to design optimal dietary intervention strategies for populations with similar gut microbiota profiles, or even a personalized nutrient regimen for each individual.

1.2 Modulating the production of gut microbiota-associated signaling molecules by pharmacological interventions

In addition to dietary interventions, treatment with antibiotics, prebiotics and probiotics, and more recently, bacterial enzyme inhibitors and bacteriophages, are currently tested as intervention strategies aiming to modulate the gut microbiota profile and function in several diseases. The section below describes the potential of such pharmacological approaches specifically in the treatment of cardiometabolic diseases.

Antibiotics, prebiotics and probiotics. Although several studies reported an association between the development of atherosclerosis and the presence of pathogens such as *Helicobacter pylori* and *Cytomegalovirus* [46-48], the use of antibiotics to selectively eliminate potentially harmful microbial species has not paid off so far. In both animal and human studies, antibiotic treatment has been associated with various metabolic disorders, such as obesity and peripheral insulin resistance [49]. Aside from this, frequent exposure of the gut microbiota to antibiotics can induce rapid genetic modification of bacteria [50], which can accelerate the development of antibiotic resistance. These findings indicate that antibiotics will probably not be a viable option for the treatment of cardiometabolic diseases.

With technological advances, holistic examination of gut microbiota responses to dietary nutrients has led to a recent expansion of the prebiotic concept, and the use of prebiotics has been proposed as a therapeutic option for cardiometabolic diseases.

7

Prebiotics are defined as selectively fermented ingredients that induce specific changes in the composition and/or function of the gut microbiota, thus conferring health benefits for the host. Favorable effects of prebiotics on cardiometabolic health have been observed in both preclinical and clinical studies [51]. However, manipulating the gut microbiota non-specifically by prebiotics can be dangerous. For example, a compositionally defined diet combined with soluble inulin can induce the development of gut microbiota-dependent hepatocellular carcinoma [52]. Thus, future studies to provide mechanistic insights into the relationship between a prebiotic and a downstream metabolic phenotype are very much needed. However, this task is very challenging, since the gut microbial community and the gut microbiota-host cross-talk are very complex. Natural modulations of the gut microbiota linked to e.g. diet, lifestyle and drug interactions, also hinder the development of prebiotic therapeutics. Another study reported that interindividual differences in the post meal glucose response are associated with individual dissimilarities in the gut microbial composition [53]. These studies indicate that a personalized strategy may be necessary and should be systematically addressed to maximally exploit the benefits of prebiotic supplements.

Meanwhile, probiotics (i.e. live microorganisms) have also been shown to exert health benefits on the host when administered in adequate amounts. For example, *Akkermansia muciniphila* (*A. muciniphila*), a SCFA producer, has been approved, in pasteurized form, as a food supplement and categorized as a novel food by the European Food Safety Authority [54]. Both live and pasteurized *A. muciniphila* were shown to improve insulin resistance and dyslipidemia both in mouse models [55] and in humans [56]. The beneficial effects of pasteurized *A. muciniphila* on cardiometabolic health was likely caused by a thermostable outer-membrane protein of *A. muciniphila* [57]. Similarly, administration of multi-strain probiotics, which contain 3 strains of *Lactobacillus*, and 3 strains of *Bifidobacterium*, was shown to reduce fasting plasma insulin levels in people with T2D [58]. Although probiotic interventions are clinically feasible and could be valuable in the treatment of cardiometabolic diseases [59], there is still no consensus on the intervention period, optimal dose and mechanistic pathways underlying the efficacy of probiotics to improve cardiometabolic diseases. It is important to point out that the current selection of probiotics is primarily in accordance to abundance-based analyses of gut microbial composition, where microorganisms whose proportions closely correlate with beneficial phenotypes are the main focus of interest. However, the keystone commensal, which organizes the gut microbial community or provides an crucial gain of function, can be a low-abundant component and is often not easily detected by current sequencing depths of analyses.

Bacterial enzyme inhibitors and bacteriophage therapy. Given the very recent insight that metabolites produced by gut bacteria may be harmful for cardiometabolic health of the host, one of the most recent lines of research focuses on developing small molecules capable of selectively targeting microbial enzymes involved in the production of those metabolites. However, data are very limited at the moment. Thus, due to high therapeutic potential, such intervention strategies represent an important avenue of future research. Bacteriophage therapy was initially described in the 1910's but has seen a recent renewal in interest with regard to the treatment of cardiometabolic diseases [60]. It was recently reported that phage therapy can be utilized to deplete susceptible gut bacteria and affect the metabolism of gut microbiota [60]. Bacteriophage therapy has been examined in a mouse model of liver diseases, showing that that bacteriophages can reduces the abundance of *Enterococcus faecalis* in the gut to improve liver damage [61]. However, using this therapy to improve cardiometabolic diseases has not been investigated outside of rodents and thus needs further investigation for its therapeutic efficacy and clinical safety.

Taken together, the gut microbiota-targeted pharmacotherapy requires a progressive and experimental pipeline approach. The first step towards developing novel therapeutics for cardiometabolic diseases would be understanding the global relationships between the gut microbiota and the host. Next, studies should focus on classifying cardiometabolic diseases based on disease phenotypes and gut microbiota profiles, so that different therapeutic strategies can be applied to different gut microbial communities. Investigating molecular mechanisms of microbiota-host interactions during pathological processes should be pursued, which would assist in developing the gut microbiota-oriented therapy. Meanwhile, bioanalytical profiling technologies, such as metagenomics and metabolomics, on human fecal samples, can be utilized to provide holistic and dynamic biochemical information, which can help researchers establish personalized gut microbiota-targeted therapeutic strategies (Gut microbiota-oriented therapies for cardiometabolic diseases are shown in **Figure 1**).
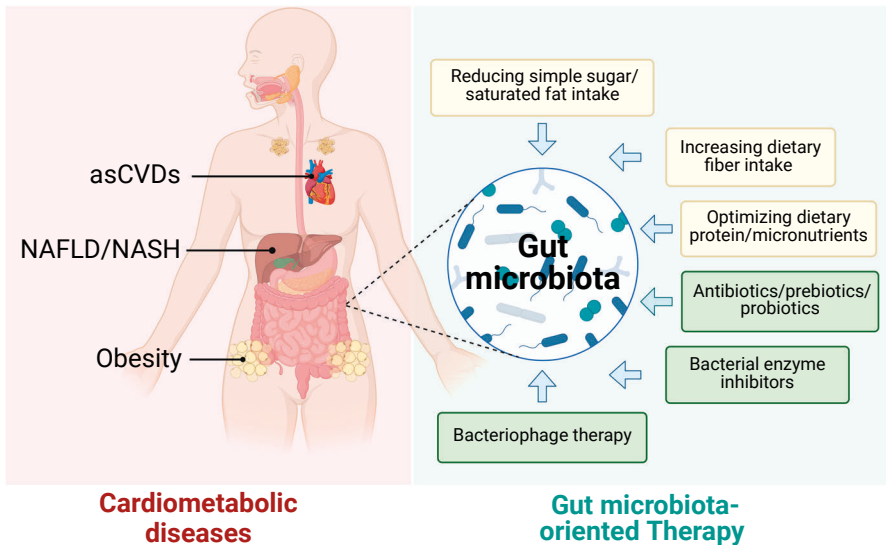
7

Figure 1. Drugging the gut microbiota to improve cardiometabolic diseases. The currently available gut-microbiota-oriented therapeutic strategies for cardiometabolic diseases, i.e. obesity, non- alcoholic fatty liver disease (NAFLD)/non-alcoholic steatohepatitis (NASH) and atherosclerotic cardiovascular disease (asCVD), are mainly dietary and pharmacological interventions. Dietary interventions, such as optimizing dietary macro- and micro-nutrient quantity and quality, can beneficially modulate gut microbiota-centered inter-organ cross-talk to combat cardiometabolic diseases. Likewise, gut microbiota-oriented pharmacological interventions, such as the use of antibiotics, prebiotics and probiotics, and more recently, bacterial enzyme inhibitors and bacteriophage therapy, have also shown therapeutic potential in the treatment of cardiometabolic diseases.

2. Targeting the liver to improve inter-organ cross-talk for combating cardiometabolic diseases

Besides the gut, the liver is another key organ that can impact cardiometabolic health and disease. Through fine-tuning circulating levels of metabolic substrates (e.g. glucose and lipids) and through producing bioactive molecules (e.g. hepatokines), the liver can communicate with various metabolic organ systems to regulate whole-body metabolism. As such, liver-centered inter-organ cross-talk is an important target for combating cardiometabolic diseases. The section below describes the therapeutic potential of targeting this cross-talk that has been investigated in this thesis.

2.1. Improving liver metabolic function by dietary and pharmacological interventions

The liver is the hub of many metabolic pathways, including those of lipids and glucose. In health, the liver is a well-controlled machinery, and it can coordinate the whole-body metabolic flexibility that is characterized by the ability to dynamically

adapt to fluctuations in energy needs and supplies. However, when the disposal of metabolic substrates of e.g. fatty acids (FAs) within the liver is overwhelmed, lipids may accumulate in the liver, thereby impairing liver metabolic function and carving the path towards to the development of NAFLD. Given that liver steatosis, an early stage of NAFLD, is an early indicator of hepatic and systemic insulin resistance, it is not surprising that NAFLD is associated with increased risk of cardiometabolic diseases. Indeed, feeding C57BL/6J mice with a HFD for 8 weeks induces liver steatosis, and mice develop more severe liver steatosis accompanied with adiposity and insulin resistance by prolonging the HFD feeding for another 8 weeks (**Chapter 4**). Likewise, in most epidemiological studies, liver fat content correlates with high body mass index (BMI) and high incidence of CVDs [62]. Moreover, by feeding *APOE*3-Leiden.CETP* mice with a high fat and high cholesterol diet (HFCD) for 23 weeks, a humanized progressive NAFLD model could be established (**Chapter 6**). Of note, compared to the liver steatosis model (**Chapter 4**), this model exhibits more severe cardiometabolic complications, such as hyperlipidemia, hyperglycemia, insulin resistance and obesity (**Chapter 6**). This is in line with recent findings demonstrating that NAFLD severity correlates positively with the severity of other cardiometabolic diseases [63]. As such, the metabolic function of the liver has become an indicator of cardiometabolic heath, and a barometer that allows the identification of individuals who are insulin resistant, who are in a metabolic state of severe adipose tissue dysfunction, and who are at a high risk of CVD development [62]. To improve liver metabolic function and cardiometabolic health, two main liver-oriented strategies are being examined in both preclinical and clinical research (i.e. dietary interventions and hepatocyte mitochondria-targeted therapy), which will be elaborated on below.

Reducing hepatic metabolite substrate influx by dietary interventions. Dietary factors can affect the metabolic function of the liver in addition to modulation of the gut microbiota-centered inter-organ cross-talk (as described in the section 1.1). Dietary interventions for NAFLD rely on the central hypothesis that optimizing the quality and quantity of dietary nutrients can reduce the influx of exogenous metabolic substrates (e.g. dietary CHOs and lipids) and endogenous metabolic substrates (e.g. white adipose tissue [WAT]-derived FAs) into the liver. Currently, diets used for improving liver metabolic function are mainly those that contain small amounts of saturated fat, free sugars and/or refined CHOs [64]. High saturated fat consumption can increase saturated free FAs in the circulation, which generally results in elevated influx of these FAs into the liver. On the other hand, excess consumption of saturated fat can cause endotoxemia, which can result in WAT inflammation and lipolysis, thereby further elevating the supply of WAT-derived FAs to the liver. In the liver, excess saturated fatty acetyl coenzyme A (acyl-CoA) can be metabolized into diacylglycerol (DAG). DAGs

7

are precursors of TGs which can be stored in the liver in the form of lipid droplets. Of note, DAGs can also activate protein kinase Cε, resulting in impaired hepatic insulin signaling [65]. Besides, saturated fatty acyl-CoAs, particularly palmitoyl-CoA, can enter to the *de novo* ceramide synthetic pathway. Ceramides can impair hepatocytic mitochondrial function, and reduce hepatic and systemic insulin signaling, thereby promoting the development of NAFLD and its associated cardiometabolic diseases [66]. Thus, reducing saturated fat intake may hold great promise in alleviation of NAFLD-associated cardiometabolic diseases. Indeed, the Mediterranean diet that contains high ratios of monounsaturated FAs (MUFAs) and polyunsaturated FAs (PUFAs) relative to saturated FAs, has been shown to reduce liver fat content and obesity in both preclinical and clinical studies [67]. Currently, the Mediterranean diet is also recommended for people with NAFLD by guidelines of the European Associations for the Study of both Obesity, Diabetes and the Liver (EASO, EASD and EASL, respectively) [68]. However, thus far limited data are available to support the use of a Mediterranean diet as a strategy for preventing and treating NAFLD. Thus, future studies are required to examine its therapeutic efficacy, preferably at various stages of NAFLD in both experimental animal models and ultimately in humans.

Reduction of dietary sugar and refined CHOs intake can reduce hepatic *de novo* lipogenesis (DNL), which is a key contributor to NAFLD. DNL is a biochemical process in which FAs are synthesized from acetyl coenzyme A (CoA) subunits which can be derived from various sources, mainly dietary CHOs. High consumption of dietary sugars can enhance DNL, which exclusively synthesized saturated FAs [69]. An intermediate in the DNL pathway, malonyl-CoA, can inhibit mitochondrial FA uptake, thereby limiting β-oxidation. Hence, reducing dietary CHOs and saturated fat may be an effective strategy for combating NAFLD and its associated cardiometabolic diseases. Consistently, a recent study has reported that short-term intervention with an isocaloric low-CHO diet induces a dramatic reduction of liver fat and other cardiometabolic risk factors paralleled by a markedly decreased DNL and largely increased mitochondrial β-oxidation [70]. These results highlight the potential of low-CHO interactions for treating NAFLD. Despite this, future studies are still needed to examine the influence of low-CHO on cardiometabolic health and disease in the long-term.

In summary, current guidelines recommend dietary modifications, in particular reducing dietary content of saturated fat, free sugars and/or refined CHOs, in the treatment of NAFLD and its associated cardiometabolic diseases. However, it remains unclear whether optimizing diet composition or following a particular dietary pattern provides greater benefit. The Mediterranean diet has received the most attention with the most promising results, and is recommended by the EASO, EASD and EASL for

people with NAFLD. Other dietary strategies, such as ketogenic, plant-based and high-protein diets, have all shown promise in beneficially affecting cardiometabolic diseases, including NAFLD. However, prospective, long-term and randomized clinical studies with liver histopathological endpoints are still required before recommendations should be developed regarding most of these dietary interventions in the specific NAFLD treatment.

Improving hepatocyte mitochondrial function by pharmacological interventions. As mentioned above, unhealthy diets lead to liver metabolic dysfunction, and dietary interventions are still the mainstay in the management of patients with NAFLD. Nevertheless, lifestyle interventions are insufficient to fully prevent/reverse NAFLD [71]. As such, pharmacological interventions that can effectively improve liver metabolic function and cardiometabolic diseases are urgently needed. Over the past decades, important advances have been made in the understanding of pathogenesis of liver damage, fibrogenesis, and carcinogenesis in relation to mitochondrial dysfunction of hepatocytes. Although liver-targeted, especially hepatocyte mitochondria-targeted medicine, is still largely in the developmental stage, we will discuss here the therapeutic potential of such a strategy in the alleviation of NAFLD and its associated cardiometabolic diseases.

The liver is composed of several cell types, among which hepatocytes, making up 70-85% of the liver mass [72]. Hepatocytes play a critical role in modulating CHO and lipid metabolism, and thus are most susceptible to cellular damage. Within these cells (i.e. hepatocytes), mitochondria are important organelles that are considered a metabolic hub for controlling hepatocyte function. Hepatocytic mitochondria orchestrate energy metabolism by substrate oxidation via a combination of β-oxidation of FAs and glycolysis of glucose, coupled to the tricarboxylic acid cycle (TCA), adenosine triphosphate (ATP) synthesis through oxidative phosphorylation (OXPHOS) and reactive oxygen species (ROS) formation [72]. Aberrant alterations in these processes can contribute to liver injury [73], indicating that improving hepatocyte mitochondrial function is a potential strategy for the alleviation of NAFLD and its associated cardiometabolic diseases. Indeed, in **Chapter 4**, we demonstrated that in developing obesity, improved hepatocyte mitochondrial function was linked to decreased sphingolipid accumulation and reduced inflammation in the liver. It is well-studied that the early onset of obesity is characterized by aberrant lipid accumulation and impaired mitochondrial function in the liver. Under obesogenic conditions, FA disposal through β-oxidation and TG formation is overwhelmed in the liver, so that excess FAs can form lipotoxic species, such as sphingolipids, that dampen mitochondrial function and induce local and systemic inflammation. With disease progression, obesity-driven

7

NAFLD is associated with impaired mitochondrial ATP synthesis in hepatocytes [74-76]. Indeed, we observed that upregulation of hepatic expression of mitochondrially encoded ATP synthase membrane subunit 6 (*mt-ATP6*), a gene encoding ATP synthase, was associated with a profound reduction of hepatic steatosis and inflammation. During progressive NAFLD, hepatic inflammation leads to hepatic stellate cell (HSC) activation, and activated HSCs are characterized by the release of retinoids, which can induce production of excessive amounts of extracellular matrix proteins and consequently promotion of liver fibrogenesis [77, 78]. In **Chapter 4**, we further reported the protective effects of improved mitochondrial function against HSC activation, as related to increased mitochondrial ATP synthesis. In agreement, depriving HSCs from retinol reduces mitochondrial ATP synthesis, while energy output increased by restoring retinol [78, 79]. Consistently, previous studies did show that within the liver, the transcription level of the *mt-ATP6* gene correlates with retinol levels [80], indicating that improvement of mitochondrial function can alleviate NASH. Notably, improved mitochondrial function of hepatocytes also contributed to reduced body fat mass accompanied by improved adipose tissue function and insulin sensitivity (**Chapter 4**). Our findings further provide convincing evidence that hepatocyte mitochondria function closely links to cardiometabolic health, and mitochondria-directed therapy holds great promise in preventing and treating NAFLD and other cardiometabolic diseases such as T2D and obesity.

In line with our findings, several drugs that are still used for treating obesity and/or T2D in the clinic have shown profound impact on hepatocyte mitochondrial function, and therefore have been proposed as potential therapeutics for NAFLD, such as metformin. Metformin can directly act on hepatocytes to decrease gluconeogenesis partially via modulation of mitochondrial complex I activity, AMP-activated protein kinase (AMPK) activation, and the AMP concentration [81-83]. It can also enhance the hepatic cytosolic redox state by inhibiting glycerol-3-phosohate dehydrogenase activity to decrease glucogenesis [84, 85]. Consistently, several clinical trials observed that metformin treatment improved hepatic steatosis and inflammation in people with NAFLD. Likewise, liraglutide, an acylated glucagon-like peptide-1 (GLP-1) agonist that is also used as anti-diabetic drug, has also been shown to improve NAFLD in HFD-fed mice by improving mitochondrial function and reducing ROS production [86]. In line with this, a randomized placebo-controlled study showed that compared with the placebo group, liraglutide treatment promoted histological resolution of NASH [87]. Although these anti-diabetic drugs thus show some promise in alleviating NAFLD, their efficacy in the treatment of more severe NAFLD, i.e. fibrotic NASH, requires further investigation. Moreover, given that these therapeutic agents do not specifically target hepatocyte mitochondria, these aforementioned findings only show an association

between improved mitochondrial function and improved progressive NAFLD. Thus, it is still unclear whether direct hepatocyte mitochondria-targeted therapy is able to combat NAFLD and its associated cardiometabolic diseases. Future studies are thus needed to evaluate the therapeutic potential of hepatocyte mitochondria-targeted therapy in the treatment of NAFLD, and in particular fibrotic NASH.

Taken together, hepatocyte mitochondria are appealing targets for treatment of liver pathologies. The development of drugs targeted to hepatocyte mitochondria is strongly encouraged, as such drugs may be able to effectively combat NAFLD, and even fibrotic NASH. This hypothesis is supported by our findings showing that improving hepatocyte mitochondrial function can inhibit HSC activation (**Chapter 4**), indicating the anti-fibrotic potential of mitochondria-targeted therapies. Currently, mitochondrial medicine is largely in the developmental stage, and future pre-clinical and clinical studies should pay more attention and efforts to explore its application in the treatment of cardiometabolic diseases.

2.2 Hepatokine FGF21-based pharmacotherapy

As an endocrine organ, the liver secretes various peptide and protein hormones, namely hepatokines, that can influence cardiometabolic health through cross-talk with multiple metabolic organ systems via autocrine, paracrine and endocrine signaling. As such, these bioactive molecules are of great interest as potential targets for the treatment of cardiometabolic diseases, especially as many of these are much easier to manipulate than other factors contributing to cardiometabolic diseases. Among these hepatokines, fibroblast growth factor (FGF) 21 has been brought to the foreground as a promising potential therapeutic for cardiometabolic diseases.

FGF21 is an atypical member of the endocrine FGF family that lacks mitogenic activity. Although *Fgf21* mRNA can be detected in numerous tissues (e.g. the liver and adipose tissue), circulating FGF21 is mainly derived from the liver [88]. Indeed, we (**Chapter 5**) and others [48, 89] observed that circulating FGF21 levels correlate well with hepatic *Fgf21* mRNA expression levels. FGF21 elicits its biological effects by binding and activating a receptor complex comprised of FGF receptors (FGFRs) and its co-receptor-klotho (KLB) [90]. Whereas FGFRs exhibit a ubiquitous expression pattern, the expression of KLB is primarily restricted to specific metabolic organs (e.g. the liver and adipose tissue) [91]. Physiologically, FGF21 is a stress-induced hormone, whose levels rise in metabolically compromised states (e.g. obesity, T2D and NAFLD) [88]. Hepatocyte lipid overload is an important signal that triggers FGF21 production and release [92]. Induction of FGF21 is thought to mediate a compensatory response to limit metabolic dysregulation, although such a physiological response is insufficient

to actually compensate [88]. Indeed, administration of (long-acting) FGF21 has shown beneficial effects on obesity and T2D, as reproducibly observed in many preclinical studies [93-95]. For instance, FGF21 administration in DIO mice reduces fat mass and improves insulin sensitivity and lipid profiles (that is, decreases in TGs and low-density lipoprotein cholesterol, and increases in high-density lipoprotein cholesterol) [95-97]. Given that native FGF21 is unsuitable for clinical use owing to poor pharmacokinetic and biophysical properties [91], a large number of long-acting FGF21 analogues have been developed. Several FGF21 analogues have even progressed to early phases of clinical trials in patients with e.g. obesity and T2D. In these trials, substantial improvements were observed in dyslipidemia and hepatic fat fractions in individuals with obesity and T2D [48, 94]. In this section, we will further discuss the therapeutic efficacy of FGF21-based pharmacotherapy on fibrotic NASH and atherosclerotic CVD.

FGF21-based pharmacotherapy in the treatment of NASH. Very recently, two phase IIa clinical trials reported that pharmacological treatment with FGF21 analogues reduce liver fat content in people with NASH [98, 99]. In **Chapter 5**, by using *APOE*3-Leiden.CETP* mice, we further demonstrated that FGF21 treatment limits all features of fibrotic NASH, including liver lipotoxicity, inflammation and fibrogenesis. We proposed that the protective effects of FGF21 on liver lipotoxicity result from the combined effects of FGF21 on adipose tissue and the liver, resulting in decreased lipid influx from adipose tissue into the liver coupled with the activation of FA oxidation and cholesterol elimination pathways in the liver [90, 91]. Our findings are in agreement with observations observed in humans showing that administration with FGF21 analogues in people with NASH not only decreased liver lipid content [100, 101], but also increased cholesterol removal, reducing the risk for further hepatocyte lipotoxicity [98]. While NASH is initiated by liver lipotoxicity, NASH progression is primarily triggered by inflammation [102]. We demonstrated that FGF21 prevented HFCD-induced inflammatory responses, as proved by improved lobular inflammation and hepatocyte ballooning and reduced numbers of inflammatory foci and crown-like structures. Notably, FGF21 reduced pro-inflammatory activation of various subsets of Kupffer cells (KCs; i.e. the resident macrophages in the liver). Furthermore, we reported that FGF21 treatment prevented liver fibrosis, which was associated with reduced numbers of lipid- and scar-associated KCs [103, 104]. Previous studies have shown that scar-associated macrophages are enriched in fibrotic liver [104-107], and these cells are able to prime quiescent primary HSCs to upregulate the expression of fibrillar collagen [104], thereby promoting liver fibrosis. As such, our findings likely indicate that FGF21 inhibits liver fibrogenesis by preventing lipid- and scar-associated macrophage accumulation, thereby inhibiting HSC activation to produce collagen. Collectively, our data further strengthen the therapeutic potential of FGF21 for treatment of NASH and provide

mechanistic insight supporting the currently ongoing clinical trials evaluating the impact of long-acting FGF21 on fibrotic NASH.

FGF21-based pharmacotherapy in the treatment of atherosclerotic CVD. While clinical trials are underway with long-acting FGF21 analogues to combat e.g. NAFLD [108], the pharmacological effects of FGF21 on atherosclerosis are far from being elucidated. Current studies evaluating the therapeutic effects of FGF21 on atherosclerosis are mainly derived from genetic studies, demonstrating that *Fgf21* deficiency in *Apoe*^{-/-} mice promotes atherosclerosis [109]. Of note, FGF21 treatment reduces hypercholesterolemia in obese non-human primates [110] and humans [111], indicating that (long-acting) FGF21 may have the ability to attenuate atherosclerosis. A study has shown reduced atherosclerotic lesion size upon FGF21 administration in *Fgf21*^{-/-}*Apoe*^{-/-} mice [109]. However, considering that APOE plays crucial role in mediating hepatic uptake of TG-rich lipoprotein remnants, *Apoe*^{-/-} mice may not be the best model to investigate potential therapeutic effects of FGF21 on atherosclerosis by modulating lipid metabolism. Therefore, in **Chapter 6**, we explored the effects of FGF21 treatment on cardiovascular risk factors, particularly on lipoprotein metabolism in relation to atherogenesis using *APOE*3-Leiden.CETP mice*. We showed that FGF21 reduces hypercholesterolemia by accelerating TG-rich lipoprotein turnover as a result of brown fat activation and white fat browning, thereby reducing atherosclerotic lesion severity and increasing atherosclerotic lesion stability index. Mechanistic studies revealed that FGF21 treatment enhances lipolytic conversion of VLDL by brown fat and by white fat. In line with this, a clinical study was reported that FGF21 administration increased thermogenesis-related gene/protein expression in human adipocytes [112]. The avid uptake of generated VLDL remnants that result from lipolysis by BAT and beige WAT by the liver is likely mediated via the APOE-LDLR pathway, as we previously found that clearance of VLDL remnants is impaired in *Ldlr*^{-/-} and *Apoe*^{-/-} mice [113]. Moreover, we showed that decreased atherosclerotic lesion area was mainly predicted by the reduction in non-high-density lipoprotein cholesterol (non-HDL-C). Indeed, clinical studies showed that early interventions to lower non-HDL-C levels in the circulation can fully block and even reverse earlier stages of atherosclerosis [114]. FGF21 also increased atherosclerotic plaque stability index by reducing the plaque macrophage content relative to the collagen and smooth muscle cell content. This suggests that in addition to lowering atherogenic cholesterol levels to reduce atherosclerosis initiation, FGF21 also suppresses inflammation. Consistently, FGF21 was shown to block foam cell formation and inhibit inflammatory responses in oxidized low-density lipoprotein-induced macrophages *in vitro* [115]. Therefore, our present data, together with available clinical data, suggest that FGF21 is a promising therapeutic for asCVD.

7

Taken together, clinical studies on FGF21 analogues conducted thus far have yielded mixed results. While the effects of FGF21 on glycemic control are disappointing, it has shown promising results in terms of liver function and lipid metabolism, making it a potential treatment for NASH and CVD comorbidities rather than T2D. It is worth noting that while many therapeutics for T2D effectively lower glucose levels, they do not have the same therapeutic effects on dyslipidemia as FGF21. Therefore, further research is needed to explore the potential benefits of combining FGF21 with these anti-diabetic drugs to treat a group of obesity-associated metabolic disorders. Additionally, large-scale clinical studies with long-term treatment periods are needed to assess whether improved lipid metabolism upon FGF21 treatment is sufficient to effectively treat NASH and asCVDs. Furthermore, to translate the therapeutic potential of FGF21-based therapeis from the laboratory to the clinic, some crucial questions need to be answered [91]. Considering that the current findings highlight the complexity and interspecies variations of FGF21 biology, future research should focus on identifying the specific tissues and cellular pathways that mediate the diverse pharmacological effects of FGF21 in humans. This would assist in developing tissue-specific FGF21 agonists with improved specificity and safety. Besides, clinical trials have observed
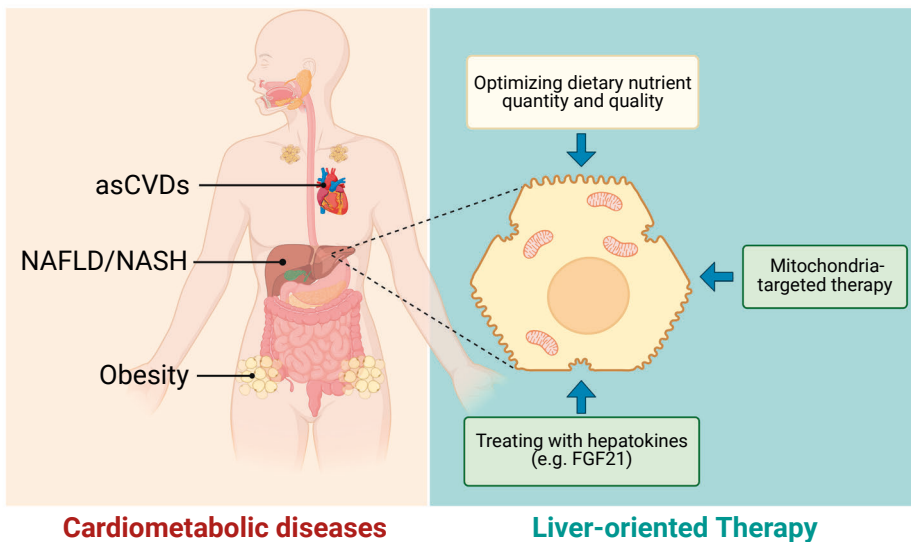

Figure 2. Improving the liver metabolic function to improve cardiometabolic diseases. Currently available liver-oriented therapeutic strategies for cardiometabolic diseases, e.g. obesity, non-alcoholic fatty liver disease (NAFLD)/non-alcoholic steatohepatitis (NASH) and atherosclerotic cardiovascular disease (asCVD), are mainly dietary and pharmacological interventions. Dietary interventions, such as optimizing dietary macro- and micro-nutrient quantity and quality can reduce liver fat which improves cardiometabolic health. Likewise, liver-oriented pharmacological interventions, such as mitochondrial-targeted therapy, and more recently, administration of hepatokines have also shown therapeutic potential in the treatment of cardiometabolic diseases, including NASH and asCVD.

large variability in plasma levels of FGF21 among individuals, indicating that people may respond differentially to (long-acting) FGF21. As such, understanding genetic and metabolic factors that influence FGF21 responsiveness is necessary for the development of personalized FGF21-based pharmacotherapies that target populations with optimal FGF21 sensitivity (Liver-oriented therapies for cardiometabolic diseases are shown in **Figure 2**).

CONCLUDING REMARKS

In multicellular organisms, maintenance of systemic homeostasis and response to nutritional and environmental challenges require the coordination of multiple organs and tissues. To adapt to changing metabolic demands, higher organisms have developed a system of inter-organ communication by which one tissue can affect metabolic processes in a distant tissue. Dysregulation of these lines of communication contributes to the development of cardiometabolic diseases (e.g. obesity, T2D, NAFLD/ NASH and asCVD), which are pressing public-health concerns worldwide. Therefore, there is an urgent need to identify novel strategies to limit cardiometabolic health risks associated with the disruption of inter-organ cross-talk.

On one hand, strategies can focus on regulating the gut microbiota-centered inter-organ cross-talk, which can be achieved by dietary and pharmacological interventions. The gut microbiota forms a bioreactor which is fueled by exogenous dietary components and endogenous compounds generated from microorganisms and the host to produce various bioactive compounds. These gut microbiota-derived metabolites signal to various metabolic organs in the body, which adds to cross-talk between the gut and the host. The gut microbiota-host interaction contains different layers, including dietary precursors, gut microbial communities and meta-organismal pathways, all of which are potential therapeutic targets for cardiometabolic diseases. The gut microbiota is most sensitive to the diet, and diet-induced changes of the gut microbiota can influence the production of the gut microbial metabolites (e.g. SCFAs). Administration of antibiotics, prebiotics or probiotics can also modulate the gut microbiota composition to affect the gut microbiota-centered inter-organ cross-talk. Moreover, bacterial enzyme inhibitors and bacteriophage therapy can also influence the production of the gut microbial metabolites by modifying the gut microbiota profile. This thesis focused on dietary intervention, as this strategy induce little discomfort and side effects. We have demonstrated that dietary interventions are efficient to modulate the gut microbiota composition and function, thereby regulating the gut microbial metabolite production. In particularly, we showed that dietary butyrate and choline

7

supplementation can beneficially modulate the gut microbiota to alleviate adiposity. Moreover, we showed that plasma levels of choline metabolite TMAO are not associated with the development of cardiometabolic diseases. Future studies are still required to evaluate the therapeutic potential of dietary butyrate and choline supplementation in the treatment of various stages of NAFLD and asCVD in both various experimental animal models and in humans.

On the other hand, therapies can also focus on liver-centered inter-organ cross-talk. Dietary and pharmacological strategies to improve hepatocyte mitochondrial function hold great promise for combating cardiometabolic diseases. Herein, we showed that improving hepatocyte mitochondrial function by γ-hydroxybutyric acid not only improves liver metabolic function, but also reverses obesity and its associated metabolic diseases including such as insulin resistance. In addition, cardiometabolic health can be improved by regulating systemic levels of hepatokines (e.g. FGF21). In this thesis, we showed that FGF21-based pharmacotherapies can regulate the cross-talk between the liver and adipose tissue to improve cardiometabolic diseases, especially fibrotic NASH and atherosclerotic CVD. Mechanistically, FGF21 upregulates FA oxidation in thermogenic tissues and in the liver, thereby improving lipid metabolism, and as a consequence largely attenuates all features of NASH and atherosclerosis development. Our data provide a strong experimental basis for the clinical development of FGF21 to treat NASH and asCVD. It will thus be very interesting to learn whether this approach is able to effectively (and safely) improve cardiometabolic health in humans in the future.

REFERENCES

1. Roth, G.A., et al., *Global Burden of Cardiovascular Diseases and Risk Factors, 1990-2019: Update From the GBD 2019 Study.* J Am Coll Cardiol, 2020. **76**(25): p. 2982-3021.

2. Collins, K.H., et al., *A High-Fat High-Sucrose Diet Rapidly Alters Muscle Integrity, Inflammation and Gut Microbiota in Male Rats.* Sci Rep, 2016. **6**: p. 37278.

3. Vors, C., et al., *Postprandial Endotoxemia Linked With Chylomicrons and Lipopolysaccharides Handling in Obese Versus Lean Men: A Lipid Dose-Effect Trial.* J Clin Endocrinol Metab, 2015. **100**(9): p. 3427-35.

4. Herman, M.A. and M.J. Birnbaum, *Molecular aspects of fructose metabolism and metabolic disease.* Cell Metab, 2021. **33**(12): p. 2329-2354.

5. Febbraio, M.A. and M. Karin, *"Sweet death": Fructose as a metabolic toxin that targets the gut-liver axis.* Cell Metabolism, 2021. **33**(12): p. 2316-2328.

6. Binienda, A., et al., *Dietary Carbohydrates and Lipids in the Pathogenesis of Leaky Gut Syndrome: An Overview.* Int J Mol Sci, 2020. **21**(21).

7. Desai, M.S., et al., *A Dietary Fiber-Deprived Gut Microbiota Degrades the Colonic Mucus Barrier and Enhances Pathogen Susceptibility.* Cell, 2016. **167**(5): p. 1339-1353 e21.

8. Cani, P.D., et al., *Metabolic endotoxemia initiates obesity and insulin resistance.* Diabetes, 2007. **56**(7): p. 1761-72.

9. Ferro, D., et al., *New Insights into the Pathogenesis of Non-Alcoholic Fatty Liver Disease: Gut-Derived Lipopolysaccharides and Oxidative Stress.* Nutrients, 2020. **12**(9).

10. Kallio, K.A., et al., *Endotoxemia, nutrition, and cardiometabolic disorders.* Acta Diabetol, 2015. **52**(2): p. 395-404.

11. Lassenius, M.I., et al., *Bacterial Endotoxin Activity in Human Serum Is Associated With Dyslipidemia, Insulin Resistance, Obesity, and Chronic Inflammation.* Diabetes Care, 2011. **34**(8): p. 1809-1815.

12. Marti, A., et al., *Higher Lipopolysaccharide Binding Protein and Chemerin Concentrations Were Associated with Metabolic Syndrome Features in Pediatric Subjects with Abdominal Obesity during a Lifestyle Intervention.* Nutrients, 2021. **13**(2).

13. Roberts, M.N., et al., *A Ketogenic Diet Extends Longevity and Healthspan in Adult Mice.* Cell Metab, 2017. **26**(3): p. 539-546 e5.

14. Paoli, A., et al., *Ketogenic Diet and Microbiota: Friends or Enemies?* Genes (Basel), 2019. **10**(7).

15. Swidsinski, A., et al., *Reduced Mass and Diversity of the Colonic Microbiome in Patients with Multiple Sclerosis and Their Improvement with Ketogenic Diet.* Frontiers in Microbiology, 2017. **8**.

16. Tagliabue, A., et al., *Short-term impact of a classical ketogenic diet on gut microbiota in GLUT1 Deficiency Syndrome: A 3-month prospective observational study.* Clin Nutr ESPEN, 2017. **17**: p. 33-37.

17. Nordmann, A.J., et al., *Effects of low-carbohydrate vs low-fat diets on weight loss and cardiovascular risk factors: a meta-analysis of randomized controlled trials.* Arch Intern Med, 2006. **166**(3): p. 285-93.

18. *Comparison of the Atkins, Zone, Ornish, and LEARN diets for change in weight and related risk factors among overweight premenopausal women: The A TO Z weight loss study: A randomized trial (vol 297, pg 969, 2007).* Jama-Journal of the American Medical Association, 2007. **298**(2): p. 178-178.

19. Gentile, C.L. and T.L. Weir, *The gut microbiota at the intersection of diet and human health.* Science, 2018. **362**(6416): p. 776-780.

7

20. Covas, M.I., et al., *The effect of polyphenols in olive oil on heart disease risk factors: a randomized trial.* Ann Intern Med, 2006. **145**(5): p. 333-41.

21. Garcia-Mantrana, I., et al., *Shifts on Gut Microbiota Associated to Mediterranean Diet Adherence and Specific Dietary Intakes on General Adult Population.* Front Microbiol, 2018. **9**: p. 890.

22. Zhang, L., et al., *Butyrate in Energy Metabolism: There Is Still More to Learn.* Trends in Endocrinology and Metabolism, 2021. **32**(3): p. 159-169.

23. Samuel, B.S., et al., *Effects of the gut microbiota on host adiposity are modulated by the short-chain fatty-acid binding G protein-coupled receptor, Gpr41.* Proc Natl Acad Sci U S A, 2008. **105**(43): p. 16767-72.

24. De Vadder, F., et al., *Microbiota-generated metabolites promote metabolic benefits via gut-brain neural circuits.* Cell, 2014. **156**(1-2): p. 84-96.

25. Li, Z., et al., *Butyrate reduces appetite and activates brown adipose tissue via the gut-brain neural circuit.* Gut, 2018. **67**(7): p. 1269-1279.

26. Salas-Salvado, J., et al., *Prevention of diabetes with Mediterranean diets: a subgroup analysis of a randomized trial.* Ann Intern Med, 2014. **160**(1): p. 1-10.

27. Turnbaugh, P.J., et al., *An obesity-associated gut microbiome with increased capacity for energy harvest.* Nature, 2006. **444**(7122): p. 1027-31.

28. Kasahara, K., et al., *Interactions between Roseburia intestinalis and diet modulate atherogenesis in a murine model.* Nature Microbiology, 2018. **3**(12): p. 1461-1471.

29. Zheng, J., et al., *Dietary N-Nitroso Compounds and Risk of Hepatocellular Carcinoma: A USA-Based Study.* Hepatology, 2021. **74**(6): p. 3161-3173.

30. Zhang, B., et al., *The Mechanism Underlying the Influence of Indole-3-Propionic Acid: A Relevance to Metabolic Disorders.* Front Endocrinol (Lausanne), 2022. **13**: p. 841703.

31. Xue, H.L., et al., *Gut Microbially Produced Indole-3-Propionic Acid Inhibits Atherosclerosis by Promoting Reverse Cholesterol Transport and Its Deficiency Is Causally Related to Atherosclerotic Cardiovascular Disease.* Circulation Research, 2022. **131**(5): p. 404-420.

32. Koeth, R.A., et al., *Intestinal microbiota metabolism of L-carnitine, a nutrient in red meat, promotes atherosclerosis.* Nat Med, 2013. **19**(5): p. 576-85.

33. Zhu, W., et al., *Gut Microbial Metabolite TMAO Enhances Platelet Hyperreactivity and Thrombosis Risk.* Cell, 2016. **165**(1): p. 111-124.

34. Wang, Z., et al., *Gut flora metabolism of phosphatidylcholine promotes cardiovascular disease.* Nature, 2011. **472**(7341): p. 57-63.

35. Tang, W.H.W. and S.L. Hazen, *The contributory role of gut microbiota in cardiovascular disease.* Journal of Clinical Investigation, 2014. **124**(10): p. 4204-4211.

36. Chang, T.Y., et al., *Optimal Dietary Intake Composition of Choline and Betaine Is Associated with Minimized Visceral Obesity-Related Hepatic Steatosis in a Case-Control Study.* Nutrients, 2022. **14**(2).

37. Bordoni, L., et al., *Trimethylamine N-oxide and the reverse cholesterol transport in cardiovascular disease: a cross-sectional study.* Sci Rep, 2020. **10**(1): p. 18675.

38. Richard, C., et al., *Impact of Egg Consumption on Cardiovascular Risk Factors in Individuals with Type 2 Diabetes and at Risk for Developing Diabetes: A Systematic Review of Randomized Nutritional Intervention Studies.* Can J Diabetes, 2017. **41**(4): p. 453-463.

39. Shin, J.Y., et al., *Egg consumption in relation to risk of cardiovascular disease and diabetes: a systematic review and meta-analysis.* Am J Clin Nutr, 2013. **98**(1): p. 146-59.

40. Meyer, K.A. and J.W. Shea, *Dietary Choline and Betaine and Risk of CVD: A Systematic Review and Meta-Analysis of Prospective Studies.* Nutrients, 2017. **9**(7).

41. Nagata, C., et al., *Choline and Betaine Intakes Are Not Associated with Cardiovascular Disease Mortality Risk in Japanese Men and Women.* J Nutr, 2015. **145**(8): p. 1787-92.

42. Wang, H., et al., *The microbial metabolite trimethylamine N-oxide promotes antitumor immunity in triple-negative breast cancer.* Cell Metab, 2022. **34**(4): p. 581-594 e8.

43. Hussein, H.M., et al., *Vitamin D mitigates diabetes-associated metabolic and cognitive dysfunction by modulating gut microbiota and colonic cannabinoid receptor 1.* Eur J Pharm Sci, 2022. **170**: p. 106105.

44. Mayneris-Perxachs, J., et al., *Iron status influences non-alcoholic fatty liver disease in obesity through the gut microbiome.* Microbiome, 2021. **9**(1).

45. Wilck, N., et al., *Salt-responsive gut commensal modulates T(H)17 axis and disease.* Nature, 2017. **551**(7682): p. 585-589.

46. Epstein, S.E., et al., *The role of infection in restenosis and atherosclerosis: focus on cytomegalovirus.* Lancet, 1996. **348 Suppl 1**: p. s13-7.

47. Patel, P., et al., *Association of Helicobacter pylori and Chlamydia pneumoniae infections with coronary heart disease and cardiovascular risk factors.* BMJ, 1995. **311**(7007): p. 711-4.

48. Saikku, P., et al., *Serological evidence of an association of a novel Chlamydia, TWAR, with chronic coronary heart disease and acute myocardial infarction.* Lancet, 1988. **2**(8618): p. 983-6.

49. Vrieze, A., et al., *Impact of oral vancomycin on gut microbiota, bile acid metabolism, and insulin sensitivity.* J Hepatol, 2014. **60**(4): p. 824-31.

50. Huemer, M., et al., *Antibiotic resistance and persistence-Implications for human health and treatment perspectives.* EMBO Rep, 2020. **21**(12): p. e51034.

51. Green, M., K. Arora, and S. Prakash, *Microbial Medicine: Prebiotic and Probiotic Functional Foods to Target Obesity and Metabolic Syndrome.* Int J Mol Sci, 2020. **21**(8).

52. Singh, V., et al., *Dysregulated Microbial Fermentation of Soluble Fiber Induces Cholestatic Liver Cancer.* Cell, 2018. **175**(3): p. 679-694 e22.

53. Zeevi, D., et al., *Personalized Nutrition by Prediction of Glycemic Responses.* Cell, 2015. **163**(5): p. 1079-1094.

54. Turck, D., et al., *Safety of pasteurised Akkermansia muciniphila as a novel food pursuant to Regulation (EU) 2015/2283.* Efsa Journal, 2021. **19**(9).

55. He, X., et al., *Akkermansia muciniphila Alters Gut Microbiota and Immune System to Improve Cardiovascular Diseases in Murine Model.* Front Microbiol, 2022. **13**: p. 906920.

56. Depommier, C., et al., *Supplementation with Akkermansia muciniphila in overweight and obese human volunteers: a proof-of-concept exploratory study.* Nat Med, 2019. **25**(7): p. 1096-1103.

57. Anhe, F.F. and A. Marette, *A microbial protein that alleviates metabolic syndrome.* Nat Med, 2017. **23**(1): p. 11-12.

58. Firouzi, S., et al., *Effect of multi-strain probiotics (multi-strain microbial cell preparation) on glycemic control and other diabetes-related outcomes in people with type 2 diabetes: a randomized controlled trial.* European Journal of Nutrition, 2017. **56**(4): p. 1535-1550.

59. Witkowski, M., T.L. Weeks, and S.L. Hazen, *Gut Microbiota and Cardiovascular Disease.* Circ Res, 2020. **127**(4): p. 553-570.

7

60. de Jonge, P.A., et al., *Gut virome profiling identifies a widespread bacteriophage family associated with metabolic syndrome.* Nat Commun, 2022. **13**(1): p. 3594.

61. Duan, Y., et al., *Bacteriophage targeting of gut bacterium attenuates alcoholic liver disease.* Nature, 2019. **575**(7783): p. 505-511.

62. Stefan, N., H.U. Haring, and K. Cusi, *Non-alcoholic fatty liver disease: causes, diagnosis, cardiometabolic consequences, and treatment strategies.* Lancet Diabetes Endocrinol, 2019. **7**(4): p. 313-324.

63. Duell, P.B., et al., *Nonalcoholic Fatty Liver Disease and Cardiovascular Risk: A Scientific Statement From the American Heart Association.* Arterioscler Thromb Vasc Biol, 2022. **42**(6): p. e168-e185.

64. Yki-Jarvinen, H., et al., *Dietary carbohydrates and fats in nonalcoholic fatty liver disease.* Nat Rev Gastroenterol Hepatol, 2021. **18**(11): p. 770-786.

65. Kotronen, A., et al., *Hepatic stearoyl-CoA desaturase (SCD)-1 activity and diacylglycerol but not ceramide concentrations are increased in the nonalcoholic human fatty liver.* Diabetes, 2009. **58**(1): p. 203-8.

66. Chaurasia, B., et al., *Targeting a ceramide double bond improves insulin resistance and hepatic steatosis.* Science, 2019. **365**(6451): p. 386-392.

67. Moore, M.P., et al., *A Fad too Far? Dietary Strategies for the Prevention and Treatment of NAFLD.* Obesity (Silver Spring), 2020. **28**(10): p. 1843-1852.

68. Sberna, A.L., et al., *European Association for the Study of the Liver (EASL), European Association for the Study of Diabetes (EASD) and European Association for the Study of Obesity (EASO) clinical practice recommendations for the management of non-alcoholic fatty liver disease: evaluation of their application in people with Type 2 diabetes.* Diabetic Medicine, 2018. **35**(3): p. 368-375.

69. Mardinoglu, A., et al., *An Integrated Understanding of the Rapid Metabolic Benefits of a Carbohydrate-Restricted Diet on Hepatic Steatosis in Humans.* Cell Metab, 2018. **27**(3): p. 559-571 e5.

70. Mardinoglu, A., et al., *An Integrated Understanding of the Rapid Metabolic Benefits of a Carbohydrate-Restricted Diet on Hepatic Steatosis in Humans.* Cell Metabolism, 2018. **27**(3): p. 559-+.

71. Romero-Gomez, M., S. Zelber-Sagi, and M. Trenell, *Treatment of NAFLD with diet, physical activity and exercise.* J Hepatol, 2017. **67**(4): p. 829-846.

72. Morio, B., et al., *Role of mitochondria in liver metabolic health and diseases.* Cell Calcium, 2021. **94**: p. 102336.

73. Serviddio, G., et al., *Targeting mitochondria: a new promising approach for the treatment of liver diseases.* Curr Med Chem, 2010. **17**(22): p. 2325-37.

74. Longo, M., et al., *Mitochondrial dynamics and nonalcoholic fatty liver disease (NAFLD): new perspectives for a fairy-tale ending?* Metabolism, 2021. **117**: p. 154708.

75. Verbeek, J., et al., *Roux-en-y gastric bypass attenuates hepatic mitochondrial dysfunction in mice with non-alcoholic steatohepatitis.* Gut, 2015. **64**(4): p. 673-83.

76. Lee, K., et al., *Hepatic Mitochondrial Defects in a Nonalcoholic Fatty Liver Disease Mouse Model Are Associated with Increased Degradation of Oxidative Phosphorylation Subunits.* Mol Cell Proteomics, 2018. **17**(12): p. 2371-2386.

77. Okuno, M., et al., *Retinoids exacerbate rat liver fibrosis by inducing the activation of latent TGF-beta in liver stellate cells.* Hepatology, 1997. **26**(4): p. 913-21.

78. Trivedi, P., S. Wang, and S.L. Friedman, *The Power of Plasticity-Metabolic Regulation of Hepatic Stellate Cells.* Cell Metab, 2021. **33**(2): p. 242-257.

79. Chiu, H.J., D.A. Fischman, and U. Hammerling, *Vitamin A depletion causes oxidative stress, mitochondrial dysfunction, and PARP-1-dependent energy deprivation.* FASEB J, 2008. **22**(11): p. 3878-87.

80. Berdanier, C.D., et al., *Role of vitamin A in mitochondrial gene expression.* Diabetes Res Clin Pract, 2001. **54 Suppl 2**: p. S11-27.

81. Zhou, G., et al., *Role of AMP-activated protein kinase in mechanism of metformin action.* J Clin Invest, 2001. **108**(8): p. 1167-74.

82. Rena, G., D.G. Hardie, and E.R. Pearson, *The mechanisms of action of metformin.* Diabetologia, 2017. **60**(9): p. 1577-1585.

83. Lien, F., et al., *Metformin interferes with bile acid homeostasis through AMPK-FXR crosstalk.* Journal of Clinical Investigation, 2014. **124**(3): p. 1037-1051.

84. Madiraju, A.K., et al., *Metformin suppresses gluconeogenesis by inhibiting mitochondrial glycerophosphate dehydrogenase.* Nature, 2014. **510**(7506): p. 542-6.

85. Madiraju, A.K., et al., *Metformin inhibits gluconeogenesis via a redox-dependent mechanism in vivo.* Nat Med, 2018. **24**(9): p. 1384-1394.

86. Tong, W.X., et al., *Liraglutide ameliorates non-alcoholic fatty liver disease by enhancing mitochondrial architecture and promoting autophagy through the SIRT1/SIRT3-FOXO3a pathway.* Hepatology Research, 2016. **46**(9): p. 933-943.

87. Armstrong, M.J., et al., *Liraglutide safety and efficacy in patients with non-alcoholic steatohepatitis (LEAN): a multicentre, double-blind, randomised, placebo-controlled phase 2 study.* Lancet, 2016. **387**(10019): p. 679-690.

88. Zarei, M., et al., *Targeting FGF21 for the Treatment of Nonalcoholic Steatohepatitis.* Trends Pharmacol Sci, 2020. **41**(3): p. 199-208.

89. Nishimura, T., et al., *Identification of a novel FGF, FGF-21, preferentially expressed in the liver.* Biochim Biophys Acta, 2000. **1492**(1): p. 203-6.

90. Fisher, F.M. and E. Maratos-Flier, *Understanding the Physiology of FGF21.* Annu Rev Physiol, 2016. **78**: p. 223-41.

91. Geng, L., K.S.L. Lam, and A. Xu, *The therapeutic potential of FGF21 in metabolic diseases: from bench to clinic.* Nat Rev Endocrinol, 2020. **16**(11): p. 654-667.

92. Priest, C. and P. Tontonoz, *Inter-organ cross-talk in metabolic syndrome.* Nat Metab, 2019. **1**(12): p. 1177-1188.

93. Kharitonenkov, A., et al., *FGF-21 as a novel metabolic regulator.* Journal of Clinical Investigation, 2005. **115**(6): p. 1627-1635.

94. Talukdar, S., et al., *A Long-Acting FGF21 Molecule, PF-05231023, Decreases Body Weight and Improves Lipid Profile in Non-human Primates and Type 2 Diabetic Subjects.* Cell Metab, 2016. **23**(3): p. 427-40.

95. Xu, J., et al., *Fibroblast growth factor 21 reverses hepatic steatosis, increases energy expenditure, and improves insulin sensitivity in diet-induced obese mice.* Diabetes, 2009. **58**(1): p. 250-9.

96. Coskun, T., et al., *Fibroblast growth factor 21 corrects obesity in mice.* Endocrinology, 2008. **149**(12): p. 6018-27.

97. Berglund, E.D., et al., *Fibroblast growth factor 21 controls glycemia via regulation of hepatic glucose flux and insulin sensitivity.* Endocrinology, 2009. **150**(9): p. 4084-93.

98. Luo, Y., et al., *Pegbelfermin selectively reduces secondary bile acid concentrations in patients with non-alcoholic steatohepatitis.* JHEP Rep, 2022. **4**(1): p. 100392.

99. Harrison, S.A., et al., *A randomized, double-blind, placebo-controlled phase IIa trial of efruxifermin for patients with compensated NASH cirrhosis.* JHEP Rep, 2023. **5**(1): p. 100563.

7

100. Sanyal, A., et al., *Pegbelfermin (BMS-986036), a PEGylated fibroblast growth factor 21 analogue, in patients with non-alcoholic steatohepatitis: a randomised, double-blind, placebo-controlled, phase 2a trial.* Lancet, 2019. **392**(10165): p. 2705-2717.

101. Harrison, S.A., et al., *Efruxifermin in non-alcoholic steatohepatitis: a randomized, double-blind, placebo-controlled, phase 2a trial.* Nat Med, 2021. **27**(7): p. 1262-1271.

102. Cai, J., X.J. Zhang, and H. Li, *The Role of Innate Immune Cells in Nonalcoholic Steatohepatitis.* Hepatology, 2019. **70**(3): p. 1026-1037.

103. Bleriot, C., et al., *A subset of Kupffer cells regulates metabolism through the expression of CD36.* Immunity, 2021. **54**(9): p. 2101-+.

104. Ramachandran, P., et al., *Resolving the fibrotic niche of human liver cirrhosis at single-cell level.* Nature, 2019. **575**(7783): p. 512-+.

105. Remmerie, A., et al., *Osteopontin Expression Identifies a Subset of Recruited Macrophages Distinct from Kupffer Cells in the Fatty Liver.* Immunity, 2020. **53**(3): p. 641-+.

106. Daemen, S., et al., *Dynamic Shifts in the Composition of Resident and Recruited Macrophages Influence Tissue Remodeling in NASH.* Cell Rep, 2021. **34**(2): p. 108626.

107. Seidman, J.S., et al., *Niche-Specific Reprogramming of Epigenetic Landscapes Drives Myeloid Cell Diversity in Nonalcoholic Steatohepatitis.* Immunity, 2020. **52**(6): p. 1057-1074 e7.

108. Sonoda, J., M.Z. Chen, and A. Baruch, *FGF21-receptor agonists: an emerging therapeutic class for obesity-related diseases.* Horm Mol Biol Clin Investig, 2017. **30**(2).

109. Lin, Z., et al., *Fibroblast growth factor 21 prevents atherosclerosis by suppression of hepatic sterol regulatory element-binding protein-2 and induction of adiponectin in mice.* Circulation, 2015. **131**(21): p. 1861-71.

110. Kharitonenkov, A., et al., *The metabolic state of diabetic monkeys is regulated by fibroblast growth factor-21.* Endocrinology, 2007. **148**(2): p. 774-781.

111. Talukdar, S., et al., *A Long-Acting FGF21 Molecule, PF-05231023, Decreases Body Weight and Improves Lipid Profile in Non-human Primates and Type 2 Diabetic Subjects.* Cell Metabolism, 2016. **23**(3): p. 427-440.

112. Lee, P., et al., *Irisin and FGF21 are cold-induced endocrine activators of brown fat function in humans.* Cell Metab, 2014. **19**(2): p. 302-9.

113. Berbee, J.F., et al., *Brown fat activation reduces hypercholesterolaemia and protects from atherosclerosis development.* Nat Commun, 2015. **6**: p. 6356.

114. Robinson, J.G., et al., *Eradicating the Burden of Atherosclerotic Cardiovascular Disease by Lowering Apolipoprotein B Lipoproteins Earlier in Life.* Journal of the American Heart Association, 2018. **7**(20).

115. Wang, N., et al., *Fibroblast growth factor 21 regulates foam cells formation and inflammatory response in Ox-LDL-induced THP-1 macrophages.* Biomed Pharmacother, 2018. **108**: p. 1825-1834.

8

Summary
Samenvatting
List of publications
Curriculum vitae
Acknowledgements

SUMMARY

Cardiometabolic health is tightly controlled by a complex network of organ communication. Dysfunction of these lines of communication is associated with the development of cardiometabolic diseases, indicating inter-organ cross-talk as a therapeutic target. In this thesis, I explored the therapeutic potential of targeting inter-organ communication in cardiometabolic diseases including obesity, atherosclerotic cardiovascular disease and non-alcoholic steatohepatitis (NASH), based on which I proposed novel therapies to tackle these diseases. **Chapter 1** provides a general introduction on inter-organ cross-talk as a gatekeeper for cardiometabolic health. It explains that various metabolic organ systems can communicate with one another to regulate whole-body metabolic processes by producing signaling molecules, such as peptide/protein hormones, bioactive lipids and functional small molecules.

Gut microbiota-derived metabolites signal to various metabolic tissues and organs in the body, which is part of the cross-talk between the gut and the host and influences cardiometabolic health of the host. For example, gut microbiota metabolize dietary choline into trimethylamine (TMA) that is delivered via the portal vein to the liver where hepatocytes rapidly oxidize TMA by flavin monooxygenases into trimethylamine-N-oxide (TMAO). Studies conducted in $Apoe^{-/-}$ and $Ldlr^{-/-}$ mice showed that TMAO aggravates atherosclerosis by promoting formation of foam cells and activating the inflammatory response. In contrast, the gut microbiota-derived bioactive molecule butyrate has been shown to beneficially modulate the gut microbiota and exert anti-inflammatory and antiatherogenic properties in the same mouse models. Therefore, in **Chapter 2**, we aimed to investigate whether butyrate can alleviate choline-induced atherosclerosis. To this end, we used *APOE*3-Leiden.CETP* mice, a well-established atherosclerosis-prone model with human-like lipoprotein metabolism, and fed these mice with an atherogenic diet alone or supplemented with choline, butyrate or their combination. Interestingly, we observed that choline protected against body fat mass gain, increased the abundance of anti-inflammatory gut microbes, and increased the expression of gut microbial genes involved in TMA and TMAO degradation. Butyrate similarly attenuated fat mass gain and beneficially modulated the gut microbiome, as shown by increased abundance of anti-inflammatory and short chain fatty acid (SCFA)-producing microbes, and inhibited expression of gut microbial genes involved in lipopolysaccharide synthesis. Both choline and butyrate upregulated hepatic expression of flavin monooxygenases, and their combination resulted in highest circulating TMAO levels. Nonetheless, choline, butyrate and their combination did not influence atherosclerosis development, and TMAO levels were not associated with

atherosclerotic lesion size. These data, obtained in a mouse model relevant to human cardiometabolic diseases, may suggest that TMAO lacks atherogenic properties in humans.

Studies in e.g. diet-induced obese (DIO) and *ob/ob* mice have linked increased dietary choline consumption also to increased incidence of obesity. However, our study described above and several clinical trials have observed anti-obesity effects of high dietary choline intake. To understand the underlying mechanisms by which choline attenuates obesity in a human-like setting, in **Chapter 3** we aimed to explore the effect of high dietary choline consumption on adiposity by using *APOE*3-Leiden.CETP* mice. We observed that dietary choline reduced body fat by activating brown adipose tissue (BAT), resulting in accelerated triglyceride-rich lipoprotein (TRL) turnover to improve hypercholesterolemia. Besides, choline ameliorated liver steatosis and damage, which was associated with an upregulation of hepatic genes involved in fatty acid oxidation. These data thus provide a mechanistic basis for the observation in human intervention trials that high choline intake is linked with reduced body weight.

Interestingly, recent clinical studies have reported that the narcolepsy drug γ-hydroxybutyric acid (GHB), a SCFA that is structurally similar to butyrate, promotes weight loss via unknown mechanisms. Narcolepsy is a clinical condition of severely disturbed sleep that causes an increase in body weight after disease onset, frequently leading to obesity. Despite being clinically used in the treatment of narcolepsy, GHB is unlikely to be prescribed as anti-obesity drug due to its central effects and its misuse-associated adverse effects (e.g. severe respiratory depression). Nonetheless, elucidating the underlying mechanisms by which GHB reduces body weight may reveal therapeutic handles for the development of effective body weight loss medications. Thus, in **Chapter 4**, we investigated the effect of oral GHB treatment on body weight control in high fat diet (HFD)-induced developing and existing obesity by using C57BL/6J mice. In existing obesity, but not in developing obesity, GHB attenuated HFD-induced fat mass gain, glucose intolerance and insulin resistance. In contrast, GHB alleviated HFD-induced hepatic steatosis and inflammation in both metabolic conditions. This was accompanied by improvement of hepatic mitochondrial dysfunction, as evidenced by upregulated hepatic expression of genes encoding mitochondrial respiratory complex. Accordingly, in developing obesity, GHB alleviated the accumulation of toxic sphingolipids both in the liver and in the circulation. In existing obesity, GHB prevented hepatic loss of retinoids and increased circulating acyl-carnitine, a substrate for combustion by BAT. Consistently, GHB alleviated HFD-induced adipose tissue dysfunction in obese mice, as evidenced by increased uncoupling protein 1 (UCP-1) abundance in BAT and decreased white adipocyte size and white adipose tissue (WAT) inflammation. Moreover, GHB

beneficially influenced the gut microbial composition, as shown by an enrichment of SCFA producers in developing obesity, and anti-inflammatory and succinate-producers in existing obesity. Taken together, GHB promotes metabolic health in developing and existing obesity, which is associated with improved hepatic mitochondrial function and likely involves beneficial modulation of the gut microbial composition. These findings thus uncover previously unknown metabolic effects of GHB related to body weight management, and provide novel insights for new therapeutic handles for treating obesity and its related diseases.

Besides gut-microbiota-associated signaling molecules, various hepatokines produced by the liver can also modulate whole-body metabolic control. A very interesting hepatokine is fibroblast growth factor 21 (FGF21), given that FGF21 analogues are in clinical development to treat obesity and type 2 diabetes. Although their glucose-lowering and insulin sensitizing effects have been largely unraveled, the mechanisms by which they alleviate liver injury have been scarcely addressed. In **Chapter 5**, we unveiled the mechanisms underlying the protective effects of FGF21 on NASH, again using *APOE*3-Leiden.CETP* mice. Liver-specific FGF21 overexpression was achieved in mice using an adeno-associated virus, followed by administration of a high-fat high-cholesterol diet for 23 weeks. We observed that hepatic FGF21 overexpression limited hepatic lipid influx and accumulation through combined endocrine and autocrine signaling, respectively, which prevents Kupffer cell activation and lowers the presence of lipid- and scar-associated macrophages to inhibit fibrogenesis. These findings provide mechanistic insight that further strengthens the therapeutic potential of FGF21 for treatment of NASH and support currently ongoing clinical trials evaluating the impact of long-acting FGF21 on NASH. In **Chapter 6**, we next investigated the importance of FGF21 in other aspects of cardiometabolic health, particularly in lipoprotein metabolism in relation to atherogenesis, by administration of a long-acting recombinant FGF21 to *APOE*3-Leiden.CETP* mice fed an atherogenic diet. We observed that FGF21 treatment reduced plasma total cholesterol levels, explained by a reduction of plasma levels of non-high-density lipoprotein (non-HDL)-cholesterol. Mechanistically, FGF21 promoted BAT activation and WAT browning, thereby enhancing the selective uptake of fatty acids from TRLs into BAT and into beige WAT, consequently accelerating the clearance of the cholesterol-enriched TRL remnants by the liver. In addition, FGF21 reduced body fat, ameliorated glucose tolerance and reduced hepatic steatosis, related to upregulated hepatic expression of genes involved in fatty acid oxidation and increased very-low density lipoprotein (VLDL)-triglyceride secretion. Ultimately, FGF21 largely decreased atherosclerotic lesion area, which was mainly explained by the reduction in non-HDL-cholesterol, as shown by linear regression analysis, decreased lesion severity, and increased atherosclerotic plaque stability index. We have thus provided additional

support for the clinical use of long-acting FGF21 in the treatment of atherosclerotic cardiometabolic diseases.

Finally, in **Chapter 7**, the results of this thesis are placed in the context of the current scientific literature, and novel strategies to combat cardiometabolic disease associated with inter-organ cross-talk disturbance are discussed. In summary, this thesis provides novel insight into targeting gut microbiota- and liver-centered inter-organ cross-talk in the treatment of cardiometabolic diseases. First of all, dietary interventions remain the most effective strategy for modulating the gut microbiota-centered inter-organ communication, and dietary choline and butyrate have beneficial impact on the gut microbiota composition and function and body weight control. In addition, hepatocyte mitochondrial function governs whole-body metabolism through orchestrating local and systemic metabolic substrate metabolism, and hepatocyte mitochondria-targeted therapy holds great promise for combating cardiometabolic diseases. Last but not least, we propose hepatokine FGF21-based pharmacotherapy as a promising strategy for the treatment of fibrotic NASH and atherosclerotic CVD. Thus, the findings described in this thesis emphasize the importance of inter-organ cross-talk for cardiometabolic diseases, and have improved our knowledge on the mechanisms that underlie the risk in the ever-increasing population of individuals who suffer from cardiometabolic diseases.

SAMENVATTING

Cardiometabole gezondheid wordt sterk gereguleerd door een complex netwerk van communicatie tussen organen. Ontregeling van dit netwerk is geassocieerd met de ontwikkeling van cardiometabole ziekten, wat aangeeft dat het netwerk van communicatie tussen organen een therapeutisch doelwit is voor deze ziekten. In dit proefschrift heb ik op basis van dit communicatienetwerk tussen organen therapeutische mogelijkheden onderzocht en therapieën voorgesteld voor de behandeling van cardiometabole ziekten zoals obesitas, hart- en vaatziekten en niet-alcoholische steatohepatitis (NASH). **Hoofdstuk 1** vormt een algemene introductie over het belang van het orgaancommunicatie voor de cardiometabole gezondheid. Hierin leg ik uit dat organen met elkaar kunnen communiceren om de stofwisseling van het hele lichaam te reguleren door het produceren van signaalmoleculen, zoals peptide/eiwit-hormonen, bioactieve lipiden en functionele kleine moleculen.

Bacteriën in de darm produceren stoffen ('metabolieten') die fungeren als signaalmoleculen richting verschillende weefsels en organen die betrokken zijn bij de stofwisseling, en op die manier de cardiometabole gezondheid van de gastheer beïnvloedt. Darmbacteriën zetten bijvoorbeeld choline uit de voeding om in trimethylamine (TMA) dat via de poortader de lever bereikt, alwaar levercellen ('hepatocyten') het TMA met behulp van specifieke enzymen ('*flavin monooxygenases*') omzetten tot trimethylamine-N-oxide (TMAO). Studies die zijn uitgevoerd in *Apoe*$^{-/-}$ en *Ldlr*$^{-/-}$ muizen toonden aan dat TMAO slagaderverkalking ('atherosclerose') verergert door de vorming van schuimcellen te bevorderen en ontstekingen te activeren. Aan de andere kant is aangetoond dat butyraat, een bioactieve stof die geproduceerd wordt door darmbacteriën als gevolg van de afbraak van voedingsvezels, in dezelfde muismodellen darmbacteriën gunstig beïnvloedt en zowel ontstekingsremmende als anti-atherogene eigenschappen heeft. Daarom hebben we in **Hoofdstuk 2** onderzocht of butyraat in staat is choline-geïnduceerde atherosclerose te verminderen. Hiertoe gebruikten we *APOE*3-Leiden.CETP* muizen, een bewezen model voor de menselijke vetstofwisseling en atherosclerose, en voerden deze muizen een atherosclerose-bevorderend dieet zonder en met choline, butyraat of de combinatie van beide. Interessant genoeg zagen we dat choline toename in lichaamsvet tegenging, de hoeveelheid ontstekingsremmende bacteriën in de darm deed toenemen en de expressie van bacteriële genen die betrokken zijn bij de afbraak van TMA en TMAO verhoogde. Butyraat verminderde op een soortgelijke manier de toename in lichaamsvet en had ook een gunstig effect op de darm, wat bleek uit een verhoogde aanwezigheid van ontstekingsremmende en korteketenvetzuren-producerende bacteriën, en een lagere

expressie van bacteriële genen die betrokken zijn bij de vorming van lipopolysaccharide, een onderdeel van bacteriën met schadelijke effecten voor de gastheer. Zowel choline als butyraat verhoogden de expressie van *flavin monooxygenases* door de lever, en de combinatie van beide resulteerde in de hoogste concentratie van TMAO in het bloed. Desondanks hadden choline, butyraat en hun combinatie geen invloed op de ontwikkeling van atherosclerose en associeerden TMAO niveaus niet met de grootte van de atherosclerotische lesies. Omdat deze gegevens verkregen zijn in een muismodel dat relevant is voor menselijke cardiometabole ziekten, suggereren zij dat TMAO geen atherogene eigenschappen heeft bij mensen.

Studies in muizen met dieet-geïnduceerde obesitas en in muizen die obees zijn door een genetische oorzaak ('*ob/ob* muizen') hebben een verband aangetoond tussen een verhoogde inname van choline in de voeding en een verhoogde incidentie van obesitas. Ons hierboven beschreven onderzoek heeft echter beschermde effecten laten zien van een hoge inname van choline op obesitas, wat overeenkomt met diverse klinische onderzoeken. Om te begrijpen waardoor choline in een menselijke setting obesitas vermindert, onderzochten we in **Hoofdstuk 3** het effect van de inname van choline op lichaamsvet, als ook de onderliggende mechanismen, door weer gebruik te maken van *APOE*3-Leiden.CETP* muizen. We toonden aan dat een dieet rijk aan choline het lichaamsvet verlaagde door bruin vetweefsel te activeren, waardoor de afbraak van triglyceridenrijke vetbolletjes ('lipoproteïnen') in het bloed werd versneld en cholesterol in het bloed werd verlaagd. Bovendien verminderde choline leververvetting en leverschade, wat gepaard ging met een verhoogde expressie van genen die betrokken zijn bij vetzuurverbranding in de lever. Deze gegevens bieden dus een mechanistische onderbouwing voor de waarneming in mensen dat een hoge inname van choline gerelateerd is aan een verminderd lichaamsgewicht.

Recente klinische studies hebben laten zien dat γ-hydroxybutyraat (GHB), een korteketenvetzuur dat sterk lijkt op butyraat en wordt gebruikt bij de behandeling van narcolepsie, gewichtsverlies bevordert via vooralsnog onbekende mechanismen. Narcolepsie is een klinische aandoening waarbij de slaap sterk wordt verstoord, wat gepaard gaat met een toename van het lichaamsgewicht en vaak leidt tot obesitas. Hoewel GHB gebruikt wordt bij de behandeling van narcolepsie, is het onwaarschijnlijk dat het als anti-obesitasmiddel wordt voorgeschreven vanwege centrale effecten en bijwerkingen die gepaard gaan met misbruik van GHB, zoals ernstige ademhalingsdepressie. Desondanks kan het ontrafelen van de onderliggende mechanismen waardoor GHB het lichaamsgewicht vermindert therapeutische aanknopingspunten opleveren voor de ontwikkeling van effectieve medicatie om af te vallen. In **Hoofdstuk 4** hebben we daarom onderzocht welk effect orale behandeling

met GHB heeft bij de preventie en behandeling van dieet-geïnduceerde obesitas in C57BL/6J muizen. Bij de behandeling van al obese muizen, maar niet bij het voorkomen van obesitas in muizen die nog slank zijn, verminderde GHB de toename van vetmassa, glucose intolerantie en insulineresistentie die ontstaan ten gevolge van het vetrijke dieet. Daarentegen verminderde GHB leververvetting en leverontsteking in zowel slanke als dikke muizen. Dit ging gepaard met verbetering van de functie van de energiefabriekjes ('mitochondriën') in de lever, aangetoond door een hogere expressie van genen in de lever betrokken bij de aanmaak van eiwitten die onderdeel zijn van de zogenaamde 'ademhalingsketen'. Hierdoor verminderde GHB bij het ontstaan van obesitas de ophoping van giftige vetten ('sfingolipiden') in de lever en in de bloedbaan. Bij bestaande obesitas voorkwam GHB de afname van retinoïden in de lever en verhoogde het de circulerende hoeveelheid acyl-carnitine, een brandstof voor bruin vetweefsel. In overeenstemming hiermee verminderde GHB de ontregeling van vetweefsel in obese muizen ten gevolge van het vetrijk dieet, aangetoond door een verhoogde aanwezigheid van het ontkoppelingseiwit-1 (*uncoupling protein-1; UCP-1*) in bruin vetweefsel en kleinere vetcellen en minder ontsteking in het wit vetweefsel. Bovendien had GHB een gunstig effect op de samenstelling van de darmbacteriën, aangetoond door een verrijking van korteketenvetzuren-producerende bacteriën tijdens het ontstaan van obesitas en ontstekingsremmende en succinaat-producerende bacteriën bij al bestaande obesitas. Samengevat bevordert GHB de metabole gezondheid tijdens zowel de preventie als behandeling van obesitas, wat samenhangt met verbetering van de mitochondriële functie in de lever en een gunstige beïnvloeding van darmbacteriën. Hiermee brengen deze bevindingen onbekende metabole effecten van GHB met betrekking tot gewichtsbeheersing aan het licht en bieden zij inzichten voor nieuwe aanknopingspunten voor het behandelen van obesitas en gerelateerde ziekten.

Naast bacteriën in de darm produceert de lever ook signaalmoleculen ('hepatokinen') die de stofwisseling in het lichaam beïnvloeden. Een zeer interessant hepatokine is fibroblast-groeifactor 21 (FGF21), aangezien analogen van FGF21 in klinische ontwikkeling zijn om obesitas en type 2 diabetes te behandelen. Hoewel hun glucose-verlagende en insuline-sensibiliserende effecten grotendeels zijn ontrafeld, zijn de mechanismen waarmee ze leverbeschadiging verminderen nog nauwelijks onderzocht. In **Hoofdstuk 5** hebben we de mechanismen die ten grondslag liggen aan de beschermende effecten van FGF21 op NASH onthuld, opnieuw door gebruik te maken van *APOE*3-Leiden.CETP* muizen. FGF21 werd specifiek in de lever van deze muizen hoog tot expressie gebracht door gebruik te maken van een genetisch gemodificeerd verkoudheidsvirus, waarna de muizen behandeld werden met een vet- en cholesterolrijk dieet gedurende 23 weken. We constateerden dat hoge expressie van FGF21 in de lever de opname en opstapeling van vet verlaagde door aan te grijpen op

zowel vetweefsel ('endocriene signalering') als de lever zelf ('autocriene signalering'). Hierdoor werd de activatie van ontstekingscellen in de lever ('Kupffercellen') voorkomen en nam de aanwezigheid van vet- en litteken-geassocieerde macrofagen af, waardoor littekenvorming in de lever werd afgeremd. Deze bevindingen bieden mechanistische inzichten die het therapeutische potentieel van FGF21 voor de behandeling van NASH verder versterken en momenteel lopende klinische trials die de impact van langwerkende FGF21 op NASH evalueren ondersteunen. Vervolgens hebben we in **Hoofdstuk 6** het belang van FGF21 onderzocht voor andere aspecten van de cardiometabole gezondheid, met name de vetstofwisseling in relatie tot atherosclerose. Hiertoe dienden we langwerkend FGF21 toe aan *APOE*3-Leiden.CETP* muizen die een atherosclerose-bevorderend dieet kregen. We toonden aan dat behandeling met langwerkend FGF21 het cholesterol in het bloed verlaagde. Dat bleek het gevolg te zijn van het activeren van bruin vetweefsel en van het zogenaamde 'verbruinen' van wit vetweefsel, waardoor de opname van vetzuren uit triglyceridenrijke lipoproteïnen door bruin en wit vetweefsel werd verbeterd en de opname van de cholesterolrijke resten van deze lipoproteïnen door de lever werd versneld. Bovendien verminderde langwerkend FGF21 het lichaamsvet, verbeterde het de glucosetolerantie en verminderde het de leververvetting, gerelateerd aan een verhoogde expressie genen in de lever die betrokken zijn bij de vetzuurverbranding en de secretie van triglyceriden in zeer lage dichtheidslipoproteïnen (*very low density lipoproteins; VLDL*) door de lever. Uiteindelijk had langwerkend FGF21 een sterk remmend effect op slagaderverkalking, wat voornamelijk werd verklaard door de vermindering van het cholesterol in het bloed, en verbeterde het de ernst en stabiliteit van atherosclerotische lesies. Deze data ondersteunen daarom de klinische toepassing van langwerkend FGF21 bij de behandeling van atherosclerotische cardiometabole ziekten.

Tenslotte werden in **Hoofdstuk 7** de resultaten van dit proefschrift in de context van de huidige wetenschappelijke literatuur geplaatst en nieuwe strategieën besproken om cardiometabole ziekten te bestrijden die geassocieerd zijn met verstoringen in de communicatie tussen organen. Samenvattend bieden de studies die beschreven zijn in dit proefschrift nieuwe inzichten in de communicatie tussen organen, met name de rol van darmbacteriën en de lever, die relevant zijn voor de behandeling van cardiometabole ziekten. Dieetinterventies blijven de meest effectieve strategie voor het beïnvloeden van darmbacteriën en hun rol in de communicatie tussen organen; zowel choline als butyraat hebben een gunstig effect op de samenstelling en functie van de darmbacteriën en gewichtsbeheersing. Daarnaast speelt de mitochondriële functie in hepatocyten een belangrijke rol in het metabolisme van de lever en het hele lichaam, en ik veronderstel dan ook dat therapieën die zich richten op de mitochondriën van hepatocyten veelbelovende mogelijkheden bieden voor het bestrijden van

cardiometabole ziekten. Tot slot stel ik FGF21-gebaseerde farmacotherapie voor als een veelbelovende strategie voor de behandeling van zowel NASH en hart- en vaatziekten die veroorzaakt worden door slagaderverkalking. De bevindingen beschreven in dit proefschrift benadrukken dus het belang van communicatie tussen organen voor de behandeling van cardiometabole ziekten en hebben ons begrip verbeterd van mechanismen die ten grondslag liggen aan cardiometabole ziekten, waaraan steeds meer mensen lijden.

LIST OF PUBLICATIONS

1. **Liu C**, Zwaan M, Verhoeven A, Schinkelshoek MS, Fronczek R, Lammers GJ, Wang Y, Giera M, Boon MR, Rensen PCN, Schönke M. γ-hydroxybutyric acid attenuates diet-induced metabolic dysfunction in developing and existing obesity. *In preparation.*

2. Zhou E, Nakashima Hiroyuki, Li R, van der Zande HJP, **Liu C**, Li Z, Müller C, Bracher F, Mohammed Y, de Boer JF, Kuipers F, Guigas B, Rensen PCN, Giera M, Wang Y. Inhibition of Δ24-dehydrocholesterol reductase ameliorates diet-induced hepatic steatosis and inflammation through liver X receptor α without inducing hyperlipidemia. *Revision submitted.*

3. **Liu C**, Song Z, Li Z, Boon MR, Schönke M, Rensen PCN, Wang Y. Dietary choline increases markers of brown fat activation and improves cholesterol metabolism in *APOE*3-Leiden.CETP* female mice**. Int J Obes 2023**; *in press.*

4. Li Z, Zhou E, **Liu C**, Wicks H, Yildiz S, Razack F, Ying Z, Kooijman S, Koonen DPY, Heijink M, Kostidis S, Giera M, Kuijper EJ, Smits WK, van Dijk KW, Rensen PCN, Wang Y. Dietary butyrate ameliorates metabolic health dependent on gut microbiota and associated with selective proliferation of *Lachnospiraceae bacterium 28-4.* **JCI Insight 2023**; 8: e166655.

5. **Liu C**, Schönke M, Spoorenberg B, Lambooij JM, van der Zande HJP, Zhou E, Tushuizen ME, Andréasson AC, Park A, Oldham S, Uhrbom M, Ahlstedt I, Ikeda Y, Wallenius K, Peng XR, Guigas B, Boon MR, Wang Y, Rensen PCN. FGF21 protects against hepatic lipotoxicity and macrophage activation to attenuate fibrogenesis in nonalcoholic steatohepatitis. **eLife 2023**; 12: e83075.

6. **Liu C**, Li Z, Song Z, Fan X, Shao H, Boon MR, Schönke M, Rensen PCN, Wang Y. Choline and butyrate beneficially modulate the gut microbiome without affecting atherosclerosis in *APOE*3-Leiden.CETP* mice. **Atherosclerosis 2022**; 362: 47-55.

7. **Liu C**, Schönke M, Zhou E, Li Z, Kooijman S, Boon MR, Larsson M, Wallenius K, Dekker N, Barlind L, Peng XR, Wang Y, Rensen PCN. Pharmacological treatment with FGF21 strongly improves plasma cholesterol metabolism to reduce atherosclerosis. **Cardiovasc Res 2022**; 118: 489-502.

8. **Liu C**, Huang S, Wu Z, Li T, Li N, Zhang B, Han D, Wang S, Zhao J, Wang J. Cohousing-mediated microbiota transfer from milk bioactive components-dosed mice ameliorate colitis by remodeling colonic mucus barrier and lamina propria macrophages. **Gut Microbes 2021**; 13: 1-23.

9. Zhou E, Li Z, Nakashima H, **Liu C**, Ying Z, Foks AC, Berbée JFP, van Dijk KW, Rensen PCN, Wang Y. Hepatic scavenger receptor class B type 1 knockdown reduces atherosclerosis and enhances the antiatherosclerotic effect of brown fat activation in *APOE*3-Leiden.CETP* mice. **Arterioscler Thromb Vasc Biol 2021**; 41: 1474-1486.

10. Huang S, Wu Z, Li T, **Liu C**, Han D, Tao S, Pi Y, Li N, Wang J. Perturbation of the lipid metabolism and intestinal inflammation in growing pigs with low birth weight is associated with the alterations of gut microbiota. **Sci Total Environ 2020**; 719: 137382.

11. Huang S, **Liu C**, Li N, Wu Z, Li T, Han D, Li Z, Zhao J, Wang J. Membrane proteomic analysis reveals the intestinal development is deteriorated by intrauterine growth restriction in piglets. **Funct Integr Genomics 2020**; 20: 277-291.

12. Huang S, Li N, **Liu C**, Li T, Wang W, Jiang L, Li Z, Han D, Tao S, Wang J. Characteristics of the gut microbiota colonization, inflammatory profile, and plasma metabolome in intrauterine growth restricted piglets during the first 12 hours after birth. **J Microbiol 2019**; 57: 748-758.

13. Hamid H, Zhang J, Li W, **Liu C**, Li M, Zhao L, Ji C, Ma Q. Interactions between the cecal microbiota and non-alcoholic steatohepatitis using laying hens as the model. **Poult Sci 2019**; 98: 2509-2521.

14. Huang S, Wu Z, **Liu C**, Han D, Feng C, Wang S, Wang J. Milk fat globule membrane supplementation promotes neonatal growth and alleviates inflammation in low-birth-weight mice treated with lipopolysaccharide. **Biomed Res Int 2019**; 2019: 4876078.

15. **Liu C**, Zhang J, Li M, Zhao L, Ji C, Ma Q. Alterations and structural resilience of the gut microbiota under dietary fat perturbations. **J Nutr Biochem 2018**; 61: 91-100.

CURRICULUM VITAE

Cong Liu was born on August 5, 1993 in Linyi, Shandong province, China. In June 2012, she graduated from the First High School in Linyi. In September 2012, she entered the bachelor program 'Animal Science' at Shandong Agricultural University, Tai'an, China, and obtained her BSc degree in June 2016.

In September 2016, she started her 2-year master program 'Animal Nutrition & Feed Science' at China Agricultural University, Beijing, China. She worked on a research project entitled 'Alterations and structural resilience of the gut microbiota under dietary fat perturbations' under supervision of Prof. dr. Jianyun Zhang and Prof. dr. Qiugang Ma, at the State Key Laboratory of Animal Nutrition, China Agricultural University. She obtained her MSc degree in June 2018. Based on increased interest in inflammatory bowel diseases in relation to the gut microbiota, she next performed a 4-month internship at the Academy of National Food and Strategic Reserves Administration, Beijing, China, under supervision of Prof. dr. Junjun Wang. During this internship she participated in five projects and was responsible for the research project entitled 'Effects of human milk bioactive components on the gut microbiome and inflammatory bowel diseases (IBD)'.

In October 2018, based on sparkled interest in cardiometabolic diseases, she joined the research group of Prof. dr. Patrick Rensen within the Department of Internal Medicine, Division of Endocrinology, of Leiden University Medical Center initially as a research assistant. By using *APOE*3-Leiden.CETP* mice, a well-established mouse model with human-like lipoprotein metabolism, she investigated the role of FGF21 in lipid metabolism in relation to atherosclerosis development. In October 2019, she started her PhD training in the same group under the supervision of Prof. dr. Patrick Rensen, Prof. dr. Yanan Wang and Dr. Milena Schönke, focusing on targeting inter-organ cross-talk in cardiometabolic diseases. The results of her research are presented in this thesis. During her PhD training, she was awarded a Young Investigator Fellowship of the 88th and 90th European Atherosclerosis Society congress in 2020 and 2022, respectively, and a Young Investigator Travel Award of the Keystone Symposium 'Inter Organ Crosstalk in Non-Alcoholic Steatohepatitis' in 2022.

In 2023, Cong will join the research group of Dr. Daniel Puleston at Tisch Cancer Institute at the Icahn School of Medicine at Mount Sinai in New York City as a postdoctoral researcher to expand her knowledge on the interplay between immunology and metabolism within cardiometabolic diseases and in tumor development.

ACKNOWLEDGEMENTS

Looking back at the past years that I have spent in The Netherlands, I have experienced difficulties and challenges mixed with lots of happiness, joy and success as well. Without the support and understanding of many, I could not have coped with the culture shock at the beginning of my study abroad and finally gone through my 3-year PhD training that has culminated in this thesis. I wish to express my sincere appreciation to everyone that I have met here, especially those who have always stood behind me and accompanied me through all the ups and downs, and those who have given me the ability to appreciate the joyful times.

Firstly, I would like to express my sincere gratitude to my mentor, Prof. dr. Patrick Rensen, who has been the most important and irreplaceable person throughout my research life. Dear Patrick, in my heart, you are not only my supervisor but also like a respected elder who always supports and helps me when I am at a loss or when I am stuck. Without you, I would not be here and would not be able to achieve my goals.

Besides, I am deeply indebted to my daily supervisors, Prof. dr. Yanan Wang and Dr. Milena Schönke. Dear Yanan, you have truly encouraged me and taken care of me like a sister. Dear Milena, thank you for giving me freedom to do science, and for helping me whenever I need you.

I would also like to pay my special gratitude to Dr. Jimmy Berbée, who unfortunately passed away in April 2020. Dear Jimmy, thank you for your kindness at the beginning of my PhD training, which was like a warm sunshine and made me feel as warm as home.

Then, I would like to thank all my fantastic ENDO colleagues. Dear Ko and Sander, thank you for your comments and suggestions on my PhD projects, which are very helpful. Dear Aashley, Borja, Carlijn, Hiroyuki, Jing, Kaiming, Leonard, Maaike[1], Maaike[2], Mariëtte, Melanie, Mohan, Nicky, Robin, Sen, Wietse, Xiaoke and Zhixiong, and dear Eva, Giulia, Jan, Jari, Max, Rob, Sekar, Sheng, Susana, Onno, Tijmen, Zhou and others, you all are amazing colleagues, and I felt the warmth of my family. Dear Arty, my sincere friend, thank you for always being willing to listen to all my happiness and complaints, and for always being willing to have lunch with me, even though I rejected many times due to a busy working schedule. Dear Salwa, my friend, thank you for helping me whenever I need you. Dear Trea, thank you very much for teaching me to do ELISA-related experiments. Dear Reshma, thank you for teaching me how to

do various stainings. Dear Amanda, thank you for teaching me all animal techniques. Dear Hetty, thank you for teaching me how to do Western blot. Dear Chris, thank you for helping me order experimental materials.

I would also like to thank our collaborators for their great support. Dear Xiao-Rong, Kristina, Ike, and the whole team at AstraZeneca, and dear Bruno, Joost, Patrick, and Maarten, thank you for all your support on my FGF21 projects - it is very much appreciated.

Besides, I would like to thank the interns in our research group, especially my students Mik, Borah, and Zikuan, for their amazing help. Without your help, I could not have completed all my projects in such a short period.

I would like to thank my friends in Europe. Dear Yilin and Fangchen, my BEST friends, without your company, I could not have had such a colorful life in The Netherlands. Dear Yingjie and Pingzhuang, you made my life full of lots of fun. Dear Enchen and Zhuang, thank you for your great help throughout my PhD training. Dear Ellen, how lucky I am to have met you and to have had you as my friend. Dear Katerina and Laura, I had a great time with you, and I am super happy to have met you in The Netherlands. River, thank you for your encouragement which helped me a lot.

Dear Ping, Mengchen, Fangtao, Shuzhen, and Feiya, my BEST friends in China, thank you for always standing behind me and supporting me.

Finally, I would like to thank my FAMILY for their unconditional love, and full support. In particular, I would like to express my sincere gratitude to my grandpa, the best engineer and the smartest person in the world. Dear grandpa, the biggest regret of my whole life is that I was unable to come back and finally meet you. Thank you for letting me know that doing science is such fun. I will not let you down, and I will try my best to become a great researcher. Dear grandma, daddy, mommy, and my younger brother, thank you for your full support!

Never Forget Why You Started